Role of Guanylate Cyclase Activating Proteins in photoreceptor cells of the retina in health and disease

Natalia López del Hoyo

Role of Guanylate Cyclase Activating Proteins in photoreceptor cells of the retina in health and disease

Tesis Doctoral

Natalia López del Hoyo

Cover drawing by Santiago Ramon y Cajal. Included in “The Structure of the Retina”

Programa de Doctorado en Biomedicina
2010/2013

Role of Guanylate Cyclase Activating Proteins in photoreceptor cells of the retina in health and disease

Memoria presentada por Natalia López del Hoyo, licenciada en Biotecnología, para aspirar al grado de Doctora en Biomedicina. Este trabajo ha sido realizado en el Departamento de Patología y Terapéutica Experimental de la Facultad de Medicina de Bellvitge (Universitat de Barcelona).

Dirigida por,

Dra. Ana Méndez Zunzunegui

Investigadora IDIBELL

Tutor,

Dr. Carles Solsona Sancho

Catedrático del Departamento de Patología y Terapéutica Experimental de la Universidad de Barcelona

Natalia López del Hoyo

Barcelona, Diciembre 2013

INSTITUT D'INVESTIGACIÓ BIOMÈDICA DE BELLVITGE

UNIVERSITAT DE BARCELONA

Con mucho cariño

a mi sobrino Ander,

a mi ahijada Marina,

a mi familia y amigos.

«On ne voit bien qu'avec le cœur;

L'essentiel est invisible pour les yeux.»

Le Petit Prince. Antoine de Saint-Exupéry

I gratefully recognize being the recipient of a PhD fellowship

from the Bellvitge Biomedical Research Institute (IDIBELL)

TABLE OF CONTENTS

I. INTRODUCTION

RESUMEN EN ESPAÑOL

Para percibir el mundo exterior, uno de los sentidos de los cuales nos valemos es LA VISTA. La visión se inicia con la llegada de luz a la retina, más específicamente, a las células fotorreceptoras, que son neuronas altamente especializadas y compartimentalizadas. En el compartimento o segmento externo de éstas, se produce la conversión de la señal lumínica a una señal eléctrica. La captura de un fotón excita el cromóforo de la molécula rodopsina, el pigmento visual, desencadenando una cascada de amplificación enzimática conocida como fototransducción, que en último término provoca una bajada en los niveles de cGMP y el cierre de los canales iónicos sensibles a cGMP en la membrana plasmática. Por lo tanto, la luz reduce la entrada de Na^+ y Ca^{2+} causando una hiperpolarización transitoria de los fotorreceptores, señal que es transmitida a neuronas de orden superior y al cerebro, dónde esta información es integrada en la corteza visual. La cinética de los procesos de fototransducción marcan la sensibilidad y la resolución del sistema visual en su conjunto. Por tanto, es imprescindible una regulación muy fina y rápida de todo el proceso, para 1) detectar pequeñas oscilaciones en los niveles de luz, y 2) no saturar el sistema cuando los niveles de luz se mantienen en el tiempo. De forma que no sólo la activación eficiente de la cascada de fototransducción es vital, sino también su inactivación, y una condición sinequanone para permitir la reapertura de los canales de Na^+/Ca^{2+} es el restablecimiento de los niveles de cGMP.

Las proteínas encargadas de la síntesis de ésta molécula, cGMP, en conos y bastones son las Guanilato Ciclasas de retina (RetGC). Y a su vez, las Proteínas Activadoras de Guanilato Ciclasa (GCAPs) confieren sensibilidad a Ca^{2+} a las RetGCs. GCAPs, pues, juegan un papel fundamental en la restauración de la respuesta a la luz y la adaptación a ésta, mediante su rol como intermediarias entre la síntesis de cGMP y los niveles de Ca^{2+} libre en la célula.

Las GCAPs, de ~25KDa, fueron descubiertas a finales de los 80 y caracterizadas durante los años 90. Pertenecen a la familia de proteínas neuronales sensoras de calcio (NCS), por lo que presentan N-miristoilación, y además poseen cuatro dominios EF de unión a Ca^{2+}, aunque el primero de ellos, en el extremo N-terminal, no une Ca^{2+}. Se ha visto, en cambio, que está implicado en el reconocimiento de RetGC por parte de las GCAPs. El resto de dominios EF cuando no unen Ca^{2+} unen Mg^{2+}.

Se han identificado hasta ocho isoformas de GCAPs diferentes en varias especies, aunque las más abundantes en mamíferos son GCAP1 y GCAP2. Éstas presentan una similitud de secuencia del 40%. Tal como se ha ido perfilando con diversos estudios *in vitro* e *in vivo* (con los modelos transgénicos de ratón y zebrafish), a pesar de tener características bioquímicas muy parecidas, la acción individual de cada una de ellas no compensa funcionalmente ni a todos los niveles la ausencia de la otra.

Nos centraremos en GCAP1 y GCAP2. Ambas isoformas forman dímeros en su forma libre de Ca^{2+}. Cuando vuelven a unir Ca^{2+}, estos dímeros se mantienen en GCAP1, pero revierten en GCAP2, correlacionándose la formación de dímeros con la capacidad de activar retGC en GCAP2. Además, tanto GCAP1 como GCAP2 están unidas a membrana independientemente de la concentración de $[Ca^{2+}]_{free}$. En conjunto, todo apunta a un modelo en que las proteínas GCAPs están constitutivamente unidas a RetGC en el segmento externo, pero oscilan entre la forma activa e inactiva según los niveles de Ca^{2+} libre en la célula. Por otra parte, se ha descrito que GCAP2 se fosforila en la serina 201. La importancia fisiológica de esta fosforilación se desconoce, aunque se ha visto *in vitro* que la proteína se fosforila cuando se encuentra libre de Ca^{2+} y unida a Mg^{2+} y que esta fosforilación no afecta a la activación de RetGC.

Estudios *in vitro* han determinado que la $[Ca^{2+}]$ necesaria para producir la transición de un estado de inactivación de RetGC a uno de activación es diferente para GCAP1 y para GCAP2, siendo EC_{50}~130nM para GCAP1 y EC_{50}~50nM para GCAP2. Los niveles de Ca^{2+} en el compartimento externo de bastones en oscuridad son de ~250nM y estos niveles caen hasta ~25nM, diez veces por debajo de los niveles de oscuridad, en condiciones de luz saturante. Al inicio de la fotorrespuesta, cuando el Ca^{2+} celular se reduce progresivamente y alcanza la concentracion de ~130 nM, GCAP1 pasa de unir Ca^{2+} a unir Mg^{2+} activando RetGC y, por tanto, empieza a promover la síntesis de cGMP. El Ca^{2+} continúa bajando, y al alcanzar $[Ca^{2+}]$ ~50 nM, GCAP2 pasa a su conformación activa, activando también a su vez RetGC. Es decir, en la activación de RetGC las GCAPs actuan de forma secuencial, por lo que a este mecanismo se le ha denominado “relevo de Ca^{2+}”. In vivo, este mecanismo de acción de las GCAPs se ha visto confirmado en modelos de ratón y de zebrafish. Por tanto, GCAP1 jugaría un papel importante en la primera fase de la respuesta, mientras que GCAP2 es fundamental cuando la luz es más intensa.

Aunque ambas proteínas se encuentran en toda la célula fotorreceptor, su localización es más abundante en el segmento externo. La presencia de GCAP1 es predominante en las células de cono y la de GCAP2, en las de bastón. Se desconocen los mecanismos que determinan la localización de GCAPs, pero se ha visto que en

ausencia de las proteínas RetGCs, las GCAPs no son transportadas al segmento externo. De hecho, en ratones knockout para la proteína rd3 (retinal degeneration 3) de 23KDa, asociada a una de las distrofias hereditarias de retina más severas, la Amaurosis Congénita de Leber tipo 12, que colocaliza e interacciona con las RetGCs, se ha observado que los niveles de RetGCs y de GCAPs se ven muy reducidos y no se transportan al compartimento externo. RD3 une RetGCs y es responsable de su transporte al segmento externo. El transporte de las proteínas GCAP, por tanto, depende del transporte de las RetGCs.

Se han identificado mutaciones en GCAPs asociadas a distrofias hereditarias de retina. Para el gen GUCA1A, que codifica GCAP1, se han descrito diez mutaciones heterocigotas que conllevan a distrofias de cono y bastón autosómicas dominantes (adCORD). En la mayoría, la activación de retGC por parte de GCAP1 se ve alterada, puesto que las mutaciones se hallan en los dominios EF-hand de unión a Ca^{2+} o en las hélices que los preceden o siguen. D100E y N104K afectan directamente el dominio de unión a Ca^{2+} EF3. L151F y E155G afectan el de EF4. E89K, Y99C, T114I, I143NT, G159V afectan las hélices α que los preceden o suceden. Por otra parte, en P50L se ve afectada la estabilidad térmica de GCAP1 y no su capacidad de unir y activar RetGC. Mientras, para GUCA1B que codifica GCAP2, únicamente se ha encontrado una mutación asociada a retinitis pigmentosa autosómica dominante G157R de la que se desconoce la causalidad de la patología.

En el caso de GCAP1, se ha visto que las mutaciones causantes de degeneración retinal reducen la afinidad de unión de Ca^{2+} a la proteína, alterando la sensibilidad a Ca^{2+} de la regulación de RetGC por GCAP1 *in vivo.* El resultado es la síntesis ininterrumpida de cGMP y la consiguiente toxicidad para la célula por los elevados niveles de cGMP y de Ca^{2+}. Sin embargo, el efecto de la mutación G157R en GCAP2 aún no se ha investigado.

1.1. THE EYE AND THE RETINA

1.1.1. The eye works as a camera

Vision begins with the formation of an external world image at the back of the eye, on a thin layer of neurons called RETINA.

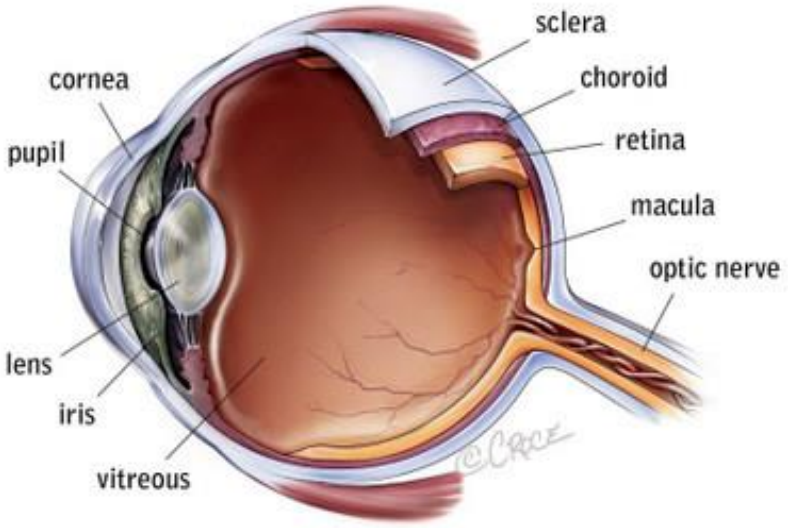

Figure I.1. ***Diagram of the different parts of a human eye.*** *From Bionic Vision Australia (http://bionicvision.org.au/eye/healthy_vision)*

Light enters the eye through the cornea. The cornea protects the eye from dust, germs, etc. and is responsible for refracting rays of light and bending them through the pupil. The iris regulates the amount of light entering the eye. In dim light the iris expands the pupil and allows more light to come in. On the contrary, in bright light, the iris contracts the pupil and less light penetrates the eye. Light crosses the lens which focuses the light upon the retina. The lens changes its shape depending on the distance of the object from the eye, making possible to “fine-tune” the focus. Afterwards, light crosses the vitreous gel, a jelly-like substance that fills the body of the eye, and it crosses the retina until reaching photoreceptor cells (Figure I.1). Photoreceptors are responsible for transforming light stimuli into an electric signal, which is then transmitted to higher order neurons in the retina, and subsequently to the visual cortex of the brain through the optic nerve (Rodieck 1998).

A homology of the eye with a photo camera is usually established. According to that functional comparison, the iris would be the diafragm regulating the entry of light, and the cornea and lens would act as the camera lens, focusing light on the thin layer of tissue covering the back of the eye, the retina, which would be the equivalent to the photographic film on which the image is impressed.

1.1.2. Rod and cone photoreceptors are compartmentalized neurons

Retina is formed by a set of different cells: photoreceptors, horizontal cells, bipolar cells, amacrine cells and ganglion cells (Rodieck 1998).

In vertebrates, there are two types of classical photoreceptors: rods and cones (Figure I.2.), although in mammals, we have a third type of retinal photoreceptor: the photosensitive ganglion cells at the inner retina (Yaun and Hardie 2009).

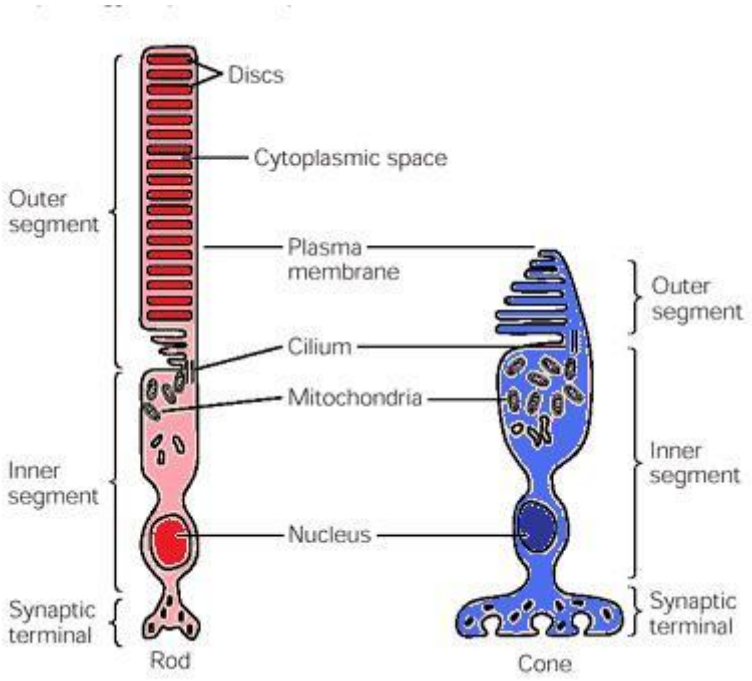

Figure I.2. ***Diagram of photoreceptor cell morphology: rod (left) and cone (right).*** *Adapted from (O'Brien 1982).*

These classical photoreceptors are highly specialized and compartmentalized neurons: they have four cell regions in which specific functions are carried out. The outer segment, where phototransduction takes places, contains a stack of membrane discs that are continuously renewed. The visual pigment, which is the most abundant protein in this compartment [at a concentration of about ~[3mM] (Otto Bruc *et al.* 1998)], is

embedded at disc membranes. In the case of rods, the non-nascent discs are not in touch with the plasma membrane, they are internalized, and the pigment is rod opsin (ó rhodopsin). However the three different types of cones in human eyes have their specific cone opsin embedded in cone invaginating membrane discs. In fact, membrane folding at cone outer segments allows having much more surface exposed, thus facilitating substances exchange, such as cromophore to regenerate the pigment or fast calcium dynamics which are key points during light adaptation (Figure I.2) (Fu and Yau 2007).

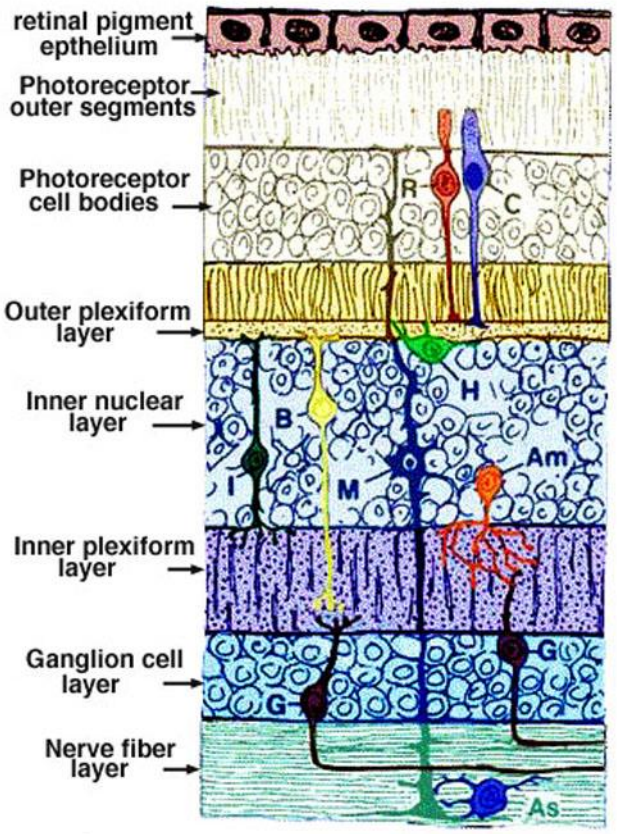

Figure I.3. ***Scheme of the layered organization of the different cell types in a human retina.*** *Different cell types in the retina organize in layers. The retinal pigment epithelium is adjacent to the retinal photoreceptor cells and nourishes them. Light-sensitive photoreceptor cells [rods(R) and cones(C)] organize in four layers: the outer segment layer (aligned outer segment compartments); inner segment layer (aligned metabolic, inner segment of the cells); outer nuclear layer (cell nuclei organized in rows); and plexiform layer (photoreceptor presynaptic terminals in contact with bipolar (B) and horizontal (H) cells dendrites). Bipolar and horizontal cell bodies locate at the inner nuclear layer alongside amacrine (A) and Müller glia (M) cell bodies, separated by the inner plexiform layer from the inner cell layer constituted by ganglion (G) cells. The ganglion cell layer continues to the optic nerve fiber layer. Astrocytes (As) are found in the ganglion cell and nerve fiber layers. Adapted from (Odgen 1989).*

The outer segment, where phototransduction takes place, is separated by a thin connecting cilium from the inner segment, the nucleus and the synaptic terminal. This implies that all phototransduction proteins, that are synthesized at the inner segment,

must pass through the cilium to get to the light sensitive compartment, the outer segment. The inner segment contains protein synthesis machinery (endoplasmic reticulum, Golgi apparatus) and an elevated number of mitochondria to supply the high amounts of proteins and energy demands. Then, it follows the nucleus, in the outer nuclear region, and finally, the synaptic terminal (Figure I.2), responsible for transmitting the change in membrane potential caused by light to the rate of neurotransmitter release to the second-order neurons: bipolar and horizontal cells. In response to light, there is hyperpolarization of the cell and a decrease in the rate of glutamate release at the outer plexiform layer. This signal travels really fast through the inner nuclear layer, to bipolar and ganglion cells in the direct pathway, to convey in the optic nerve (Figure I.3). Furthermore, horizontal and amacrine cells enrich the variety of connections established between photoreceptors, bipolar and ganglion cells (Rodieck 1998).

While photoreceptor cells “measure” the light intensity at different points of the visual image, this information is transmitted to bipolar and ganglion cells in a way in which some important integration occurs, so that the output of ganglion cells to the brain is based on contrasts of light intensity, and on movement, rather than on the light intensity of the natural world. The integration of visual information starts at the retina, and in that sense the retina is usually referred to as an “outpost” of the brain (Rodieck 1998).

1.2. THE PHOTOTRANSDUCTION CASCADE

1.2.1. Activation and recovery phase

Our visual system relies on the two types of photoreceptor cells described above: rods and cones, to cover the broad range of light intensities present in the natural world. As rods are more abundant in humans and higher mammals (97% in mouse retina) than cones, phototransduction has been better studied in rods (Fu and Yau 2007). Rods cover the range of dim light intensities. They are extraordinarily sensitive to light, and saturate at much dimer light intensities than cones, that cover the range of bright light (Fu and Yau 2007).

Therefore, when one photon of light is captured by the chromophore of rhodopsin, it causes its photoisomerization from 11-cis retinal to all-trans retinal, and a conformational change in the rhodopsin protein, that acquires its functional state (Rodieck 1998).

In its active state, rhodopsin activates the G_{α} subunit protein of transducin, by promoting the exchange of GDP for GTP in its α subunit and causing its separation from G_{β} and G_{γ}

subunits. G_α-GTP activates PDE6, retina-specific phosphodiesterase, whose catalytic sites cleave cGMP into GMP (Figure I.4). A single activated rhodopsin molecule activates ~20 G_α molecules, or what it is the same, ~ 0.2% of them (Krispel *et al.* 2006), producing a substantial amplification of the signal. cGMP-gated channels, which have a high probability of being in the open state in darkness, opened when they have 4 molecules of cGMP bound to them, allow the entrance of Ca^{2+} and Na^{2+} to the cell. The reduction of cGMP levels caused by the activation of rhodopsin promotes the closure of the channels reducing the entry of cations (Na^+ and Ca^{2+}) and therefore causing the hyperpolarization of the cell (Yaun and Hardie 2009). This hyperpolarization decreases, or even stops, the release of glutamate neurotransmitter which is sensed by the secondary neurons. One single activated rhodopsin molecule causes a reduction of ~0.7%, which corresponds to the closure of ~2% of the channels that are normally open in the dark state (Rodieck 1998).

As the exposure to light ends, everything that has been activated has to be inactivated in order to restore the darkness equilibrium. Photoactivated rhodopsin is phosphorylated by a rhodopsin kinase, GRK1 (G protein-coupled-receptor-kinase 1), and quenched by arrestin. In the case of the effector complex formed by transducin G_α and PDE in rods, inactivation resides in a GAP (GTPase activating complex) consisting of RGS9 (G-protein signaling 9), a RGS9-anchoring protein (R9AP) and an orphan G protein β subunit (Gβ5) that accelerate the intrinsic GTPase activity of G_α subunit, promoting the exchange of GTP for GDP (Yaun and Hardie 2009). Also, the cGMP levels have to be reestablished to the dark levels to reset the sensitivity of photoreceptors when the light ceases. cGMP is restored to dark levels by activation of retGCs by GCAPs, this causes the reopening of cGMP channels thus allowing the entrance of Na^+ and Ca^{2+}, and the dark current and membrane potential, and also the levels of intracellular Ca^{2+} to 500nM (Figure I.4) (Lucas *et al.* 2000).

The plasma membrane potential in photoreceptors is determined, in part, by the number of cGMP open channels which depends on the levels of cGMP in the cytoplasm, and that is ultimately controlled by the opposing effects of PDE6 and retGCs: when light leads to the activation of PDE producing cGMP hydrolysis and a drop in [cGMP], light also sets in motion a Ca^{2+} feedback loop that activates RetGCs in order to replenish cGMP levels in the cell and ultimately restore sensitivity to photoreceptors (Lucas *et al.* 2000). This Ca^{2+} feedback loop to cGMP synthesis mediated by RetGC/ GCAPs, by opposing the effect of light, constitutes an essential step of termination of the light-response, and of light adaptation (Dizhoor 2000).

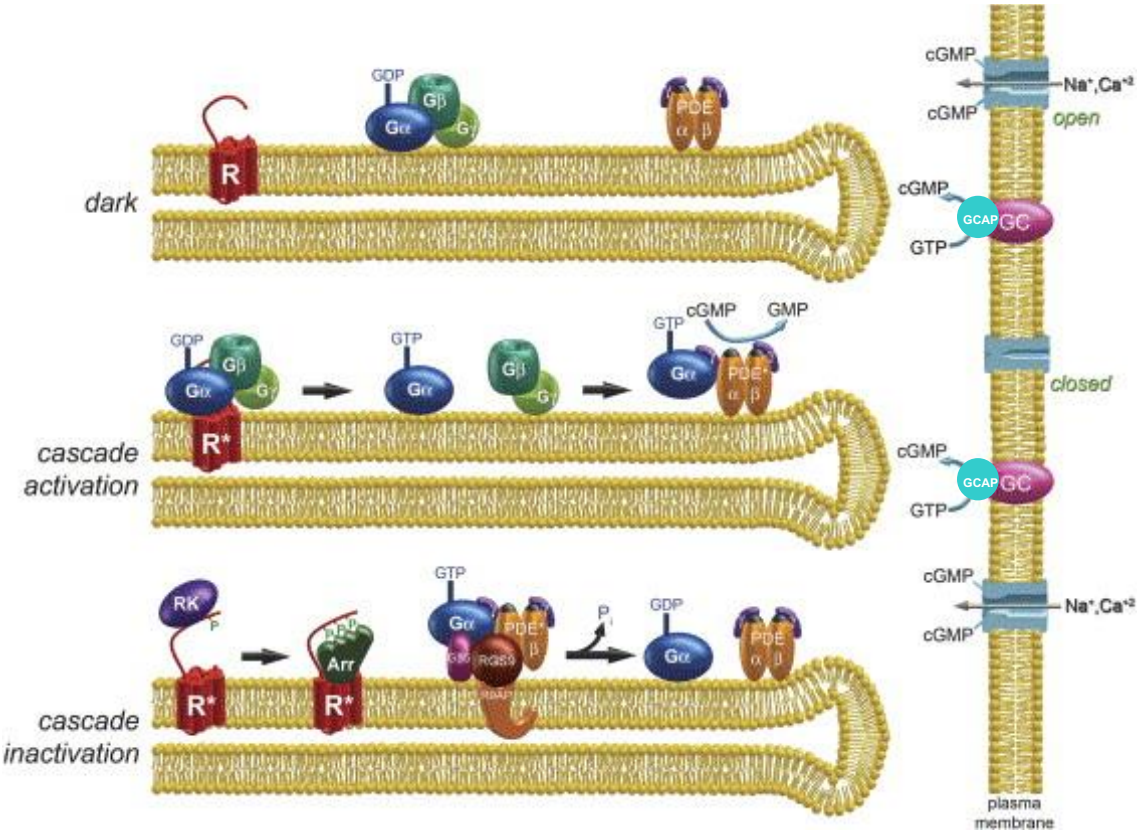

Figure I.4. ***Activation and deactivation of the phototransduction cascade***. *In darkness, rhodopsin (R), transducin (G_α, Gβ and Gγ subunits), and PDE (α, β and γ subunits) are in their inactive form, as represented in the upper disc membrane. Light causes the photoactivation of rhodopsin, leading to the dissociation of GTP-bound transducin alpha (G_α) from the Gβ and Gγ subunits. G_α-GTP in turn activates cGMP-PDE by forming the so-called "effector complex", as illustrated in the middle disc membrane. Once the photoreceptor cell has responded to light, when the light ceases every protein that has acquired an active state must be deactivated in order to restore the darkness equilibrium. Deactivation reactions are illustrated in the lower disc membrane: R* is inactivated through phosphorylation by rhodopsin kinase (RK) followed by arrestin (Arr) binding; the effector (transducin/PDE) inactivation is mediated by a GAP- complex: the RGS9-1–Gβ5–R9AP, that catalyzes the intrinsic GTPase activity of G_α. Also required to restore the darkness equilibrium is the reinstatement of cGMP to the dark levels by new synthesis. The Guanylate cyclase/GCAP complex (RetGC/GCAP) are responsible for de novo cGMP synthesis in photoreceptor cells, here illustrated at the plasma membrane. Modified from (Burns and Arshavsky 2005)*

1.2.2. Mechanisms of light adaptation

As the intensity of light in the surface of the planet varies over ten orders of magnitude, photoreceptors respond constinuously to changes in background light intensity. As mentioned before, rods cover the low range (*scotopic vision*). They are extraordinarily sensitive to light, with a threshold of one photon every 85 minutes, and saturate at relatively low intensities; whereas cones are less sensitive to light but can operate over a broader range of light intensities. Cones carry out daylight response to light (*photopic vision*), but they are not as sensitive as rods. Cones have better temporal resolution than rods and are responsible for color vision (Rodieck 1998).

In order to prevent saturation, and be able to respond to light in the natural world at highly varying ambient light intensities, photoreceptors adjust their sensitivity depending on the background light intensity. This sensitivity adjustment is mediated by a Ca^{2+} negative feedback to the transduction cascade that serves to counteract the effect of light. As light leads to cGMP- channel closure, the Ca^{2+} influx is reduced, while Ca^{2+} extrussion continues through the Na^{+}/Ca^{2+} exchanger. Therefore there is a decrease in the $[Ca^{2+}]$ during the light response. This drop in Ca^{2+} is sensed at different steps in the phototransduction cascade: it serves to release recoverin from its interaction with GRK1, therefore accelerating rhodopsin phosphorylation and inactivation. It serves to increase the affinity for cGMP of the cGMP-gated channels, through the action of CaM, and most importantly it serves to cause the transition of the GCAP proteins from their inhibitory to their activator state of the RetGCs, therefore accelerating cGMP synthesis (Pugh *et al.* 1999) (Fain *et al.* 2001) (Burns *et al.* 2002).

The synthesis of cGMP contributes to the opening of cGMP-channels, therefore serving to restore a fraction of the dark current even in the presence of a background light, so that makes it possible to respond to an overimposed light stimulus. This process of adjusting light sensitivity to the intensity of the ambient light is known as light adaptation (Pugh *et al.* 1999).

1.3. THE GUANYLATE CYCLASE ACTIVATING PROTEINS, GCAPS

1.3.1. GCAPs are Neuronal Calcium Sensor proteins

Guanylate cyclase activating proteins (GCAPs) belong to the neuronal calcium sensor (NCS) family. NCS proteins transduce Ca^{2+} signals into different changes in neuronal function (Koch 2012). Ca^{2+} changes in neurons can vary greatly in magnitude, space and time. Neuronal calcium sensor proteins selectively respond to defined Ca^{2+} signals due to variations in their on-rate kinetics, Ca^{2+}-affinities and localization (Burgoyne and Haynes 2012).

The NCS protein family is encoded by 14 genes in the human genome (http://www.liv.ac.uk/physioogy/ncs/index.html) that carry out distinct non-redundant roles. (McCue *et al.* 2010). NCS proteins are about 22 kDa proteins, with 30-70 percent protein sequence identity to each other. They are high-affinity Ca^{2+}-binding proteins that

act as Ca^{2+} sensors rather than Ca^{2+} buffers. The NCS proteins possess four EF-hands, a helix-loop-helix motif, of which only two or three bind Ca^{2+} (Haynes and Burgoyne 2010).

Subgroup	First appearance in evolution	Mammalian protein	Expressed human splice variants	Proposed functions
A	Yeast	NCS-1	1	Regulation of neurotransmission, stimulation of constitutive and regulated exocytosis, learning, short-term synaptic plasticity, Ca^{2+} channel and Kv4 channel regulation, phosphoinositide metabolism, dopamine D2 receptor endocytosis, GDNF signalling, neuronal growth and survival
B	Nematodes	Hippocalcin	1	Anti-apoptotic, AMPA receptor recycling in LTD, MAPK signalling, learning
		Neurocalcin-δ	1	GC activation
		VILIP1	1	GC activation and recycling, traffic of nicotinic receptors, increase of cAMP levels and secretion
		VILIP2	1	Regulation of P/Q-type Ca^{2+} channels
		VILIP3	1	Unknown
C	Fish	Recoverin	1	Light adaptation by inhibition of rhodopsin kinase
D	Fish	GCAP1	1	Regulation of retGCs
		GCAP2	1	Regulation of retGCs
		GCAP3	1	Regulation of retGCs
E	Insects	KchIP1	3	Regulation of Kv4 and Kv 1.5 channels, repression of transcription
		KchIP2	5	Regulation of Kv4 and Kv 1.5 channels, repression of transcription
		KchIP3	2	Regulation of Kv4 channels, presenilin processing, APP processing, repression of transcription, pro-apoptotic, regulates ER Ca^{2+}
		KchIP4	6	Regulation of Kv4, presenilin processing, channels, repression of transcription

Table I.1. ***Neuronal Calcium Sensor proteins and their proposed functions in mammalian systems. F****rom (Burgoyne 2007).*

Specifically, the N-terminal EF-hand does not bind Ca^{2+} in all family members. Many members of the family are N-terminally myristoylated. In many cases, this modification

facilitates the protein association to membranes, thereby facilitating the regulation of its target (Ames and Lim 2012).

Five different NCS classes have been characterized in higher organisms: class A encompasses NCS-1; class B, visinin-like proteins (VSNLs); class C, recoverin; class D, GCAPs and class E, K+ channel-interacting proteins (KChIPs) (Table I.1) (Burgoyne 2007) .

Depending on sequence variations in their EF domains, N- and C-terminal regions and protein structure, each type differ among the others in its Ca^{2+}-affinity. Nevertheless, they all show cooperation in calcium binding *in vitro*, responding to subtle oscillations in intracellular Ca^{2+}. Consequently, NCS proteins undergo conformational changes upon Ca^{2+} binding, thus regulating their targets. (Burgoyne *et al.* 2004)

1.3.2. Historical perspective: purification, cloning and biochemical characterization of GCAPs

By the late 70s it was known that illumination of bovine rod outer segment membrane preparations or amphibian intact photoreceptors led to changes in cGMP and Ca^{2+} (Papermaster *et al.* 1978). These two molecules were the prime candidates to carry the message from the photon absorption by the visual pigment at the disc membrane to the ion channels at the plasma membrane of photoreceptor outer segments. It was in the mid-eighties, with the identification, purification and functional reconstitution of the cyclic GMP-dependent channel from rod photoreceptors, that cGMP was established as the second messenger of phototransduction (Fesenko *et al.* 1985). It was clear that light, by causing the photoisomerization of the chromophore in rhodopsin, initiated an enzymatic amplification cascade that culminated with the hydrolysis of cGMP. This drop of cGMP caused the closure of a fraction of cGMP-gated channels at the plasma membrane, reducing the inward current of Na^+ and Ca^{2+} and leading to the hyperpolarization of the cell. Once cGMP was established as the second messenger for light transduction, numerous studies followed to show that Ca^{2+} ions played an important role at promoting the recovery of the light response and mediating light adaptation, that is, adjusting photoreceptor sensitivity to the level of background illumination.

Since cGMP levels drop during the light response, recovery of the dark state once the light is dimmed or extinguished requires that cGMP levels are restored through new synthesis. cGMP is synthesized by the retinal guanylate cyclase (RetGCs) enzyme, an integral membrane protein.

RetGCs are transmembrane proteins located in the disc membranes of photoreceptor cells that are active as dimers. An extracellular domain lies within the lumen of the disc membranes, but unlike homologous GCs in other tissues that are activated by ligand binding to the extracellular domain; no ligand has been identified for RetGC1 and RetGC2 (Dizhoor 2000). In fact, they can be activated even when the extracellular domain, or the transmembrane domain, have been truncated (Laura *et al.* 1996). Instead, retGCs are regulated by GCAPs, as it was discovered in the late eighties (Dizhoor 2000).

In 1988, a seminal paper in Nature by Karl-Wilhelm Koch and Lubert Stryer showed that cGMP synthesis in bovine rod outer segment membranes (bovROS) was steeply dependent on Ca^{2+}, in the physiological range of intracellular Ca^{2+} concentrations (Koch and Stryer 1988). The rate of cGMP synthesis increased 5 to 20-fold when [Ca^{2+}] was changed from 1μM to 10nM. This Ca^{2+} regulation of RetGC activity was not direct, but mediated by a soluble factor. Ca^{2+}-regulation was lost when membranes were washed with a hypotonic solution, and restored when the washed fraction (containing the proteins stripped from the membrane) was restored to membranes. This pioneering study predicted the existence of a soluble Ca^{2+}-binding protein in photoreceptor cells that would activate RetGC upon sensing the drop in Ca^{2+} that happens in response to light. That is, this protein would maximally activate RetGC upon losing Ca^{2+}, therefore working in the opposite direction from CaM regulation of its targets, and it would do so with high Ca^{2+} cooperativity (Koch and Stryer 1988).

In 1994, two independent groups at the University of Washington, Seattle, were able to purify the Ca^{2+}-binding proteins responsible for RetGC regulation from the soluble fraction of bovine rod outer segments. They did so by subjecting the low salt-wash fraction of bovROS to a series of chromatographic steps, and identifying the fraction that retained GC stimulating activity. Two related but not identical proteins were purified, of 21 and 24 kDa, that were termed guanylate cyclase activating protein 1 (Subbaraya *et al.* 1994) (Gorczyca *et al.* 1995) and guanylate cyclase activating protein 2 (Dizhoor *et al.* 1994) (Dizhoor *et al.* 1995), that were shown to decrease the sensitivity, time-to-peak and recovery time of the light response following their introduction into intact photoreceptor cells.

The subsequent molecular cloning of GCAPs from different species revealed that these ~200 aminoacidic proteins presented strong sequence conservation at four EF-hand motifs, out of which only EF-2 to EF-4 bind Ca^{2+}, and revealed its relation to Ca^{2+}-binding proteins of the NCS superfamily (Figure I.5). In GCAPs, the N-terminal EF-1 domain does not bind Ca^{2+}, and is instead involved in RetGC1 recognition (Gorczyca *et*

al. 1995) (Ermilov *et al.* 2001). GCAP1 and GCAP2 show overall 40% identity and they are both myristoylated at the NH_2 terminus.

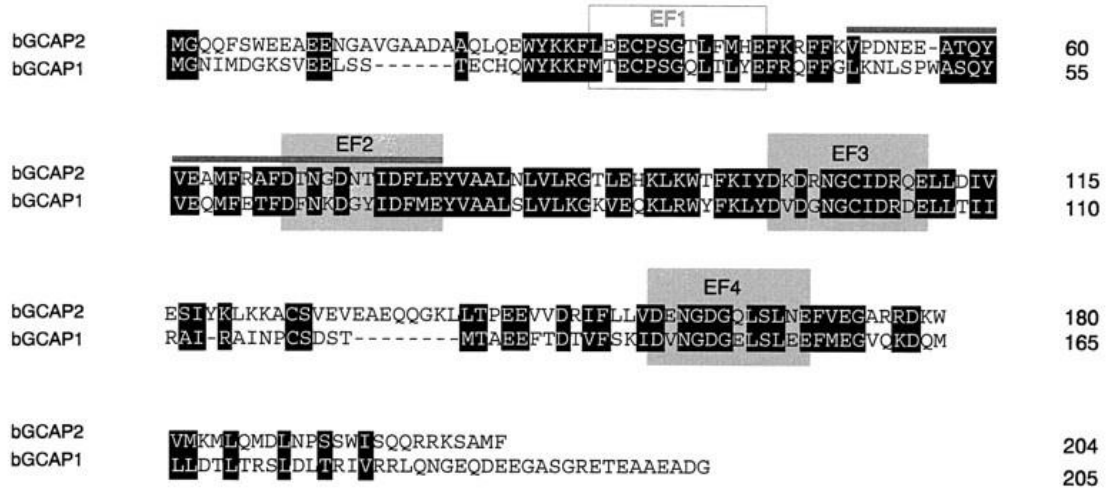

Figure I.5. ***Aminoacid sequence alignment of bovine GCAP2 and GCAP1.*** *For optimal alignment of the two proteins, several gaps (hyphens) were introduced. Predicted calcium binding domains are shaded in gray, while amino acids on black background represent identity or conservative replacement (L = I = V = M; Y = F; K = R; S = T = A). From (Gorczyca 1995)*

Because GCAPs associate to membranes independently of the $[Ca^{2+}]_{free}$, GCAPs are thought to form a stable complex with RetGC independent of the $[Ca^{2+}]_{free}$ (Peshenko *et al.* 2008). These complexes may switch between two conformations, active and inactive, with the binding and dissociation of Ca^{2+}. GCAPs activate the cyclase at free Ca^{2+} concentrations below 100nM characteristic of light adapted rods, and inhibit the cyclase at free Ca^{2+} concentrations above 500nM characteristic of the dark-adapted photoreceptors. In contrast to other known EF-hand proteins which regulate their effectors in their Ca^{2+}-loaded form, GCAPs activate RetGC in their Ca^{2+}-free (Mg^{2+}-bound) form, and inhibit RetGC in their Ca^{2+}-loaded form (Peshenko and Dizhoor 2004) (Peshenko *et al.* 2004a) (Peshenko and Dizhoor 2006)

To study the mechanism of Ca^{2+}-sensitive modulation of RetGC, the role of individual EF-hands of GCAP1 and GCAP2 in RetGC inactivation was analyzed by mutagenesis. Individual EF-hands of GCAP1 and GCAP2 play similar but not identical roles. Disabling mutations in EF-3 and EF-4 domains of GCAP1 impair GCAP1 convertion from activator to inhibitor of RetGC, with the mutants retaining partial constitutive activity. Therefore, EF-3 and EF-4 hand-motifs are the most critical domains for Ca^{2+}-sensitive inactivation in GCAP1, while EF-2 contributes little to Ca^{2+}-sensitive GCAP1 inactivation (Rudnicka-

Nawrot *et al.* 1998) (Sokal *et al.* 1999) (Peshenko and Dizhoor 2007). In contrast, all three EF-hands of GCAP2 contribute to the inhibitory effect of Ca^{2+} (Dizhoor and Hurley 1996) (Ames *et al.* 1999). GCAP1 and GCAP2 are thought to interact with RetGC at the same or at a partially overlapping binding site, based on the fact that both GCAP1 and GCAP2 in their Ca^{2+}-loaded forms can compete the constitutive activity of the GCAP1 mutant with disabled EF-hands (Peshenko *et al.* 2008).

Another property of GCAPs relevant to understand their mode of action is that both GCAP1 and GCAP2 can form dimers upon Ca^{2+} dissociation (Olshevskaya *et al.* 1999b). It has been shown that the capacity to dimerize in GCAP2 correlates with the ability to activate RetGC. That is, GCAP2 has to form a dimer to be active. A subtle difference is that while in GCAP2 dimerization is reversed by Ca^{2+} binding, GCAP1 dimerization is resistant to the presence of Ca^{2+} (Olshevskaya *et al.* 1999b). This implies that Ca^{2+} triggers different conformational changes in GCAP1 and GCAP2 in the RetGC-GCAP complexes.

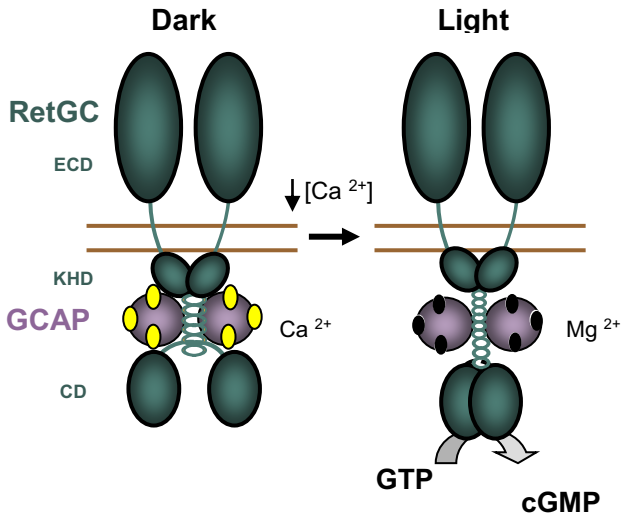

Figure I.6. ***Model of retGC regulation by GCAPs.*** *RetGCs are active as dimers (Yu et al. 1999). GCAPs are presumed to be permanently bound to RetGC, regulating its catalytic activity as they bind or release Ca^{2+}. The Ca^{2+}-loaded form of the GCAP proteins, typical of the high Ca^{2+} levels in the dark-adapted state, (left), inhibit the catalytic activity of RetGC. The Ca^{2+}-free form of GCAPs that would emerge as a result of light exposure as Ca^{2+} drops (Ca^{2+}-free, Mg^{2+}-loaded GCAP form, right) robustly stimulate RetGC activity by promoting the dimerization of retGC catalytic domains (CD). KHD (kinase homology domain), ECD (extracellular domain).*

Taken together, these biochemical results point to a RetGC model of regulation by GCAPs in which GCAPs are permanently bound to RetGCs, and oscillate between an activator and an inhibitor state depending on the $[Ca^{2+}]_{free}$ (Figure I.6).

GCAP1

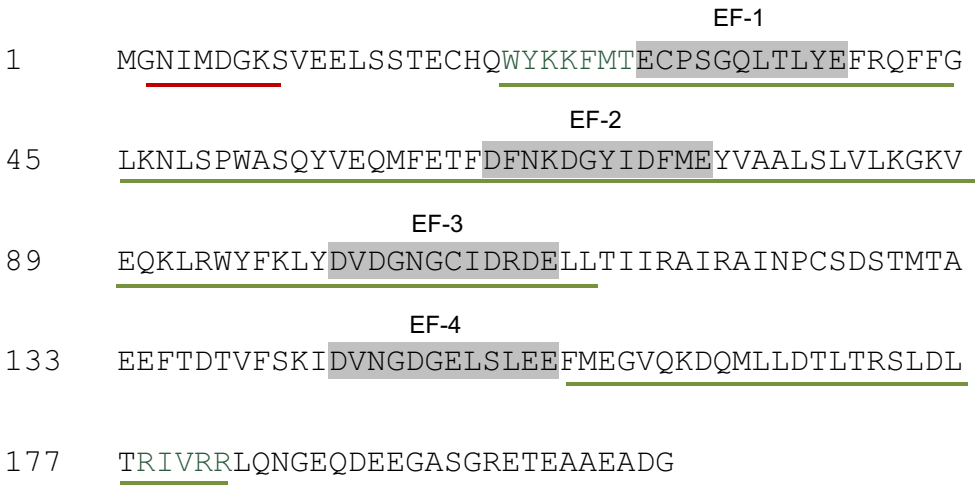

GCAP2

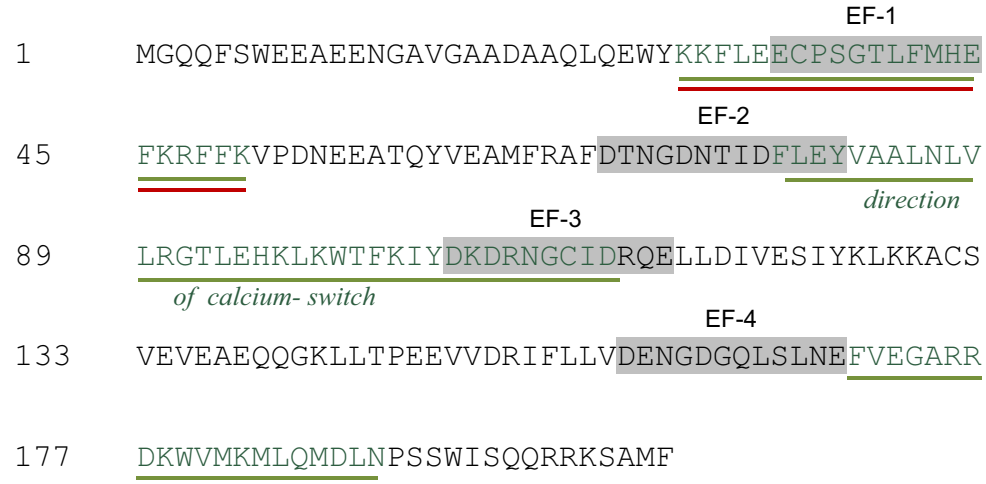

Figure I.7. ***Map of functional domains in GCAP1 and GCAP2.*** *Regions necessary for RetGC activation are underlined in green, with essential sequences in green font. Regions necessary for RetGC inhibition underlined in red. The interdomain region between EF-2 and EF-3 determines the direction of the calcium switch in GCAP2.*

Several biochemical studies then addressed the mapping of functional domains in GCAP1 and GCAP2 involved in activation or inhibition of RetGC by analysis of deletion mutants and chimeric proteins in which different regions of the GCAP proteins were substituted by the corresponding regions of recoverin or neurocalcin (Olshevskaya *et al.* 1999a) (Krylov *et al.* 1999).

It was determined that several regions of the GCAP molecules are required for RetGC activation (Figure I.7): a) a region whithin the N-terminal region starting at Trp21 (numbering corresponding to GCAP1) that comprises a 5 to 7 amino acid stretch preceding EF-1, the EF-1 domain -non-functional at Ca^{2+} coordination- and some additional amino acids; b) the region between EF-hands 2 and 3, representing the "interdomain" or "hinge" region between the NH_2- and COOH- terminal globular domains in the structure of GCAPs, is required for activation and determines the direction of the Ca^{2+}-switch in GCAP2; and c) a stretch of about 20 amino acids starting at Phe156 immediately adjacent to EF-4 within the COOH-terminal domain (Olshevskaya *et al.* 1999a) (Krylov *et al.* 1999).

Whithin these domains, the stretches of amino acids Trp21-Thr27 preceding EF-1 in the NH_2-terminal region, and Thr177-Arg182 within the COOH-terminal region in GCAP1 (Krylov *et al.* 1999), and the corresponding regions in GCAP2, appear to be critical for RetGC activation (Olshevskaya *et al.* 1999a). Therefore, a picture is emerging in which the signal in the GCAP proteins involved in RetGC recognition is discontinuous, involving the NH2- and COOH-terminal regions.

In contrast, inhibition of RetGC requires the first 9 aa of GCAP1 (Krylov *et al.* 1999), and the EF-1 domain in GCAP2 (Olshevskaya *et al.* 1999a).

1.3.3. GCAPs regulation of RetGCs: the calcium relay model

Two to eight different GCAP isoforms have been identified in species from fish to human, for example, GCAP3 is specifically found in human and zebrafish retinas (Imanishi *et al.* 2002). Surprisingly it is in fishes where we see more variety, probably arising from gene duplications: in zebrafish there are 6 isoforms (GCAP1–5, GCAP7) and 8 in pufferfish and carp (GCAP4-8). In frogs, we find a GCAPs homolog, Guanylate Cyclase Inhibiting Protein (GCIP) (Imanishi *et al.* 2004). GCAP1 and GCAP2 are the major isoforms in higher mammals. When two different isoforms of a protein are expressed in the human retina, the first question to address is whether one isoform might be specific for rods and the other for cones. However, in the case of GCAP1 and GCAP2 it was established that they are both expressed in rod and cone cell types (see *GCAPs localization* for details). This apparently redundant expression of GCAP1 and GCAP2 was initially puzzling, since they exhibited very similar biochemical properties. However, when mice became available that lacked either GCAP1 or GCAP2, their electrophysiological recordings indicated that these neuronal calcium sensors had

somewhat different roles in shaping the light response of a rod cell. GCAP1 was responsible for the initial rapid recovery phase, while GCAP2 was responsible for the slower recovery to the baseline [(Mendez and Chen 2002) (Howes *et al.* 2002) (Pennesi *et al.* 2003), see *GCAP physiological functions revealed by the study of mouse models* for details]. At about the same time as the initial electrophysiological report, more detailed biochemical studies showed that the Ca^{2+}-sensitivity of the RetGC activation profile of bovine GCAP1 differed from that of GCAP2 (Hwang *et al.* 2003). It was determined that the EC_{50} for Ca^{2+} inhibition of retGC stimulation was higher for GCAP1 than for GCAP2 [Ca^{2+} EC_{50} for GCAP1 ~130nM; for GCAP2 ~50nM], providing a molecular basis for the interpretation of the electrophysiological data (Peshenko *et al.* 2011b).

Light exposure results in up to a 10-fold decline in the intracellular free [Ca^{2+}], from ~250nM in darkness to 23nM in saturating light in mouse rod outer segments. The difference in the EC_{50} values means that this Ca^{2+} decrease is first sensed at GC/GCAP complexes comprising GCAP1 (Ca^{2+} EC_{50} for GCAP1 ~130nM) and successively, when Ca^{2+} has dropped to lower levels, at those comprising GCAP2 [Ca^{2+} EC_{50} for GCAP2 ~50nM], in a sequential mode of action that is today referred to as “the Ca^{2+}-relay model” (Kock and Dell’Orco 2013).

In a physiological context, during the single flash response of a rod cell, the Ca^{2+} concentration drops from its dark value to below 100nM. Within the first 50ms the cytoplasmic Ca^{2+} has dropped but has not reached its final value. During this “intermediate state” the activation of GCAP1 is triggered, causing a first pulse of cGMP synthesis responsible for the characteristic “fast recovery phase” that is absent in mice lacking GCAP1. A further decrease in cytoplasmic Ca^{2+} on a time-scale of 0.5-1s triggers the dissociation of Ca^{2+} from GCAP2 causing its conformational change to the activator state and stimulating the cGMP synthesis that restores the rod sensitivity to its baseline (Kock and Dell’Orco 2013).

That is, the regulation of retGC by GCAPs is a two-step process in which GCAP1 mediates the first-response as $[Ca^{2+}]_i$ starts to fall with illumination, whereas GCAP2 provides additional retGC stimulation of cGMP synthesis only after $[Ca^{2+}]_i$ drops substantially (e.g. in brighter light). Altogether, the rate of cGMP synthesis upon light exposure is stimulated up to ~12-fold over its basal levels, serving to restore the cGMP levels and to reopen the channels during the recovery of the light response and light adaptation (Peshenko *et al.* 2012b).

This Ca^{2+} relay mode of operation of GCAPs makes the cell highly responsive to changes in intracellular calcium along the wide range of physiological Ca^{2+} concentrations.

1.3.4. GCAPs structure

To complement the biochemical characterization of GCAPs, structural studies have aimed in recent years at elucidating the Ca^{2+}-induced conformational changes in GCAP1 that control activation of RetGC by pursuing the atomic resolution structures of GCAP1 in both the Ca^{2+}-bound (inhibitor) and Mg^{2+}-bound (activator) states. The structure of the Mg^{2+}-bound activator state of GCAP1 has been elusive so far, due to this form of the protein being highly unstable and difficult to maintain in solution. Neither the crystal structure nor the nuclear magnetic resonance (NMR) structure of the activator state of

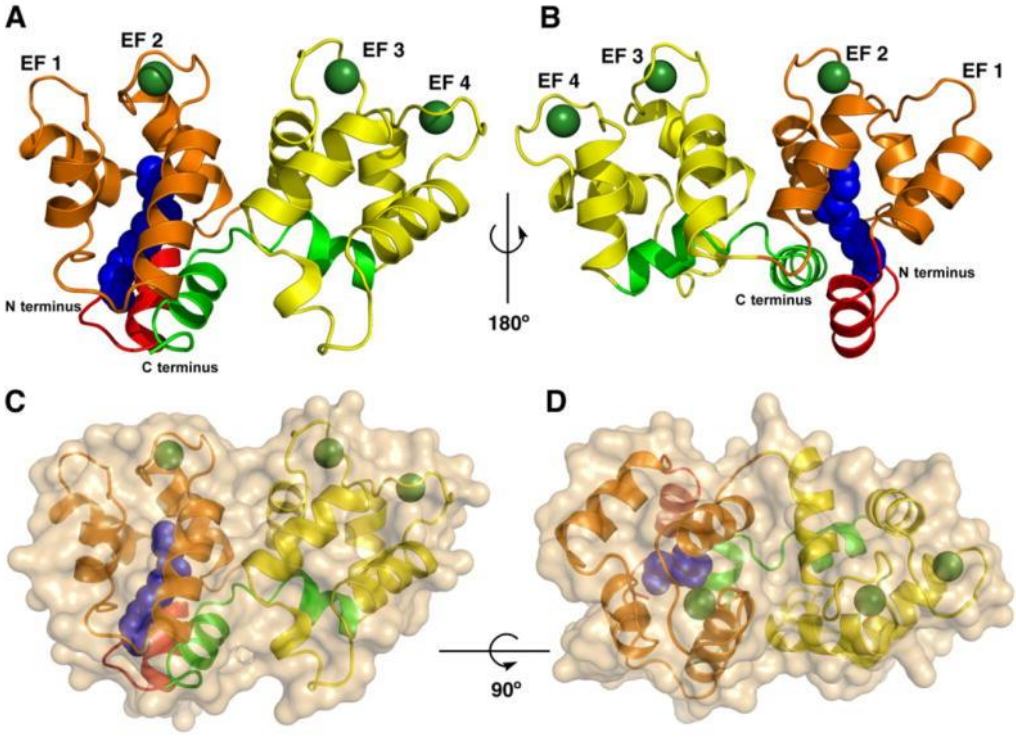

Figure I.8. ***Crystal structure of myrGCAP1 in its Ca^{2+} bound (inhibitor) state. A*** *and* ***B*** *represent the front and back view, respectively, of myrGCAP1. N-terminal helix is coloured in red and C-terminal helix is coloured in green. The N-terminal globular domain, which encompasses EF-1 and EF-2 is orange, while the C-terminal domain, containing EF-3 and EF-4, is yellow. Ca^{2+} ions are shown as dark green spheres and the myristoyl group is represented by dark blue space-filling spheres.* ***C*** *and* ***D*** *are surface representations of front and top views of myrGCAP1, respectively. Semitransparent surface reveal the cartoon representation (already described for A and B) and the buried myristoyl group.See text for details. From (Stephen et al. 2007)*

GCAP1 could be determined so far. Only the structure of the Ca^{2+}-bound (inhibitor) state of GCAP1 has been obtained. The crystal structure of myristoylated GCAP1 in its Ca^{2+}-bound form has been resolved at a 2.0 Å resolution (Stephen *et al.* 2007).

In this crystal structure, the four EF-hand motifs are arranged in two domains in Ca^{2+}-bound myrGCAP1. EF-1 (residues 17-42) and EF-2 (residues 50-82) form the N-terminal domain, whereas EF-3 (residues 87-118) and EF-4 (residues 130-160) form the C-terminal domain. A short loop between EF-2 and EF-3 links these domains together (Stephen *et al.* 2007).

The overall structure of myrGCAP1 is quite compact. In contrast to Ca^{2+}-bound recoverin, the myristoyl group in Ca^{2+}-bound GCAP1 (blue in Figure I.8) is completely buried in the core of the N-terminal domain. The binding pocket for the myristoyl group in Ca^{2+}-bound GCAP1 is formed by hydrophobic side chains contributed from residues from EF-1 (W20, F38, and F42), EF-2 (V55, M58, F62, Y75, L79 and V82), the N-terminal helix (M4, V9 and L12) and the C-terminal portion of the kinked C-terminal helix (L174, I177, V178 and I181). The link between the N- and C- terminal domains is strengthened by an interaction between the N- and C-terminal helices. The C-terminal helix (green in Figure I.8) is partially unraveled and sharply kinked and it interacts in an antiparallel orientation with the N-terminal helix (red in Figure I.8) tying the two domains together (Stephen *et al.* 2007) (Lim *et al.* 2009). *Note: see Appendix for amino acid code and properties table.*

The packing of the myristoyl group in Ca^{2+}-bound GCAP1 is opposite to what is observed for the acyl group in the Ca^{2+}-bound recoverin. This is also attributable to Ca^{2+}-bound GCAP2 (Hughes *et al.* 1998) (Ames *et al.* 1999). In myr-recoverin the acyl group is completely exposed in the Ca^{2+}-bound state, and it is the transition to its Ca^{2+}-free conformation that is accompanied by sequestration of the acyl group in its N-terminal domain, in the so-called “calcium-myristoyl switch”. That way recoverin is soluble in the Ca^{2+}-free state (myristoyl group buried) and is recruited to the membrane in the Ca^{2+}-bound state, where it regulates its target. In GCAP1, an analysis of the solvent exposure of the acyl group has determined that the myristoyl group is buried in the molecule both in the Ca^{2+}-bound and in the Ca^{2+}-free states. There is no “calcium-myristoyl switch” regulating the membrane association of GCAP1. Amino-terminal myristoylation of GCAP1 is required for full activity at physiological concentrations of Ca^{2+} (Otto-Bruc *et al.* 1997) (Hwang and Koch 2002) (Peshenko *et al.* 2012a). The GCAP1 structure shows that the myristoyl group is a central feature in the hydrophobic core of the N-terminal domain, that by contacting the kinked C-terminal domain it helps

to stabilize the bridge between N- terminal residues and the C-terminal residues 175-183, previously identified as crucial for GCAP1 activity (Figure I.8 –important domains involved in RetGc activation) (Stephen *et al.* 2007) (Lim *et al.* 2009). Therefore, the myristoyl group in GCAP1 is crucial to provide structural stability and to tune GCAP1/Ret-GC complex affinity and activation (Peshenko *et al.* 2012b). Instead, myristoylation of GCAP2 affects its overall structural stability without affecting RetGC regulation (Hwang and Koch 2002) (Olshevskaya *et al.* 2007) (Schröder *et al.* 2011).

Overall, the crystal structure of GCAP1 points to the clustering of the N- and C-terminal helices and the myristoyl group as responsible for GCAP1 inhibition of photoreceptor RetGC at high concentrations of Ca^{2+}. It also suggests that a transition to the Ca^{2+}-free state of GCAP1 might pull these two helices apart, yielding the conformation responsible for RetGC activation at low Ca^{2+} concentrations (Stephen *et al.* 2007).

This prediction based on the crystal structure could be somewhat confirmed with the recent determination of the NMR structure of a functional mimic of GCAP1 in the Ca^{2+}-free/Mg^{2+} bound activator state (the D144/D148G mutant or EF4 mutant). As mentioned above, the Ca^{2+}-free/Mg^{2+} bound GCAP1 protein is unstable and tends to aggregate under NMR conditions, but a mutant with the EF-4 hand inactivated that is constitutively active in reconstituted assays turned out to be more stable under NMR conditions. A comparison of NMR chemical shifts for the inhibitor and activator states of GCAP1 revealed that residues at the GCAP1 domain interface (exiting helix of EF2 and entering helix of EF3) have broad NMR resonances indicating they are conformationally dynamic, and pointing to a Ca^{2+}-induced domain swiveling (that would separate N- and C-terminal helices apart) taking place, albeit to a much lesser extent than the reported for recoverin. Single mutations in some residues of the domain interface (V77, A78, L82, W94) abolish or dramatically decrease cyclase activity, emphasizing the importance of the swiveling between domains (Lim *et al.* 2013).

These results are also in line with earlier biochemical studies of the Ca^{2+}-induced conformational changes in GCAP2, that showed that the Ca^{2+}-free form of GCAP2 or its functional mimic EF^{-}GCAP2 present a more exposed C-terminal helix as revealed by the exposure of the C-terminus to a protein kinase that phosphorylates GCAP2 at Ser201, and to limited proteolysis. The physiological significance of Ser201 phosphorylation is not known yet (Peshenko *et al.* 2004b).

Biochemical analysis of Ca^{2+}-induced conformational changes in GCAP1 had also revealed that at high $[Ca^{2+}]_{free}$ the central portion of the protein was protected from

proteolysis, while at low $[Ca^{2+}]_{free}$ the central portion of the protein was more vulnerable to proteolysis.

Taken together, structural analysis of GCAP1 and GCAP2 point to a more compact and stable structure of these proteins in their Ca^{2+}-bound (inhibitor) form, and a more open structure in which the N- and C-terminal helixes pull apart in the Mg^{2+}-bound (active) form. The myristoyl group would be buried in the N-terminal domain in both states, contributing to the thermal stability of the protein (Orban *et al.* 2013).

1.3.5. GCAPs localization in rods and cones

GCAP1 and GCAP2 are present at different levels in the retina. In bovine retinas, the GCAP1: GCAP2 ratio is estimated to be between 3:1 and 4:1. Furthermore, initial localization studies of GCAP1 and GCAP2 in different species showed that both isoforms are present at the rod outer segment compartment of rods and cones, where phototransduction takes place, albeit at apparently different levels. Although the localization of GCAP1 and GCAP2 might differ in different species, there is the consensus that GCAP1 is more abundant at cone outer segments than at rod outer segments in higher mammals, whereas GCAP2 localizes primarily to rods and at lower levels in cones (Howes *et al.* 1998) (Cuenca *et al.* 1998) (Kachi *et al.* 1998).

Besides localizing to rod outer segments, GCAPs are also present at proximal compartments of the cell. GCAP1 is present (to a lesser extent than at rod outer segments) at the inner segment and synaptic terminals of cones and rods, where its function is unknown (Howes *et al.* 1998). GCAP2 localization in rods is not restricted to rod outer segments either. GCAP2 is present at rod inner segments at the same or higher levels, and at lower levels in more proximal compartments of the cell like the synaptic terminal. However, because the range of $[Ca^{2+}]_i$ at synaptic terminals is considerably higher than that at rod outer segments, a function of GCAPs in stimulation of cGMP synthesis was deemed unlikely. The role of GCAPs at the synaptic terminal is currently unknown. Therefore our interest in pursuing the identification of new GCAP protein interactors, in order to identify new GCAPs molecular targets at this compartment.

The mechanisms that determine GCAPs subcellular distribution are largely unknown, but it has been reported that GCAPs localization to the rod outer segments (where phototransduction takes place) requires RetGC1 and RetGC2 expression (two RetGCs are expressed in retinal photoreceptors) (Karan *et al.* 2010). GCAP1 preferentially

activates RetGC1 *in vivo*, while GCAP2 seems to bind to the two retGCs identified in mammalian rod and cone cells. RetGC2 is expressed at a lower molar ratio, although this ratio differs among species. RetGC1:RetGC2 ratio in bovine ROS is 25:1, while in murine ROS is 4:1 (Helten *et al.* 2007). In the double knockout mice in RetGC1 and RetGC2, both GCAP1 and GCAP2 appear to be excluded from the outer segment and accumulate at the inner segment. Mutations in RetGC1 (GUCY2D) are associated with one of the most severe forms of inherited blindness that accounts for approximately 5% of all retinal dystrophies: Leber's Congenital Amaurosis type 1 (LCA-1), characterized by extinguished scotopic and photopic ERGs at very early onsets (Jacobson *et al.* 2013). In mice, the RetGC1/RetGC2 double knockout phenotypically resembles human LCA1 with extinguished ERGs and rod/cone degeneration. In these mice, GCAPs fail to be transported to the outer segment and accumulate at the inner segment (Coleman *et al.* 2004) (Baehr *et al.* 2007). This observation suggests that GCAPs are transported to the sensory compartment following their association to Ret-GCs (as GCAP/RetGC complexes) (Baehr *et al.* 2007). It has been proposed that the RetGC proteins may contain ciliary trafficking signals, and could guide a subtype of vesicular transport carriers from the endoplasmic reticulum to the cilium that would carry the peripheral membrane proteins involved in cGMP metabolism (Karan *et al.* 2010).

However, an attempt to map these ciliary targeting sequences in RetGC1 by generating fusion proteins of its C-terminal region or its cytosolic domains with GFP and studying whether they are targeted to rod outer segments in transgenic frogs failed to define a linear targeting signal. These results suggest that either the signal is discontinuous or there are accessory proteins in this RetGC1 guided trafficking to the cilium (Karan *et al.* 2011).

Actually, it was recently found that the protein of 23 kDa responsible for Leber's Congenital Amaurosis type 12 in patients and for a blindness phenotype in a naturally occurring strain of mice called rd3, interacts and colocalizes with RetGC1 (Friedman *et al.* 2006). The absence of the protein RD3 (retinal degeneration 3) in naturally occurring rd3 mice causes a dramatic decrease in RetGC1 and RetGC2 protein levels and their absence at the outer segment compartments of rods and cones (Peshenko *et al.* 2011a). Interestingly, and consistent with the observations in RetGC1/RetGC2 double knock-out mice, RD3 absence also causes a decrease in GCAP protein levels and their exclusion from the outer segments. It was suggested that RD3 has the ability to recruit RetGC1 from the ER to endosomal vesicles, by interacting with a small stretch of amino acids at the RetGC1 COOH-terminal domain, in the cytosolic fragment of the protein (Karan et al 2010) (Azadi *et al.* 2010) (Molday *et al.* 2013). When RD3 binds RetGC,

avoids RetGC/GCAPs activity, independent of Ca^{2+} levels. Therefore RD3 is a RetGC1 binding protein required for the stable expression and membrane vesicle trafficking of RetGCs (and consequently of GCAPs) in photoreceptors (Azadi *et al.* 2010) (Peshenko *et al.* 2011a).

1.3.6. GCAP physiological functions revealed by the study of mouse models

A number of mouse models have been developed to study the role of GCAP proteins *in vivo*. The first mouse model consisted on the abrogation of expression of both genes (GCAP1 and GCAP2), to target the Ca^{2+} feedback to RetGC activity in order to determine its kinetic contribution to termination of the light response and to the process of light adaptation. Because the genes encoding GCAP1 and GCAP2 (GUCA1A and GUCA1B respectively) are organized in a tail-to-tail array (Surguchov *et al.* 1997), suggesting ancient gene duplication and inversion events (see Figure I.9) (Howes *et al.* 1998), individual knock-outs were not pursued in this original study, because the double knockout would have never been obtained by the breeding of individual knockouts. Therefore, a double knockout in GCAP1 and GCAP2 was obtained with a single replacement vector (Mendez *et al.* 2001) (Mendez and Chen 2002) (Figure I.9).

GCAPs-/- mice preserved a mostly normal retinal morphology (Figure I.9 C) The expression levels of other genes involved in cGMP turnover, such as RetGCs and PDE were not affected in these mice, indicating that GCAPs ablation did not lead to noticeable compensatory changes (Figure I.9 B) (Mendez *et al.* 2001) (Mendez and Chen 2002).

Rods from these mice were much more sensitive to light than wildtype rods. Dim flash responses from GCAPs-/- mice rose for a longer time and to a larger peak amplitude than wildtype responses (Burns *et al.* 2002). The mean single photon response amplitude in GCAP1/GCAP2-/- mice was nearly five times larger than that of wildtype rods (Figure I.10). The flash strength required to elicit a half-maximal response, was about 8-fold lower in the GCAPs-/- rods. That is: GCAPs-/- mice gave much larger responses than wildtype mice to the same light stimulus; or, put it in the other way, they required much lower light intensities than wildtype mice to elicit the same response. It was concluded that Ca^{2+} feedback to GC via GCAP1 and GCAP2 potently reduces the flash sensitivity of wildtype dark-adapted rods, and significantly shortens the dark-adapted flash response (Mendez *et al.* 2001) (Mendez and Chen 2002).

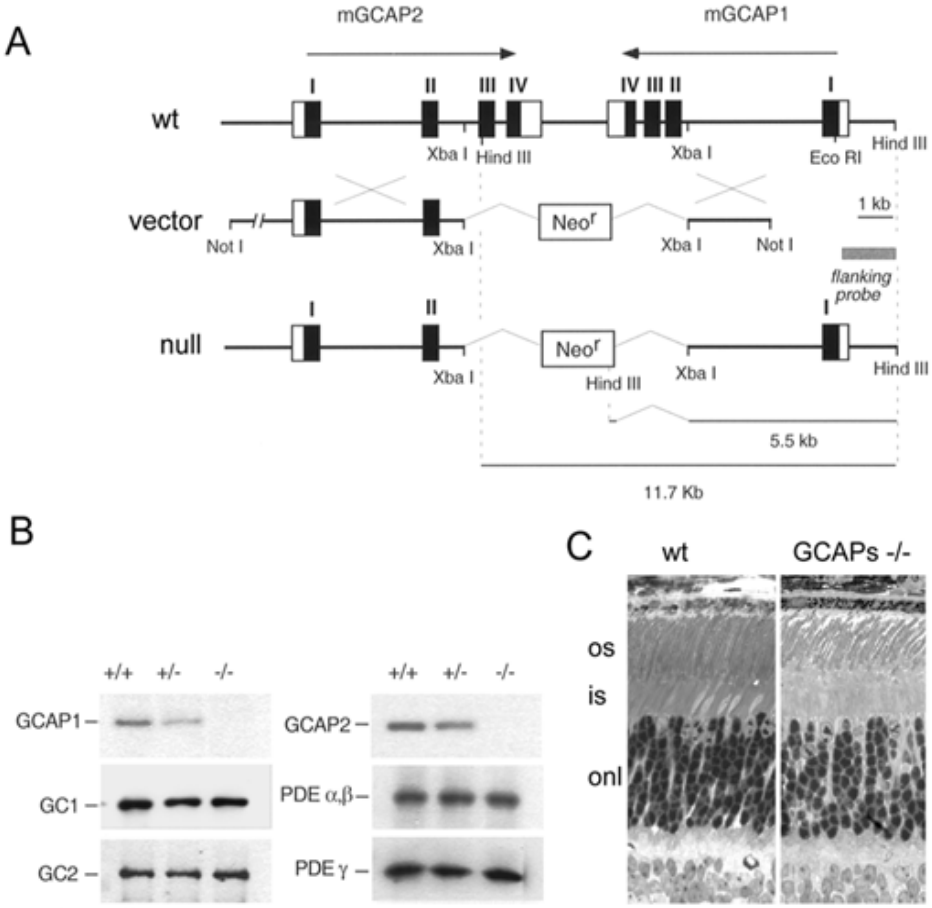

Figure I.9. ***Development of GCAP1 and GCAP2 knockout mice.*** *A. Targeting strategy to replace. 6.3 kb of genomic DNA (GCAP1 exons 2 to 4 and GCAP2 exons 3 to 4) for a neomicyn resistance cassette by homologous recombination. B. Immunoblots analysis of GCAPs +/+, GCAPs +/- and GCAPs -/- retinal homogenates detecting GCAPs, RetGCs, and PDE subunits . C. Light micrographs of GCAPs+/+ (wt) and -/- retinal sections of 3 month-old mice. os, outer segment; is, inner segment; onl, outer nuclear layer. From (Mendez et al. 2001).*

GCAP1 and GCAP2 were then individually restored in the GCAPs-/- background, and although there was some variability in the flash responses due to small variations in transgene expression levels from cell to cell, it was clear that the initial rapid recovery phase observed in wildtype responses was observed when GCAP1 individual expression was restored (Howes *et al.* 2002) (Pennesi *et al.* 2003), but not when GCAP2 individual expression was restored. However, after exposure to saturating light intensities, GCAP2 alone could drive maximal RetGC activity and restore current to its baseline (Mendez and Chen 2002).

These studies were basically confirmed and further expanded more recently with the generation of individual GCAP1 and GCAP2 knockout mice by the group of Alexander

Dizhoor (Makino *et al.* 2008) (Makino *et al.* 2012). In the absence of GCAP1, the initial rapid recovery phase of dark-adapted responses was absent, but given enough time, responses recovered to the baseline due to the action of GCAP2 (Makino *et al.* 2012). In contrast, responses of rods that lacked GCAP2 maintained the initial rapid component of the recovery, but presented abnormally prolonged responses in the sense that restoration of current to the baseline took longer times (Makino *et al.* 2008).

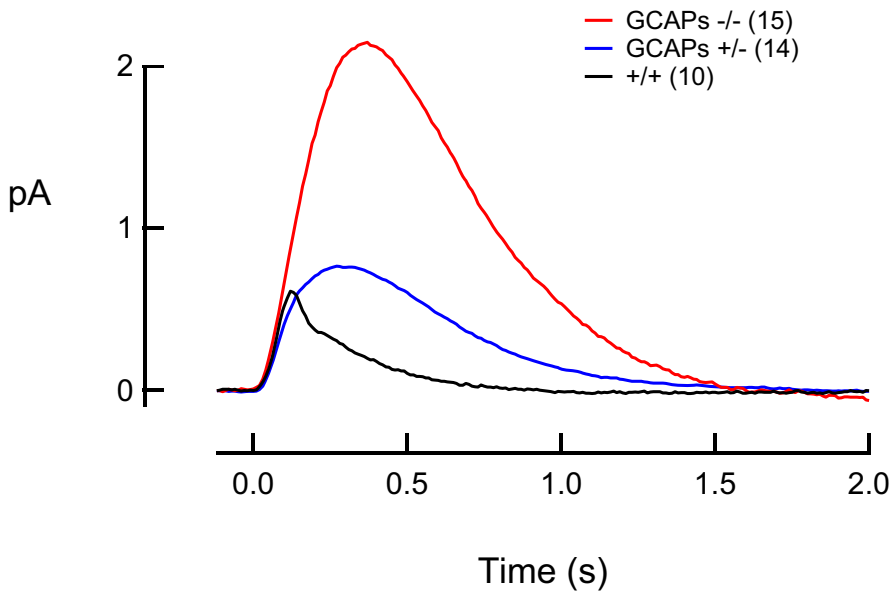

Figure I.10. ***Overimposed single photon responses from GCAPs -/-, GCAPs +/- and GCAPs +/+ mouse rods.*** *From (Mendez et al. 2001)*

These results where the origin of the Ca^{2+}-relay model, a model that was subsequently confirmed by the detailed biochemical characterization of GCAP1 and GCAP2, as outlined in previous sections (Peshenko *et al.* 2011b).

The Ca^{2+}-relay model has been further ratified in the zebrafish model (Scholten and Koch 2011). Zebrafish have three types of cones: double cones (long-wavelength sensitive), long single cones (short-wavelenght sensitive) and short single cones (UV-sensitive) which express six different zGCAP isoforms (1-5 and 7) (Table I.2).

Each zGCAP has a different EC_{50} for Ca^{2+}regulation of RetGC: they have either EC_{50} ~30 nM (zGCAP1, 2 and 3) or around EC_{50} ~400 nM (zGCAP4, 5 and 7) (Table I.2). As shown in the table below, each type of cone has at least a GCAP isoform with a high EC_{50} and at least one GCAP isoform with a low EC50, so that RetGC activation is regulated on a step-by-step basis (Koch 2013).

EC_{50} (nm)	Level of activation (x-fold activation)		
	Double cones	**Long single cones**	**Short single cones**
~30	zGCAP3 +++	zGCAP3 +++	zGCAP1 ++ zGCAP2 ++++ zGCAP3 +++
~400	zGCAP4 ++++ zGCAP5 + zGCAP7 +	zGCAP4 ++++ zGCAP5 + zGCAP7 +	zGCAP4 ++++ zGCAP5 + zGCAP7 +

Table I.2. ***Summary of zGCAP expression in different cone types.*** *Some isoforms of zGCAPs regulate GC with a low IC_{50} value (around 30 nM free $[Ca^{2+}]$) (in red), and others regulate GC with a high IC_{50} around 400 nM $[Ca^{2+}]$ (in blue). Their levels of activation (x-fold) corresponds to >10-fold: ++++; 5–10-fold: +++; 3–5-fold: ++; <3-fold +, in the different cone types: double cones (long-wavelength sensitive), long single cones (short-wavelength sensitive) and short single cones (UV-sensitive). Adapted from (Scholten and Koch 2011).*

1.3.7. Molecular basis of inherited retinal dystrophies: GCAPs mutations and disease.

Inherited retinal dystrophies affect 1 in 4000 individuals worldwide. Mutations may primarily affect rods and lead to retinitis pigmentosa (RP, characterized by night blindness), or may primarily affect cone function and lead to cone-dystrophies, cone-rod dystrophies or macular degeneration (Hamel *et al.* 2006). Mutations that affect essential proteins for both rod and cone function are associated to a severe form of congenital blindness, Lebers Congenital Amaurosis (LCA) (den Hollander *et al.* 2008).

Retinitis pigmentosas are the most prevalent forms of inherited retinal dystrophies, and are genetically and clinically very heterogeneous disorders (Chang *et al.* 2011). Twenty-five genes have been associated to adRP (30-40% of total RP), and forty-three genes linked to arRP (50-60%), whereas three different genes have been associated to X-linked RP (5-15%) (https://sph.uth.edu/Retnet/sum-dis.htm#B-diseases) (Hartong *et al.* 2006). Therefore, more than 70 different genes when mutated lead to RP, and all possible patterns of inheritance are possible. Mutations associated to RP commonly affect rod function first, initially causing the loss of peripheral sight and nyctalopia (night blindness). As the disease progresses with age, once a certain threshold of rod cell death is reached, cones start dying as well (as a result of the loss of rod's support or rod's function), and central vision and visual acuity are affected ultimately leading to total blindness. The rate of progression of the disease may vary considerably depending on the mutation, and it could take years or decades from initial symptons of nyctalopia (in the adolescence or young adulthood), to the loss of central vision (adulthood) (Hartong

et al. 2006). These diseases may also manifest incomplete penetrability, with variable clinical manifestations between affected members of the same family, indicating the existence of modifier genes (Hartong *et al.* 2006) (Chang *et al.* 2011).

A sample of genes that have been associated to RP follows (Figure I.11).

Autosomal-recessive RP, 50-60% of cases

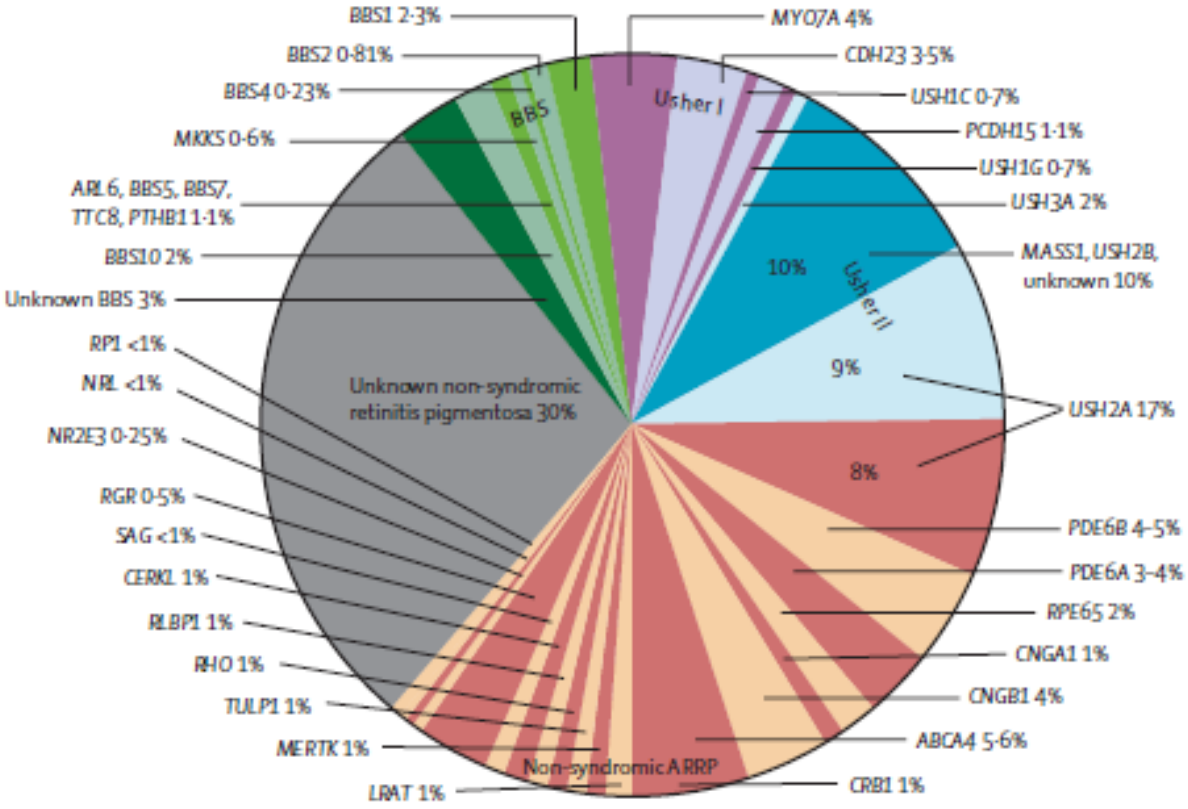

Autosomal-dominant RP, 30-40% of cases

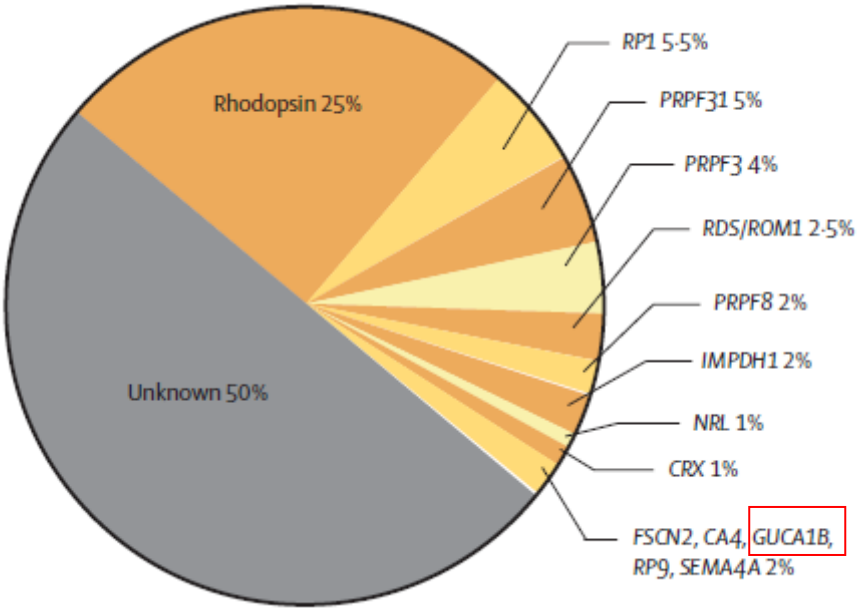

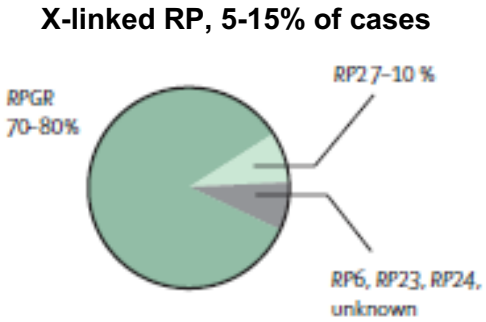

Figure I.11. ***Prevalence of gene mutations contributing to autosomal recessive retinitis pigmentosa*** *(arRP)****, autosomal dominant retinitis pigmentosa*** *(adRP). and* ***X-linked retinitis pigmentosa*** *(X-linked RP)****.*** *From (Hartong et al. 2006). The GUCA1B gene encoding GCAP2 is highlighted in a red square.*

LCA (Leber's Congenital Amaurosis) is a severe retinal dystrophy leading to visual impairment in the first year of life (Perrault *et al.* 1996). In fact, it is the most common cause of blindness in kids. Affected children present normal fundus, but an almost flat ERG, as both rod and cone function is typically affected. They also present nystagmus and amaurotic pupils. Other symptoms, such as night blindness or photoaversion show high variability between patients suffering the disease. At later stages of the disease, the retina could have a similar appearance to that of final RP (Chapple *et al.* 2001) (den Hollander *et al.* 2008).

LCA was first reported by Theodore Leber in 1869 (Leber 1869) (van der Spuy *et al.* 2002). Today, there are 21 genes that have been identified as causative of LCA when mutated: *GUCY2D*(LCA1), *RPE65*(LCA2), *SPATA7*(LCA3), *AIPL1*(LCA4), *LCA5*(LCA5), *RPGRIP1*(LCA6), *CRX*(LCA7), *CRB1*(LCA8), *NMNAT1*(LCA9), *CEP290*(LCA10), I*MPDH1*(LCA11), RD3(LCA12), *RDH12*(LCA13), *LRAT*(LCA14), *TULP1*(LCA15), *KCNJ13*(LCA16), *IQCB1, KCNJ3, OTX2, CABP4, DTHD1*, (Figure I.12) (Weleber *et al.* updated 2013) (https://sph.uth.edu/Retnet/sum-dis.htm#B-diseases) .

Autosomal dominant cone/rod dystrophies (adCORDs) are diseases characterized by the loss of color vision and central visual acuity in the first decade of life (as cones degenerate first), with the retention of peripheral sight, that eventually lead to total blindness, usually at the age of 50 or earlier (Hamel 2007).

Mutations in GCAP1 cause autosomal dominant cone dystrophies or cone/rod dystrophies (in agreement with the more abundant localization of GCAP1 in cones, see *GCAPs localization in rods and cones*). Ten mutations in GCAP1 and one in GCAP2 have been linked to inherited retinal dystrophies to date (see below, and Table A.2. in Appendix).

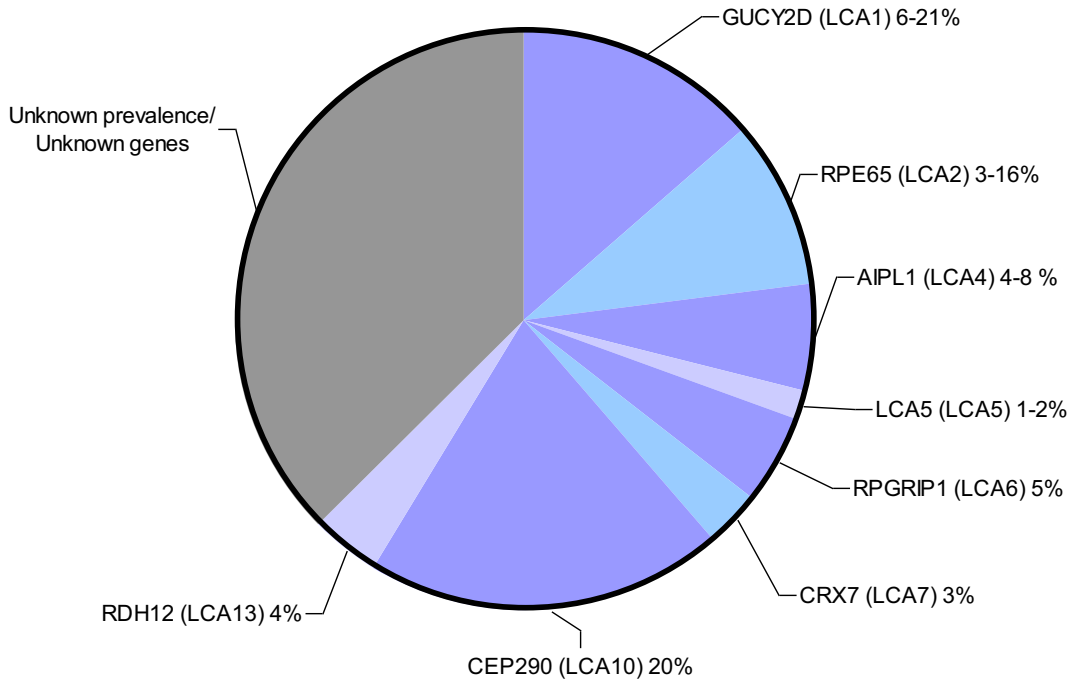

Figure I.12. ***Prevalence of gene mutations contributing to Leber's Congenital Amaurosis (LCA).*** *Based on data from (Weleber et al. updated 2013).*

Despite the importance of GCAPs-mediated Ca^{2+}-feedback on cGMP synthesis in the control of sensitivity, deletion of GCAP1 and GCAP2 in mice does not lead to significant effects on retinal morphology (see *GCAP physiological functions revealed by the study of mouse models*). This indicates that GCAPs are not essential for the development or maintenance of retinal organization. However, mutations in the GCAP1 and GCAP2 genes have been linked to inherited autosomal dominant retinopathies. So far, ten heterozygous mutations in the GUCA1A gene encoding GCAP1 have been identified to cause autosomal dominant cone dystrophy (adCD), cone rod dystrophy (adCORD) or macular degeneration (adMD): P50L, Y99C, N104K, T114I, I143NT, L151F, E155G, G89K, D100E and G159V (Dizhoor *et al.* 1998) (Downes *et al.* 2001) (Jiang *et al.* 2005) (Jiang *et al.* 2008) (Kitiratschky *et al.* 2009) (Michaelides *et al.* 2005) (Nishiguchi *et al.* 2004) (Payne *et al.* 1998) (Sokal *et al.* 2005) (Wilkie *et al.* 2001). Until now, only one mutation in the GUCA1B gene, G157R, has been associated to autosomal dominant retinitis pigmentosa (adRP) (Sato *et al.* 2005) (Figure I.13).

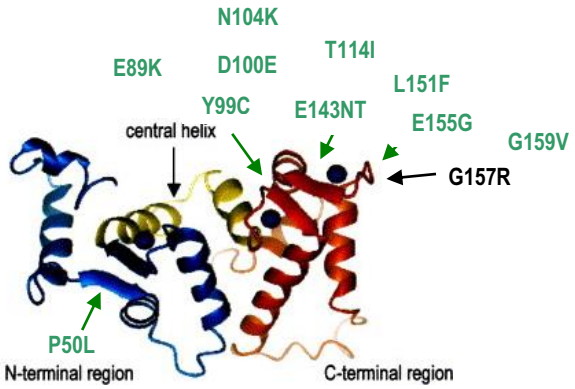

Figure I.13. ***Genetic mutations in Guanylate Cyclase Activating Proteins (GCAPs) that have been linked to human blindness.*** *In* ***green****, mutations that have been described in GUCA1A encoding GCAP1. In* ***black****, mutation described in GUCA1B encoding GCAP2. Most of the mutations* ***(E89K,Y99C, D100E, N104K, T114I,E143NT, L151F, E155G, G159V)*** *directly or indirectly affect GCAPs* Ca^{2+} *binding affinity and have been shown to affect their thermal stability and activity. Others are predicted to affect primarily the folding of the protein (****P50L****,* ***G157R****) and lead to a conformational disorder.* In the case of E143NT and P50L it has been suggested that the conformation of the mutant proteins are unstable and susceptible to proteolysis.

Most of these mutations map at EF-hand domains and affect Ca^{2+} coordination directly (like D100E and N104K at EF-3 or L151F and E155G at EF-4 (Wilkie *et al.* 2001) (Jiang *et al.* 2005) (Jiang *et al.* 2008) (Kitiratschky *et al.* 2009)), or map at the incoming or outgoing α-helixes in EF-3 and EF-4 domains, like E89K, Y99C, T114I, I143NT and G159V (Payne *et al.* 1998) (Nishiguchi *et al.* 2004) (Kitiratschky *et al.* 2009), causing conformational distorsions that make Ca^{2+} binding less favorable. These mutations shift the Ca^{2+} IC_{50} of GC activation to higher free [Ca^{2+}], so that *in vitro* the mutant proteins fail to switch to the inhibitory state and lead to persistent activation of RetGC in the whole physiological range of $[Ca^{2+}]_i$.

In vitro studies anticipated that the molecular basis of these disorders *in vivo* would be the abnormal elevation of cGMP levels in rod outer segments that would lead to an increase in the number of open cGMP-gated channels, a subsequent increase in $[Ca^{2+}]_i$ and the trigger of apoptosis (Wilkie *et al.* 2001) (Olshevskaya *et al.* 2004) (Dizhoor *et al.* 1998) (Sokal *et al.* 1998) (Kitiratschky *et al.* 2009). It has been demonstrated in vivo that this mechanism accounts for the pathology of Y99C, which was the first mutation to be identified by 1998 (Payne *et al.* 1998) (Dizhoor *et al.* 1998), and E155G GCAP1 mutations. Expression of these mutants in transgenic mice resulted in a shift in the Ca^{2+} sensitivity of the cyclase, above 100 μM in some cases, that lead to sustained cGMP synthesis *in vivo*, with the subsequent elevation of both cGMP and Ca^{2+} in rods, and a retinal degeneration that could be significantly prevented by conditions that promoted constitutive stimulation of cGMP-PDE either by equivalent light generated by the G90D

rhodopsin mutant or by constant light exposure (Olshevskaya *et al.* 2004) (Woodruff *et al.* 2007) (Dizhoor *et al.* 2008) (Buch *et al.* 2011).

Another example of a different pathogenic mechanism for naturally occurring mutations affecting GCAPs is the P50L mutation in GCAP1 that activates RetGC with the same Ca^{2+}-sensitivity as the wildtype protein *in vitro* (Newbold *et al.* 2001) but shows reduced thermal stability by circular dicroism and in *in vitro* GC assays (Newbold *et al.* 2001). Therefore this autosomal dominant mutation in GCAP1 anticipates that some GCAP mutations will also cause rod and cone cell death by a mechanism distinct from cGMP accumulation, likely related to conformational instability. In this respect, the G157R mutation in the EF-4 domain of GCAP2, which has been associated with autosomal dominant retinal dystrophies ranging from retinitis pigmentosa to macular degeneration in the Japanese population (Sato *et al.* 2005), has not been explored *in vitro* or *in vivo*.

1. 4. GCAP2 AT THE SYNAPTIC TERMINAL

1.4.1. Photoreceptor synapses must sustain tonic neurotransmitter release

Because light intensities in the natural world can vary over ten orders of magnitude, one fundamental ability of rod and cone photoreceptor cells is to sense and reliably transmit fine gradations in light intensity covering a broad dynamic range. To accomplish this, photoreceptor cells avoid spikes and finely grade the quantized synaptic output with graded changes in membrane potential (Parsons 2003) (Thoreson 2007). Like sensory receptors in the auditory and vestibular systems, they rely on specialized synapses that support the continuous neurotransmitter release at high rates (von Gersdorff 2001) (Prescott and Zenisek 2005). A hallmark of these synapses is a specialized structure, the “ribbon” or “dense body”, a plate-like proteinaceous scaffold that anchors to the active zone just adjacent to the clustered voltage-gated calcium channels, anchoring synaptic vesicles to it (Figure I.14) (Tom Dieck and Brandstatter 2006) (LoGiudice and Matthews 2009) (Schmitz 2009) (Zanazzi and Matthews 2009). Ribbons presumably facilitate focal exocytosis at high throughput by targeting vesicular fusion and the molecular components that trigger this fusion to the proximity of sites of Ca^{2+} influx (Zenisek *et al.* 2004) (Snellman *et al.* 2011) (Zampighi *et al.* 2011). In mammalian rods there is a single synaptic ribbon at the terminal, of about 0.77 μm^2 (35nm thick, 1µm in height and several micrometers in length) and about 770 synaptic vesicles bound to it.

This planar, plate-shaped structure is not anchored directly to the plasma membrane, but through the arciform density (Sterling and Matthews 2005) (Schmitz *et al.* 2009).

The vesicles that are close to the presynaptic membrane and are primed (ready to fusion) are considered the readily releasable pool (RRP). The release rate at mammalian rods has been stimated at about 500 vesicles/s/ribbon at high Ca^{2+} levels in the dark, as compared to other synapses at the hippocampus, for instance, where maximal release rate is about 20 vesicles/s/ribbon. This high rate of exocytosis of synaptic vesicles at rods sustains high neurotransmitter tonic release in darkness, so that gradual changes in membrane potential caused by small changes in the light stimulus can generate detectable changes in glutamate release. That way, photoreceptors are able to transduce a broad bandwidth of stimulus intensities by avoiding spikes and causing gradual changes in neurotransmitter release instead, through fine gradations in membrane potential that determine the intracellular Ca^{2+} levels at the synaptic terminal (Heidelberger *et al.* 2005).

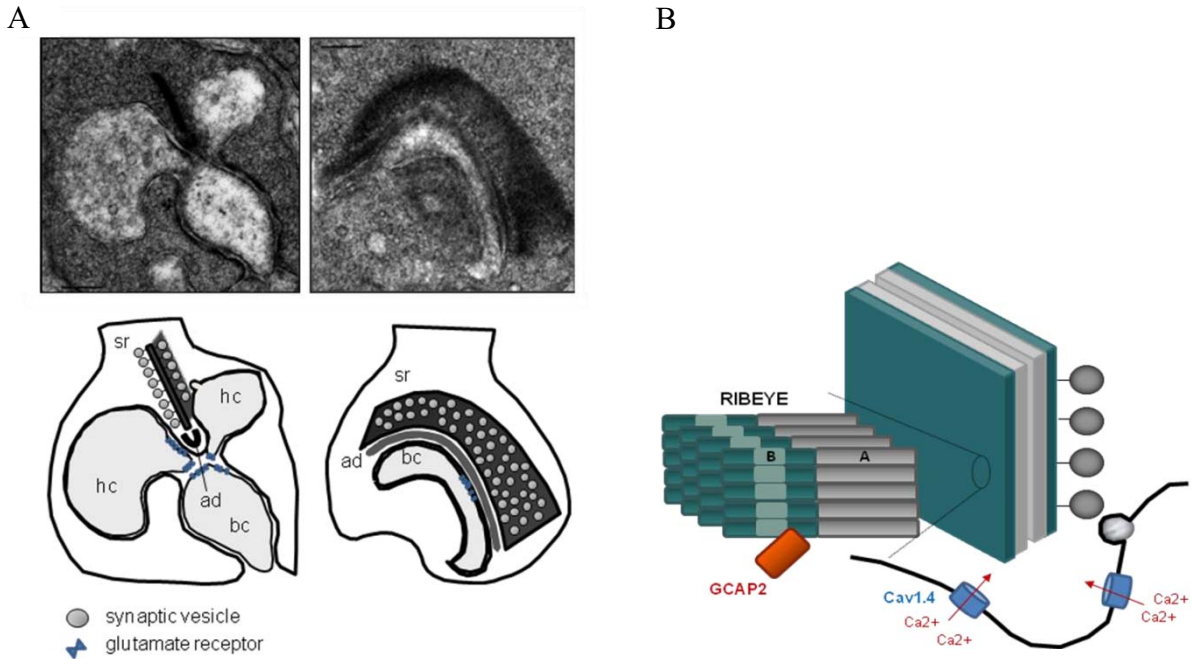

Figure I.14. ***Ultrastructure of synaptic ribbons.*** *(A) Transmission electron micrographs and diagrams of rod synapses from murine retinas (pictures from our lab). Cross-section (left) shows a bar-shaped synaptic ribbon (sr) anchored at the arciform density (ad). Saggital section (right) shows the horseshoe-shaped plate-like nature of ribbons. Numerous synaptic vesicles associate with the ribbon. Hc, horizontal cell; bc, bipolar cell. (B) GCAP2 C- terminal interacts with hinge2 region of RIBEYE, the protein scaffold. Sketch based on (Venkatesan et al. 2010).*

The specific mechanism by which ribbons increase the rate of synaptic vesicle release is not clear yet, and it has been suggested that they may serve to secure or accelerate the RRP at the proximity of the Ca^{2+} voltage channels (Diamond 2011).

1.4.2. Ribbon morphology and dynamics

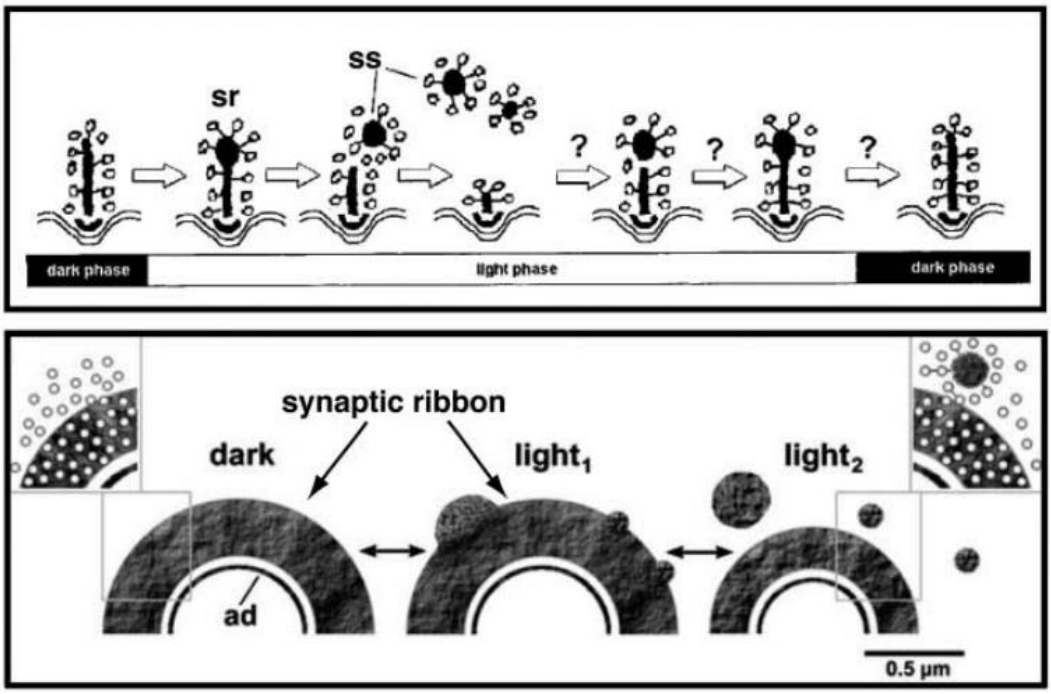

Figure I.15. ***Scheme of retinal ribbon changes in relation to ambient lighting conditions.*** *In the dark, when synaptic activity is high, the horseshoe-shaped ribbons are large and do not show protrusions. Soon after light exposure (beginning of light phase in the upper image or light$_1$ in the lower image), when synaptic activity is depressed, protrusions develop at the outer circumference of the ribbon and detach from it (middle of light phase in the upper image or light$_2$ in the lower image), resulting in smaller ribbons. After dark exposure, the changes are reversed. (Upper) A disassembling synaptic ribbon (sr). The bar-shaped synaptic ribbon (sr) disassembles through synaptic spheres (ss), which "bud off" from the distal end of the ribbon in response to light. (Lower) The insets show the synaptic vesicles in relation to the ribbon and detached spheres also surrounded by synaptic vesicles (inset in the upper right-hand corner). ad, arciform density. The upper image is modified from (Adly et al. 1999) and the lower image from (Spiwoks-Becker et al. 2004). Both images are also included in a more recent review (Schmitz 2009)*

Synaptic ribbons are heterogeneous organelles present in various forms in different cell types, such as spherical, ellipsoid, or bar-shaped structures, with different shapes in hair cells being associated with different functional properties (von Gersdorff 2001) (LoGiudice and Matthews 2009). In rod synapses of the mouse retina of the albino Balb/c strain synaptic ribbons undergo dynamic turn-over changes depending on illumination. Ribbons tend to disassemble in response to illumination by releasing ribbon material in spherical modules; and elongate by regaining ribbon material during

dark-adaptation (Vollrath and Spiwoks-Becker 1996) (Vollrath *et al.* 2001) (Balkema *et al.* 2001) (Spiwoks-Becker *et al.* 2004). In darkness, synaptic ribbons are large and smooth, and during illumination they are smaller and may present spherical and club-shaped forms, forms that are considered “disassembly intermediates” due to the release of protrusions (Figure I.15) (Adly *et al.* 1999). This illumination-dependent ribbon remodeling was reported to affect visual function in Balb/c mice (Balkema *et al.* 2001). Whether these light-dependent ribbon turn-over changes can be regarded as a general mechanism for light adaptation is questioned, based on the variability observed between mouse strains. Illumination-dependent ribbon remodeling changes are less dramatic in pigmented C57Bl/6 mice compared to Balb/c (Fuchs *et al.* 2012). Therefore the physiological significance of the light-dependent ribbon turn-over changes is not yet clear.

Mechanistically, the illumination-dependent disassembly of ribbons is known to depend on the drop in intracellular Ca^{2+} at the synapse caused by the light-triggered hyperpolarization of the cell. Disassembly has been experimentally induced in *in situ* retinas by chelating extracellular Ca^{2+} with EGTA/BAPTA (Vollrath and Spiwoks-Becker 1996) (Vollrath *et al.* 2001) (Spiwoks-Becker *et al.* 2004) (Regus-Leidig *et al.* 2010a).

A breakthrough in the study of the molecular composition of the ribbon structure came with the discovery from Frank Schmidt´s group in the year 2000 that a 120 kDa protein named RIBEYE with the ability to self-associate constituted the main protein component (the scaffold) of the ribbon (Schmitz et al 2000). RIBEYE has two domains: an N-terminal RIBEYE(A) domain that contains three different domains for RIBEYE-RIBEYE interaction, and a C-terminal RIBEYE(B) domain that is identical to the transcription factor CtBP2 (Figure I.16). This C-terminal domain binds NAD(H), and is also involved in RIBEYE-RIBEYE interactions. By establishing homodomain and heterodomain RIBEYE-RIBEYE interactions, RIBEYE self-associates and constitutes the scaffold to which other protein constituents of the ribbon bind, modelling a plastic, dynamic macromolecular structure (Magupalli *et al.* 2008).

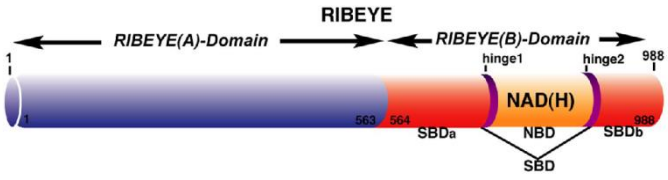

Figure I.16. ***Scheme of RIBEYE structure.*** *RIBEYE is composed by two parts: an N-terminal A domain and a C-terminal B domain which is identical to CtBP2 and binds nicotinamide adenine dinucleotide (NADH) by nicotinamide binding domain (NBD). RIBEYE B also has a substrate binding domain (SBD). From (Venkatesan 2010)*

RIM1 and RIM2, Munc13, ELKC/CAST/ERC, bassoon and piccolo are other important proteins located at ribbons. RIM1 and 2 are important for vesicle priming and Ca^{2+}-dependent synaptic vesicle release. They interact with Munc 13 and ELKC/CAST/ERC. CAST also binds bassoon and piccolo. Bassoon is responsible for anchoring the ribbon to the synaptic membrane, occupying the proximal part of the ribbon. Piccolo is responsible for the refilling of the ribbon, the distal half of it. It has been suggested that the formation of protrusions at the distal part of the ribbon could be to diminish piccolo levels at the synapse. KIF3A is also found at ribbons, with an unknown function (Schmitz *et al.* 2009) (Zanazzi and Matthews 2009).

As mentioned in GCAPs localization in rods and cones, GCAP1 and GCAP2 are also localized in synaptic terminals of photoreceptor cells. However, because the range of $[Ca^{2+}]_i$ at synaptic terminals is considerably higher than that in rod outer segments, a function of GCAPs in stimulation of cGMP synthesis was deemed unlikely. Therefore, the function of GCAPs at the synaptic terminal is currently unknown (Howes *et al.* 1998) (Venkatesan *et al.* 2010).

Three years ago, Frank Schmidt´s group, in a search for RIBEYE interactors identified GCAP2. It was reported that the C-terminus of GCAP2 interacts with the hinge 2 region of RIBEYE B domain. Based on this observation, it was hypothesized that GCAP2 could be mediating the ribbon plasticity due to the chelation of Ca^{2+} by GCAP2 at the proximity of the ribbon. This observation raised the important question of whether the GCAPs proteins may be playing a novel role in light adaptation by regulating the dynamic plasticity of ribbon structures (Venkatesan *et al.* 2010).

1.5. 14-3-3 PROTEINS

14-3-3 proteins are highly conserved acidic proteins of ~28-33 KDa in eukaryotes, initially identified in brain lysates where they are very abundant (Boston and Jackson 1980) (Steinacker *et al.* 2011), but expressed in many different tissues. They owe their name to the particular migration pattern on 2D DEAE-cellulose chromatography. There are seven homologs or isoforms in mammals, named with greek letters: (α) β, γ, (δ), ε, ζ, η, τ, σ, (being α and δ the phosphorylated forms of β and ζ, respectively), depending on the order of elution by HPLC. The seven isoforms are almost identical to each other (Aitken 1996).

14-3-3 proteins are phosphobinding proteins, that work as dimers (homo or heterodimers) with a rigid structure that forms a groove with two separate binding sites

that allows the binding of one protein after two coincident phosphorylation events, or the simultaneous binding of two independent phosphorylated client proteins, which are then linked by their interaction with 14-3-3 (Figure I.17). Phosphorylation of client proteins at Ser or Thr residues at consensus sequences drastically increases the affinity of 14-3-3 binding to these sites, although prior phosphorylation of the substrate is not required in all cases (Muslin *et al.* 1996).

A comparison with known 14-3-3 binding proteins revealed consensus sequences capable of mediating interactions with all 14-3-3 isoforms. Mode I binding sites have the consensus sequence R(S/X)XpSXP and mode II have the consensus sequence RXXXpSXP, where X denotes any aminoacid residue and pS denotes phosphorylated serine. Binding motif III is the same as motif I but lacking the C-terminal proline, RXXpSX -COOH. Client proteins that bind to 14-3-3 that lack these consensus sequences have also been described (Smith *et al.* 2011).

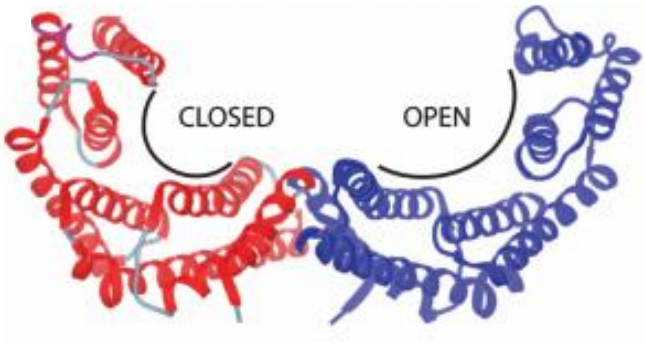

Figure I.17. ***Dynamic nature of the 14-3-3 dimers.*** *Crystal structure of the apo-β isoform. The two binding grooves are represented in an open and closed conformation for the individual monomers indicating that by modifying its groove conformation 14-3-3 proteins are flexible and adapt to their interactor . From (Yang et al. 2006)*

14-3-3 proteins are associated with a broad variety of functions in the cell. 14-3-3 proteins are thought to modify the properties of client proteins by one of three functional mechanisms: clamping, masking and scaffolding. First, due to its inherent rigidity, the binding of 14-3-3 is thought to stabilize certain conformations of client proteins, refered to as **clamping** function. An example is how 14-3-3 fixes the active conformational state of the plant plasma membrane H^+-ATPase (PMA), favoring the arrangement of PMA into large H+ conducting complexes. Second, 14-3-3s could physically **mask** some specific sorting signals of target proteins. One well characterized example is how 14-3-3 regulate ER export of certain targets by binding to consensus binding sites adjacent to RXR motifs required for COPI binding, therefore interfering with COPI binding when masking

RXR motifs. Third, 14-3-3 proteins may facilitate interactions between the target protein and other proteins, by providing a platform for protein anchoring **(scaffolding)**. An example is 14-3-3 binding to nicotinic acetylcholine receptors, which triggers the asembly of a multi-subunit protein complex providing a link to the microtubule cytoskeleton. By modifying target proteins in one of these ways, 14-3-3 proteins exert a diverse range of regulatory roles in protein stability, metabolism, trafficking or integration of cell survival versus cell death pathways (Smith *et al.* 2011).

Importantly for the interpretation of our results in this study, a close association has been established between 14-3-3 proteins and progressive neurodegenerative diseases. 14-3-3 proteins have been shown to colocalize with Alzheimer Disease (AD) neurofibrillary tangles that are composed primarily of hyperphosphorylated tau proteins (Layfield *et al.* 1996) (Lee *et al.* 2001). In Parkinson´s disease (PD), 14-3-3 is detectable in Lewy bodies which accumulate α-synuclein (Kawamoto *et al.* 2002); and 14-3-3 colocalization was also reported with mutant ataxin in spinocerebellar ataxia (SCA) (Chen *et al.* 2003). Furthermore, 14-3-3 zeta and epsilon binding to phosphorylated ataxin-1 at S776 was shown to aggravate neurodegeneration by stabilizing mutant ataxin, retarding its degradation and enhancing its aggregation in transfected cells and transgenic flies (Chen *et al.* 2003). The requirement of 14-3-3 zeta for Htt86Q aggregate formation has also been established in cells (Omi *et al.* 2008). In summary, 14-3-3 proteins have been shown to bind to conformationally unstable proteins with a tendency to form amyloid deposits. By stabilizing thermally unstable proteins they seem to gradually promote their accumulation, and ultimaly they aggravate the pathology upon a certain threshold of toxic protein build-up.

In the retina, 14-3-3 proteins are expressed in all cell types. In photoreceptor cells they distribute to the cytosolic fraction of proximal cell compartments: the inner segment, perinuclear region and synaptic terminal of the cell, but they are excluded from the outer segment. The only well-characterized role of 14-3-3 in the retina is the regulation of the intracellular distribution of phosducin, by retaining it at the inner segment and proximal compartments upon phosducin phosphorylation. Phosducin is a protein that binds to transducing beta/gamma dimers, and by oscillating between phosphorylated and unphosphorylated states, it regulates the subcellular distribution of $Gt_{\beta\gamma}$ during light/dark periods (Nakano *et al.* 2001). Phosducin modulation of the localization of $Gt_{\beta\gamma}$ dimers is one of the factors that determine the amount of $Tr_{\alpha\beta\gamma}$ trimer at rod outer segments, and, as such, one of the factors that modulate the sensitivity of rod photoreceptors (Thulin *et al.* 2001).

II. SCIENTIFIC AIMS

RESUMEN EN ESPAÑOL

Las Proteínas Activadoras de Guanilato Ciclasa (GCAPs) juegan un papel fundamental en las células fotorreceptoras de la retina durante la terminación de la respuesta a luz y en el proceso de adaptación a luz, confiriendo sensibilidad a Ca^{2+} a la síntesis de cGMP. Además de su papel modulando la síntesis de cGMP en el compartimento fotosensible, GCAPs pueden desempeñar otras funciones en conos y bastones, dado que también localizan en el segmento interno y la terminal sináptica. Mutaciones en los genes GUCA1A y GUCA1B, que codifican GCAP1 y GCAP2, las isoformas mayoritarias en humanos, causan distrofias retinales. Nuestro principal objetivo fue abordar cómo mutaciones en GCAP conducen a enfermedades *in vivo*, y caracterizar nuevas posibles funciones de las proteínas GCAP en estas células.

Objetivos específicos:

1- El primer objetivo es investigar las bases de la patología en una línea transgénica de ratón que expresa en bastones una forma mutante de Proteína Activadora de Guanilato Ciclasa 2 (GCAP2) impedida para unir Ca^{2+}: EF^{-} GCAP2, para entender mejor la patología causada por mutaciones en GUCA1A y GUCA1B asociadas a distrofias hereditarias de retina. Nos basamos en las siguientes tres razones: 1) la mayoría de las mutaciones en GCAP asociadas a enfermedad afectan a la afinidad de unión de Ca^{2+} de GCAP; 2) GCAP2 es la isoforma más abundante en bastones; y 3) los bastones son más manejables que los conos para para estudios morfológicos, bioquímicos y fisiológicos en un sistema como el de ratón que es bastón-dominante.

2- El segundo objetivo es caracterizar posibles nuevas funciones de la Proteína Activadora de Guanilato Ciclasa (GCAP2) en la terminal sináptica y compartimentos proximales de la célula, mediante un análisis detallado del fenótipo de modelos de ratón de ganancia y pérdida de función.

AIMS

Guanylate Cyclase Activating Proteins (GCAPs) play a fundamental role in photoreceptor cells of the retina during termination of the light response and in the process of light adaptation, by confering Ca^{2+} regulation to cGMP synthesis. Besides their role in modulation of cGMP synthesis at the light sensitive compartment, GCAPs may have other roles in rods and cones, given that they also localize to the inner segment and synaptic terminal compartments. Mutations in the GUCA1A and GUCA1B genes encoding GCAP1 and GCAP2, the major isoforms in humans, lead to retinal dystrophies. Our main aim was to address how GCAP mutations lead to disease *in vivo*, and to characterize novel putative functions of GCAP proteins in these cells.

Specific aims:

1. First aim is to investigate the basis of the pathology in a mouse transgenic line expressing in rods a mutant form of Guanylate Cyclase Activating Protein 2 (GCAP2) impaired to bind Ca^{2+}: EF^{-}GCAP2, to gain insight into the pathology caused by mutations in GUCA1A and GUCA1B associated to inherited retinal dystrophies. Based on the following three reasons: 1) most GCAP mutations associated to disease affect GCAP binding affinity to Ca^{2+}; 2) GCAP2 is the most abundant GCAP isoform in rods; and 3) rods are more amenable than cones for morphological, biochemical and physiological studies in the rod-dominated murine system.

2. Second aim is to characterize putative new roles of Guanylate Cyclase Activating Protein 2 (GCAP2) at the synaptic terminal and proximal compartments of the cell, by doing a detailed analysis of the synaptic phenotype of loss of function and gain of function of GCAP mouse models.

III. MATERIALS AND METHODS

3.1. Mouse Genetic Models used in the study

The care and use of animals was done in compliance with Acts 5/1995 and 214/1997 for the welfare of experimental animals of the Autonomous Community (Generalitat) of Catalonia, and approved by the Ethics Committee on Animal Experiments of the University of Barcelona. To do these studies the following mouse strains were used:

Line nomenclature Chapter 1	**Line nomenclature Chapter 2**	**Background**	**GCAP1 and GCAP2 expression levels (expressed as a function of endogenous level)**
C57Bl/6 (WT)	C57Bl/6 (WT)	GCAPs +/+	GCAP1 **1** GCAP2 **1**
bGCAP2 E	GCAP2 +	GCAPs +/+	GCAP1 **1** GCAP2 **2 + 1**
-	GCAP2 +/+	GCAPs +/+	GCAP1 **1** GCAP2 **2 + 2 + 1**
bEF$^-$GCAP2 (A)	-	GCAPs +/+	GCAP1 **1** GCAP2 **1** EF-GCAP2 **2.76**
bEF$^-$GCAP2 (B)	-	GCAPs +/+	GCAP1 **1** GCAP2 **1** EF- GCAP2 **3.85**
GCAPs -/-	GCAPs -/-	GCAPs -/-	GCAP1 **0** GCAP2 **0**
GCAPs -/- bGCAP2 E	GCAPs -/- GCAP2+	GCAPs -/-	GCAP1 **0** GCAP2 **2**
GCAPs -/- bEF$^-$GCAP2 (A)	-	GCAPs -/-	GCAP1 **0** EF-GCAP2 **2.76**
GCAPs -/- bEF$^-$GCAP2 (B)	-	GCAPs -/-	GCAP1 **0** EF-GCAP2 **3.85**

Table M.1. ***Compilation of transgenic mouse lines used in the study.*** *Given the number of transgenic lines used in the study, and their manipulation in the GCAPs+/+ and GCAPs-/- background as well as homozygosity or heterozygosity of the transgene, we here present a compilation of the used strains, that states the nomenclature used to refer to each line in each chapter, as well as the overall expression level (transgene + endogenous) of GCAP1, GCAP2 or EF$^-$GCAP2.*

The detailed description of the generation of these transgenic mice is found in *Mouse models to study GCAP functions in intact photoreceptors* (Mendez and Chen 2002).

These mice were developed in accordance with the ARVO statement for the Use of Animals in Ophthalmic and Vision Research and approved by the Ethics Committee on Animal Experiments of the University of Southern California. The GCAP2 expression vectors used to generate transgenic mice were obtained by assembling the 4.4 kb mouse opsin promoter with bovine wildtype GCAP2 cDNA or mutant bEF$^-$GCAP2 [GCAP2 E80Q/E116Q/D158N] (Dizhoor and Hurley 1996) cDNA (0.7 kb), and a 0.6 kb fragment containing the mouse protamine 1 polyadenylation sequence, into pBluescript II SK (Stratagene, La Jolla, California). The resulting fusion gene, 5.7 kb in size, was excised from the plasmid, gel purified and microinjected at 1µg/ml into the pronuclei of C57Bl6/J x DBA/2J F1 hybrid mouse embryos (The Jackson Laboratories, Bar Harbor, Maine). Injected embryos were implanted into pseudopregnant females, and progenie was screened for founders by PCR amplification of tail genomic DNA.

A protocol to screen for transgene-positive mice by PCR amplification of tail DNA was developed, in order to a) identify founders, when the mouse colonies were developed, and b) genotype every new litter in subsequent generations.

3.1.1.DNA purification

A tiny piece of mouse tail (2 mm) was snipped off and collected in an eppendorf tube. Tails were digested in 200µl of "Tailing Buffer" (0.05% proteinase K, 50mM TrisHCl pH 8.0, 100mM EDTA and 0.5% SDS) at 55ºC overnight. Hair particles were pelleted by centrifugation and supernatants were transferred to clean eppendorf tubes. 100µl 8M NH_4OAc and 600µl of 96% ethanol were added and samples were vortexed. DNA precipitation occurred at this step. Samples were spinned for 5min at 13000 rpm. Supernatants were discarded and pellets were washed three times with 70% ethanol. Pellets were either air-dried or dried under the vacuum and resuspended in 100µl of TE buffer (10mM TrisHCl pH8.0, 0.1mM EDTA) or ddH_2O. At this point, DNAs were ready for PCR genotyping. If storage was required, DNAs at this stage were kept at -20ºC.

3.1.2.PCR: polymerase chain reaction

To amplify heterologous GCAP2 in transgenic mice, the following primer set was used: (~450bp amplification product)

Rh1.1.*:* *5'GTGCCTGGAGTTGCGCTGTGGG3'* *(forward)*

p24: *5'TGGCCTCCTCGTTGTCCGGGACCTT3' (reverse).*

Equal volumes of both primers at a 20pmol/µl stock were mixed 1:1, and 0.5µl of the mix were used per 20µl-reaction.

The reaction mixture combined 2 µL of 10x PCR buffer (Invitrogen), 0.6 µL 50mM $MgCl_2$ (Invitrogen), 0.16 µL 25mM dNTPmix (Roche), 0.5µl of primer mix Rh1.1-p24 at 10 pmol/ µl each (SIGMA), 0.12µM Taq DNA polymerase (Invitrogen), 15.62µl ddH_2O and 1µl of DNA sample.

PCR conditions: An initial dissociation step		95ºC,	3.5 min.
30 cycles:	Denaturing step	94ºC	1 min
	Annealing step	64ºC	1.5 min
	Extension	72ºC	1.5 min
A final extension		72ºC	10 min

PCR reactions were analyzed in 1% agarose gels in TAE (40mM Tris, 20mM acetic acid, and 1mM EDTA) to screen for the appearnce of the ~450bp-PCR amplification product that would indicate the presence of the transgene.

METHODS CHAPTER 1

3.2. Determination of transgenic levels of expression in bEF-GCAP2 mice by Western Blot

Founder mice were bred to C57Bl/6 mice to maintain the transgene in a pigmented wildtype genetic background, or to GCAPs-/- to generate GCAPs-/- bEF-GCAP2 mice. To detect transgenic GCAP2 expression by immunoblot, retinas from mice of each genotype were obtained at either postnatal day 22 (p22) (for WT and mice from line B) or p40 (lines A and E), and were homogenized in 100µl of homogenization buffer [80mM TrisHCl, pH 8.0, 4mM $MgCl_2$, 0.5mg/ml Pefabloc SC, 0.5mg/ml Complete Mini protease inhibitors (Roche, Basel, Switzerland)]. After addition of SDS Laemmli sample buffer, samples were boiled for 5 min, and fractions corresponding to 1/40 of a retina were resolved by SDS-PAGE in a 12% tris-glycine gel and transferred to nitrocellulose membranes (Protran, Schleicher & Schuell, Keene, NH). Membranes were incubated with polyclonal antibodies to bovine GCAP2 [p24ΔN (Dizhoor *et al.* 1995), a gift from A. Dizhoor, Pennsylvania College of Optometry, Elkins Park, Pennsylvania], [GC1 and GC2 (Yang *et al.* 1999), a gift from D. Garbers, HHMI and UT Southwestern Medical Center, Dallas] and PDE (αβγ2, Cytosignal, Irvine, CA). Immunopositive protein bands were detected with a peroxidase-conjugated goat anti-rabbit IgG with the ECL system (Amersham, UK).For determination of the precise level of expression of the transgene (expressed as a function of the endogenous), retinal extracts from mice from bEF-GCAP2 line B and line A (2-fold serial dilutions of retinal extracts obtained as described above) were directly compared to retinal extracts from the bGCAP2 control line (2-fold dilutions). The expression level of bGCAP2 in this line was previously established as 2-fold the endogenous levels (Mendez *et al.* 2001). The 2-fold serial dilutions in each sample were used to obtain the integration values of those bands present in the linear range in the same gel, for a direct comparison. The expression of bEF-GCAP2 line A was determined to be 2.76 $\pm$ 0.12 –fold the endogenous levels (average $\pm$ St Dev, n=3). The expression of bEF-GCAP2 line B was estimated to be about 1.4-fold higher than line A, that is, about 3.85-fold the endogenous levels.

3.3. Histology and Retinal Morphometry of ONL thickness

Histological analysis of the retina by light microscopy and retinal morphometry measurements were performed as previously described (Concepcion, Mendez *et al.*

2002). The indicated mice (GCAPs-/-bEF$^-$GCAP2 and GCAPs-/-bGCAP2 control mice) were either reared in constant darkness or under constant light exposure (fluorescent light, 1500 lux intensity) and processed for analysis at postnatal day 20 or 40. Eyecups were marked for orientation, embedded in epoxy resin and sectioned at 1 µm thickness as described (Concepcion, Mendez *et al.* 2002) (Lopez-del Hoyo, Fazioli *et al.* 2012).

Measurements of ONL thickness were taken by making use of a camera lucida attached to a microscope, with the aid of a graphics tablet (WACOM, Vancouver, WA) and the Axiovision LE Rel.4.1. imaging software (Carl Zeiss Inc., Germany). A stage micrometer (Klarmann Rulings, Litchfield, NH) was used for calibration. Each retina half (superior and inferior) was divided into ten equal segments from the optic nerve to the tip (excluding a radius of 100 µm from the optic nerve, due to the natural thinning of the ONL at this region). Three independent measurements were taken per segment, and the average value was obtained. In this manner 60 independent measurements were obtained per section (20 segments x 3 measurements/segment). The mice analyzed per genotype were: GCAPs-/-bEF$^-$GCAP2 line A, n= 4 for each dark and light conditions; GCAPs-/-GCAP2 line E, n= 3 for each dark and light conditions; and GCAPs -/- control line, n=2 for each condition.

3.4. Electroretinogram

Electroretinogram responses to flash stimuli were recorded on a Nicolet Electrovisual Diagnostic System. Mice were dark-adapted for 12 h and then anesthesized under dim red light by intraperitoneal administration of Ketamine HCl (100mg/kg) and Xylazine HCl (10 mg/kg). Phenylephrine HCl (2.5%) and Tropicamide (0.5%) were applied to the cornea to dilate the pupils, and mice were dark-adapted again for 10 min previous to the recording. Following administration of Tetracaine HCl (0.5%) eyedrops as a topical corneal anesthetic, the mice are placed on a heated pad at 37^{o}C in a Faraday cage. The corneal electrode consisted of a carbon-fiber moistened in saline. A 1ms light flash was delivered through a fiber optic centered vertically over a few millimeter of the corneal surface. Mice from the different genotypes were recorded over the course of eight months under identical conditions.

3.5. Guanylate Cyclase assays

Guanylate cyclase activity was assayed in mouse retinal homogenates. Six retinas from dark-adapted mice of each genotype were dissected under infrared illumination, pooled and homogenized in 112µl of 2X assay buffer (100mM MOPS-KOH pH 7.5, 16mM NaCl, 200mM KCl, 2mM IBMX, 20mM $MgCl_2$, 14mM 2-β-mercaptoethanol). From this, 12.5µl aliquots were mixed with either 7.5µl of 1.33mM EGTA (for a final concentration of 0.4mM EGTA per reaction, the "low Ca^{2+}" condition) or 7.5µl of 6.6µM $CaCl_2$ (for a final concentration of 2µM Ca^{2+}, the "high Ca^{2+}" condition) and preincubated at 30ºC for 10 min. Reactions were initiated by addition of 5µl of 5x substrate mix (1.0mM GTP, 0.2µCi/µl of [α-^{32}P]GTP, 1.0mM ATP), and allowed to proceed for 15 min at 30ºC. Reactions were terminated by addition of 500µl of ice-cold 120mM $Zn(OAc)_2$, neutralized with 500µl of Na_2CO_3, kept at -80^0 C for 15 min and centrifuged at 14,000g, 4ºC for 20 min. Radiolabeled cGMP in the supernatants was separated from radiolabeled GTP by alumina column chromatography as described (Domino *et al.* 1991). Protein concentration in retinal homogenates was determined by Bradford. Results are the average and standard deviation of four independent experiments performed in duplicate, with mice that were between p20 and p30. Guanylate cyclase activity was also determined in all retinal homogenates after the addition of 3µM recombinant GCAP2 as a control for the presence of active RetGCs.

3.6. Expression and purification of GCAP2 mutant proteins

BovGCAP2 and its mutants (bovEF$^-$ GCAP2 and bovG161R GCAP2) were expressed in bacteria, by quemical transformation of *E. coli* BL21 (DE3) strain with pET-15b plasmids with the respective cDNAs. Protein expression was induced in bacterial cultures when OD_{600} = 0.6, by addition of IPTG to 1mM final concentration, and expression was allowed to proceed at 37ºC for 5 hours. Cell cultures were centrifuged for 30 minutes at 8000 rpm (JA-14 rotor from Beckman) and resuspended in lysis buffer (0.1M NaH_2PO4, 0.01M TrisHCl, 1mM EDTA, 7mM β-mercaptoetanol, 50µM PMSF, 0.2 mg/mL lysozyme, pH 8). Bacteria lysis was performed by 6 to 12 pulses of sonication on ice, for 30 seconds each at an amplitude of 50 mAmp. Lysates were centrifuge at 15000 rpm (JA-20 rotor from Beckman) for 30 minutes and pellets were collected. This process was repeated 4-6 times, to gradually purify and collect inclusion bodies. Final pellets were solubilized in a denaturing buffer with a chaotropic agent (0.1M NaH_2PO_4, 6M Guanidinium-HCl, 10mM TrisHCl, 20mM imidazole, 2.5mM β-

mercaptoetanol, pH8) and incubated for 1-2 hour at room temperature, with gentle stirring. Solubilized inclusion bodies were then clarified by centrifugation, at 15000 rpm (JA-20 rotor from Beckman) for 30 minutes, supernatants were loaded to 5ml His-Trap™ Chelating HP Columns (GE Healthcare) pre-charged with Ni^{2+} and pre-equilibrated in solubilization buffer.

We then performed "on-column refolding" of GCAP2 and its mutants at the HPLC set, by subjecting the columns to a buffer exchange from 6M Guanidinium to 6M Urea, and then to a decreasing Urea gradient. First step, 5 CV (column volumes) of Refolding Buffer (0.1M NaH_2PO_4, 6M Urea, 10mM TrisHCl, 20mM imidazole, 2.5mM β-mercaptoetanol, pH 8). Second step, 30CV gradient step from 100% Refolding Buffer to 100% Washing Buffer (0.1M NaH_2PO_4, 10mM TrisHCl, 20mM imidazole, 2.5mM β-mercaptoetanol, pH 8). Third step, 5CV of Washing Buffer. Fourth step, gradient step for Elution, 4CV from 100% Washing Buffer to 100% Elution Buffer (0.1M NaH_2PO_4, 10mM TrisHCl, 0.5M imidazole, 2.5mM β-mercaptoetanol, pH 8). Fifth step, 2CV of Elution Buffer. Fractions of 2.5ml were collected and analized by SDS-PAGE. Peak fractions were pooled and concentrated with centricones. Protein concentration was determined with a Bradford Assay. Proteins were stored at -80ºC in 50% glycerol.

3.7. GCAP2 Immunoprecipitation and protein identification by LC-MS/MS

For GCAP2 immunoprecipitation in order to identify protein interacting partners in the different phenotypes [GCAPs-/- bovGCAP2, GCAPs-/- bovEF$^-$GCAP2 and GCAPs-/- control mice] forty retinas per phenotype were pooled and homogenized in HEPES buffer [10mM HEPES pH 8.0, 5mM KCl, 135mM NaCl, 1.5mM $MgCl_2$, 4mM EGTA, 1mM PMSF, 1mM NaF, 1mM β-mercaptoethanol, 1% Triton-X100 and a protease inhibitor cocktail (Complete Mini, Roche, Basel, Switzerland)], and clarified by centrifugation. Supernatants were incubated with anti-GCAP2 monoclonal antibody-covalently crosslinked to magnetic beads (Dynabeads, Life Technologies, Carlsbad, California) for 45 minutes at room temperature (anti-GCAP2 mAb2235, Millipore, Billerica, MA). Following extensive washing, elution was performed with 0.2M Glycine-HCl pH 2.5. Elution fractions were neutralized and concentrated by ethanol precipitation, reduced and alkylated with 45mM DTT at 60ºC followed by 100mM iodoacetamide at room temperature, dehydrated and rehydrated with sequencing grade trypsin in 25mM ammonium bicarbonate for 12h. For LC-MS/MS samples were resuspended in 0.1% formic acid and injected into a series Proxeon LC nanoEASY system (Thermo Fisher Scientific, West Palm Beach, Florida) coupled to a LTQ-Velos

Orbitrap (Thermo Fisher Scientific, West Palm Beach, Florida). The resulting mass spectral peak lists were searched with the Sequest search engine (v.2.1.04, Matrix Sciences, London, UK) against the merged BOVIN-MOUSE UP SP r 2011-1.fasta sequence library. Immunoprecipitation assays and LC-MS/MS analysis with the indicated mouse phenotypes were performed in three independent experiments, with similar results.

3.8. In vitro phosphorylation of GCAP2 and pull-down assays with mock- or phosphorylated-GCAP2.

For *in vitro* phosphorylation of GCAP2 in the presence of radioactivity, 20µl reaction mixtures contained 8.5µg of purified recombinant wildtype bGCAP2, bEF$^-$GCAP2 or bG161R/GCAP2, purified PKGIα (100 units, Calbiochem, Billerica, MA) and 3µCi of ^{33}P- γATP (Perkin Elmer, Massachusetts, USA) in phosphorylation reaction buffer (30mM Tris-HCl pH 7.5, 5mM $MgCl_2$, 5mM sodium phosphate buffer pH 7.5, 6mM DTT, 0.1mM EGTA and 10µM ATP). For reactions in Ca^{2+} or EGTA conditions, the 0.1mM EGTA in the reaction buffer was substituted to 5mM $CaCl_2$ or 2mM EGTA, respectively. cGMP was added to 500µM (to obtain phosphorylated GCAP2 or P-GCAP2) or not added (mock- controls). After incubation for 2 h at 30ºC and overnight at 4ºC, each reaction mixture was diluted with Laemmli buffer and resolved by 15% SDS-PAGE. Following transfer to a nitrocellulose membrane, an autoradiograph of the ^{33}P phosphorylation products was obtained by 15 min of exposure to a Kodak X-ray film. The nitrocellulose membrane was subsequently incubated with a pAb anti-GCAP2 and IRDye 800CW Goat Anti-rabbit IgG for GCAP2 immunodetection.

To obtain phosphorylated bGCAP2 or bEF$^-$GCAP2 for pull-down assays in the absence of radioactivity, the same procedure was used except that 25µg of bGCAP2 or bEF$^-$GCAP2 protein and 230 units of purified PKGIα were used per reaction. The product of each reaction was cross-linked to 2.5mg of magnetic beads (Life Technologies, Carlsbad, California) and used in pull-down assays with solubilized bovine retina. Each sample was incubated with material corresponding to 1/8 of a bovine retina, previously homogenized in binding buffer (10mM HEPES, 135mM NaCl, 5mM KCl, 1mM PMSF, 1mM NaFl, 1mM β-mercaptoethanol, 1% Triton X-100, 4mM EGTA, 2mM EDTA, Complete Mini protease inhibitors, pH 7.4) and pre-cleared by centrifugation. After 1h incubation at room temperature, beads were washed and bound proteins were eluted under acidic conditions, equilibrated and ethanol precipitated. Samples were resolved by 15% SDS-PAGE and transferred to a nitrocellulose membrane. For Western

detection of GCAP2 and 14-3-3 the following antibodies were used: a polyclonal anti-GCAP2 (López-del Hoyo *et al.* 2012), a pAb to 14-3-3pan (JP18649, IBL International, Hamburg, Germany), a mAb to 14-3-3ε (EPR3918, abcam, Cambridge, UK), a IRDye 800CW Goat anti-rabbit IgG and a IRDye 680CW Goat anti-mouse IgG (Tebu Bio, Offenbach, Germany). Image was acquired at the Odyssey Imaging System (LI-COR, Lincol, Nebraska USA).

3.9. In Situ phosphorylation assays

All mice for *in situ* phosphorylation assays were 30-36 days old. Mice were dark-adapted for a minimum of 14h prior to use. Retinas were dissected under infrared light (two retinas per phenotype per light condition) and incubated for 90 min in 600µl of bicarbonate-buffered Locke's solution (112.5mM NaCl, 3.6mM KCl, 2.4mM $MgCl_2$, 1.2mM $CaCl_2$, 10mM HEPES, 0.02mM EDTA, 20mM $NaHCO_3$, 10mM glucose, 3mM sodium succinate, 0.5mM sodium glutamate, 0.1% vitamin and amino acids supplement) containing 1 mCi/ml [$^{32}P_i$]H_3PO_4 (10mCi/ml, Perkin Elmer, Massachusetts, USA) in the dark in a 5% CO_2 incubator to allow incorporation of ^{32}P in the endogenous ATP pool. Following incubation, retinas were washed with Locke´s solution and immediately homogenized in 200µl of solubilization buffer [10mM HEPES, 135 mM NaCl, 5mM KCl, 1mM PMSF, 2mM NaFl, 4 mM EGTA, 1.5mM $MgCl_2$, 2mM EDTA, 1% Triton X100, Complete Mini protease inhibitors (Roche Applied Sciences, Basel, Switzerland), pH 7.4] in the dark, or exposed to bright white light for 5 min prior to homogenization. Samples were clarified by centrifugation at 13,000g for 20 min at 4°C and supernatants were transferred to new tubes. From these samples, 10ul aliquots were resolved by 15% SDS-PAGE to obtain an autoradiograph of the input samples. Visualization of inputs required 4h of exposure with a Kodak X-ray film. The remaining volume of samples (180µl) were used to immunoprecipitate GCAP2 with an anti-GCAP2 monoclonal antibody (anti-GCAP2 mAb2235, Millipore, Billerica, MA) coupled to magnetic beads (Dynabeads, Life Technologies, Carlsbad, California) as described above. After acidic elution of bound fractions, samples were neutralized and proteins precipitated with ethanol. Protein pellets were resolved by 15% SDS-PAGE and transferred to a nitrocellulose membrane. Visualization of phosphorylated proteins in the bound fractions by autoradiography required 4 days of exposure with a Kodak X-ray film. The membrane was subsequently incubated with a polyclonal antibody anti-GCAP2 and IRDye 800CW Goat Anti-rabbit IgG; and a polyclonal antibody to 14-3-3pan (JP18649 IBL International, Hamburg, Germany) and IRDye 680CW Goat Anti-

mouse IgG, and scanned at an Odyssey Image Acquisition system (LI-COR, Lincoln, Nebraska USA).

3.10. Isoelectric focusing (IEF)

Retinas from mice of the indicated phenotypes were dissected under infrared light, and each retina was solubilized in 150µl of buffer (10mM HEPES pH7.5, 1mM $MgCl_2$, 10mM NaCl, 0.1mM EDTA, 1% dodecyl-maltoside, 1mM DTT, 50mM NaFl) overnight at 4°C. Samples were centrifuged at 14000 rpm for 5min, and a 15µl aliquot of the supernatant was loaded onto an isoelectrofocusing gel (pH range 3-8) on a Pharmacia FBE 300 flat bed apparatus, and focused for 2h at 23W. Proteins were transferred to a nitrocellulose membrane by capillary action and incubated with GCAP2 pAb. Bands were visualized with the ECL system (Pharmacia).

3.11. Size-exclusion chromatography.

Sixteen freshly dissected retinas from GCAPs-/- bGCAP2 or GCAPs-/- bEF$^-$GCAP2 mice were solubilized in 500µl of buffer (10mM HEPES pH7.4, 135mM NaCl, 5mM KCl, 1mM PMSF, 1% Triton X100 and Complete Mini protease inhibitors), precleared by centrifugation, filtered and injected into pre-equilibrated columns: Ultrahydrogel 500 column coupled to Ultrahydrogel 250 column (Waters Corporation), in a Waters 2695 Alliance HPLC separation module. Flow rate was 0.3mL/min and the fraction volume collected was 0.6mL. For Triton X100 resistant, SDS-solubilized samples, the pellet fraction from the Triton-X100 preclearing step above was solubilized in SDS buffer (10mM Hepes pH7.4, 135mM NaCl, 5mM KCl, 1mM PMSF, 1% SDS and Complete Mini protease inhibitors), precleared, filtered and injected in the same column extensively pre-equilibrated with the SDS buffer. Collected fractions were individually concentrated with 3000 MWCO Centricons (Millipore), precipitated with ethanol and resolved by 12% SDS-PAGE. Proteins were transferred to nitrocellulose membranes and sequentially incubated with: anti-GCAP2 pAb (visualized in green) and anti-14-3-3ε mAb (visualized in red) for Triton X100 sample-panels; and with GCAP2 mAb (visualized in red) and sequentially with anti-14-3-3ε mAb (also visualized in red) for SDS-sample-panels.

3.12. In vivo electroporation of plasmid DNA following its injection in the subretinal space

Expression vectors for the mutants bS201G/EF$^-$GCAP2 and bG161R/GCAP2 were obtained by site-directed mutagenesis of the expression vectors described above for bGCAP2 and bEF$^-$GCAP2 based on the 4.4kb version of the mouse opsin promoter. Site-directed mutagenesis was performed with the QuikChange II site-directed mutagenesis kit (Agilent, Santa Clara, CA, USA) using primers:

bGCAP2_S201G_Fw: CTCAGCAGAGGCGGAAAGGTGCCATGTTC;

bGCAP2_S201G_Rv: GAACATGGCACCTTTCCGCCTCTGCTGAG;

bGCAP2_G161R_Fw: CCTTCTGGTGGATGAAAATCGAGATGGTCAGCTG;

and bGCAP2_G161R_Rv: CAGCTGACCATCTCGATTTTCATCCACCAGAAGG.

Mutagenesis in each case was confirmed by sequencing. Mice were electroporated at p0 according Matsuda and Cepko, (Matsuda and Cepko 2004) and processed at p28-30. Briefly, 0.5µl at a concentration of 6µg/µl of DNA mix in PBS was injected into the subretinal space, by making use of a Nanojet microinjector and micromanipulator (Drummond Scientific, Broomall, PA). The DNA mix consisted of the expression vector for the specific GCAP2 mutant (GCAP2, G161R/GCAP2, EF$^-$GCAP2 or S201G/EF$^-$GCAP2) in circular form and a tracer plasmid [pL_UG, expressesing the green fluorescent protein (GFP) driven by the Ubiquitin C promoter, (Zavzavadjian, Couture *et al.* 2007) also in circular form, at a mass ratio of 2:1. Electroporation was performed with a square-wave electroporator (CUI21, Nepagene, Japan) by triggering 5 pulses of 80V with a 50ms duration and an interval time of 950ms. Electroporated pups were raised under standard cyclic light conditions and sacrificed at p28-30 for immunofluorescence analysis. Briefly, eyes were fixed in 4% paraformaldehyde in PBS at pH 7.4, embedded in acrylamide mix and frozen as described [34]. Retinal cryosections were obtained at 22µm thickness. An antigen retrieval protocol was performed preceding the immunofluorescence studies: glass slides were incubated with proteinase K in PBS pH 7.4 (0.05mg/ml) for 2 min and heated at 70^{o}C for 8 sec. Sections were incubated in blocking solution (1% BSA, 3% normal goat serum, 0.1% Triton X100, PBS pH 7.4); primary antibody solution (1% BSA, 3% normal goat serum, PBS pH 7.4 containing 0.01mg/ml polyclonal antibody to GCAP2 and 0.00025mg/ml mAb 1D4 to rhodopsin); and secondary antibody solution [1% BSA, 3% normal goat serum, PBS pH7.4 containing Alexa Fluor 647 anti-rabbit IgG (signal converted to red in figures); and Alexa Fluor 555 anti-mouse IgG (signal converted to blue in figures)]. Images were acquired in a Leica confocal microscope. GCAP2 and rhodopsin signal

profiles were obtained for the individual cells shown by tracing a line along the inner segment compartment, and another line along the outer segment compartment, and plotting the summation of the red and the green signal along both lines from the collection of planes in a z-stack that covers the whole volume of the cell, by using the Leica confocal software (Leica Microsystems).

3.13. Immunocytochemistry

To obtain retinal sections for immunofluorescence analysis mouse eyecups were fixed, infiltrated in sucrose or acrylamide, embedded in OCT and cryosectioned as described (Lopez-del Hoyo, Fazioli *et al.* 2012) . Sections were incubated with blocking solution (3% normal goat serum, 1% BSA, 0.3% Triton X100 in PBS pH 7.4, 1 h at room temperature); primary antibody (14 h at 4ºC), secondary antibody (1 h at room temperature), and fixed for 15 min in 4% paraformaldehyde prior to being mounted with Mowiol [Calbiochem, Billerica, MA]. An antigen retrieval treatment of retinal sections [incubation in 0.05mg/ml proteinase K in PBS pH 7.4 for 2 min at room temperature followed by a heat shock at 70ºC for 10 sec] was needed for GCAP2 immunostaining. Antibodies used were: a polyclonal anti-GCAP2 (Lopez-del Hoyo, Fazioli *et al.* 2012), monoclonal anti-GCAP2 [mAb2235, Millipore, Billerica, MA], rabbit monoclonal anti-14-3-3ε [EPR3918, abcam, Cambridge, UK]. Secondary antibodies for immunofluorescence were Alexa 488 goat anti-rabbit IgG and Alexa 555 goat anti-mouse IgG [Molecular Probes, Eugene, Oregon]. Images were acquired at a laser scanning confocal microscope (Leica TCS-SL and TCS-SP2).

METHODS CHAPTER 2

3.14. Immunofluorescence microscopy

For immunofluorescence microscopy, mice were sacrificed and eyes were marked at the superior center for orientation purposes. Immediately after enucleation the eyes were punctured with a needle and submerged in fixative: 4% paraformaldehyde; 0,02% glutaraldehyde in phosphate buffer saline at pH7.4. At 5 min into the fixation step the cornea was excised, at 20 min the lens was removed and eye cups were further fixed for a total of 2h at room temperature. Eye cups were infiltrated in acrylamide (8,4% acrylamide, 0,014% bisacrylamide in PBS pH7.4 for 14h before acrylamide polymerization was induced) or in sucrose (30% w/v in PBS pH7.4 for 14h), and included in OCT compound. Cryosections along the vertical axis of the eyecup were obtained at 20µm-thickness using a CM1510S Leica cryostat (Leica Microsystems). Sections were incubated with blocking solution (3% normal goat serum, 1% BSA, 0,3% Triton X100 in PBS pH7.4, 1h at room temperature); first antibody (14h at 4^{o}C), secondary antibody (1h at room temperature), and fixed for 15 min in 4% paraformaldehyde prior to being mounted with Mowiol [Calbiochem 475904]. An antigen retrieval treatment of retinal sections [incubation in 0,05 mg/ml proteinase K in PBS pH7.4 for 2 min at room temperature followed by a heat shock at 70^{o}C for 10 sec] was needed for GCAP2 immunostaining. Images were acquired at a laser scanning confocal microscope (Leica TCS-SL and TCS-SP2).

The GCAP2 antibody used in Western blots, indirect immunofluorescence assays and electron microscopic immunolocalization is a polyclonal antibody raised in rabbit against a His-tagged recombinant form of bovGCAP2 expressed in bacteria. Antibodies were affinity-purified with a recombinant GCAP2 affinity column. For indirect immunofluorescence assays GCAP2 Ab was used at a 1:400 working dilution from a 1 mg/ml stock. Ribeye immunolabeling of synaptic ribbons was performed with a monoclonal antibody anti-CtBP2 [BD biosciences 612044, 1:250]. The GCAP1 antibody is a polyclonal antibody raised in rabbit against a His-tagged recombinant form of human GCAP1, and was affinity-purified.

To label retinal cell types we used primary antibodies directed against the following molecules: Transducin Gγ c subunit [Cytosignal PAB-00801-G Ab, 1:200, for cone pedicules]; Calbindin D [Swant CB-38a Ab, 1:500, for horizontal cells]; Protein Kinase C α isoform, PKCα [Santa Cruz Biotechnology sc-10800 Ab, 1:100, for rod-on bipolar cells]; Bassoon [Stressgen VAM-PS003 mAb, 1:1000, for arciform densities in rods and

cones]; and Synaptophysin, SYP [Chemicon MAB5258 mAb, 1:1000, for rod spherules and cone pedicules]. Secondary antibodies for immunofluorescence were Alexa 488 goat anti-rabbit IgG [Molecular Probes A-21206]; Alexa 555 goat anti-mouse IgG [Molecular Probes A-31570] and Alexa 633 goat anti-guinea pig IgG [Molecular Probes A-21105], used at a 1:100 dilution.

3.14.1. OPL measurements

For measurements of outer plexiform layer (OPL) thickness, pictures were taken at four different positions in the retinal vertical meridian (A, B, C and D). These regions, at 800 µm from the superior edge (A), equidistant from point A and the optic nerve (B), at 750µm from the optic nerve in the inferior retina (C) and equidistant from C and the inferior edge (D) were marked at 10x magnification by photobleaching the fluorescent signal next to the point of interest. By using the photobleached areas as a reference, pictures at A, B, C and D positions were taken at 63x magnification. Measurements of OPL thickness were taken at each point in the different phenotypes by determining the width of the GCAP2 (or RIBEYE) immunolabeled bands with the Leica LAS AF Lite image acquisition software. Three different measurements were taken per point to calculate the average for each retina specimen, and at least four mice per phenotype were analyzed to calculate the mean.

3.15. Retinal preparation for light microscopy and electron microscopy

For the ultrastructural analysis of rod synaptic terminals the different mouse lines were raised in constant darkness by maintaining cages in aerated dark cabinets. They were sacrificed under dim red light at postnatal day 40 (dark conditions); or exposed to 1500 lux white fluorescent light for 1 or 5h after pupil dilation with a mixture of 0.75% tropicamide and 2.5% phenylephrine hydrochloride (light conditions) and immediately sacrificed. For orientation purposes, a mark was imprinted at the superior center of the eye before enucleation. Immediately after enucleation the eye was punctured with a 30-G needle and fixed in 2% paraformaldehyde, 2.5% glutaraldehyde in 0.1M cacodylate buffer for 5 min. An incision was made arround the ora serrata and fixation was allowed to proceed for 1h. The cornea and lens were removed and the eye cup was further fixed for 12h at 4ºC. After this fixation step, eye cups were washed with 0.1M cacodylate buffer and fixed with 1% osmium tetroxide (OsO4) in 0.1M cacodylate

buffer for 2h at room temperature. Specimens were dehydrated in ethanol (30-100%) or acetone, infiltrated with propylene oxide and embedded in Epoxi embedding medium (Fluka Analytical). To measure synaptic ribbons in GCAP2+ and WT littermate control mice, 4 GCAP2+ and 3 WT littermate controls were raised in 12h:12h dark-light standard cyclic light and were processed at p60 at the end of the dark period. Processing of the eyes for conventional electron microscopy was done as described.

3.16. Ultrathin sectioning, image acquisition and analysis at the transmission electron microscope

Ultrathin sections (70-90nm) in the vertical meridian of the eye cup were made using a Reichert Ultracut S ultramicrotome (Leica), collected on 200 mesh copper grids, counterstained with heavy metal staining (2% uranyl acetate in 50% ethanol for 30 min) and contrasted with 2% lead citrate for 10 min. Ultrathin sections were analyzed in a JEOL 1010 or a Tecnai Spirit Twin [FEI] 120 Kv LaB6 transmission electron microscope. Images were obtained with a Bioscan Gatan wide angle slow scan CCD camera. In order to determine the ribbon length in the different mouse lines, at least two different specimens were analyzed per phenotype. Two to ten 16 x 16 µm frames at 8,000 x magnification were delimited per Epon block, that typically contained 10 to 22 rod synaptic terminals. At a given plane of sectioning along the vertical axis in the center of the eye cup, the synaptic ribbon was visible in about 60-70% of the synaptic terminals, and about 40% of all terminals presented ribbons discernible as resulting from transversal cuts (Supplementary Table I). Contrary to ribbons from longitudinal or oblique cuts that result in variable shapes and sizes, transversal cuts are easily recognized as defined lines anchored at the arciform density between the two invaginating processes of horizontal cells, and their length should represent the length of the ribbon plate at any point. Therefore, once the 8,000x magnification frames were delimited, all synaptic terminals contained in the frame were individually scanned at 100,000x magnification, and length measurements were taken from ribbons resulting from tangential cuts by using the ImageJ software. Cone synaptic terminals were excluded from the analysis.

For determination of synaptic terminal size [μm^2], micrographs of the OPL area were obtained at the electron microscope at low magnification [x8000], and the ImageJ software was used to obtain the dimensions of delimited regions of interest with the form of the synaptic terminals.

To determine the percentage of synaptic terminals containing a synaptic ribbon, the number of total synaptic terminals was determined in five 16x16 -μm^2 frames per fenotype, and the number of terminals containing a longitudinal, transversal or sagittal ribbon were counted. A percentage was calculated per frame, and the five results obtained per phenotype were averaged.

3.17. Immunoelectron microscopy

For immunoelectron labeling of GCAP2 and RIBEYE in GCAPs-/-GCAP2+ mice and GCAPs-/- negative control mice, dark-reared mice at p40 were sacrificed in dim light. The eyes were marked, enucleated and immediately fixed in 2% paraformaldehyde in phosphate buffer saline at pH 7.4 for 2h at room temperature, following the puncture and dissection steps described above. In order to preserve antigenicity while maintaining ultrastructure, immediately after fixation eye cups were processed by a progressive lowering temperature (PLT) protocol of dehydration and embedding in Lowicryl resin. Dehydration protocol was: [0ºC, 30 min 30% ethanol; -20ºC, 60 min 50% ethanol; -35ºC, 60 min 70% ethanol; -35ºC, 60 min 95% ethanol; -35ºC, 60 min 100% ethanol; -35ºC, 60 min 100% ethanol]. Infiltration was performed with Lowicryl embedding media K4M: [-35ºC, 60 min resin:ethanol 1:3; -35ºC, 60 min pure resin; -35ºC, 16h pure resin]. The resin was polymerized by long wavelength UV irradiation for at least 24h. Ultrathin sections were incubated at room temperature in blocking solution (1% BSA, 20mM glycine in PBS pH7.4, for 30 min), first antibody (anti-RIBEYE Ab, for 2h) and secondary antibody (5nm or 15nm gold-conjugated goat anti-mouse IgG, BBInternational, for 1h); and the process subsequently repeated for GCAP2 immunolabeling, by repeating the blocking step and incubating with antibody (anti-GCAP2 Ab, for 2h) and secondary antibody (5nm or 15nm gold-conjugated goat anti-rabbit IgG, BBInternational, for 1h). After washes, sections in the gold grids were counterstained with heavy metal staining (2% uranyl acetate in 50% ethanol for 10 min) and contrasted with 2% lead citrate for 5 min.

Sections were observed at a JEOL JEM1010 transmission electron microscope at 80 Kv and images were obtained with a Bioscan Gatan wide angle slow scan CCD camera.

To assess specificity of the association of gold-particles to GCAP2 antigenicity in the GCAPs-/-GCAP2+ specimens, the number of gold particles associated to synaptic ribbons were counted in 74 synaptic terminals randomly selected from two specimens,

and compared to that of GCAPs-/- negative control samples. Out of 74 randomly selected synaptic terminals in the GCAPs-/-GCAP2+ sample, 12 out of 74 (about 16%) had at least one gold particle associated to the synaptic ribbon, and 20 out of 74 (about 27%) showed association of gold particles to the presynaptic plasma membrane in apposition to the invaginated processes of horizontal cells; whereas in the GCAPs-/- only 6% of the ribbons analyzed showed associated gold particles and only 16% showed association of gold particles to the membrane delineating the invaginating horizontal dendritic processes. Therefore, we consider the micrographs selected in Fig 6 to be an accurate illustration of GCAP2 intracellular localization at the synaptic terminal.

3.18. Electroretinogram analysis

Electroretinogram (ERG) recordings were performed in 12h dark-adapted deeply anesthetized mice. Recordings were acquired with a Burian-Allen mouse electrode set on a corneal lens specifically designed to fit the mouse eye (Hansen Ophthalmic Development Lab), with the reference electrode positioned at the mouth and the ground grasped on the tail. Pupil from the right eye was dilated, and flash-induced ERG responses were recorded in response to light stimuli produced with a Gansfeld stimulator. The intensity of light stimuli ranged from -4 to 2 log cd.s.m^{-2}. For each light intensity, responses from four consecutive light presentations were averaged. The range of light intensities from -4 to -1,52 log cd.s.m^{-2} elicited rod-mediated responses. In the range from -1,52 to 0,48 log cd.s.m^{-2} ERG recordings reflected mixed responses from rods and cones. Pure cone responses were recorded after inducing rod saturation by exposing the mouse to a 30cd/m^2 background light for 10 min, and then applying light stimuli in the range of -0,52 to 2 log cd.s.m^{-2} superimposed to the background. ERG signals were amplified and band filtered between 0.3 and 1000 Hz (Grass CP511 AC amplifier), digitized at 10kHz with a Power Lab data acquisition board (ADI instruments) and analyzed off-line by measuring the amplitudes of the a-wave (from the baseline to the peak of the a-wave) and of the b-wave (from the peak of the a-wave to the peak of the b-wave). ERG measurements were done on a blind basis with respect to the mouse phenotype.

3.19. Retinal Morphometry

For retinal morphometry analysis of GCAPs-/- and GCAPs-/-GCAP2+ retinas, a high magnification picture of the whole retina under study was obtained by fusion (HUGIN software) of three 20x overlapping frames covering the length of a vertical section from central retina. Pictures were taken with the ProgResCapturePro 2.6 software in a Stereo Lumar V12 stereoscopic microscope (Zeiss) coupled to a Jenoptik camera. On whole retina-pictures, lines were traced from an imaginary point at the center of the retina semicircumference to the optic nerve and to the superior and inferior borders, dividing the retina in its superior and inferior quadrants; and then to marks traced at 200 µm intervals starting from the optic nerve that divided the superior retina into 12 equal divisions and the inferior retina into 11 divisions. Marks were numbered 1 to 10 starting at the second mark from the optic nerve towards the superior edge, and from -1 to -10 at equivalent positions in the inferior retina. At each marked position the onl thickness was determined by taking three measurements with the ProgResCapturePro 2.6 software and averaging them. To obtain the graph comparing the morphometric analysis in GCAPs-/-GCAP2+ versus GCAPs-/-, at least three animals per phenotype were used.

IV. CHAPTER 1

RESUMEN EN ESPAÑOL

Para estudiar el efecto *in vivo* de mutaciones en GCAP2 que afectan a su afinidad de unión a Ca^{2+}, en este estudio llevamos a cabo la generación y caracterización de ratones transgénicos que expresan una forma mutada de GCAP2 con los tres dominios de unión a Ca^{2+} inactivados: GCAP2(E80Q/E116Q/D158N) ó bEF$^-$GCAP2. Para discriminar el efecto de las mutaciones del efecto que la sobreexpresión del transgén pueda tener *in vivo*, se incluyó una línea transgénica control que sobreexpresa la isoforma bovina de GCAP2 wildtype. Las líneas transgénicas en que se ha basado este estudio son: las líneas transgénicas bEF$^-$GCAP2 A y B (con expresión del transgén a un ratio 2.76:1 y 3.85:1 con respecto a la expresión endógena de GCAP2) y la línea transgénica control bGCAP2 E (expresión 2.5:1).

Las líneas transgénicas bEF$^-$GCAP2 A y B condujeron a una degeneración retinal progresiva que se correlacionó con los niveles de expresión del transgén. Esta degeneración se caracterizó haciendo un seguimiento de la morfología de la retina con la edad en las tres líneas, que reveló que el número de células fotorreceptor se ve aproximadamente reducido a la mitad en la línea B a los 40 días, y en la línea A a los tres meses. En ambas líneas los ratones alcanzan la ceguera total (respuesta plana en electrorretinograma) entre los 5 y los 8 meses de edad. Podemos afirmar con seguridad que esta degeneración se atribuye al efecto de las mutaciones (a un efecto de las proteínas mutantes en la célula) y no a un efecto de sobreexpresión heteróloga en fotorreceptores de la isoforma de GCAP2 bovina, porque la línea transgénica control no presenta degeneración.

La proteína mutada GCAP2(E80Q/E116Q/D158N) ó bEF$^-$GCAP2 conduce en ensayos de reconstitución *in vitro* a la actividad constitutiva del enzima guanilato ciclasa. Este mutante se comporta *in vitro* como los mutantes en GCAP1 impedidos para unir Ca^{2+}, es decir, al no unir Ca^{2+} la proteína se bloquea en su estado "activo", y no adquiere su estado "inactivo" o "inhibidor de la ciclasa" en respuesta a las elevaciones en $[Ca^{2+}]_i$. Nuestra sorpresa fue que *in vivo*, en ensayos de actividad guanilato ciclasa realizados en homogenados de retina de ratones bEF$^-$GCAP2, la proteína transgénica mutante no mostró actividad constitutiva. En realidad, no mostró una actividad apreciable en los ensayos, ni en condiciones de alto Ca^{2+} ni en ausencia de Ca^{2+}. La expresión de la proteína transgénica control, por el contrario, restauró la regulación de la guanilato ciclasa en ratones GCAPs-/- según lo esperado.

El análisis de la localización de bGCAP2 en ratones transgénicos GCAPs-/-bGCAP2 (línea control) en secciones de retina reveló que la proteína transgénica control

reproduce la localización de la proteína GCAP2 endógena en ratones wildtype. Sin embargo en ratones transgénicos GCAPs-/-bEF$^-$GCAP2, la proteína bEF$^-$GCAP2 ("bloqueada" en su forma libre de Ca^{2+}) se acumula en el segmento interno y compartimentos proximales de la célula y no se transporta al segmento externo. Estos resultados, junto con los resultados de falta de activación de la guanilato ciclasa en homogenados de retina, apuntan a que la proteína mutante se acumula en forma inactiva en el segmento interno.

Para investigar si la proteína mutante es retenida en el segmento interno por su interacción con alguna otra proteína, llevamos a cabo ensayos de inmunoprecipitación de GCAP2 y caracterización de las proteínas que coinmunoprecipitan por espectrometría de masas. Los ensayos de inmunoprecipitación se llevaron a cabo en paralelo en ratones GCAPs-/-bGCAP2 y GCAPs-/-bEF$^-$GCAP2, para identificar proteínas que interaccionaran específicamente con la forma mutada de GCAP2. En este tipo de ensayos identificamos las proteínas 14-3-3 como interactores preferentes de GCAP2 en su forma libre de Ca^{2+}.

Dado que las 14-3-3 son proteínas que se unen a sus blancos de interacción en respuesta a la fosforilación de los mismos, investigamos si la forma libre de Ca^{2+} de GCAP2 se fosforila en extractos de retina de ratones transgénicos. Tanto ensayos de fosforilación *in situ* por marcado metabólico con ^{32}Pi, como ensayos de resolución de extractos de retina por geles de isoelectroenfoque, revelaron que la proteína bEF$^-$GCAP2 en retinas de ratones transgénicos se encontraba fosforilada a un nivel mucho mayor que la proteína bGCAP2. Una sorpresa de los ensayos de isoelectroenfoque fue la revelación de que aproximadamente el 50% de la proteína GCAP2 endógena en ratones wildtype se encuentra fosforilada tanto en estadíos de luz como de oscuridad. En línea con estos resultados, ensayos de cromatografía de exclusión por tamaño de extractos de retina mostraron que bGCAP2 está asociado a 14-3-3 en ratones de la línea control, y que lo está también y en mayor medida la proteína bEF$^-$GCAP2 en la línea mutante. Por tanto, la fosforilación de GCAP2 y su unión a 14-3-3 es algo que ocurre en la proteína wildtype a cierto nivel (es, por tanto, un proceso fisiológico), y que ocurre de forma magnificada cuando la proteína GCAP2 se ve bloqueada en su forma libre de Ca^{2+}.

Dado que las distintas isoformas de 14-3-3 se localizan en células fotorreceptor en el segmento interno y compartimentos proximales pero excluídas del segmento externo, la fosforilación de GCAP2 y su interacción con 14-3-3 podría ser la causante de su retención en el segmento interno. Para probar esta hipótesis recurrimos a una estrategia genética. Expresamos el mutante de GCAP2: bS201G/EF$^-$GCAP2 en

fotorreceptores de ratones GCAPs-/-, por transgénesis transitoria mediante inyección subretinal del DNA y electroporación *in vivo*. El análisis de localización de la proteína en las células bastón transfectadas de esta forma en la retina reveló que la mutación de la Ser201 (el único residuo que se fosforila en GCAP2) revirtió la distribución de GCAP2, precluyendo su retención en el segmento interno. La proteína bS201G/EF^{-} GCAP2 se localizó mayormente en el segmento externo.

Conjuntamente, estos resultados nos llevan a proponer un modelo en que la distribución intracelular de GCAP2 está regulada por fosforilación y unión de 14-3-3. En condiciones fisiológicas, GCAP2 oscila entre su forma unida a Ca^{2+} (cuando el Ca^{2+} es alto, en oscuridad) y su forma libre de Ca^{2+} (cuando el Ca^{2+} baja durante exposiciones prolongadas a luz). Proponemos que la fracción de GCAP2 que se sintetiza en el período de oscuridad une Ca2+ y es transportada al segmento externo, mientras que la fracción de GCAP2 que se sintetiza durante períodos lumínicos, al estar en su forma libre de Ca2+, es fosforilada y se une a 14-3-3, siendo retenida en el segmento interno y compartimentos proximales de la célula. De esta forma, los ratones wildtype que se mantienen en el estabulario en ciclos de luz-oscuridad estándar, resultan en células fotorreceptor que contienen aproximadamente un 50% de GCAP2 en el segmento externo y un 50% de GCAP2 en el compartimento interno. Aquellas condiciones que desequilibran esta regulación, como es el bloqueo de GCAP2 en su forma libre de Ca^{2+}, no sólo producen un cambio en la distribución intracelular de GCAP2 (que se acumula fundamentalmente en el segmento interno), sino que conducen a una degeneración retinal rápida. Proponemos que la causa de la toxicidad de la forma libre de Ca^{2+} de GCAP2 reside en su inestabilidad térmica y su tendencia a la agregación. Una de las atribuciones descritas para 14-3-3 es su papel de chaperona para proteínas con tendencia a agregar y a formar depósitos amiloides, del tipo de los observados en Alzheimer, Parkinson, Huntington, etc. Creemos que la toxicidad de las mutaciones que afectan a la unión de Ca^{2+} en GCAP2 es de carácter de desorden conformacional, e independiente del metabolismo de cGMP. Este resultado, además de para las mutaciones descritas en el gen GUCA1B, tiene implicaciones para aquellas distrofias hereditarias de retina que resultan en un fenotipo "luz-equivalente" (un fenotipo que cabría esperar tras exposiciones a luz anormalmente altas o prolongadas). Estas distrofias suelen resultar en una bajada prolongada en la $[Ca^{2+}]_i$, y por tanto resultarían en la acumulación de GCAP2 en su forma libre de Ca^{2+}.

4.1. CONTRIBUCIONES

Las líneas transgénicas descritas en este trabajo fueron generadas originalmente por A. Méndez en el laboratorio de la Dra. Jeannie Chen en la University of Southern California, Los Angeles, y trasladadas a Barcelona para su caracterización. Los ensayos de actividad guanilato ciclasa y el análisis por ERG fueron realizados por A. Méndez. Tanto la construcción de los plásmidos de expresión para la transgénesis transitoria de los mutantes bS201G/EF$^-$GCAP2 y bG161R/GCAP2, como la electroporación de los plásmidos en retina *in vivo*, el análisis de la localización de las proteínas mutantes por ensayos de inmunofluorescencia y la obtención y análisis de imágenes al microscopio confocal fueron realizados por S. López-Begines. Los ensayos de isoelectroenfoque fueron aportados por el laboratorio de la Dra. Jeannie Chen, USC, Los Angeles.

La contribución experimental de N. López del Hoyo a este capítulo ha sido: 1) el mantenimiento y genotipaje de rutina de las cepas de ratón descritas, 2) la puesta a punto de los ensayos de proteómica, tanto por inmunoprecipitación como por pull-down seguidos de análisis de espectrometría de masas, y por tanto de la obtención de las Tablas de proteómica, 3) los pull-downs de verificación de la interacción GCAP2-14-3-3, 4) la expresión y purificación de GCAP2 y sus mutantes en bacteria, 5) los ensayos de fosforilación *in vitro* e *in situ* por marcado metabólico de GCAP2, 6) los ensayos por cromatografía de exclusión en tamaño.

4.2. BRIEF INTRODUCTION

Although GCAPs are not essential for the development and maintenance of retinal morphology (Mendez *et al.* 2011), mutations in GCAPs genes have been linked to inherited autosomal dominant retinopathies. Nine from ten mutations in GUCA1A gene, coding for GCAP1 (E89K, Y99C, D100E, N104K, T114I, E143NT, L151F, E155G and G159V), affect Ca^{2+}binding affinity (directly or indirectly), producing cGMP elevated levels *in vitro*. In Y99C and E155G mutations it was proved *in vivo* that these abnormal cGMP levels cause rods and cones death. P50L, the other GCAP1 mutation, is predicted to affect the folding of the protein and hypothesized to cause cell death by another pathogenic mechanism. G157R, the only mutation identified in GUCA1B gene, has not been explored.

To study the effect of mutations in GCAP2 that affect Ca^{2+} binding *in vivo*, we expressed a mutant form of GCAP2 with inactivated EF hands: GCAP2(E80Q/E116Q/D158N), hereafter referred to as bEF$^-$GCAP2, in the rod photoreceptors of transgenic mice (Figure R.2A). It was previously shown that inactivation of the three functional EF hands in bGCAP2 abolishes its capacity to bind Ca^{2+} (Dizhoor *et al.* 1996).

4.3. RESULTS

4.3.1. Transgenic expression of bEF$^-$GCAP2 in mouse rods leads to progressive retinal degeneration

To generate transgenic mice we expressed the cDNA of the bovine GCAP2 isoform, so that the transgene product could be distinguished from the endogenous murine form by SDS-PAGE electrophoretic mobility. To discriminate the effect of the mutations in GCAP2 from the effect that overexpression of GCAP2 might have on the cell, we included in the study a control transgenic line that expresses wildtype bovine GCAP2 (line E, Figure R.2A,B). This line was reported to express wildtype bovine GCAP2 at a ~2:1 ratio relative to endogenous GCAP2 (Mendez *et al.* 2001).

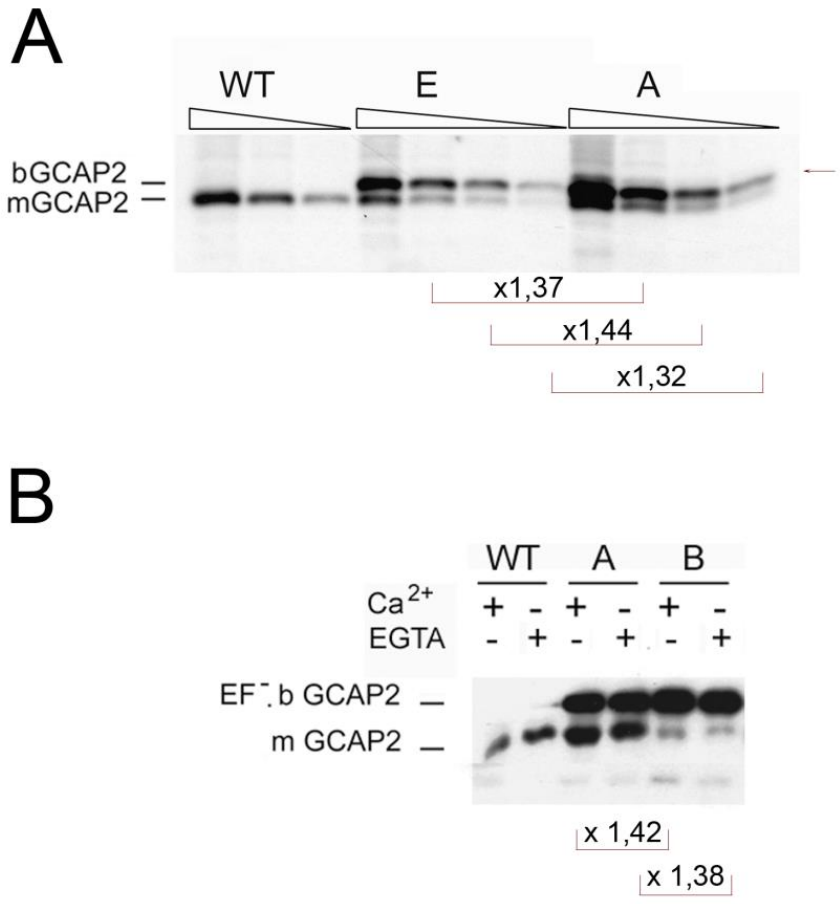

Figure R.1. ***Determination of bEF$^-$GCAP2 transgenic expression levels in lines A and B. A.*** *The level of expression of bEF$^-$GCAP2 in line A was determined by direct comparison with that of bGCAP2 in line E, by loading in the same gel two-fold serial dilutions of a retinal homogenate representing 1/40 of a retina. Expression of bEF$^-$GCAP2 was determined to be 1.38-fold higher (± 0.06 St Dev) than that of bGCAP2 in control line E. Because line E was previously established to express 2-fold the endogenous levels of GCAP2 (Mendez et al. 2001), line A is determined to express 2,76-fold the endogenous levels of GCAP2. B. Likewise, by comparison to line A, line B was determined to express 1.4-fold more transgene, or 3.86-fold the endogenous GCAP2 levels.*

We established two independent transgenic lines that expressed different levels of bEF$^-$GCAP2. Line A expressed bEF$^-$GCAP2 at a ratio of 2.76:1 relative to endogenous GCAP2, whereas line B had a higher relative level of expression (3.85:1 ratio), Figure. R.2B and Figure R1.1, see Methods.

To assess whether bEF$^-$GCAP2 expression in rods causes compensatory changes in the expression levels of other proteins involved in cGMP metabolism, we compared the level of expression of PDE6 and Ret-GCs in retinal homogenates from wildtype and transgenic mice from lines A and B (Figure R.2C). Levels of PDE α, β and γ subunits, or GC1 and GC2 were mostly unaffected in mice from line A, whereas a reduction in all proteins was observed in line B at postnatal day 22 (p22), which can be explained by the dramatic shortening and disorganization of rod outer segments observed from a very early age in this line (Figure R.2D).

Mice expressing bEF$^-$GCAP2 showed a progressive retinal degeneration whose severity correlated with the level of expression of the transgene. Figure R2.D shows normal retinal morphology in the control transgenic line E at p40 and at 3 months of age. In contrast, clear signs of retinal degeneration were observed in mice expressing bEF$^-$GCAP2 from lines A and B. Mice from line B, which express the highest levels of bEF$^-$GCAP2, presented a substantial shortening of rod outer segments and a noticeable reduction of outer nuclear layer (ONL) thickness as early as p40, with ONL thickness reduced to 6-7 rows of nuclei. Mice from line A showed a slower progression of the disease, noticeable at 3 months, when the ONL thickness was reduced to 7-9 rows of nuclei.

Because expression of wildtype bGCAP2 did not cause retinal degeneration for up to one year of age in line E (results not shown), the retinal degeneration observed in mice from lines A and B likely results from distinctive properties of the mutant form of GCAP2 impaired to bind Ca^{2+}. However, due to the different transgene expression levels, we could not exclude that the observed phenotype may result from overexpression of bGCAP2. To rule out this possibility, we bred the control line E to homozygosity, to obtain a line that expressed bGCAP2 to equivalent levels as mutant line A. This line showed normal outer segment length and organization, as well as normal outer nuclear layer thickness for up to six months of age when raised in cyclic light (López-del Hoyo *et al.* 2012). From these results we conclude that mutations that impair Ca^{2+} binding in GCAP2 lead to retinal degeneration *in vivo*.

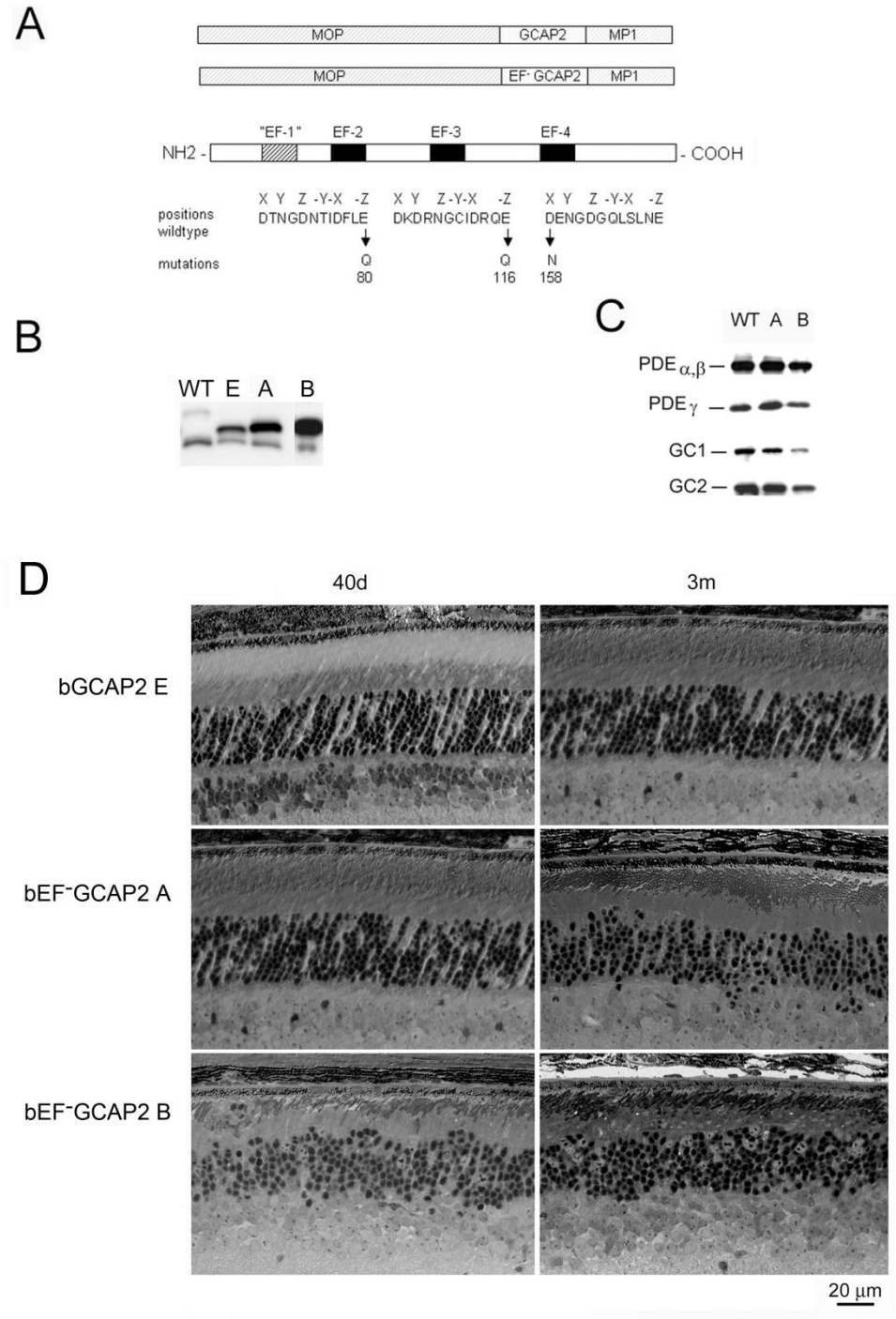

Figure R.2. ***Transgene expression of EF-GCAP2 in rods leads to retinal degeneration. A****. Design of transgene expression vector. The cDNA of bovine GCAP2 with the three functional EF hands disrupted [GCAP2 (E80Q, E116Q, D158N) or EF-GCAP2] was expressed under the mouse opsin promoter (MOP), with the polyadenilation signal of the mouse protamine 1 (MP1) gene.* ***B.*** *Western showing the level of expression of the transgene in bGCAP2 line E and bEF-GCAP2 lines A and B, compared to wildtype mice. Equivalent fractions of a retina were resolved by SDS-PAGE from wt (22d of age), line E (40d) and lines A (40d) and B (22d, showed from independent gel). An earlier time point was chosen for the strongest line (B) to reduce the effect that its rapid retinal degeneration has on total retinal protein content. Bovine and murine GCAP2 differ in size by three amino acids and can be distinguished by mobility.* ***C.*** *Compensatory changes in proteins involved in cGMP metabolism were not observed. The levels of PDEα,β and γ subunits, or GC1 and GC2 were mostly unaffected in mice from line A, whereas a reduction in all proteins was observed in line B at 22d of age, due to the shortened outer segments in this line.* ***D.*** *Light micrographs of retinal sections from mice expressing bGCAP2 (line E) or bEF-GCAP2 transgene (lines A and B) in the GCAPs+/+ background at 40d or 3m.*

4.3.2. Retinal degeneration by bEF-GCAP2 is reproduced in the GCAPs -/- background, and correlates with the loss of visual function.

Mutations in the GUCA1A and GUCA1B genes show an autosomal dominant pattern of inheritance of the associated retinal dystrophies. Therefore, transgene expression of mutant GCAPs in the normal GCAPs+/+ genetic background should constitute good models of the disease. However, the presence of the endogenous GCAPs interferes with the study of the mutant protein localization and function in the cell. Hence we bred the transgenic lines to GCAPs-/- mice, to study the effects of the mutant protein on cell physiology.

The relative levels of expression of the transgene in the independent transgenic lines were maintained in the GCAPs-/- background (Figure R.3A). Expression of bEF-GCAP2 in the GCAPs-/- background slightly accelerated the rate of retinal degeneration observed in the GCAPs+/+ background. Mice from the control lines GCAPs-/- and GCAPs-/- bGCAP2 E showed largely normal retinas with an outer nuclear layer (ONL) thickness of 10 rows of nuclei for up to 5 months of age (Figure R.3B), and preserved normal visual function when raised in cyclic light conditions as assessed by electroretinogram (ERG) (López-del Hoyo *et al.* 2012). In contrast, GCAPs-/- expressing bEF-GCAP2 showed a progressive retinal degeneration that correlated with loss of visual function (Figure R.4). In retinas from line B the ONL was reduced to six rows of nuclei and outer segments were much shorter than normal as early as p30 (Figure R.3B), when the A and B-wave amplitudes of ERG responses were half the size of normal responses from littermate controls (not shown). At 3 months of age the ONL was reduced to 4 rows of nuclei, and by 5 months it was limited to a single row. Mice were unresponsive to light (flat ERG traces) by 7 months (Figure R.4). A slightly slower retinal degeneration was observed in mice from line A that went from a normal outer nuclear layer thickness of 12 rows of nuclei at p30 to about 5 rows by 3 months of age. ERG responses of these mice resembled normal responses at very early ages, but A- and B-wave amplitudes were reduced by half by 4 months, correlating with a dramatic cell loss in these mice between p20 and 5 months of age (Figure R.3B and Figure R.4). Most of these mice are non responsive to light by ERG by 7-8 months (Figure R.4).

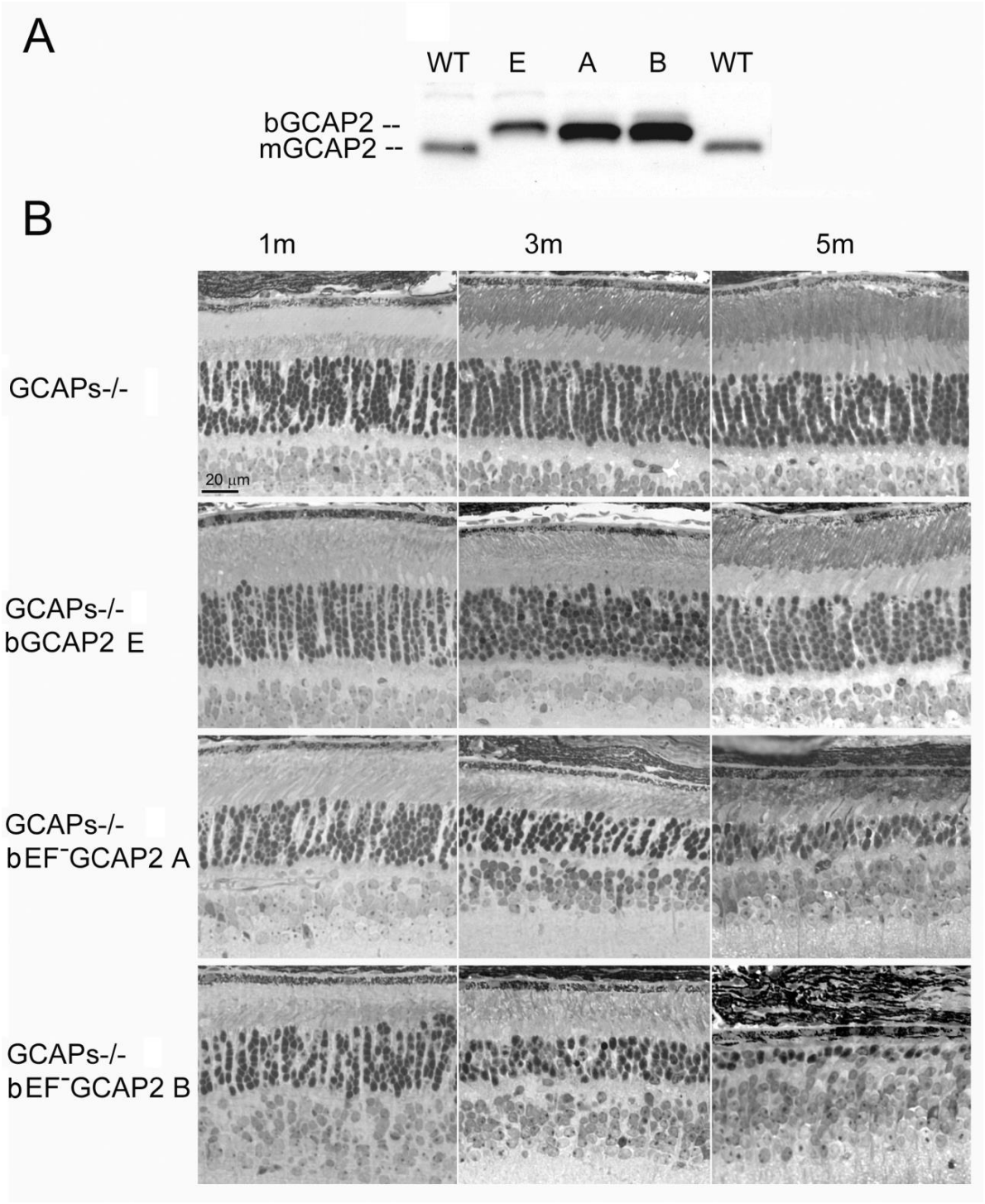

Figure R.3. ***Transgenic expression and rate of retinal degeneration in the GCAPs-/- background.*** ***A****. Levels of transgene expression in the GCAPs-/- background in mouse retinas from line E (ctrl bGCAP2) and lines A, B (bEF-GCAP2). Equal fractions of the retina were loaded from mice at 30d of age. Transgene expression levels estimated in the GCAPs+/+ background were maintained in the GCAPs-/- background.* ***B****. Light micrographs of retinal sections from mice of the indicated genotypes at 1, 3 and 5 months of age, standard cyclic light rearing. Lines A and B show a progressive retinal degeneration in the GCAPs-/- background, that reduces the ONL thickness to 4-5 rows of nuclei at three months, and to 3 rows at five months (line A) or to a single row by five months of age (line B).*

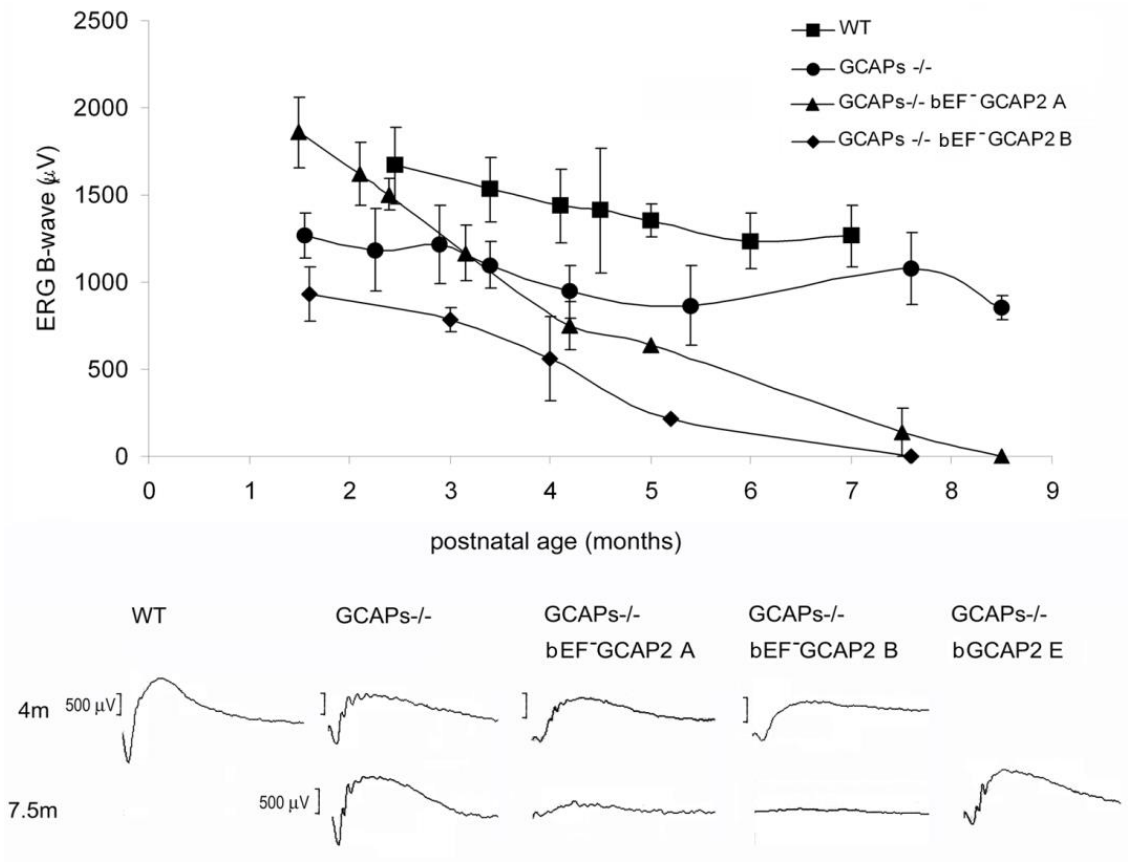

Figure R.4. ***Timecourse for the loss of visual function in bEF⁻GCAP2 expressing mice as assessed by electroretinogram.*** *ERG B-wave amplitudes (μV) are plotted to postnatal age of mice (months). Representative ERG responses are shown for each phenotype at 4 and 7.5 months of age.*

4.3.3. bEF⁻GCAP2 protein accumulates in inactive form at the inner segment of the cell

In vitro studies have shown that recombinant bEF⁻GCAP2 leads to maximal activation of RetGCs in reconstitution studies using washed bovine rod outer segment membrane preparations independently of free Ca^{2+} in the whole physiological range of [Ca^{2+}] (Dizhoor and Hurley 1996). To assay whether the transgenic bEF⁻GCAP2 protein has the capacity to activate RetGC activity in retinal extracts from mice in a similar manner as in *in vitro* studies we performed guanylate cyclase activity assays in retinal extracts from the mutant or control mice obtained prior to significant retinal degeneration - between p20 and p30- under 0μM Ca^{2+} or 2μM Ca^{2+} (Figure R.5).

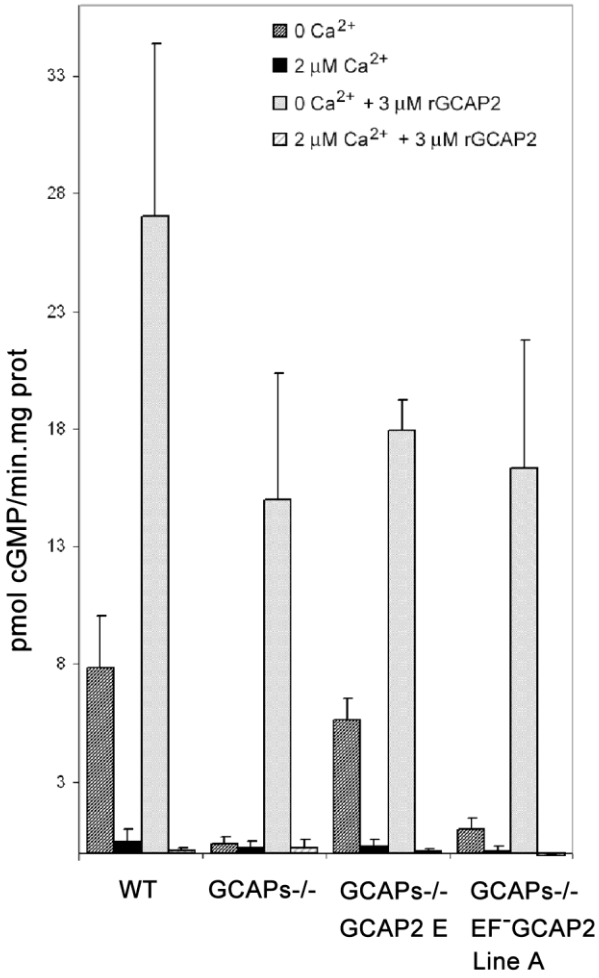

Figure R.5. *Guanylate cyclase activity in retinal homogenates of transgenic mice at 0 [Ca^{2+}] and 2µM [Ca^{2+}]. Guanylate cyclase activity (pmol cGMP/min.mg prot) was determined in WT, GCAPs-/-, GCAPs-/- bGCAP2 line E and GCAPs-/- bEF^{-}GCAP2 line A retinal extracts at 0 [Ca^{2+}] or 2 µM [Ca^{2+}] conditions, in the absence or presence of 3 µM recombinant GCAP2. In WT retinal homogenates at 0 [Ca^{2+}] the endogenous GCAPs activate RetGC activity about 8-fold over the activity at 2 µM [Ca^{2+}]. This stimulation of RetGC activity at 0 [Ca^{2+}] is lost in GCAPs-/- retinal homogenates, but restored in the GCAPs-/- bGCAP2 line E, which indicates that the control bGCAP2 protein expressed in vivo as a transgene is active in these assays. However, retinal homogenates from GCAPs-/- bEF^{-}GCAP2 line A mice showed greatly reduced RetGC activity at 0 [Ca^{2+}] and no activity at 2 µM [Ca^{2+}] conditions. Addition of 3µM recombinant GCAP2 elicited activation of RetGC at 0 [Ca^{2+}] in all retinal homogenates, indicating the presence of functional RetGC in all samples. These results show that bEF^{-}GCAP2 was present, but mostly inactive, in GCAPs-/- bEF^{-}GCAP2 line A retinal homogenates. Results show the mean and standard deviation of at least four independent experiments.*

Ca^{2+}-dependent modulation of RetGC activity was observed in retinal homogenates from wildtype mice and control GCAPs-/- bGCAP2 E line. As expected, the Ca^{2+}-sensitive guanylate cyclase activity was undetectable in GCAPs-/- retinal extracts, indicating that the guanylate cyclase activity that is measurable in whole mouse retinal extracts originates essentially from photoreceptor cells in a GCAPs-dependent manner. As a control for the presence of functional RetGCs in retinal extracts, guanylate cyclase activity was also measured after addition of 3µM recombinant

bGCAP2, which restored robust activity in a Ca^{2+} dependent manner. Surprisingly, retinal extracts from GCAPs-/- bEF$^-$GCAP2 B mice resembled those of GCAPs-/-. They showed little detectable retGC activity at either 0 Ca^{2+} or high Ca^{2+}. Even though the levels of Ret-GCs and bEF$^-$GCAP2 were reduced to some extent in these retinal extracts due to the shortening of the rod outer segments in this line, the addition of recombinant bGCAP2 showed that there was functional RetGCs in these extracts at levels that were sufficient to elicit a measurable activity. The results shown are the average of four independent experiments. These results indicate that while the transgenic bGCAP2 control protein expressed in the GCAPs-/- background reproduced normal activity, the transgenic mutant form of bGCAP2 impaired to bind Ca^{2+} showed very little detectable activity *in vivo*.

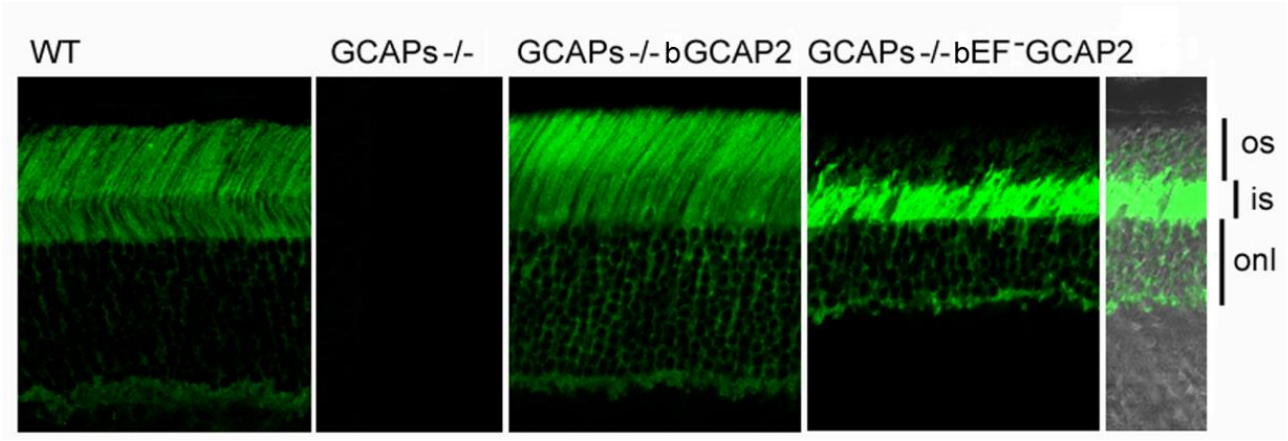

Figure R.6. *b**EF$^-$GCAP2 mislocalizes in transgenic retinas, accumulating at the inner segment compartment of the cell.** Cryosections of central retina from WT, GCAPs-/-, GCAPs-/- bGCAP2 line E and GCAPs-/- bEF$^-$GCAP2 line B, immunostained with an anti-GCAP2 polyclonal Ab. Endogenous GCAP2 in WT retinas distributes to the cytosolic space of rod cells, at the rod outer segment, inner segment, outer nuclear and outer plexiform layers of the retina. This pattern of staining is lost in GCAPs-/- retinas and restored in GCAPs-/-bGCAP2 line E retinas. However, in GCAPs-/- bEF$^-$GCAP2 line B the pattern of staining is shifted, with the GCAP2 signal being much stronger at the inner segment and proximal compartments of the cell than at the outer segment. os, outer segment; is, inner segment; onl, outer nuclear layer.*

To study whether the bEF$^-$GCAP2 protein reproduced the localization pattern of endogenous GCAP2 in transgenic mice, we immunostained GCAP2 in retinal cryosections. Whereas transgenic bGCAP2 in the control line mimicked the localization of endogenous GCAP2 in wildtype retinas (staining the outer segment, inner segment, cytosol of outer nuclear layer and outer plexiform layers of the retina, with the signal being most intense at rod outer segments); this pattern was shifted in the case of bEF$^-$GCAP2, with the signal being most intense at the rod proximal compartments, particularly at the inner segment layer (Figure R.6). These results show that bEF$^-$GCAP2, when expressed in the GCAPs-/- background, tend to accumulate at the metabolic compartment of the cell.

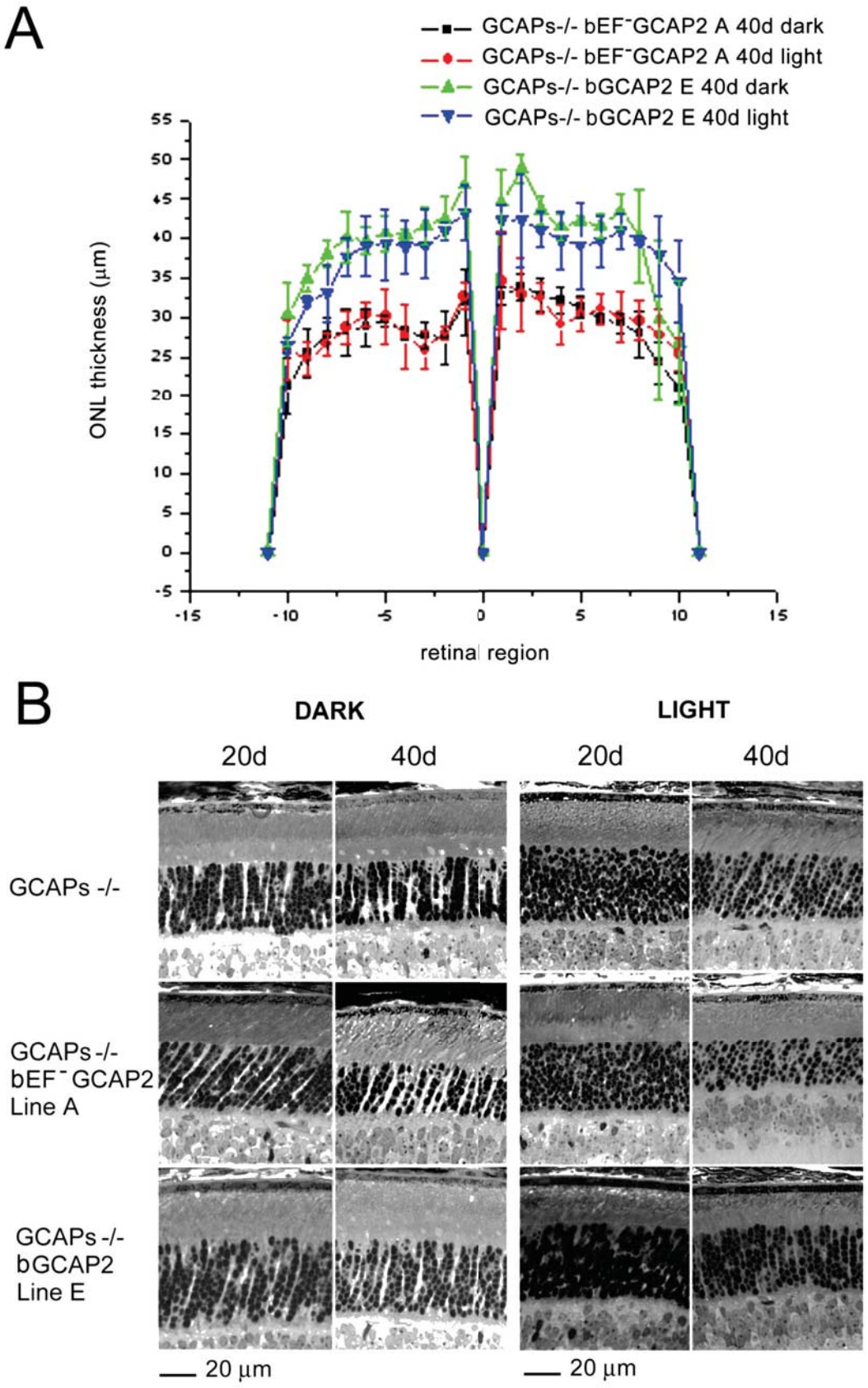

Figure R.7. Light-rearing does not prevent or delay retinal degeneration in bEF-GCAP2 transgenic mice. *Rationale. If bEF-GCAP2 expression led to unabated cGMP synthesis in vivo and accumulation of cGMP was the basis of the pathology, then conditions of constant light exposure would slow the retinal degeneration by causing the sustained activation of PDE6 activity and cGMP hydrolysis. Light induced*

sustained cGMP hydrolysis would counteract unabated cGMP synthesis. ***A.*** *Statistical comparison of ONL thickness at fixed regions along the central retina between bEF-GCAP2 transgenic mice reared in complete darkness or under constant light exposure (1,500 lux fluorescent light) at postnatal day 40. Measurements of ONL thickness (μm) were taken at ten equal intervals along the superior and inferior hemispheres of the retina, indicated in abscissas as positive values (superior retina) and negative values (inferior retina) from the optic nerve (position 0). The superimposition of the red and black lines indicate that retinal degeneration (shortening of ONL thickness along the retina) was observed to the same extent in dark-reared or constant light-reared bEF-GCAP2 mice. ONL thickness in GCAPs-/- bGCAP2 line E control mice are shown as a reference of normal retina values.* ***B.*** *Representative pictures from central superior retinas of dark-reared and constant light-reared GCAPs-/- bEF-GCAP2 line A and control mice at 20 and 40 postnatal days.*

These results indicate that bEF-GCAP2 in the retinas of transgenic mice has a greatly reduced capacity to activate the cyclase and accumulates at the inner segment of the cell, indicating that the pathology in these mice does not result from unabated cGMP synthesis. Furthermore, the retinal degeneration in bEF-GCAP2 mice could not be prevented by raising the mice in constant light exposure that would counteract the increase in cGMP synthesis by continuous cGMP hydrolysis (Figure R.7), as was the case in Y99C-GCAP1 mice (Woodruff *et al.* 2007).

Taken together, these results point to a mechanism independent of cGMP metabolism as the molecular basis for the neurodegeneration in these mice.

4.3.4. bEF-GCAP2 protein is phosphorylated to high levels in vivo and binds to 14-3-3 in a phosphorylation-dependent manner

We reasoned that the accumulation of bEF-GCAP2 at the proximal compartments of the cell rather than its absence at the rod outer segment was the cause of the progressive retinal degeneration in these mice, given that the absence of GCAP1 and GCAP2 in GCAPs-/- mice does not affect gross retinal morphology (Mendez *et al.* 2001). To address why bEF-GCAP2 fails to be distributed to the rod outer segment and how its retention and accumulation at the inner segment leads to toxicity, we investigated the protein-protein interactions that the mutant form of the protein establishes in a specific manner. Immunoprecipitation assays were conducted with an anti-GCAP2 monoclonal antibody cross-linked to magnetic beads, using Triton X100-solubilized whole retinal extracts from GCAPs-/- bGCAP2 E and GCAPs-/- bEF-GCAP2 B mice. Retinal extracts from GCAPs-/- mice were carried to define the background. The pool of proteins immunoprecipitated in each case was identified by directly subjecting the elution fractions to trypsin-digestion and liquid chromatography-tandem mass spectrometry analysis (LC-MS/MS). We searched for proteins identified in the GCAPs-/- bEF-GCAP2 B sample with an spectral counting at least 1.5-fold over

the GCAPs-/- bGCAP2 and GCAPs-/- control lines). We found that only the distinct isoforms of 14-3-3 proteins fulfilled these criteria, being identified with a considerably higher number of peptides [1.33 to 3.2-fold higher] in the GCAPs-/-bEF$^-$GCAP2 B than in control samples in at least two independent experiments (Table R.1). Spectral counting of 14-3-3 isoforms were between 1.6-fold and 5-fold higher in the GCAPs-/-bEF$^-$GCAP2 B samples than in control samples in the two experiments (Table R.2).

				Exp 1			Exp 2		
Protein	**UniProtKB/ Swiss-Prot entry name**	**Primary accession number**	**Gene name**	**line E**	**line B**	**ctrl**	**line E**	**line B**	**ctrl**
GCAP 2	GUC1B-BOVIN	P51177	GUCA1B	12	10	0	9	6	0
14-3-3 protein ε	1433E-MOUSE	P62259	Ywhae	11	19	6	5	10	5
14-3-3 protein γ	1433G-MOUSE	P61982	Ywhag	9	12	4	4	8	3
14-3-3 protein ζ/δ	1433Z-MOUSE	P63101	Ywhaz	7	15	9	6	9	6
14-3-3 protein β/α	1433B-MOUSE	Q9CQV8	Ywhab	6	13	6	0	8	0
14-3-3 protein τ	1433T-MOUSE	P68254	Ywhaq	5	16	5	3	7	3

Table R.1: ***Proteins identified by LC-MS/MS in GCAP2 immunoprecipitation experiments***. *The table lists proteins identified in GCAP2 immunoprecipitation assays from retinal homogenates of GCAPs-/- GCAP2 line E, GCAPs-/- EF$^-$GCAP2 line B and GCAPs-/- mice (ctrl). Data is shown from two independent experiments (three columns per experiment). Last six columns indicate the number of peptides identified for each protein in each sample, indicative of the relative levels of coimmunoprecipitated proteins. GCAP2 was immunoprecipitated to similar levels in control line E and mutant line B, but 14-3-3 isoforms coimmunoprecipitation with GCAP2 occurred substantially more efficiently in mutant line B than in control line E, indicating 14-3-3 selective binding to GCAP2 locked in its Ca^{2+}-free form. GCAP2, guanylate cyclase activating protein 2.*

				Exp 1						
				bGCAP2 ctrl line E		bEF-GCAP2 Line B		GCAPs -/- ctrl		Ratio of spectra (EF-GCAP2 / ctrl line E) normalized to ratio of GCAP2 spectra (EF-GCAP2 / ctrl line E)
				peptides	spectra	peptides	spectra	peptides	spectra	
Guanylate cyclase activating protein 2	GUC1B-BOVIN	P51177	GUCA1B	12	49	10	140	0	0	x1
14-3-3 protein epsilon	1433E-MOUSE	P62259	Ywhae	11	28	19	134	6	12	x1.9
14-3-3 protein gamma	1433G-MOUSE	P61982	Ywhag	9	11	12	47	4	7	x1.6
14-3-3 protein zeta/delta	1433Z-MOUSE	P63101	Ywhaz	7	10	15	59	9	15	x2.1
14-3-3 protein beta/alpha	1433B-MOUSE	Q9CQV8	Ywhab	6	8	13	45	6	9	x2.1
14-3-3 protein theta	1433T-MOUSE	P68254	Ywhaq	5	7	16	50	5	8	x2.6
14-3-3 protein eta	1433F_MOUSE	P68510	Ywhah	5	7	13	40	3	6	x2
14-3-3 protein sigma	1433S_MOUSE	O70456	Sfn	3	5	4	22	0	0	x1.7
				Exp 2						
				bGCAP2 ctrl line E		bEF-GCAP2 Line B		GCAPs -/- ctrl		Ratio of spectra (EF-GCAP2 / ctrl line E) normalized to ratio of GCAP2 spectra (EF-GCAP2 / ctrl line E)
				peptides	spectra	peptides	spectra	peptides	spectra	
Guanylate cyclase activating protein 2	GUC1B-BOVIN	P51177	GUCA1B	9	44	6	32	0	0	x1
14-3-3 protein epsilon	1433E-MOUSE	P62259	Ywhae	5	7	10	29	5	5	x5.6
14-3-3 protein gamma	1433G-MOUSE	P61982	Ywhag	4	5	8	16	3	3	x4.4
14-3-3 protein zeta/delta	1433Z-MOUSE	P63101	Ywhaz	6	8	9	24	6	6	x4.1
14-3-3 protein beta/alpha	1433B-MOUSE	Q9CQV8	Ywhab	0	0	8	17	0	0	ND
14-3-3 protein theta	1433T-MOUSE	P68254	Ywhaq	3	4	7	15	3	3	x5.1

Table R.2: ***Spectral counting of Proteins identified by LC-MS/MS in GCAP2 immunoprecipitation experiments***

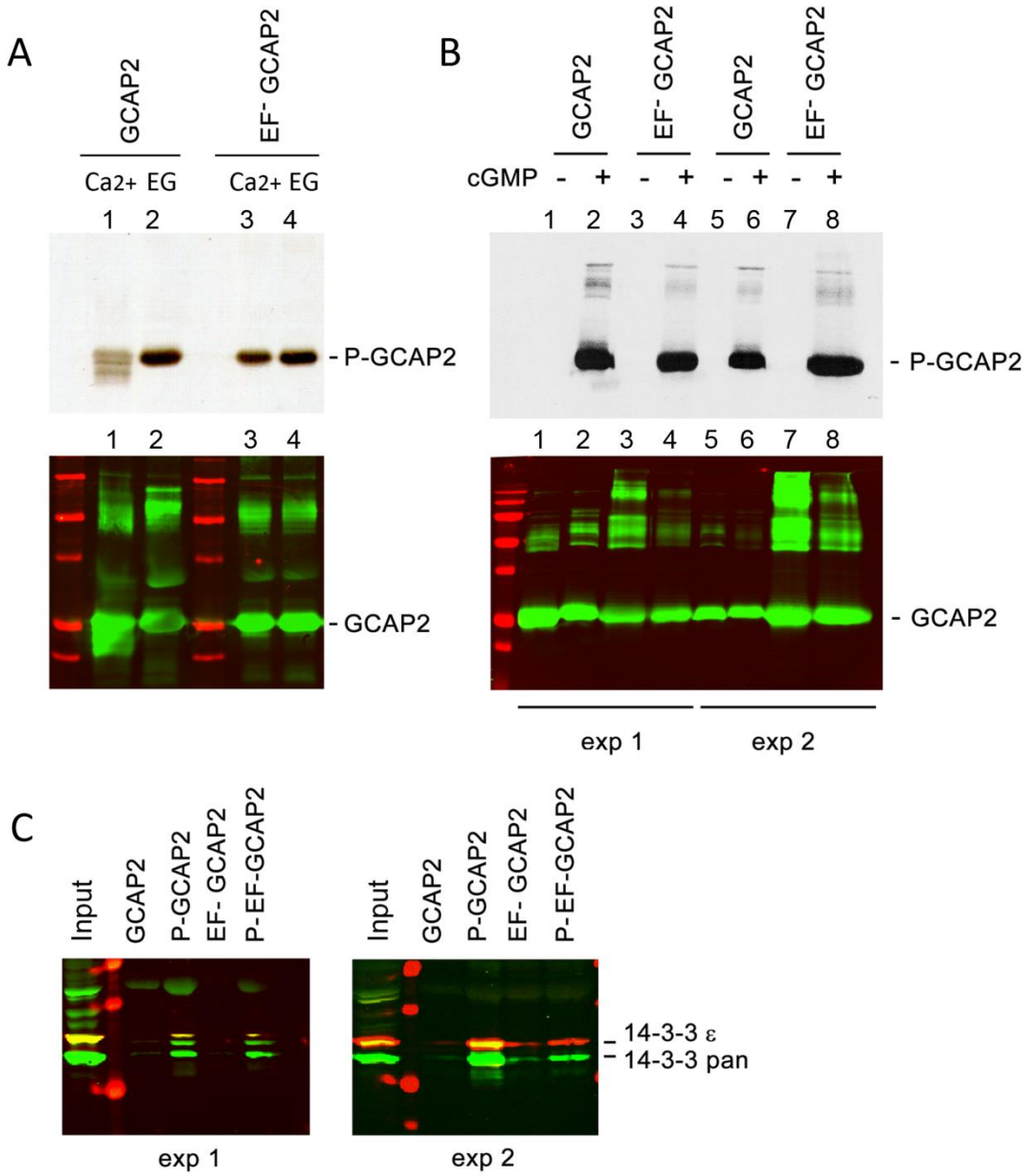

Figure R.8. ***The protein 14-3-3 binds to recombinant GCAP2 in a phosphorylation-dependent manner. A.*** *In vitro, Ca^{2+}-free bGCAP2 is phosphorylated more efficiently than Ca^{2+}-bound bGCAP2. Upper panel shows an autoradiograph of ^{33}P phosphorylation products from an in vitro phosphorylation reaction of recombinant wildtype bGCAP2 or bEF$^-$GCAP2 with protein kinase G (PKG), in the presence or absence of free Ca^{2+}. The 20μ reaction mixture contained 8.5μg of purified recombinant wildtype bGCAP2 or bEF$^-$GCAP2, purified PKGIα (100 units, Calbiochem) and 3μCi of ^{33}P- γATP in phosphorylation reaction buffer, containing either $CaCl_2$ or EGTA (see Methods). After incubation, reaction mixtures were resolved by 15% SDS-PAGE and transferred to a nitrocellulose membrane. Lower panel shows immunostained GCAP2. Recombinant bGCAP2 or bEF$^-$GCAP2 proteins were present to similar amounts in all reaction tubes.* ***B.*** *In vitro phosphorylated or mock-treated bGCAP2 and bEF$^-$GCAP2 were generated for pull-down assays. Phosphorylation reactions were performed as above, in the presence of EGTA, except that cGMP was added to 500μM (+ lanes) or not added (- lanes). Immunostaining of GCAP2 in the same nitrocellulose membrane shows the GCAP2 monomer at 25kDa and upper bands corresponding to dimers and multimers of GCAP2, observed to a higher extent in the EF$^-$GCAP2 lanes. Molecular mass (MW) markers (Precision Plus Protein Standards, BioRad) are 20, 25, 37, 50, 75, 100 and 150 kDa. Experiment shown in duplicate.* ***C.*** *The 14-3-3 protein isoforms bind more efficiently to phosphorylated bGCAP2 and bEF$^-$GCAP2 than to unphosphorylated counterparts.*

Phosphorylated or mock- proteins were cross-liked to magnetic beads and pull-down assays were performed with whole bovine retinal extracts obtained in 1% Triton-X100. Panels show the input and bound fractions for the indicated phospho- or mock-proteins, resolved by 15% SDS-PAGE. Membrane was sequentially incubated with a pAb to 14-3-3pan (IBL International, Hamburg, Germany), a mAb to 14-3-3ε (abcam, Cambridge, UK), an IRDye 800CW Goat Anti-rabbit IgG and an IRDye 680CW Goat Anti-mouse IgG (Tebu-Bio, Offenbach, Germany). Image was acquired at the Odyssey Imaging System (LI-COR). Therefore 14-3-3pan isoforms (30kDa) are shown in green, while 14-3-3ε (33kDa) is shown in red. Experiment shown in duplicate.

Because 14-3-3 proteins typically bind to their targets in response to phosphorylation (Smith *et al.* 2011), and since phosphorylation of GCAP2 has been reported to occur *in vitro* at a conserved Ser at position 201 in bGCAP2 (Peshenko *et al.* 2004b), we next assayed whether the binding of 14-3-3 to GCAP2 was phosphorylation dependent. We first reproduced the observation that GCAP2 can be phosphorylated *in vitro* by PKG, with Ca^{2+}-free bGCAP2 being a better substrate for the kinase than Ca^{2+}-loaded bGCAP2 (Figure R.8A). Subsequently, we used recombinant bGCAP2 or bEF$^-$GCAP2 in *in vitro* phosphorylation reactions with PKG to generate phosphorylated-bGCAP2 or mock-treated bGCAP2 for pull-down assays with bovine whole retinal homogenates (Figure R.8B). As seen in Figure R.8C, 14-3-3 showed preferential binding to the phosphorylated form of bGCAP2 or bEF$^-$GCAP2 in two independent experiments.

The observations that 14-3-3 binds more efficiently to bEF$^-$GCAP2 than to bGCAP2 *in vivo* and that 14-3-3 binds to bGCAP2 in a phosphorylation dependent manner, together with the reported higher efficiency of GCAP2 phosphorylation in its Ca^{2+}-free rather than its Ca^{2+}-bound conformational state led us to hypothesize that bEF$^-$GCAP2 might be abnormally phosphorylated in the living cell. To test this hypothesis we performed a $^{32}P_i$ -metabolic labeling of GCAPs-/- bGCAP2 and GCAPs-/- bEF$^-$GCAP2 retinas *in situ*, followed by GCAP2 immunoprecipitation and SDS-PAGE analysis. Following the incorporation of $^{32}P_i$ into the retinas of dark-adapted mice for 2h, retinas were either kept in darkness or exposed to 5 min of bright white light and immediately subjected to Triton X100-solubilization and GCAP2 immunoprecipitation. GCAPs-/- retinas were carried as a negative control.

Figure R.9A shows equal fractions of the Triton X100-solubilized retinas after $^{32}P_i$-incorporation and 5min dark- or light-exposure. The overall pattern of bands in this panel shows that incorporation of $^{32}P_i$ into the ATP pool of the retina occurred at comparable levels in all samples, allowing the detection of phosphorylated proteins and changes in the overall phosphorylation pattern caused by light (e.g. the light-dependent phosphorylation of rhodopsin is observed at 35-37 kDa). GCAP2 phosphorylation could not be detected in whole retinal extracts, so these samples were used as inputs for the GCAP2 immunoprecipitation assay shown in Figure R.9B.

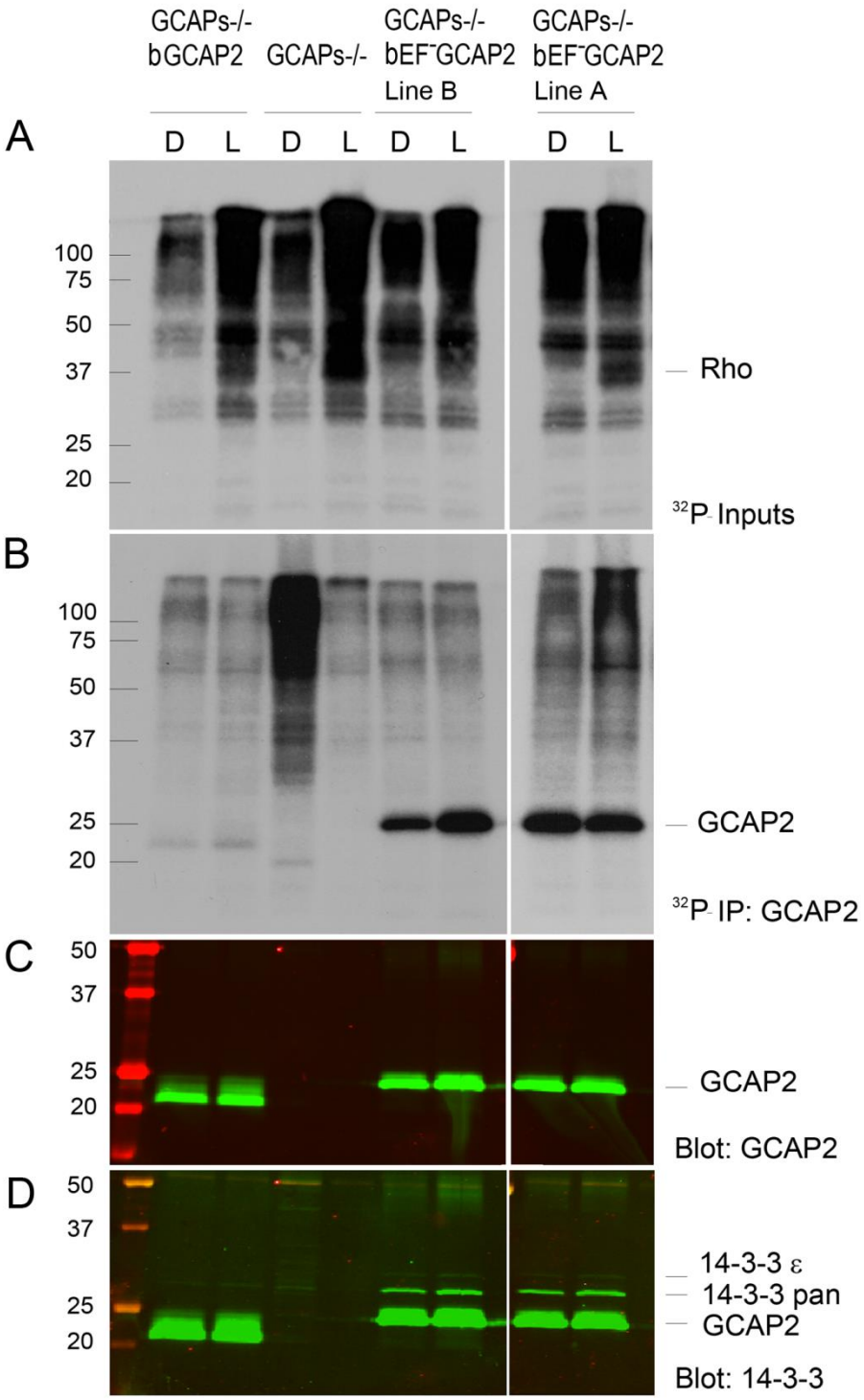

Figure R.9. ***$^{32}P_i$ metabolic labeling reveals phosphorylation of bEF-GCAP2 to a higher extent than bGCAP2 in living retinas. A.*** *In situ phosphorylation assay. Retinas from dark-adapted mice from the indicated phenotypes were dissected under dim red light, incubated in bicarbonate buffered Locke's solution containing 1 mCi/mL of ^{32}P-H_3PO_4 for 90min in a 5% CO_2 incubator and exposed to white light for 5min (L) or maintained in darkness (D). Retinas were homogenized in Triton X100-solubilization buffer and pre-cleared by centrifugation. Aliquots corresponding to one tenth of a retina were resolved by 15% SDS-PAGE and blotted to a nitrocellulose membrane. Phosphorylated proteins were visualized by autoradiography upon 4h of exposure.* ***B.*** *GCAP2 immunoprecipitation in ^{32}P-labeled samples.*

Solubilized samples corresponding to two retinas per phenotype and condition were used as inputs for GCAP2 immunoprecipitation with an anti-GCAP2 mAb. Elution fractions were resolved by 15% SDS-PAGE, blotted to a nitrocellulose membrane and visualized by autoradiography after 4 days of exposure. ***C.*** *Western blot of samples in (B) using a polyclonal antibody anti-GCAP2 show that the amount of GCAP2 in the control GCAPs-/- bGCAP2 E line was comparable to that in mutant lines GCAPs-/- b EF$^-$ GCAP2 A and B.* ***D.*** *Immunostaining of 14-3-3 proteins in the same membrane, by using a pAb to 14-3-3pan (IBL International, Hamburg, Germany).*

GCAP2 was phosphorylated to low levels in the GCAPs-/- bGCAP2 sample in the dark, and to a slightly higher extent when the retina was exposed to light. No 24 kDa bands were observed in the GCAPs-/- samples. Strikingly high levels of bEF$^-$GCAP2 phosphorylation were observed in GCAPs-/- bEF$^-$GCAP2 samples (lines A and B). A GCAP2 immunoblot of the ^{32}P-labeled membrane confirmed that comparable levels of GCAP2 were immunoprecipitated in GCAPs-/- bGCAP2 and GCAPs-/- bEF$^-$GCAP2 samples (Figure R.9C). Figure R.9D shows the subsequent immunostaining of the 14-3-3 pan and epsilon isoforms in the same membrane, further confirming the selective binding of 14-3-3 to the phosphorylated mutant form of GCAP2 impaired to bind Ca^{2+}.

GCAP2 phosphorylation was further characterized by isoelectrofocusing gel analysis followed by immunoblotting with a GCAP2 antibody (Figure R.10). Under room light conditions wildtype C57BL/6 mice showed two bands of roughly equal intensity corresponding to the pI of the unphosphorylated (4.92) and singly phosphorylated (4.85) mGCAP2. The intensity of the 4.85 band was greatly diminished when NaFl, a broad phosphatase inhibitor, was omitted from the samples, thus confirming the identity of this band as phosphorylated GCAP2 (Figure R.10A). We conclude that about half of the total GCAP2 protein is phosphorylated in wildtype mice under standard room light conditions. The extent to which endogenous mGCAP2 was phosphorylated in wildtype mice under room light conditions was higher than that of bGCAP2 in GCAPs-/- bGCAP2 transgenic mice.

To address whether GCAP2 phosphorylation takes place differentially in dark/light conditions, wildtype mice that were adapted to room light for 1h were dark-adapted for up to 14h, and GCAP2 phosphorylation was analyzed at 1,2,3,5 and 14h.Figure R.10B shows that the ratio of unphosphorylated to phosphorylated GCAP2 did not vary substantially during the 14h dark-adaptation period. If we presume that GCAP2 is preferentially phosphorylated during periods of light exposure when in its Ca^{2+}-free conformation, results may indicate that a few hours of dark- or light-adaptation are not enough to have a noticeable effect on the overall GCAP2 population. This would not be surprising if only newly synthesized GCAP2 was subjected to the kinase/phosphatase regulation (see Discussion).

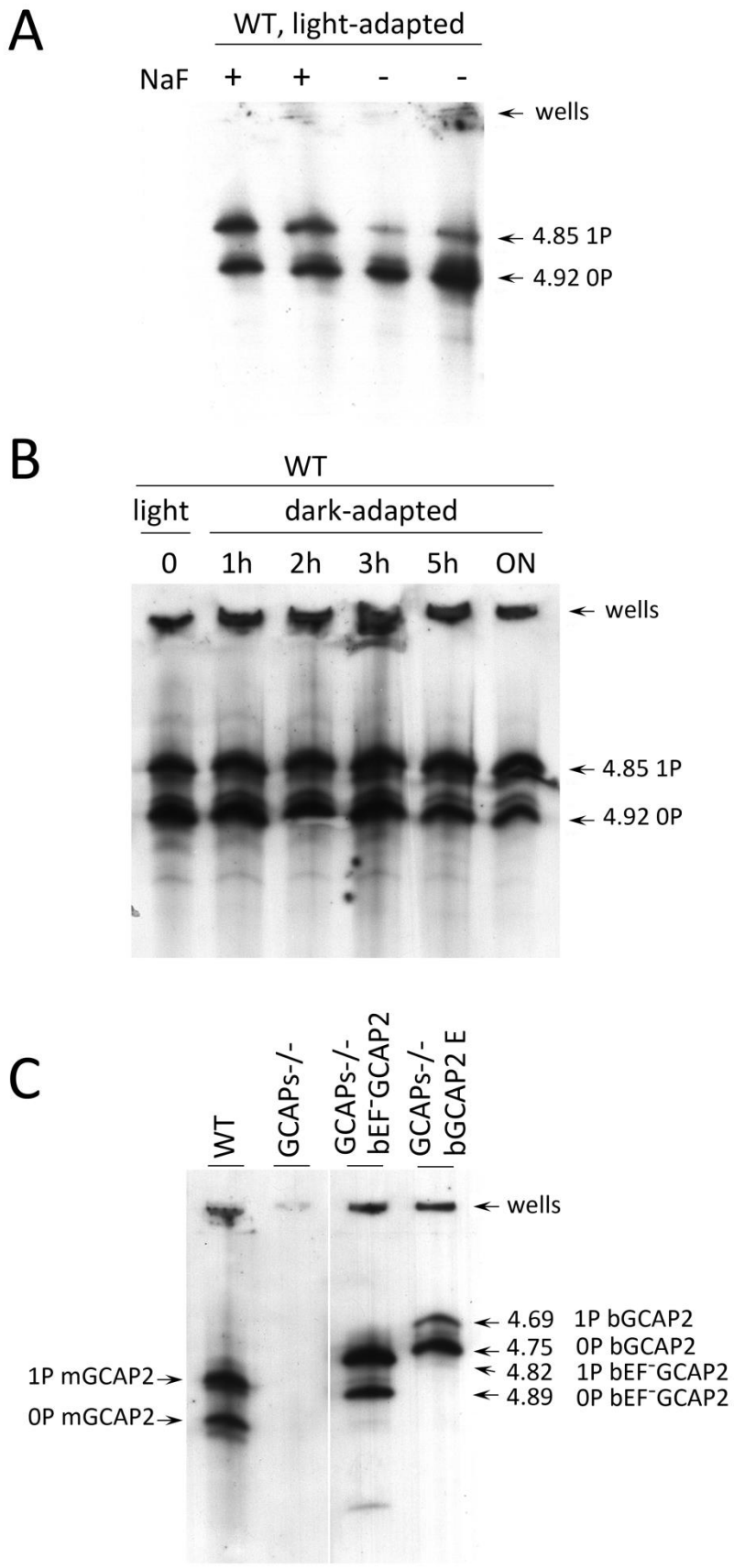

Figure R.10. ***Analysis of GCAP2 phosphorylation by isoelectrofocusing. A***. *Isoelectrofocusing (IEF) gel of light-adapted wildtype mouse retinal homogenates. Mice were light-adapted to room light. Retinas*

were obtained, solubilized in a saline buffer with 1% dodecyl maltoside, in the presence or absence of 50mM NaF (phosphatase inhibitor). Samples were clarified, loaded onto an electrofocusing gel (pH range 3-8) and focused for 2h at 23W. Proteins were transferred to a nitrocellulose membrane and incubated with an anti-GCAP2 Ab. Two prominent bands are observed at 4.92 and 4.85 isoelectric point, that correspond to unphosphorylated and monophosphorylated mGCAP2, respectively. ***B****. The overall phosphorylation status of GCAP2 does not change significantly during a 12h period of dark-adaptation. Mice were light-adapted to room light for 1h, and subjected to dark-adaptation for a period of up to 14h. Retinas were analyzed as above.* ***C****. Analysis of GCAP2 phosphorylation status in the indicated mouse lines. Transgenic bGCAP2 is phosphorylated to a lesser extent than the endogenous mGCAP2, whereas bEF$^-$GCAP2 is phosphorylated to a much higher extent. Note that the isoelectric point of bGCAP2 differs from that of mGCAP2, and that the isoelectric point of bEF$^-$GCAP2 (E80Q,E116Q,D158N GCAP2) is shifted versus that of bGCAP2. Results from the isoelectrofocusing gels confirm that transgenic bEF$^-$GCAP2 is phosphorylated to a much higher extent than the control transgenic bGCAP2.*

Isoelectrofocusing of retinal samples from GCAPs-/- bEF$^-$GCAP2 and GCAPs-/- bGCAP2 were performed to assay the steady-state relative levels of non-phosphorylated and phosphorylated GCAP2 (Figure R.10C). Whereas endogenous GCAP2 in wildtype C57BL/6 mice showed similar proportions of non-phosphorylated and phosphorylated GCAP2, the GCAPs-/- bEF$^-$GCAP2 sample showed a larger fraction of phosphorylated GCAP2 and the GCAPs-/- bGCAP2 sample showed the reverse: a larger fraction of non-phosphorylated GCAP2. These results are consistent with the metabolic labeling results, namely, low levels of phosphorylation in the GCAPs-/- bGCAP2 control line, and much higher phosphorylation levels in the GCAPs-/- bEF$^-$GCAP2 line (Figure R.10C and Figure R.9B).

We next tested whether GCAP2 and 14-3-3 association could be inferred by analysis of solubilized retinal extracts by size-exclusion chromatography, and whether this association was stronger in the mutant than in the control line. Sixteen retinas from GCAPs-/- bEF$^-$GCAP2 or GCAPs-/- bGCAP2 mice were solubilized in 1% Triton X-100 buffer, clarified and separated by size exclusion chromatography in a column with a separation range of 10,000 to 400,000 kDa. Results are shown in Figure R.11. The upper panels show that the peak of GCAP2 appears in the same fraction as the peak of 14-3-3 in retinal extracts from both the mutant and the control lines, indicating an association between both proteins. This association appears stronger in the mutant line, for which the percentage of GCAP2 (from the total) that is present in the same fraction as 14-3-3 is higher than in the control line.

To test whether bEF$^-$GCAP2 might have a higher tendency than bGCAP2 to aggregate and compromise its solubility *in vivo,* the Triton-X100 resistant fraction at the clarification step was solubilized in buffer containing 1% SDS and also subjected to gel filtration. Figure R.11 lower panels show that GCAP2 is more enriched at higher molecular weight fractions in SDS-solubilized samples than in Triton-X100 samples,

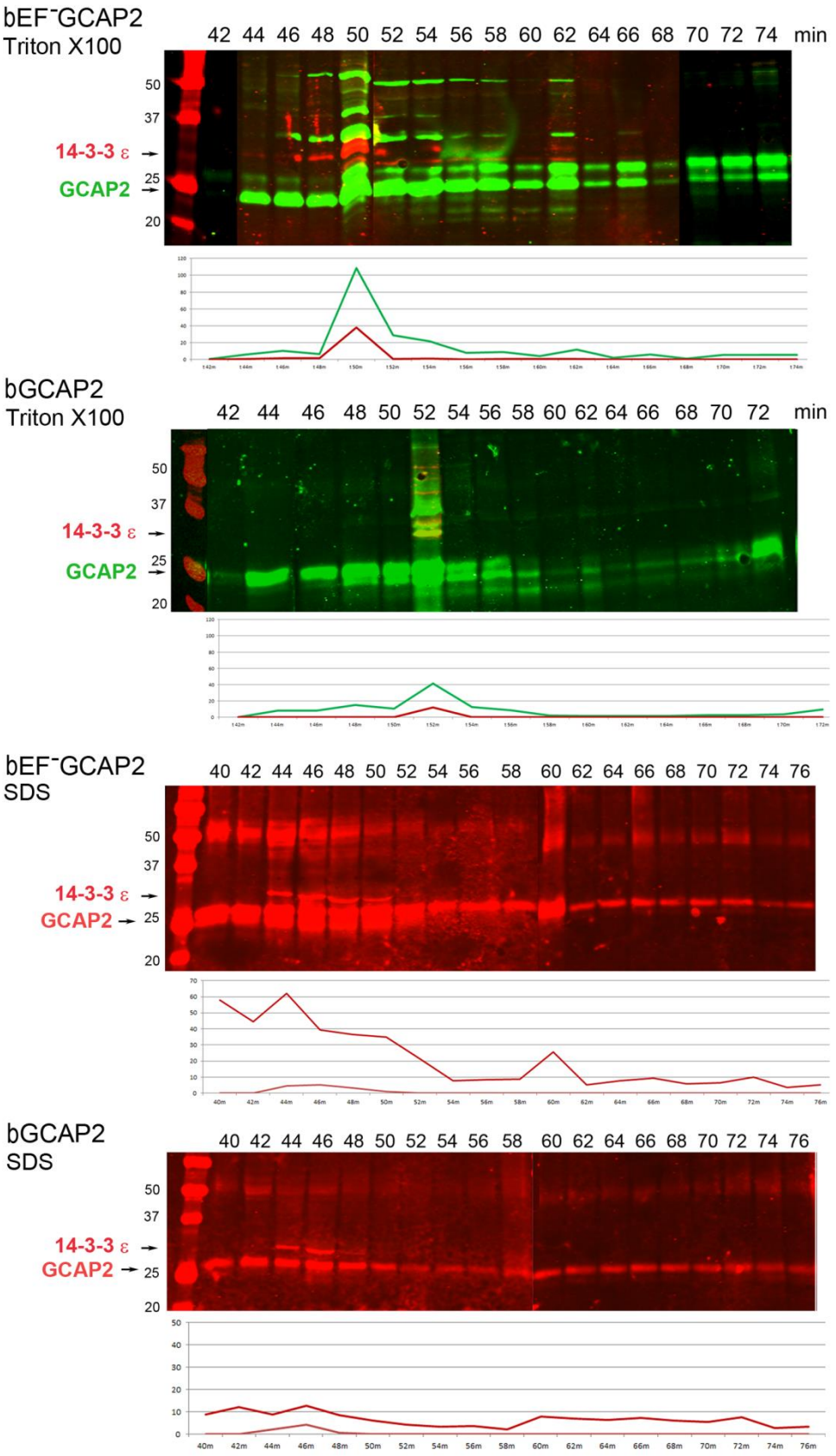

Figure R.11. ***Size-exclusion chromatography analysis of GCAP2 and 14-3-3 in solubilized retinas from bGCAP2 and bEF-GCAP mice.*** *Sixteen retinas from GCAPs-/- bEF-GCAP2 or GCAPs-/- bGCAP2*

mice were obtained at p20-25, and solubilized in buffer containing 1% Triton-X100 (10mM Hepes, 135mM NaCl, 5mM KCl, 1.5mM MgCl2, 2mM EDTA, 1mM PMSF, 1% Triton X100). The Triton-X100-soluble fraction was kept, and the Triton X100-resistant fraction was solubilized in 1% SDS buffer (10mM Hepes, 135mM NaCl, 5mM KCl, 1.5mM MgCl2, 2mM EDTA, 1mM PMSF, 1% SDS). Triton X100-soluble and SDS-soluble fractions were separated in a ultrahydrogel 500 column with a molecular weight range of 10,000-400,000 kDa. Fractions were collected each 2 min, concentrated with 3,000 MWCO Amicons and loaded into a 12% SDS-PAGE. Proteins were transferred to nitrocellulose membranes and incubated with a pAb to GCAP2 (green signal) and a mAb to 14-3-3ε (abcam, Cambridge, UK, red signal) for the two upper panels. For the lower panels, membranes were sequentially incubated with a mAb to GCAP2 (Affinity Bioreagents, Golden, Colorado, USA) and a mAb to 14-3-3ε (abcam, Cambridge, UK), both signals in red. Image was acquired at the Odyssey Imaging System (LI-COR). The integrated intensities of all bands were obtained using the Odyssey software, and the added values for each lane (in arbitrary units) were plotted in the graphs underneath each panel. An association between GCAP2 and 14-3-3 epsilon was observed at the GCAP2 peak fraction in Triton X100-soluble fractions. The percentage of total GCAP2 that maps at the peak fraction with 14-3-3 was higher in the EF$^-$GCAP2 than in the GCAP2 sample. SDS-soluble samples revealed a tendency for GCAP2 to be enriched at higher molecular weight fractions, more clearly manifested at the bEF$^-$GCAP2 than at the bGCAP2 sample.

and this enrichment happens to a higher extent in bEF$^-$GCAP2 samples than in control samples.

To address whether 14-3-3 binding to phosphorylated GCAP2 might be the cause of its retention at inner segments, we analyzed the localization of the 14-3-3 proteins in retinal sections from GCAPs-/- bGCAP2 and GCAPs-/- bEF$^-$GCAP2 samples. Figure R.12 shows that 14-3-3 epsilon localizes to all cell layers of the retina; the ganglion cell layer, the inner cell layer and the photoreceptor cell layer of the retina. In photoreceptor cells it appears to distribute to the inner segment, the perinuclear region and the synaptic terminal, but it is excluded from the outer segment. This isoform of 14-3-3 colocalized with GCAP2 mainly at the inner segment of GCAPs-/- bGCAP2 samples, but also to the perinuclear region and synaptic terminals in the GCAPs-/- bEF$^-$GCAP2 samples. From these results we infer that the localization pattern of 14-3-3ε in photoreceptor cells would be consistent with a role of GCAP2 phosphorylation and 14-3-3 binding at retaining the mutant form of GCAP2 impaired to bind Ca^{2+} at the proximal compartments of the cell.

4.3.5. Phosphorylation at Ser201 is required for the retention of bEF$^-$GCAP2 at the proximal compartments of the photoreceptor cell in vivo

To address whether phosphorylation of GCAP2 is what causes the retention of bEF$^-$GCAP2 at the inner segment and proximal compartments of the cell, we expressed a mutant form of bEF$^-$GCAP2 in which Ser201 was mutated to Gly as a transient transgene in rod cells, given that Ser201 is the only residue that was found to be phosphorylated in GCAP2 (Peshenko *et al.* 2004b).

The bS201G/EF-GCAP2 cDNA was expressed under the rod opsin promoter by subretinal injection and *in vivo* electroporation of the DNA in neonatal GCAPs-/- mice as described (Matsuda and Cepko 2004). Both bGCAP2 and bEF-GCAP2 cDNAs were carried out in parallel in order to compare the localization of the mutants under equivalent experimental conditions. A plasmid expressing the green fluorescent protein (GFP) under the Ubiquitin C promoter was coinjected to identify the region arround the injection site in which DNA transfection was efficient, and electroporated retinas were analyzed at p28.

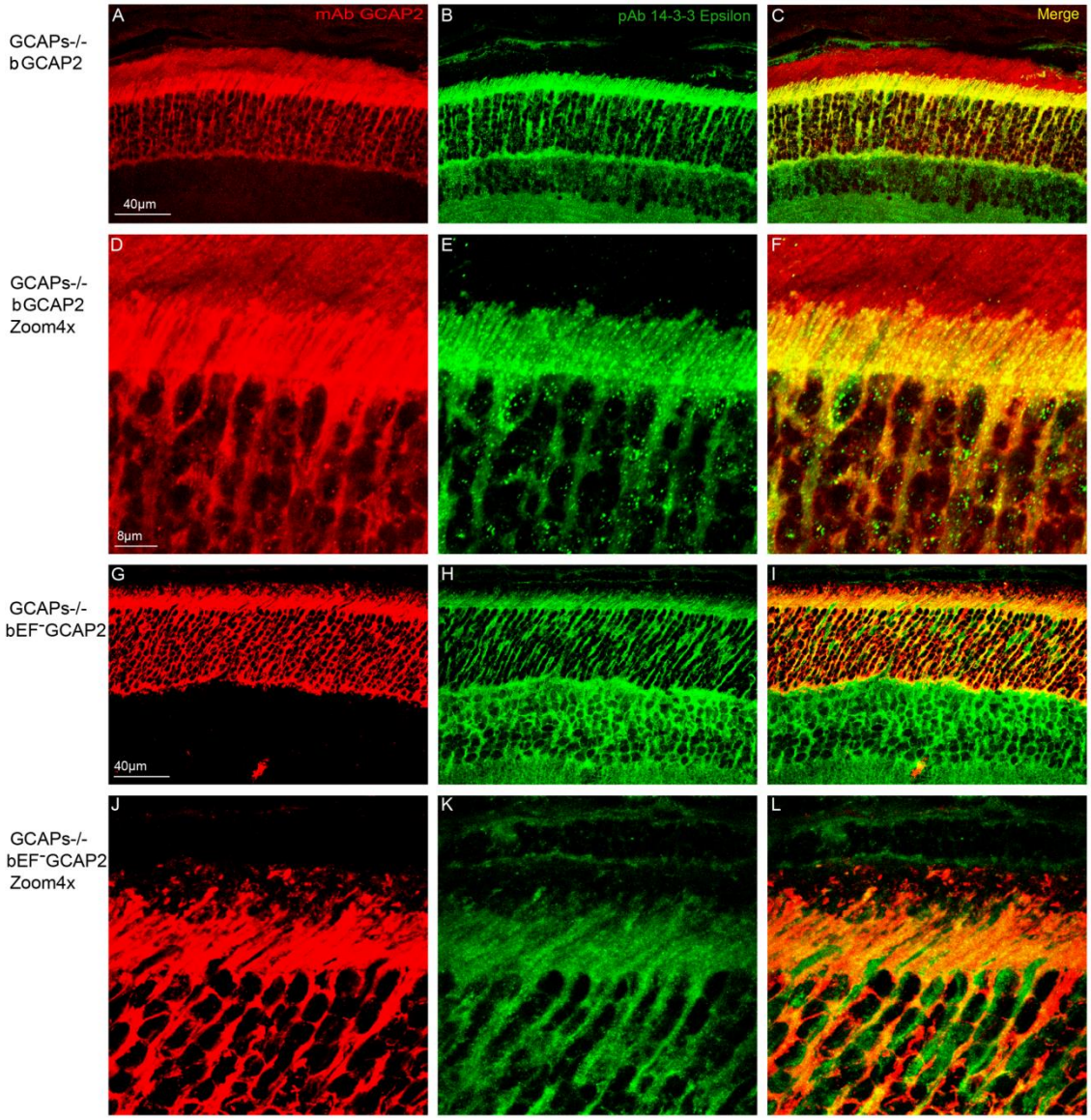

Figure R.12. ***Coimmunolocalization of 14-3-3ε with GCAP2 in retinas from GCAPs-/-GCAP2 E and GCAPs-/- EF-GCAP2 B mice.*** *Cryosections of central retina from the indicated lines at 20 days of age were immunostained with an anti-GCAP2 mAb (Affinity Bioreagents, Golden, Colorado, USA) and an anti-14-3-3ε rabbit monoclonal (abcam, Cambridge, UK), by indirect immunofluorescence staining with the Alexa 488 goat anti-rabbit IgG and Alexa 555 goat anti-mouse IgG (Molecular Probes, Eugene, Oregon). GCAP2 signal in red, 14-3-3ε signal in green. GCAP2 and 14-3-3 proteins colocalize at the inner segment and proximal compartments of photoreceptor cells.*

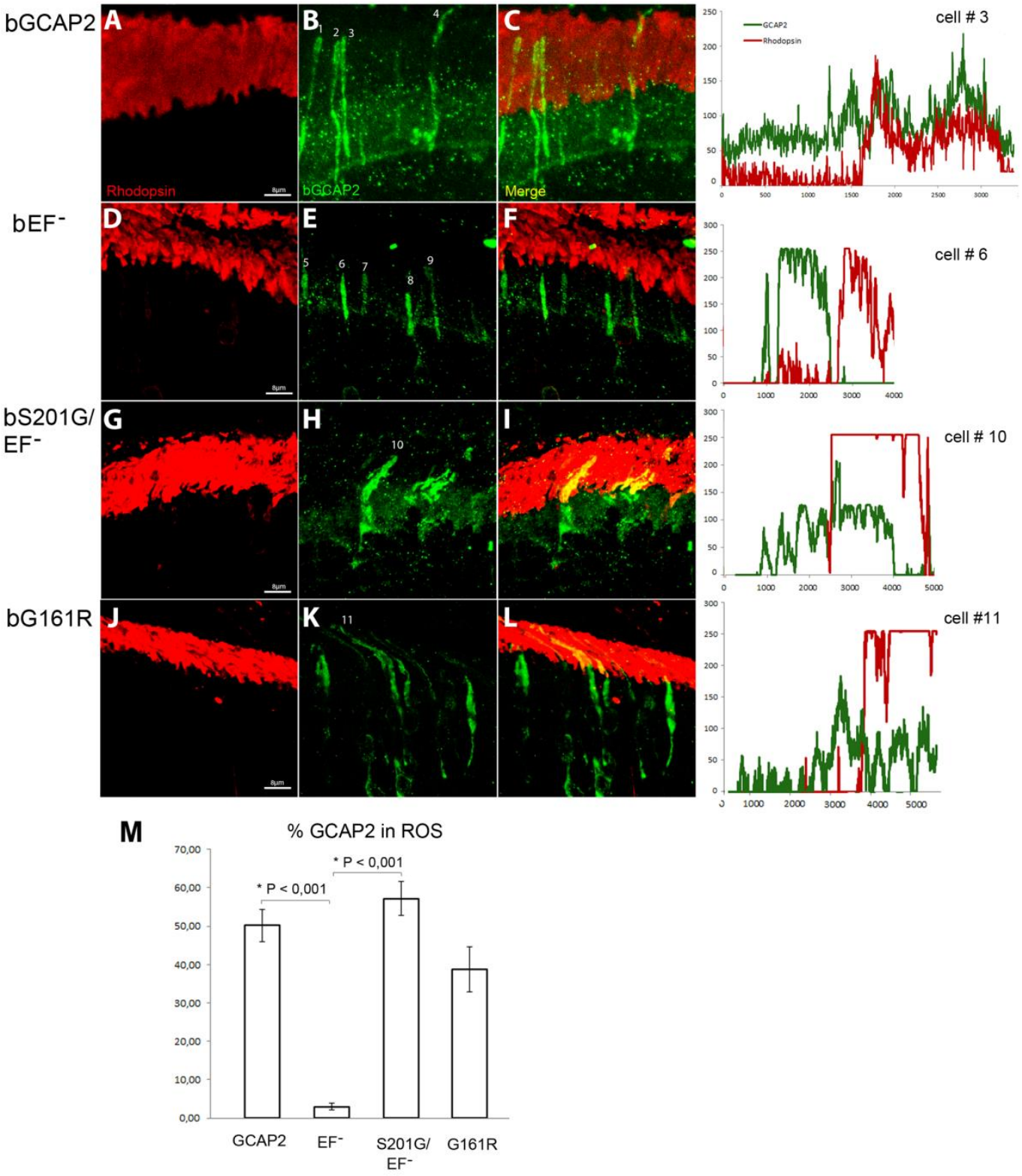

Figure R.13. ***Mutation of Ser201 in bEF-GCAP2 precludes protein retention at the inner segment.*** *Wildtype bGCAP2, bEF-GCAP2, bS201G/EF-GCAP2 or bG161R/GCAP2 were transiently expressed in the rod photoreceptor cells of GCAPs-/- mice by in vivo DNA electroporation of neonates following subretinal injection. A plasmid expressing GFP driven by the Ubiquitin C promoter was coinjected in order to identify transfected areas in the eye at postnatal day 28 (p28). Cryosections were immunostained for GCAP2 with a polyclonal GCAP2 Ab and an Alexa Fluor 555 anti-rabbit IgG (signal converted to green); and for rhodopsin with monoclonal Ab 1D4 and an Alexa Fluor 647 anti-mouse IgG (red signal). Transient expression of wildtype bGCAP2 by electroporation reproduced the reported localization pattern in the stable transgenic line, namely, its almost equal distribution between the inner and outer segments (panels*

B, C). bEF-GCAP2 was mostly retained at the inner segments, being excluded from outer segments (panels E, F, and profile for cell N.6), which also reproduced the observation from the stable bEF-GCAP2 transgenic lines. In contrast, b201G/EF-GCAP2 localized to some extent at the inner segment but mostly distributed to rod outer segments, showing a clear colocalization with rhodopsin (panels H, I, and profile from cell N.10). bG161R/GCAP2 showed, on average, a higher retention at inner segments than the wildtype protein, but an statistical analysis showed no significative difference with wildtype GCAP2 distribution. Panel M shows a histogram of the mean percentage of GCAP2 distribution to ROS for each phenotype and the standard error of the mean, as determined by calculating: (the intensity of GCAP2 that colocalizes with rhodopsin) / (intensity of GCAP2 that colocalizes with rhodopsin + intensity of GCAP2 at the inner segment), see Methods. (Five cells were analyzed for the WT, twelve cells for bEF-GCAP2, thirteen cells for bS201G/GCAP2 and four cells for bG161R/GCAP2).

Figure R.13 shows that the localization of bGCAP2 and bEF-GCAP2 in the transient transgenic mice obtained by electroporation reproduced the localization observed in stable transgenics: specifically, bEF-GCAP2 was retained at the inner segment and proximal compartments of transfected photoreceptors. bEF-GCAP2 was excluded from the outer segment, which is demarcated by rhodopsin immunofluorescence (red) (Figure R.13 panels E, F and profile from cell N.6, Figure R.14 for additional images and profiles). In contrast, the mutant bS201G/EF-GCAP2 distributed to the proximal compartments of the cell but also to rod outer segments. As shown in panels H -I of Figure R.13 and in the profile from cell N. 10, the GCAP2 signal -in green- co-labeled with rhodopsin (red) in all transfected cells (thirteen cells analyzed, 57% of GCAP2 signal co-labeled with rhodopsin on average, see Figure R.14), indicating its redistribution to rod outer segments. On average, 50% of the protein distributed to rod outer segments when bGCAP2 was expressed, whereas virtually all bEF-GCAP2 was retained at the inner segment and proximal compartments. Mutating S201 to Gly in bEF-GCAP2 reverted this retention, resulting in 57% of the protein distributing to rod outer segment (histogram in Figure R.13M).

These results indicate that phosphorylation at Ser201 in the mutant form of GCAP2 impaired to bind Ca^{2+} is what causes its accumulation at the inner segment and proximal compartments of the cell, ultimately leading to toxicity.

4.3.6. Toxicity resulting from the retention and accumulation of GCAP2 at the inner segment may contribute to the pathology of the human mutation G157R in GCAP2 associated to retinitis pigmentosa.

The G157R mutation in GCAP2 has been reported to cause autosomal dominant RP and macular degeneration in Japanese patients (Sato *et al.* 2005). To address whether this mutation would cause GCAP2 accumulation at the proximal compartments *in vivo*, we expressed the corresponding mutation in bovine GCAP2 (bG161R/GCAP2)

in rod cells by transient transgenesis. Results are shown in Figure R.13 panels K-L and M, and Figure R.14. bG161R/GCAP2 was,on average, retained at inner segments to a higher extent than the wildtype protein, since the percentage of the protein distributing to ROS was less (38.7 ± 5.9 %, n=4 of bG161R/GCAP2 localized to ROS versus 50.1 + 4.2% of bGCAP2, n=5). However the difference was subtle, and was not statistically significant based on the number of cells analyzed (histogram in Figure R.13M). This result was in line with results obtained from the analysis of bG161R/GCAP2 susceptibility to *in vitro* phosphorylation in Ca^{2+} versus EGTA conditions (Figure R.15), that showed phosphorylation levels at the Ca^{2+} condition that

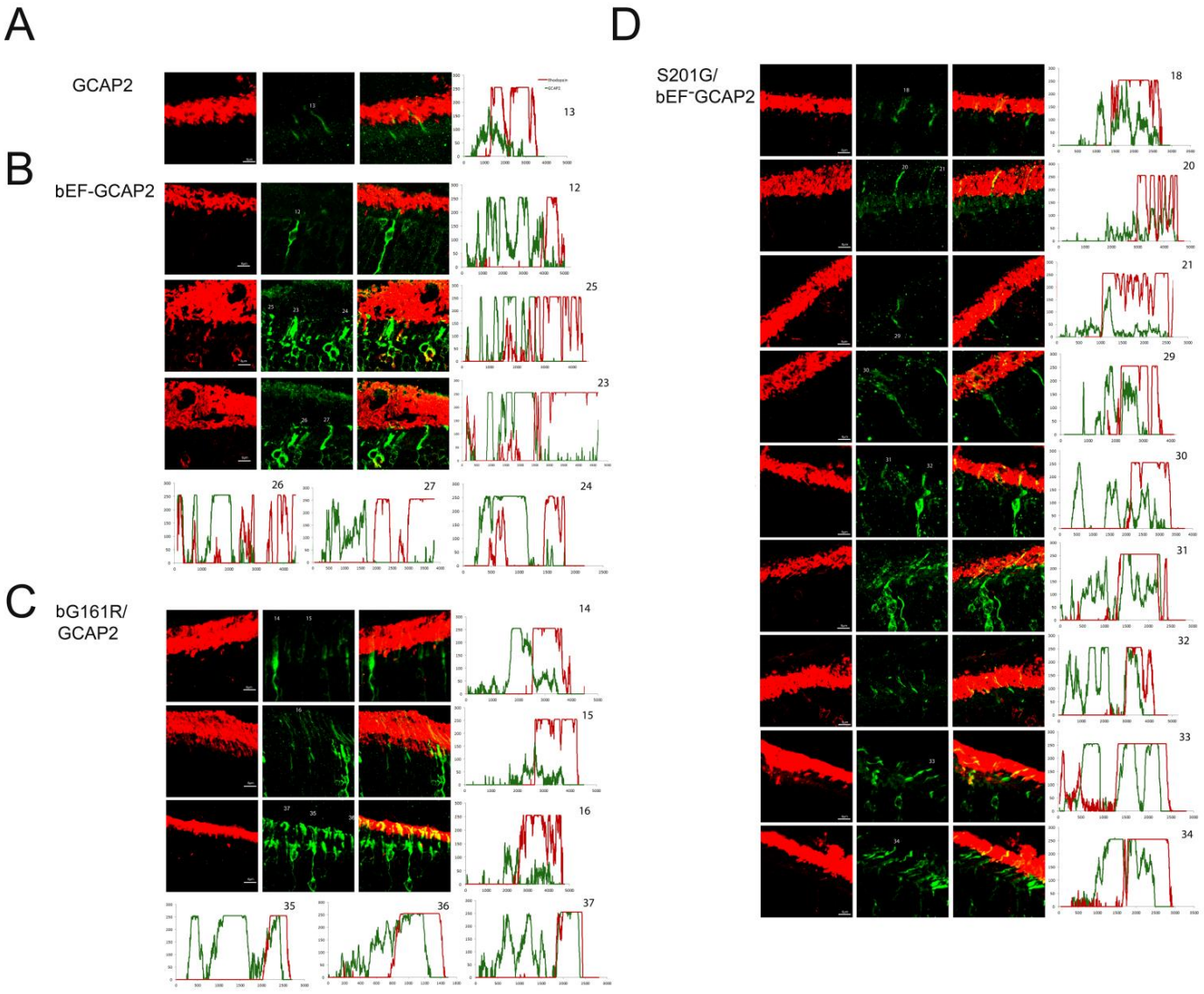

Figure R.14. ***Additional images and GCAP2 staining profiles of cells from electroporated mice.*** *Photoreceptor cells from electroporated mice with bGCAP2 (1 cell), bEF-GCAP2 (6 cells), bS201G/EF-GCAP2 (9 cells) and bG161R/GCAP2 (6 cells). GCAP2 stained in green, rhodopsin in red.*

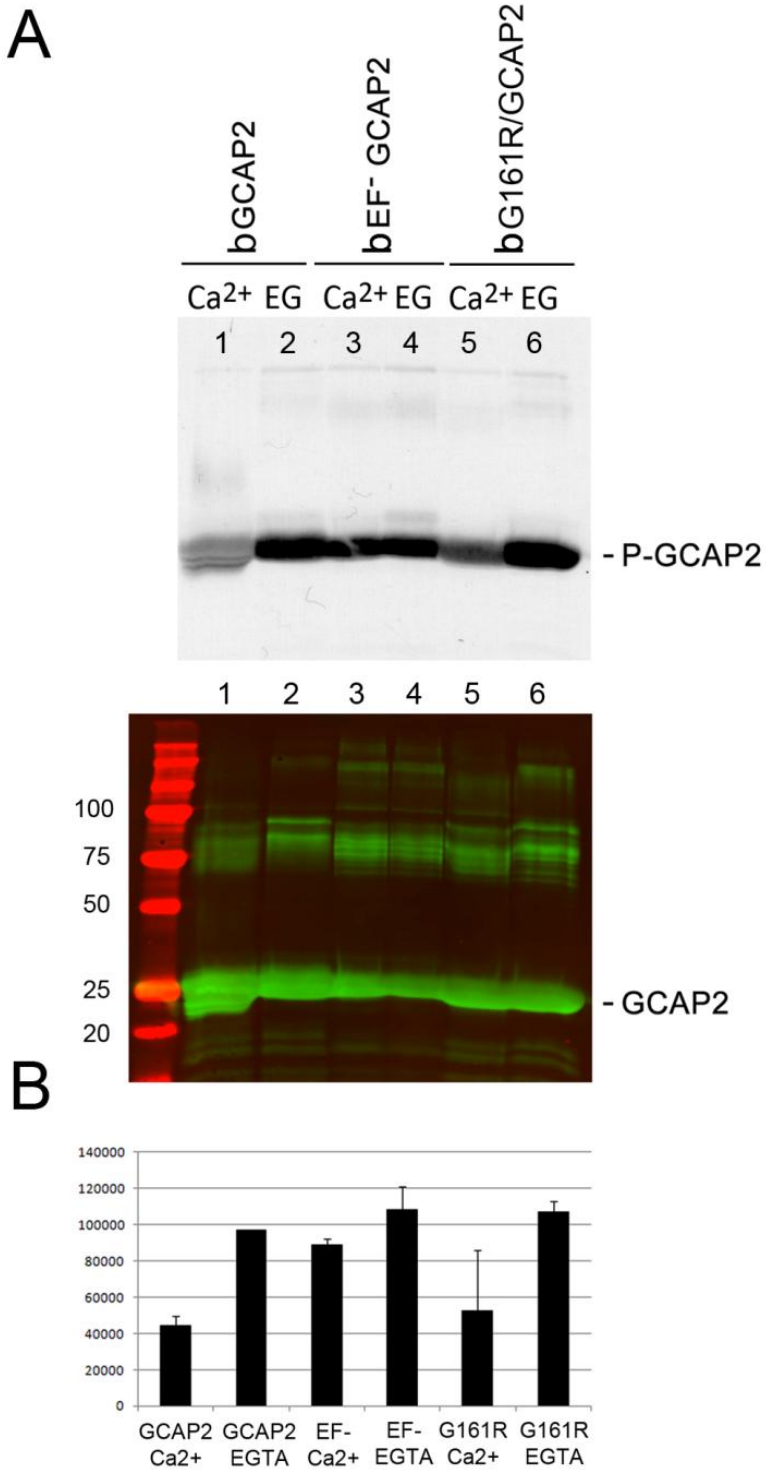

Figure R.15. ***In vitro phosphorylation of bG161R/GCAP2 in conditions of Ca^{2+} or EGTA***. *Upper panel shows an autoradiograph of ^{33}P phosphorylation products from an in vitro phosphorylation reaction of recombinant wildtype bGCAP2, bEF⁻GCAP2 or bG161R/GCAP2 with protein kinase G (PKG), in the presence or absence of free Ca^{2+}. The 20µl reaction mixture contained 8.5µg of the corresponding purified recombinant protein, purified PKGIα (100 units, Calbiochem) and 3µCi of ^{33}P- γATP in phosphorylation reaction buffer, containing either $CaCl_2$ or EGTA (see Methods). After incubation, reaction mixtures were resolved by 15% SDS-PAGE and transferred to a nitrocellulose membrane. Lower panel shows immunostained GCAP2. GCAP2 mutants were present to similar amounts in all reaction tubes.*

were on average intermediate between the levels of wildtype and bEF$^-$GCAP2 proteins. This difference was also subtle, so that the standard deviation between assays precludes us from concluding whether it might be physiologically relevant.

4.4. DISCUSSION

4.4.1. The *in vivo* effect of mutations that preclude Ca^{2+} binding in GCAP2 is different from mutations that impair Ca^{2+} binding in GCAP1

We here report that a form of GCAP2 with mutations that impair Ca^{2+} coordination at the three functional EF-loops (bEF$^-$GCAP2) led to retinal degeneration when expressed in rods in transgenic mice. *In vitro* the bEF$^-$GCAP2 mutant shows a similar shift in Ca^{2+} sensitivity of guanylate cyclase regulation as the Y99C, E155G and other GCAP1 mutants that directly or indirectly affect Ca^{2+} coordination (Dizhoor and Hurley. 1996) (Dizhoor *et al.* 1998) (Sokal *et al.* 1998). These GCAP1 mutants have been demonstrated to cause retinal degeneration *in vivo* by leading to persistent activation of the cyclase, causing elevated levels of cGMP and Ca^{2+} (Olshevskaya *et al.* 2004) (Woodruff *et al.* 2007) (Buch *et al.* 2011). Intriguingly, we found that the retinal degeneration caused by bEF$^-$GCAP2 expression in rods was independent of cGMP metabolism. When guanylate cyclase activity was measured in retinal homogenates from bEF$^-$GCAP2 transgenic mice, instead of constitutive activation of the cyclase we found very diminished cyclase activity independently of the [Ca^{2+}] conditions, which contrasts with the normal cyclase activity observed in homogenates of wildtype and bGCAP2 control-transgenic mice (Figure R.5). Furthermore, retinal degeneration in bEF$^-$GCAP2 transgenic mice could not be prevented or delayed by raising the mice under constant light exposure (Figure R.7). These results show for the first time that mutations that affect the conformation of GCAP2 can cause cell death *in vivo* by a mechanism independent of guanylate cyclase regulation.

4.4.2. Phosphorylation of GCAP2 and 14-3-3 binding as a new *in vivo* mechanism controling GCAP2 subcellular distribution that causes toxicity when overly deregulated

In contrast to the bGCAP2 control-transgenic protein that reproduced the endogenous mGCAP2 subcellular localization, bEF$^-$GCAP2 largely accumulated at inner segment

and proximal compartments of the rod when it was expressed in the GCAPs-/- background (Figure R.6). At this compartment, bEF$^-$GCAP2 was phosphorylated to a much higher extent than the control transgenic protein in *in situ* phosphorylation assays as well as under steady state level in the intact rod as shown by IEF, and it was found to bind 14-3-3 proteins (Table R.1, Figures R.8-R.10). This constitutes the first report that GCAP2 is phosphorylated *in vivo*, at much higher levels when locked in its Ca^{2+}-free conformation, and that phosphorylation of GCAP2 triggers 14-3-3 binding. We show that 14-3-3 localization in rod photoreceptors is restricted to proximal compartments and excluded from the outer segments (Figure R.12). Furthermore, we demonstrate that phosphorylation is required for bEF$^-$GCAP2 retention at proximal compartments by showing that replacing Ser201 by Gly in bEF$^-$GCAP2 substantially reverts this retention (Figure R.13). On average 57% of bSer201/EF$^-$GCAP2 localized to rod outer segments (Figure R.13 histogram, n=13 cells). We believe that the reason that a 100% reversion was not observed is that 14-3-3 shows some affinity for unphosphorylated bEF$^-$GCAP2 as well (Figure R.8). We therefore infer that 14-3-3 binding to phosphorylated GCAP2 retains the protein at proximal compartments, in what clearly represents an important step in the regulation of GCAP2 subcellular distribution *in vivo* (Figure R.13), somewhat analogous to 14-3-3 regulation of phosducin availability during dark and light adaptation.

14-3-3 proteins are a family of phosphobinding proteins of about 30 kDa that comprises seven homologs in mammals. They exist as homo- or hetero-dimers that are rigid in structure, with each 14-3-3 dimer binding to two different phospho-binding sites either in the same or in two independent target proteins. By masking an epitope, clasping epitopes or promoting the scaffolding of their clients, 14-3-3 proteins exert a diverse range of regulatory roles in metabolism, trafficking or integration of cell survival versus cell death pathways (Smith *et al.* 2011). In the retina, 14-3-3 proteins interact with phosducin at rod inner segments, regulating the amount of free phosducin during dark- and light-adaptation (Nakano *et al.* 2001), (Thulin *et al.* 2001). Phosducin modulates the amount of $Tr_{\alpha\beta\gamma}$ heterotrimer through competition with Gt_α subunit for binding to the $Gt_{\beta\gamma}$ complex. When light exposure activates Gt, releasing $Gt_{\beta\gamma}$ from Gt_α at rod outer segments, phosducin association to $Gt_{\beta\gamma}$ facilitates $Gt_{\beta\gamma}$ and Pd-$Gt_{\beta\gamma}$ independent translocation to the inner segment compartment (Sokolov *et al.* 2004). At the inner segment during dark-adaptation phosducin is simultaneously phosphorylated at Ser-54 and Ser-73 residues by PKA and CaMK, which causes a competing interaction with the 14-3-3 protein that dramatically reduces phosducin binding to $Gt_{\beta\gamma}$ (Lee *et al.* 2004). This allows the redistribution of Gt_α and $Gt_{\beta\gamma}$ to rod outer segments,

the former assisted by UNC119 and the latter by PrBP (Zhang *et al.* 2011), (Zhang *et al.* 2012). At rod outer segments Tr subunits are discharged to membranes and a heterotrimer forms again.

How 14-3-3 binding to phosphorylated GCAP2 fits with GCAP2 overall role in photoreceptor cell physiology and inherited retinal dystrophies is only emerging. It is clear from this work that GCAP2 is phosphorylated preferentially in its Ca^{2+}-free form *in vivo*. Because it is well established that GCAP2 in its Ca^{2+}-free form forms dimers (Olshevskaya *et al.* 1999b), and that 14-3-3 exists as dimers that bind to two consensus binding sites in client proteins (Smith *et al.* 2011), it seems straightforward to propose that a dimer of 14-3-3 would bind to a dimer of GCAP2, presumably to stabilize it (Figure R.16). Because GCAP1 and GCAP2, unlike recoverin or phosducin, were shown not to redistribute between subcellular compartments during dark- or light-adaptation (Strissel *et al.* 2005), we deduce that this mechanism would mainly affect the cytosolic distribution of newly synthesized protein.

We propose a model in which the GCAP2 molecules synthesized during the dark period (predominantly in the Ca^{2+}-loaded state) would bind to RetGC and be transported to rod outer segments, whereas the GCAP2 molecules synthesized in the light period (GCAP2 in its Ca^{2+}-free state) would be phosphorylated and retained at proximal compartments by 14-3-3 binding (Figure R.16). Such a scenario would result in the phosphorylation and retention to proximal compartments of about 50% of GCAP2 molecules in a physiological situation (wildtype mice raised in standard cyclic light). This is what we observe by IEF (Figure R.10) and by immunolocalization analysis (Figure R.6). This model would also explain why 12h of dark-adaptation did not have a noticeable effect on the steady-state phosphorylation levels of GCAP2 (Figure R.10).

We propose that GCAP2 phosphorylation and 14-3-3 binding constitute a major molecular determinant of GCAP2 subcellular localization upon its synthesis. What is its physiological relevance? A possibility is that 14-3-3 binding to GCAP2, by trapping GCAP2 to proximal compartments, might work to secure a reservoir of GCAP2 at these compartments, where GCAP2 may be exerting other roles at the synaptic terminal (López-del Hoyo *et al.* 2012), (Venkatesan *et al.* 2010). Alternatively, the 14-3-3 trapping of Ca^{2+}-free GCAP2 upon its phosphorylation might serve as a protein quality control mechanism, to avoid that an excess of Ca^{2+}-free, aggregation-prone GCAP2 molecules would reach the rod outer segment. Irrespective of its physiological significance, this regulatory enzymatic step is specific of GCAP2, given that GCAP1 is not phosphorylated, and might have evolved because it is more relevant for rods than

cones. Conditions that substantially alter this regulatory mechanism increasing the protein retention at the inner segment would have toxic consequences for the cell. We propose that toxicity in this scenario would arise from GCAP2 natural tendency to aggregate (see below).

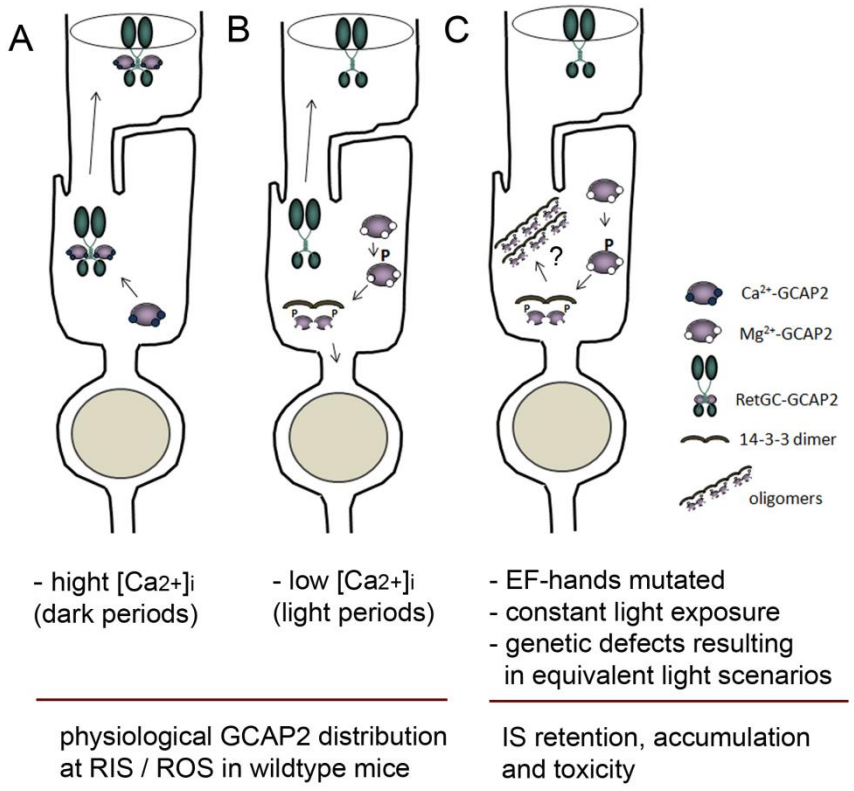

Figure R.16. ***Model depicting a mechanism regulating GCAP2 distribution in rods involving GCAP2 phosphorylation and 14-3-3 binding.*** *Under high Ca^{2+} conditions typical of the dark-steady state, the Ca^{2+}-loaded form of GCAP2 would bind to Ret-GC and be transported to rod outer segments (A); whereas under low Ca^{2+} conditions (e.g. light periods), the Ca^{2+}-free form of GCAP2 would be retained by 14-3-3 at proximal compartments (B). These alternating scenarios would result in approximately half of GCAP2 distributing to the inner segment and proximal compartments of the cell, and half to the outer segment compartment in a physiological situation (e.g. in wildtype mice raised in standard cyclic light). However, a prolonged light exposure or genetic conditions that would result in an abnormal accumulation of GCAP2 in its Ca^{2+}-free form (e.g. mutations in GCAP2 that impair Ca^{2+} binding, or mutations in components of the phototransduction cascade causing unabated signaling and a prolonged reduction in $[Ca^{2+}]_i$) would lead to neurodegeneration likely by inducing GCAP2 aggregation, or by GCAP2-mediated toxicity some other way (C).*

4.4.3. Physiological implications of GCAP2 phosphorylation and 14-3-3 binding for inherited retinal dystrophies

GCAP2 phosphorylation and 14-3-3 binding are observed to a more moderate extent in the bGCAP2 control transgenic line (IEF gel in Figure R.10) than in wildtype mice, presumably because bovine GCAP2 is not such a good substrate for the murine

kinase as the endogenous murine GCAP2. In wildtype mice phosphorylated GCAP2 at steady state constitutes about 50% of the total protein, consistent with about 50% of the protein retention at rod proximal compartments. This indicates that GCAP2 phosphorylation and 14-3-3 binding are not in itself toxic for the cell. It is therefore the deregulation of this mechanism– when all GCAP2 molecules are impaired to coordinate Ca^{2+} and GCAP2 phosphorylation and 14-3-3 binding are happening to a much larger extent- that correlates with severe retinal degeneration in the bEF^{-}GCAP2 line.

How does the accumulation of GCAP2-14-3-3 complexes at the rod inner segment lead to cell death? We hypothesize that accumulation of these complexes might result in pathology due to the formation of misfolded GCAP2 oligomers, in much a similar way to which synuclein, APP, Tau, Huntingtin or ataxin lead to neuronal cell death in Parkinson's (PD), Alzheimer (AD), Huntington's (HD) or spinocerebellar ataxia (SCA) diseases. GCAP2 shows a natural tendency to aggregate. Structural studies have shown that the Ca^{2+}-free form of GCAP proteins, and particularly of GCAP2, are difficult to maintain in solution and are prone to aggregation (Ames *et al.* 1999). When expressed in bacteria, recombinant GCAP2 accumulates in inclusion bodies, is only solubilized at high concentrations of guanidinium or urea, and is difficult to maintain in solution after refolding (Dizhoor *et al.* 1995). Dimers and high molecular weight aggregates can typically be distinguished by SDS-PAGE, more prominently for EF^{-}GCAP2 than for the wildtype form of the protein (e.g. this study, Figure R.8B). On the other hand, previous studies have found a close association between 14-3-3 and progressive neurodegenerative diseases. 14-3-3 proteins have been shown to colocalize with AD neurofibrillary tangles that are composed primarily of hyperphosphorylated tau proteins (Layfield *et al.* 1996), (Lee *et al.* 2001). In PD, 14-3-3 is detectable in Lewy bodies which accumulate α-synuclein (Kawamoto *et al.* 2002); and 14-3-3 colocalization was also reported for mutant ataxin in SCA (Chen *et al.* 2003). Furthermore, 14-3-3 zeta and epsilon binding to phosphorylated ataxin-1 at S776 was shown to aggravate neurodegeneration by stabilizing mutant ataxin, retarding its degradation and enhancing its aggregation in transfected cells and transgenic flies (Chen *et al.* 2003). The requirement of 14-3-3 zeta for Htt86Q aggregate formation has also been established in cells (Omi *et al.* 2008).

We propose that the mutant form of GCAP2 locked in its Ca^{2+}-free conformation results in toxicity *in vivo* by the progressive formation of soluble high molecular weight oligomers of GCAP2-14-3-3 that are toxic for the cell. Consistent with this, we observe a much higher fraction of bEF^{-}GCAP2 than of control bGCAP2 associated to 14-3-3 in

the fractionation of mouse retinal extracts by size exclusion chromatography (Figure R.11). Fractions showing GCAP2 and 14-3-3 association show also GCAP2 higher molecular species including dimers. The compromised solubility of accumulating bEF$^-$GCAP2-14-3-3 complexes is manifested in the fraction of bEF$^-$GCAP2 associated to 14-3-3 found in the Triton-X100 resistant, SDS-soluble fraction (Figure R.11). Inclusion bodies were not detected in our immunofluorescence assays with the polyclonal or monoclonal anti-GCAP2 antibodies used, or the anti-14-3-3ε monoclonal antibody. It may happen that these antibodies do not recognize inclusion bodies or that their absence would result from a relatively efficient clearance of the mutant protein and therefore slow formation of putative deposits. In this sense we have observed that inhibition of the proteasome results in an increase of EF$^-$GCAP2 levels (López-del Hoyo and Méndez, unpublished observation).

We investigated whether phosphorylation at Ser201 and 14-3-3 binding may underlie the toxicity of G161R-GCAP2, the bovine equivalent to the human G157R-GCAP2 mutation linked to adRP (Figure R.13). We found that, while G161R-GCAP2 showed on average a higher susceptibility to *in vitro* phosphorylation in the presence of free Ca^{2+} than the wildtype protein (Figure R.15) and a higher retention at the inner segment (Figure R.13), these changes were subtle. The nature of these assays precluded us from undertaking the number of assays that would be required to achieve statistical significance, and we foresee the requirement of a stable transgenic line to determine to what extent the mechanism here described contributes to retinal dystrophies associated to the human G157R-GCAP2 mutation.

This mechanism of toxicity caused by GCAP2 misfolding may contribute to the pathology of genetic mutations causing “equivalent-light” damage that result in a sustained reduction in the level of intracellular Ca^{2+}: mutations impairing termination of the light response or mutations in the visual cycle or the visual pigment resulting in opsin basal constitutive activity (e.g. null mutations in RPE65 or G90D opsin (Dizhoor *et al.* 2008) (Singhal *et al.* 2013), (Woodruff *et al.* 2003). Furthermore, this mechanism of toxicity is likely to contribute to cell death and retinal degeneration in those cases of Lebers Congenital Amaurosis (LCA) in which two conditions converge: GCAPs accumulation at the inner segment and a sustained reduction in the level of intracellular Ca^{2+}. Those conditions are met, for instance, in LCA1 caused by null mutations in RetGC-E (GUCY1E) or LCA12 caused by mutations in RD3, two severe and prevalent inherited retinal dystrophies.

In conclusion, we propose that GCAP2 may be a mediator of “equivalent-light” genetic damage, by its natural tendency to aggregate when in its Ca^{2+}-free form, in a process

regulated by phosphorylation and 14-3-3 binding. Future studies will be addressed at further characterizing the stoichiometry, solubility and turn-over of GCAP2-14-3-3 complexes, as well as their effects on the normal functions of the cell.

V. CHAPTER 2

RESUMEN EN ESPAÑOL

Realizamos un minucioso estudio de la ultraestrutura de las terminales sinápticas de bastones en modelos de ratón de pérdida de función de GCAP1 y GCAP2 (GCAP1/GCAP2 doble "knockout"), y modelos de ratón de ganancia de función de GCAP2, por la sobreexpresión de este transgén.

Las cintillas sinápticas de los ratones GCAPs-/- no difieren de las del fenotipo salvaje, cuando los ratones son crecidos en oscuridad constante. Esto indicaría que las proteínas GCAPs no son requeridas para el ensamblaje y maduración inicial de las cintillas. Por lo que vemos a continuación, es el mantenimiento de los niveles entre ambas isoformas, GCAP1 y GCAP2, lo que es relevante para la preservación de la integridad de la terminal sináptica.

En cambio, la sobreexpresión de GCAP2 en el fenotipo salvaje (GCAP2 +/+) en bastones lleva a un acortamiento de las cintillas sinápticas y a un aumento de los intermediarios de ensamblaje de éstas, como son las cintillas esféricas y las que adoptan la forma de "palo de golf". Sin embargo, cuando la sobreexpresión de GCAP2 es en el fenotipo knockout para GCAPs (GCAP-/- GCAP2+), porque se restaura la expresión de GCAP2, esto es, la expresión de GCAP2 en ausencia de GCAP1 endógeno, esta sobreexpresión tiene el sorprendente efecto de acortar la longitud de las cintillas mucho más que la sobreexpresión de GCAP2 en el fenotipo salvaje, así como también acentúa la reducción del grosor de la capa plexiforme externa (OPL) sin verse afectado el numero de fotorreceptores bastón. Además, esta sobreexpresión en ausencia de GCAP1 exacerba el desensamblaje de las cintillas sinápticas. Por otra parte, comprobamos por IHC que GCAP1 y RIBEYE colocalizan parcialmente. Creemos pues, que ambas proteínas, y más específicamente, sus niveles relativos contribuyen a los cambios morfológicos dependientes de luz que tienen lugar en las cintillas sinápticas. Estos cambios pueden deberse a un efecto indirecto de la desregulación de niveles de cGMP en el segmento externo, o a un efecto directo de las GCAPs sobre las cintillas.

Cuando realizamos la immunolocalización con oro coloidal a nivel de microscopia electrónica, observamos que GCAP2 y RIBEYE estarían colocalizando formando lo que parecen focos de desensamblaje. Con esta técnica, confirmamos la presencia de GCAP2 en las cintillas sinápticas, avalando un papel directo para las GCAPs como mediadoras del efecto de la luz en los cambios morfológicos que tienen lugar en estas estructuras.

Además, también poseemos estudios funcionales del efecto de variar los niveles de GCAP1:GCAP2 en la terminal sináptica, mediante registros de ERG para las distintas líneas de ratón. Al comparar la respuesta de ratones GCAPs-/- GCAP2+, cuyas cintillas son las más reducidas, que han sido crecidos en oscuridad, con ratones de la misma línea que se han crecido 12 horas oscuridad: 12 horas luz. En el caso de los primeros, los cambios en la cintilla podrían ser un efecto secundario debido a los niveles alterados de cGMP que se acumulan en el segmento externo, por la descompensación de GCAP1:GCAP2, y que en última instancia, provoca una variación en los niveles de Ca^{2+} en la sinapsis. En el caso de los segundos, el ERG muestra que la respuesta en los bastones es como la de los ratones salvajes, por lo que los cambios en el tamaño de las cintillas no se explica por el efecto secundario de los anteriores. Pero mostraría que las cintillas pueden verse sometidas a cambios agudos en sus dimensiones (de ~ 40%) sin verse afectada su funcionalidad. Como ya postuló Venkatesan en “Nicotinamide adenine dinucleotide-dependent binding of the neuronal Ca2+ sensor protein GCAP2 to photoreceptor synaptic ribbons” (Venkatesan *et al.* 2010), cambios en los niveles de Ca^{2+} serían los desencadenantes de que GCAPs promuevan cambios en las cintillas sinápticas.

Finalmente, nuestra demostración de la immunolocalización de GCAP2 en las cintillas sinápticas a nivel ultrastructural avalaría un papel *in situ* para las GCAPs como mediadoras del efecto de la luz en los cambios morfológicos que tienen lugar en estas cintas sinápticas.

5.1. CONTRIBUCIONES

Las líneas transgénicas descritas en este trabajo fueron generadas originalmente por A. Méndez en el laboratorio de la Dra. Jeannie Chen en la University of Southern California, Los Angeles, y trasladadas a Barcelona para su caracterización. Los ensayos de coinmunolocalizacion de GCAP2 y RIBEYE a nivel de microscopia confocal y microscopia electrónica fueron realizados por Lucrezia Fazioli y A. Mendez, con la inestimable ayuda técnica de Almudena Garcia y Nuria Cortadellas, en la plataforma cientificotécnica de microscopia electronica del Hospital Clinic, CCiT-UB, y del Dr. Benjamín Torrejon en CCiT-UB Bellvitge. Las figuras de análisis de la conectividad sináptica de los distintos tipos neuronales con marcadores especificos por IHC fueron realizadas por Lucrezia Fazioli en colaboración con Laura Fernandez-Sanchez del laboratorio del Dr. Nicolas Cuenca en la Universidad de Alicante. Los ensayos de ERG fueron realizados en el laboratorio del Dr. Pedro de la Villa en la Universidad de Alicante, con la valiosa ayuda técnica de Laura Ramírez.

La contribución experimental de N. López del Hoyo a este capítulo ha sido: 1) el mantenimiento y genotipaje de rutina de las cepas de ratón descritas, 2) la preparación de colecciones de ojos en bloques de resina Epoxi o Spur para el análisis ultraestructural, 3) la observación y captacion de imágenes al microscopio electrónico de cientos de terminales sinápticas por fenotipo 4) las mediciones de las cintillas sinápticas en las imágenes captadas, y el análisis estadístico.

5.2. BRIEF INTRODUCTION

A fundamental ability of photoreceptor cells in the retina is to sense light stimuli over a broad dynamic range of ambient light intensities in the natural world, by reliably transmiting fine gradations in membrane potential that set the rate of neurotransmitter release to bipolar and horizontal cells (Parsons *et al.* 2003) (Thoreson 2007) (Werblin 2011).

To accomplish this, they rely on specialized synapses that support the continuous neurotransmitter release at high rates: synaptic ribbons (von Gersdorff 2001) (Prescott and Zenisek. 2005). It is known that intracellular Ca^{2+} levels cause illumination-dependent remodeling of ribbons. A recent study has proposed Guanylate Cyclase Activating Protein 2 (GCAP2) as a prime candidate for mediating the Ca^{2+}-dependent structural changes of ribbons, based on the following observations: 1) GCAP2 interacts with RIBEYE, the main protein component of synaptic ribbons; 2) GCAP2 colocalizes with RIBEYE at ribbon synapses; and 3) GCAP2 overexpression in photoreceptor cells achieved by viral infection of retinal explants led to the disassembly of the synaptic ribbon in a high percentage of synaptic terminals (Venkatesan *et al.* 2010).

In order to gain insight into the roles that GCAP1 and GCAP2 may play at the synaptic terminal, and whether they might mediate the light-triggered morphological changes of photoreceptor ribbons, we performed a detailed morphological analysis of the outer plexiform layer (OPL) and rod synaptic terminals in retinas from mouse models of gain-of-function of GCAP2 and loss-of-function of GCAP1 and GCAP2.

5.3. RESULTS

5.3.1. Mouse Models of Gain-of-function and Loss-of-function of GCAP2 Show Morphological Alterations at the Outer Plexiform Layer

The mouse lines used in this study are summarized in Figure R.17 and Table R.3. To study the effect of GCAP2 overexpression on the morphology and function of rod synaptic terminals *in vivo*, we used a previously characterized transgenic line that expresses GCAP2 in rods under the mouse opsin promoter (Figure R.17A). This line expresses heterologous GCAP2 (bovine GCAP2, bigger than the murine isoform in three amino acids) at 1.5-fold the endogenous GCAP2 levels (Figure R.17B), and is referred to as GCAP2+ in Table R.3. By breeding this original transgenic line to transgene homozygosis we obtained a line in which transgenic GCAP2 was expressed to 3-fold the endogenous level of GCAP2 (GCAP2+/+, Figure R.17D, Table R.3). These mice showed virtually normal retinas for up to six months of age when raised in standard cyclic light conditions. No noticeable signs of retinal degeneration were observed by light microscopy in mice raised in constant darkness at postnatal day 40 (Figure R.17C).

As a mouse model of loss-of-function we used the double knock-out in GCAP1 and GCAP2, referred to as GCAPs−/− (Mendez *et al.* 2001). These mice were originally obtained by homologous recombination in embryonic stem cells with a single replacement vector, because the GUCA1A and GUCA1B genes encoding GCAP1 and GCAP2 are contiguous in the genome. Mice deficient in GCAP1 and GCAP2 lack the rapid and robust Ca^{2+} feedback signal to cGMP synthesis set in place by light, and show slower light response kinetics, enhanced sensitivity to light and impaired light adaptation. Despite this marked functional phenotype, retinas from GCAPs−/− mice show normal appearance for up to 5 months of age when mice are raised in standard cyclic light (Mendez *et al.* 2001) (Figure R.17E). A transgenic line that expresses GCAP2 in the absence of GCAP1 was obtained by breeding the GCAP2+ line to the GCAPs−/− line. GCAP2 expression in this line restores the endogenous GCAP2 localization and function (Mendez *et al.* 2001). Retinas from these mice show a normal outer nuclear layer thickness for at least 5 months of age (Figure R.17E).

To study whether the loss of expression of both GCAP1 and GCAP2 in the GCAPs−/− mice or the selective restoration of GCAP2 expression in this line has an effect on the synaptic terminals of rods and cones, the OPL in retinal sections from p40 mice was immunolabeled with an antibody anti-RIBEYE, the major protein component of synaptic

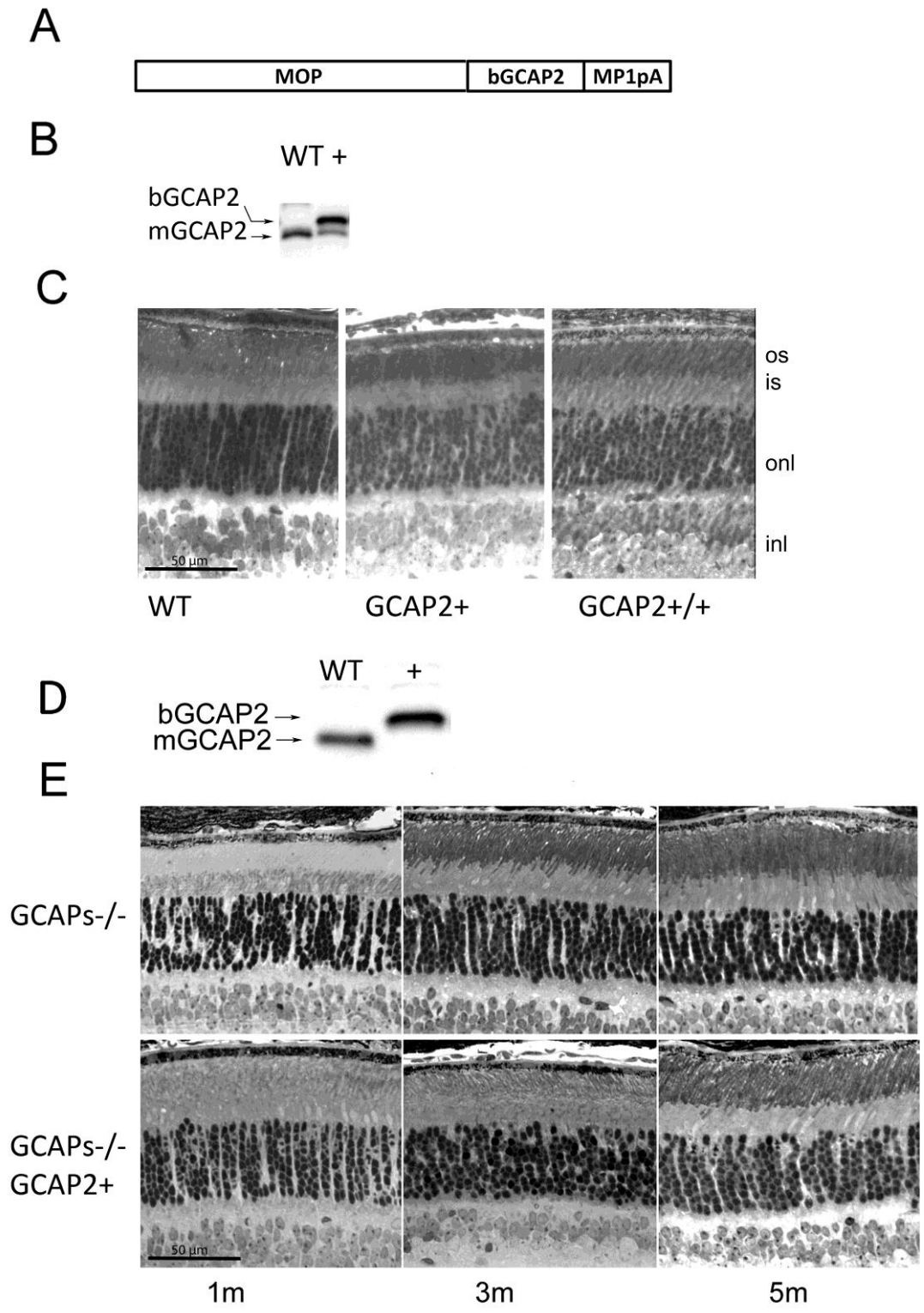

Figure R.17. ***Mouse models of overexpression of GCAP2 and loss-of-function of GCAP1 and GCAP2 used in the study A****. GCAP2 transgene construct. MOP, 4.4 kb-version of the mouse opsin promoter; bGCAP2, cDNA of bovine GUCA1B gene encoding guanylate cyclase activator protein 2 (GCAP2); MP1pA, polyadenylation signal of mouse protamine gene 1.* ***B.*** *Western blot of total retinal homogenates illustrating GCAP2 level of expression in the GCAP2+ line. Equivalent fractions of a retina (1/10) of WT and GCAP2+ mice were resolved in a 12% SDS-PAGE, transferred to a nitrocellulose membrane and incubated with a polyclonal Ab anti-GCAP2. The bovine (transgenic) and murine (endogenous) isoforms of GCAP2 can be resolved on the basis of their 3-aa difference in size. In the GCAP2+ transgenic line bGCAP2 is expressed to 1.5-fold the endogenous GCAP2 expression (Mendez et al. 2001).* ***C.*** *Light micrographs of vertical sections of the retina of dark-reared WT, GCAP2+ and*

GCAP2+/+ (transgenic line bred to homozygosity, that expresses transgenic GCAP2 to 3-fold the endogenous GCAP2 level) at postnatal day 40. Mice overexpressing GCAP2 show at this age a normal retinal morphology. ***D.*** *Expression of bGCAP2 transgene in the GCAP1/GCAP2 double knockout background (GCAPs−/− background). Western blot shows expression of transgenic bGCAP2 in the absence of endogenous GCAP2 in the GCAPs−/−GCAP2+ mice.* ***E.*** *Light micrographs of vertical sections of the retina from GCAPs−/− and GCAPs−/−GCAP2+ at 1, 3 or 5 months of age, when reared in standard cyclic light. Mice lacking GCAP1 and GCAP2 retain the normal thickness of outer nuclear layer, that is, the normal number of photoreceptor cells for up to 8 months of age. Mice in which GCAP2 expression is restored in the GCAPs−/− background do not show obvious signs of retinal degeneration at the light microscopy level.*

ribbons. Sections were co-stained with an antibody anti-GCAP2. Measurements of OPL thickness were taken at the confocal microscope at four points along the retinal vertical meridian (A, B, C and D shown in Figure R.18B inset, see Methods). The retinas analyzed in this study were obtained from mice raised in complete darkness to avoid secondary changes at the synaptic terminal that could derive from differences in the gain of the light response at the rod outer segment among different mouse models. The absence of both GCAP1 and GCAP2 in the GCAPs−/− mice had a minor effect on OPL thickness, which was significant only in the upper retina. However, expression of GCAP2 in the absence of GCAP1 caused a 40% reduction in OPL thickness along the entire length of the retina, indicating that the size or the number of synaptic terminals was reduced (Figure R.18A).

Mouse strain	GCAP1 expression *	GCAP2 expression *
WT (C57Bl)	1 -fold	1 –fold
GCAPs-/-	0	0
GCAPs-/-GCAP2+	0	1.5 –fold
GCAP2+	1 -fold	1.5 + 1 = 2.5 –fold
GCAP2+/+	1 -fold	3 + 1 = 4 –fold

***** expressed respect to the endogenous protein level (1 -fold)

Table R.3. ***Transgene expression levels in the different mouse lines.***

This reduction of OPL thickness was not preceded by photoreceptor cell death. GCAP2 expression in the absence of GCAP1 did not cause noticeable morphological changes at the outer segment, inner segment or outer nuclear layers of the retina (Figure R.18A). GCAPs−/−GCAP2+ mice showed an outer nuclear layer undistinguishable in thickness from that of GCAPs−/− littermate control mice along the entire length of the retina (Figure R.18C), indicating that the thinning of the OPL was not a secondary consequence of ongoing photoreceptor cell death.

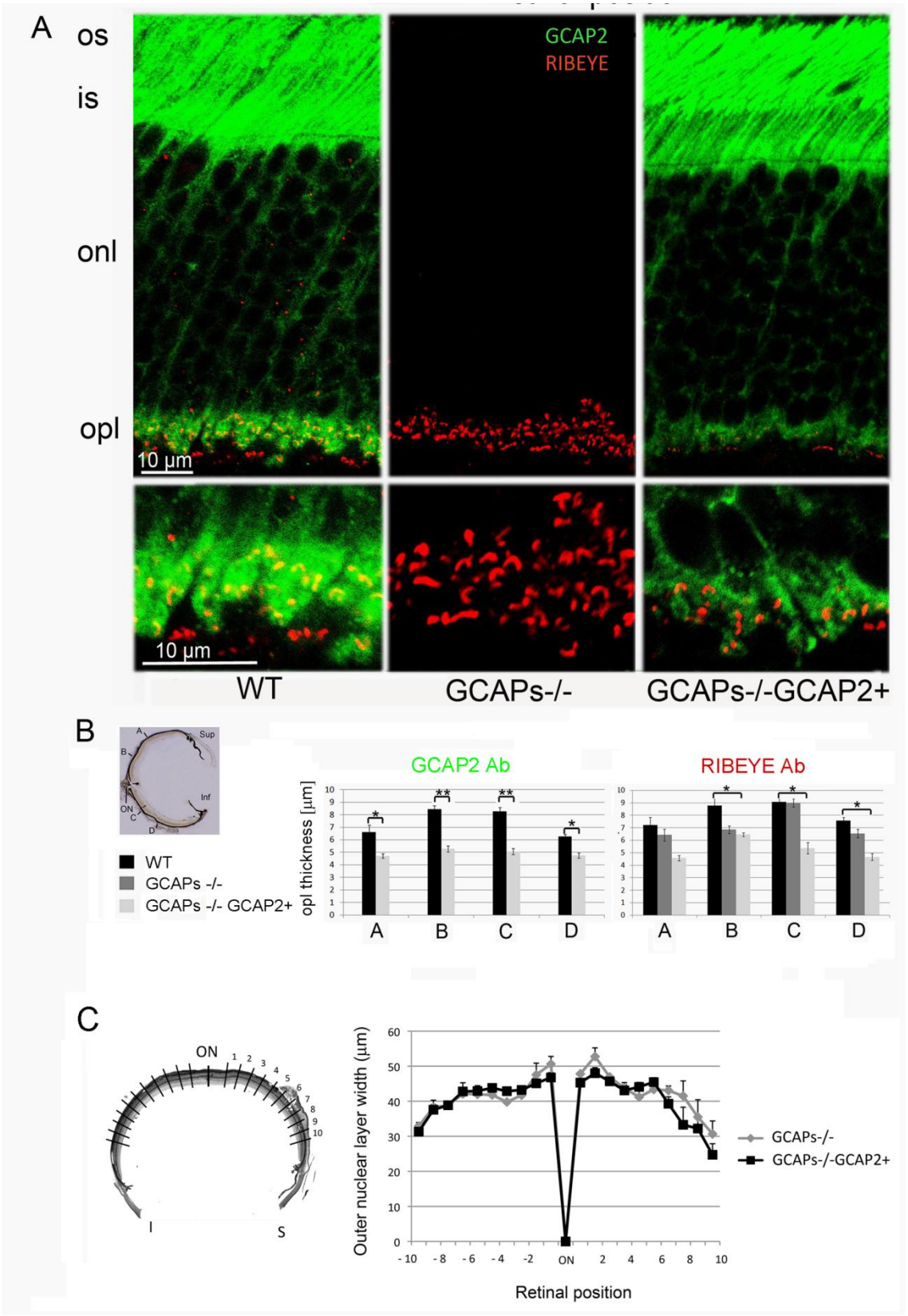

Figure R.18. ***Mice that express GCAP2 in the GCAPs−/− background show a reduction of outer plexiform layer (OPL) thickness compared to wildtype mice. A.*** *Immunolabeling of vertical retinal sections from WT, GCAPs−/− and GCAPs−/−GCAP2+ mice with rabbit polyclonal antibodies anti-GCAP2 and a monoclonal antibody against RIBEYE(B)/CtBP2. GCAP2 antibodies give a strong immunolabeling signal at the outer segment (os), inner segment (is) and outer plexiform layer (opl) of the retina. This signal is absent in GCAPs−/− mice, and is restored in GCAPs−/−GCAP2+ mice, in which the GCAP2 transgenic*

protein reproduces the endogenous GCAP2 intracellular localization. GCAP2 partially colocalizes with RIBEYE at ribbon synapses, as pointed by white arrows in WT magnified OPL panel, as previously reported (Venkatesan, Natarajan et al. 2010). This figure shows that the expression of GCAP2 in the GCAPs−/− background, that is, GCAP2 expression in the absence of GCAP1, leads to a substantial shortening of the OPL: compare immunolabeling intensity and thickness of the OPL in WT and GCAPs−/−GCAP2+ panels. ***B.*** *Statistical analysis of the outer plexiform layer thickness in the WT, GCAPs−/− and GCAPs−/−GCAP2+ phenotypes. Measurements of OPL thickness were taken at four different regions along vertical sections of the central retina (A, B, C and D in inset) for each phenotype. WT, GCAPs−/− and GCAPs−/−GCAP2+ mice were raised in constant darkness and processed at p40. OPL thickness was determined at each position based on measurements of the anti-GCAP2 Ab immunolabeled region (left histogram) or anti-RIBEYE mAb immunolabeled region (right histogram) at the laser scanning confocal microscope. In GCAPs−/−GCAP2+ mice the OPL thickness is reduced to 60–65% of the wildtype OPL. Values in histograms are the mean ± standard deviation from measurements taken from four mice per phenotype. * denotes P<0.01; ** denotes P<0.001 in the Student's t-test.* ***C.*** *Mice that express GCAP2 in the absence of GCAP1 (GCAPs−/−GCAP2+) retain the normal quantity of photoreceptor cells at p40 when raised in constant darkness. The retinal morphometry analysis shows that outer nuclear layer thickness (in µm) at 200 µm intervals covering the whole length of the vertical central retina (left diagram) is undistinguishable in GCAPs−/− and GCAPs−/−GCAP2+ mice at p40 (overlapping graphs). Mean values ± standard error were obtained from at least three littermate mice per phenotype.*

To study whether the magnitude of the reduction of the OPL thickness in the GCAPs−/−GCAP2+ mice depends on whether the mice are raised in constant darkness (with constant intracellular Ca^{2+} levels at rod outer segments and tonic neurotransmitter release at the synapse) or exposed to regular 12 h:12 h dark:light cycles (with photoreceptor intracellular Ca^{2+} levels varying daily between its dark and daylight values), the OPL from 40 day-old mice raised either in constant darkness or in standard 12 h:12 h dark:light cycles was stained with an anti-Bassoon antibody (Figure R.19) and measurements of OPL thickness were taken at four points in the retina vertical meridian. GCAPs−/−GCAP2+ mice raised in cyclic light also presented an statistically significant reduction in OPL thickness when compared to wildtype controls, although slightly lower in magnitude than when mice were raised in constant darkness (20–30% reduction of OPL thickness depending on the retinal region, versus the 40% uniform reduction in dark reared-mice, data not shown). Immunolabeling of cone pedicules with an antibody for the Transducin Gγ c subunit did not reveal noticeable alterations in the synaptic terminals of cones or the density of their synaptic ribbons among the different mouse phenotypes (Figure R.19).

To determine whether the connections between photoreceptor cells and horizontal and bipolar cells were affected, horizontal and bipolar cells were immunolabeled with antibodies for Calbindin and PKCα, respectively (Figure R.20). Photoreceptor synaptic terminals were highlighted with an antibody for Synaptophysin, SYP. There was a reduction in the density and size of horizontal cell processes, both in GCAPs−/− and in GCAPs−/−GCAP2+ mice. Remodeling changes were also apparent in the dendrites of bipolar cells, which were more dramatic in GCAPs−/−GCAP2+ mice that were raised in constant darkness than in mice raised in cyclic light, with shorter bipolar dendrites and

loss of dendritic tip terminals. Immunostaining of retinal sections with Bassoon also showed a reduction in the density and size of synaptic ribbons in the OPL of GCAPs−/−GCAP2+ mice respect to wildtype mice, while no variation in OPL thickness is observed in GCAPs−/− mice versus wildtype mice.

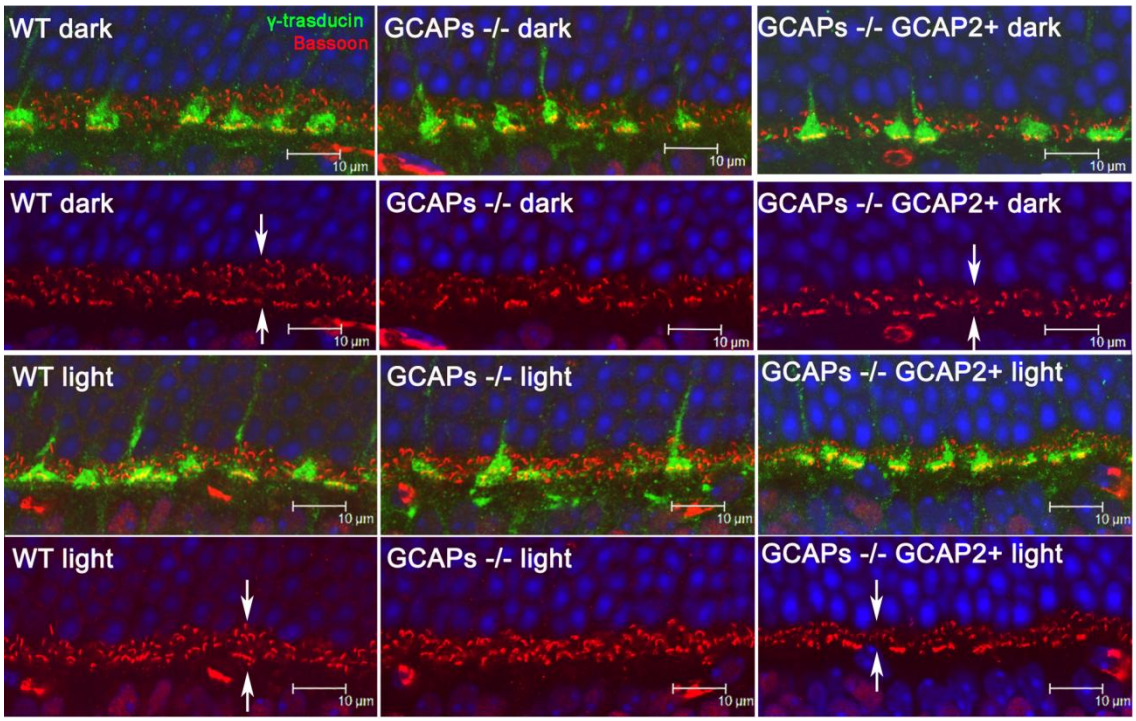

Figure R.19. ***Outer plexiform layer reduction in GCAPs−/−GCAP2+ mice takes place regardless of whether the mice are raised in constant darkness or in 12h dark : 12h light cyclic light.*** *Immunolabeling of synaptic active zones (arciform densities) with a monoclonal antibody anti-Bassoon (in red), and cone pedicules with a polyclonal antibody anti-transducin γ (in green) in WT, GCAPs−/− and GCAPs−/−GCAP2+ retinas. Mice were either raised in darkness (two upper rows) or were raised in standard 12 h dark : 12 h cyclic light (two lower rows) and processed at p40. OPL thickness in GCAPs−/−GCAP2+ mice was reduced to about 65% of wildtype thickness independently of the light-rearing conditions [compare OPL thickness in WT and GCAPs−/− GCAP2+ panels, arrows].*

Together these results show that mice that express GCAP2 in the absence of GCAP1 have a severe reduction in the thickness of the OPL, with a decrease in the density of synaptic ribbons. GCAP2 expression effect on retinal morphology is specific to the outer plexiform layer, and is not accompanied by photoreceptor cell loss by postnatal day 40. These OPL alterations are more dramatic when mice are raised in constant darkness than when they are raised under cyclic light conditions, and are accompanied by remodeling changes that reduce the density of connecting horizontal and bipolar cell processes.

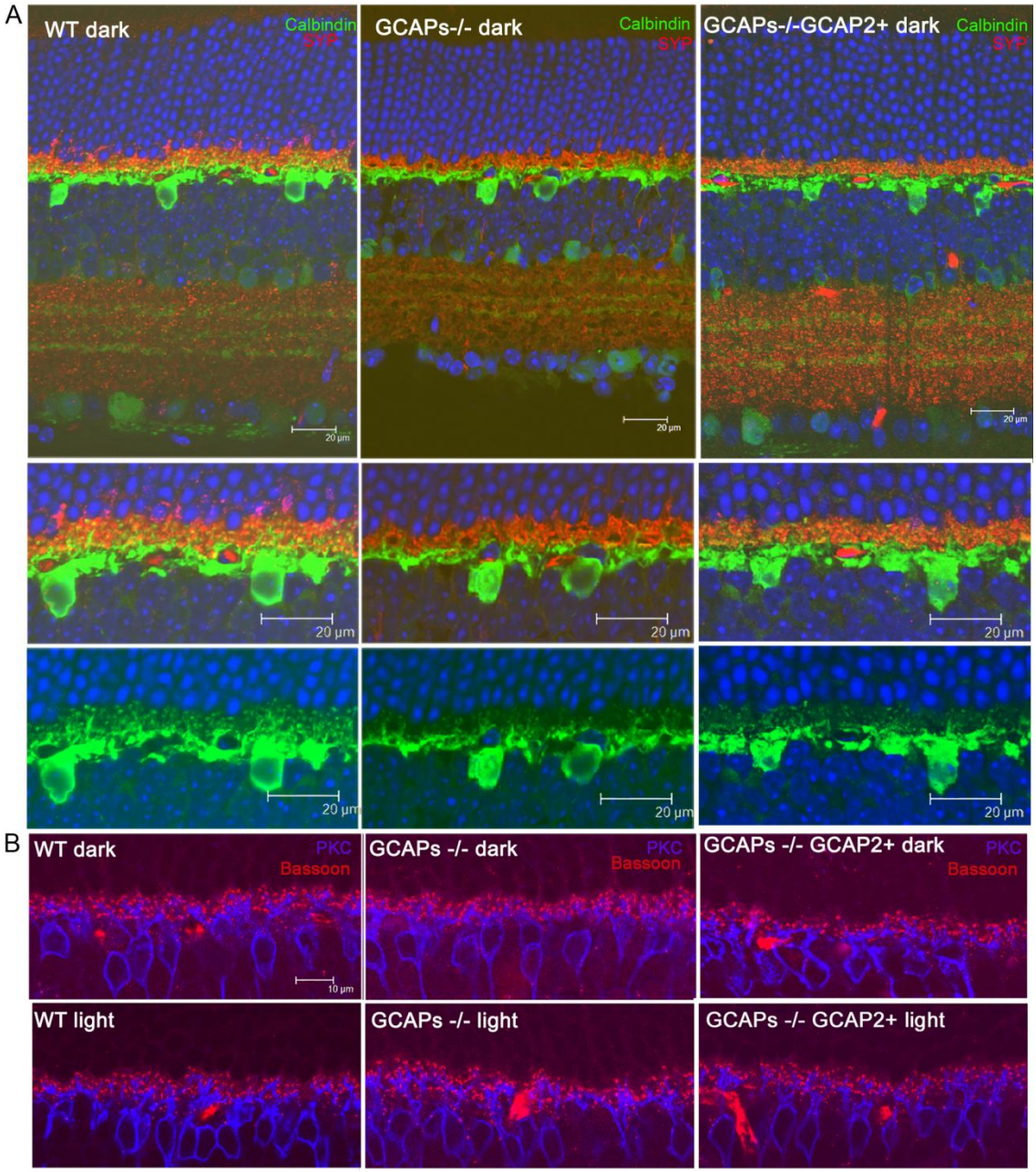

Figure R.20. Reduction in the density of horizontal and bipolar cell dendritic processes in mice that express GCAP2 in the GCAPs−/− background. A. *Immunolabeling of horizontal cells by indirect immunofluorescence with anti-Calbindin polyclonal antibodies [green signal] and rod and cone synaptic terminals with a monoclonal antibody anti-Synaptophysin [SYP, red signal] in WT, GCAPs−/− and GCAPs−/−GCAP2+ mice raised in constant darkness. Note the reduction in density and complexity of horizontal cell processes in GCAPs−/− and GCAPs−/−GCAP2+ retinas compared to WT samples.* ***B.*** *Immunolabeling of bipolar cells with a polyclonal antibody against PKCα [blue signal] and detection of arciform densities in rod and cone synaptic terminals with a monoclonal antibody anti-Bassoon [red signal]. Note the remodeling of bipolar cell dendrites that is taking place at p40 in GCAPs−/−GCAP2+ samples associated to a reduction in the number and dimensions of synaptic ribbons and arciform density structures at rod and cone synaptic terminals.*

5.3.2. Overexpression of GCAP2 in Rod Photoreceptors Leads to Shorter Synaptic Ribbons and Increases the Abundance of Ribbon Assembly Intermediates

To study whether GCAP2 overexpression in rods leads to the shortening of synaptic ribbons at the ultrastructural level, the OPL region of retinal ultrathin sections from transgenic mice expressing GCAP2 to 2.5 or 4-fold the endogenous GCAP2 levels (GCAP2+ or GCAP2+/+ transgenic mice respectively, see Table R.3) was examined by transmission electron microscopy. The lengths of transversal rod synaptic ribbons contained in two to eight 16×16-µm frames of OPL per specimen from at least two specimens per phenotype were determined and averaged, and compared to those of C57Bl control mice (Figure R.21 and Table R.4, see Methods). Mice were reared in complete darkness and sacrificed at p40 under dark-adapted conditions or following a 1–5 h period of light exposure.

C57Bl mice that were raised in constant darkness to postnatal day 40 and were processed in darkness presented ribbons that measured on average 0,2915±0,0066 µm (n = 103 synaptic ribbons from 5 mice), whereas littermate mice that were processed after 1–5 h of light exposure showed ribbons that measured on average 0,2534±0,0082 (n = 98 synaptic ribbons from 5 mice), Table R.4. This represents a 13% reduction of ribbon length in C57Bl mice following a 1–5 h period of light exposure that was statistically significant (Figure R.21A and R.21C)

Transgenic expression of GCAP2 led to a shortening of synaptic ribbons that correlated with transgene dosage, independently of whether the mice were sacrificed in the dark or following light exposure. GCAP2+ mice presented a 9,6% reduction whereas GCAP2+/+ mice presented a 13,7% reduction in ribbon length versus the C57Bl control when processed under dark-adapted conditions (representative ribbons shown in Figure R.21A, statistical analysis shown by black bars in Figure R.21C, see Table R.4). Under light-adapted conditions the reduction was of 4% for GCAP2+ and of 17% for GCAP2+/+ when compared to the C57Bl light value (Figure R.21A, grey bars in Figure R.21C).

Because illumination-dependent changes of photoreceptor ribbon structure were shown to differ between mouse strains (Fuchs *et al.* 2013) it was important to discard that minor variations in the genetic background between GCAP2-transgenic and C57Bl mice may account for the phenotype observed, given that the analysis of GCAP2 gene dosage effect on ribbon length could not be performed on littermate mice. Although the GCAP2- expressing transgenic mice used in this study were back-crossed to C57Bl/6

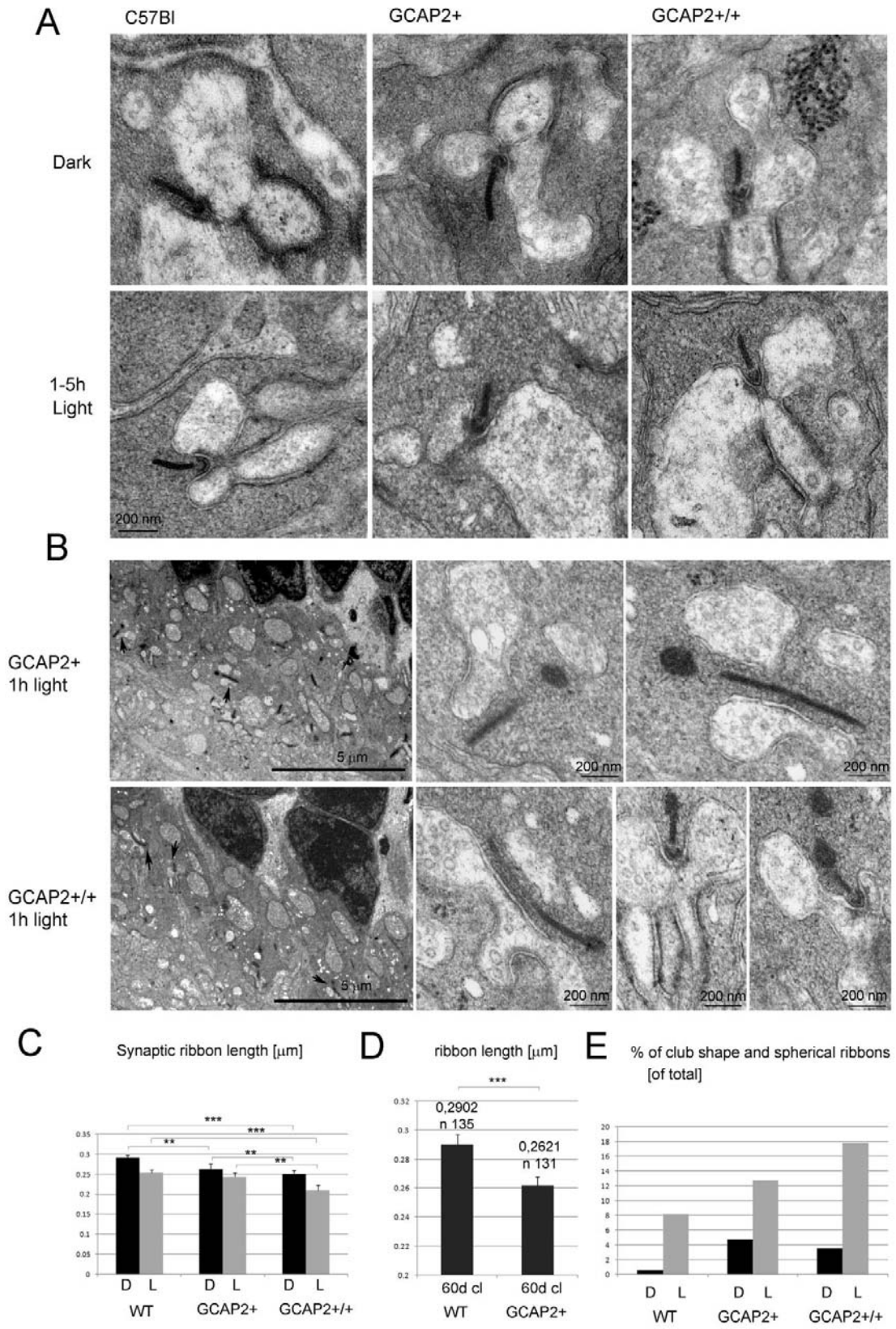

Figure R.21. ***Overexpression of GCAP2 in transgenic mice leads to shortening of ribbon length and to an increase in the fraction of club-shaped and spherical morphologies representing disassembling ribbons. A.*** *Electron micrographs of rod synaptic terminals of dark-reared C57Bl, GCAP2+ or GCAP2+/+ mice at p40 that were processed in darkness or immediately after 1–5 h of light exposure, showing transversal sections of synaptic ribbons. Notice the difference in length in C57Bl [left], GCAP2+ [middle] and GCAP2+/+ [right panel] ribbons. In addition to synaptic vesicles, vesicle-like*

particles that are smaller in diameter than synaptic vesicles were seen forming clusters in the cytosol [GCAP2+/+ panel]. These clusters found in the vicinity of the ribbons were more extensive in GCAP2+/+ samples than in C57Bl samples. ***B.*** *Club-shaped ribbons were more abundant in GCAP2+ and GCAP2+/+ than in C57Bl samples. Two examples of the density of club-shaped and spherical-ribbons are shown in 8,000× visual fields of GCAP2+ and GCAP2+/+ retinal sections. Club-shaped and spherical ribbons pointed by arrows are shown at higher magnification in the right panels.* ***C.*** *Statistical analysis of ribbon length in C57Bl, GCAP2+ and GCAP2+/+ mice that were either raised in constant darkness (D); or raised in constant darkness and subsequently exposed to 1–5 h light (L). A minimum of forty synaptic ribbons were measured from at least two mice per phenotype. Plotted in the histogram are mean values ± standard error. *** denotes P<0.0001 in Student's t-test. ** denotes P≤0,001 in Student's t-test. *denotes PP≤0,01 in Student's t-test.* ***D.*** *Statistical analysis of ribbon length in GCAP2+ and WT littermate control mice raised in standard cyclic light and processed at p60. GCAP2-expressing mice showed a 10% reduction in ribbon length compared to WT littermate controls. Notice the difference in the Y-axis scale. *** denotes P≤0,0001 in Student's t-test.* ***E.*** *Histogram comparing the percentage of club-shaped and spherical ribbons [of total synaptic ribbons] in C57Bl, GCAP2+ and GCAP2+/+ at p40 processed in darkness [D] or immediately after 1 h or 5 h of light exposure.*

for at least four generations, they were originally obtained in a C57Bl × DBA mixed genetic background (Mendez *et al.* 2001)

To discard the contribution of genetic background effects, synaptic ribbon length was compared in GCAP2+ versus transgene-negative control mice (herein called WT) in the same litter, raised in the same cage under standard cyclic light and analyzed at p60. GCAP2 transgene expression led to a 10% reduction in ribbon length compared to WT mice [0,2621±0,0059 µm in transgene-positive mice, n = 131 from four mice; versus 0,2902±0,0067 µm in WT mice, n = 135 from three mice; Student's t = 3,114, 264d.f., P = 0,002] (Figure R.21D).

Taken together these results indicate that the overexpression of GCAP2 promotes the loss of ribbon material, both in dark-adapted and light-adapted retinas.

It has been reported that as synaptic ribbons loose material in the light adaptation process, different morphologies are observed at the ultrastructural level, such as club-shaped ribbons (csr) or ribbons with a spherical form (sr) in tangential sections. This is probably due to the fact that the ribbons, laminar in nature, assemble and disassemble material in preformed spherical blocks at focal points (Vollrath *et al.* 1996) (Vollrath *et al.* 2001) (Spiwoks-Becker *et al.*2004).

To study whether the overexpression of GCAP2 led to a higher abundance of these "assembly intermediate" morphologies, the percentage of club-shaped and spherical ribbons was determined in GCAP2+ and GCAP2+/+ versus C57Bl mice (Histogram in Figure R.21E, Table R.4). While C57Bl mice that were raised in darkness showed less than 1% of club-shaped/spherical ribbons, GCAP2+ and GCAP2+/+ mice raised in darkness showed a 4.8% and 3.6% of these structures respectively, which represents at least a four-fold increase in their relative abundance (Table R.4). In C57Bl mice that

Phenotype; dark/light condition	Mouse ID: [N. of rod synaptic terminals, rod terminals with ribbon, rod terminals with measurable tangential ribbon] per 16 x 16 μm frame (2-10 frames per Epon block, separated by semicolons)	Synaptic ribbon length (μm) ± standard error	% of club-shape ribbons (csr) and spherical ribbons (sr)
C57Bl 40d dark	#1: [19,8,**5**]; [12,8,**6**] #2: [19,13,**9**]; [12,9,**7**]; [10,7,**6**]; [14,9,**7**]; [12,11,**8**] #3: [18,6,**5**]; [14,9,**4**]; [15,9,**7**]; [18,8,**4**] #4: [22,9,**3**]; [22,19,**10**] #5: [7,6,**6**]; [12,6,**4**]; [12,7,**4**]; [11,10,**8**] [Total rod synaptic terminals: 249; Total rod synaptic ribbons: 154; Tangential ribbons: 103]	0,2915 ± 0,0066 (n=103)	#1: 0; 0 #2: 1csr; 0; 0; 0; 0 #3: 0; 0; 0; 0 #4: 0; 0 #5: 0; 0; 0; 0 **Percentage csr/sr: 0,65%**
C57Bl 40d dark 1-5h light	#6: [16,10,**8**]; [10,9,**5**]; [14,9,**8**]; [15,5,**2**]; [17,13,**8**] #7: [15,9,**5**]; [19,14,**9**]; [13,10,**8**]; [13,11,**8**]; [15,11,**6**] #8: [10,3,**2**] #9: [11,3,**3**]; [17,10,**7**]; [13,6,**3**]; [14,8,**5**]; [15,5,**4**]; [8,4,**2**] #10: [5,3,**3**]; [9,3,**2**] [Total rod synaptic terminals: 249; Total rod synaptic ribbons: 146; Tangential ribbons: 98]	0,2534 ± 0,0082 (n=98)	#6: 0; 1; 0; 1; 2 #7: 2; 1; 0; 0; 1 #8: 0 #9: 1; 2; 0; 0; 1; 0 #10: 0; 0 **Percentage csr/sr: 8,2%**
GCAP2+ 40d dark	#11: [15,14,**8**]; [18,11,**7**]; [16,16,**13**]; [12,10,**9**]; [13,11,**4**] [Total rod synaptic terminals: 74; Total rod synaptic ribbons: 62; Tangential ribbons: 41]	0,2634 ± 0.013 (n=41)	#11: 0; 0; 1; 2; 0 **Percentage csr/sr: 4,8%**
GCAP2+ 40d dark 1-5h light	#12: [14,14,**8**]; [16,8,**4**]; [12,8,**3**]; [15,7,**3**]; [21,12,**6**]; [9,6,**4**]; [16,11,**5**]; [17,12,**11**] #13: [8,8,**2**]; [18,6,**3**]; [18,9,**3**]; [12,10,**5**]; [10,8,**3**]; [9,7,**5**]; [16,8,**5**]; [18,14,**6**] [Total rod synaptic terminals: 229; Total rod synaptic ribbons: 148; Tangential ribbons: 76]	0,2439 ± 0.010 (n=76)	#12: 1; 2; 2; 2; 3; 1; 2; 1 #13: 0; 0; 0; 0; 1; 2; 2; 0 **Percentage csr/sr: 12,8 %**
GCAP2+/+ 40d dark	#14: [15,7,**5**]; [13,10,**7**]; [13,10,**6**]; [17,13,**9**]; [13,8,**5**] #15: [12,7,**4**]; [14,7,**5**]; [11,7,**4**]; [13,11,**3**]; [11,8,**6**] #16: [16,9,**8**]; [22,11,**7**]; [14,7,**5**]; [15,11,**7**]; [16,11,**8**] [Total rod synaptic terminals: 215; Total rod synaptic ribbons: 137; Tangential ribbons: 89]	0,2516 ± 0,0085 (n=89)	#14: 0; 1csr; 1csr; 0; 1csr #15: 0; 0; 0; 1csr; 1sr #16: 0; 0; 0; 0; 0 **Percentage csr/sr: 3,6%**
GCAP2+/+ 40d dark 1-5h light	#17: [16,9,**5**]; [13,7,**5**]; [8,5,**3**] #18: [17,11,**7**]; [13,8,**8**]; [14,13,**9**]; [11,9,**5**]; [13,11,**7**] [Total rod synaptic terminals: 105; Total rod synaptic ribbons: 73; Tangential ribbons: 49]	0,2098 ± 0,0134 (n=49)	#17: 1csr,1sr; 1csr,1sr; 0 #18: 1csr,1sr; 2csr; 1csr,2sr; 1csr; 1sr **Percentage csr/sr: 17,8%**
WT 60d cyclic light	**#19**: [16,12,**12**]; [11,5,**3**]; [14,9,**8**]; [18,8,**5**]; [15,8,**6**]; [10,9,**9**] **#20**: [9,4,**3**]; [9,5,**4**]; [13,6,**4**]; [13,5,**5**]; [14,10,**8**]; [10,10,**9**] **#21:** [11,8,**8**]; [15,8,**7**]; [13,7,**6**]; [15,10,**9**]; [12,5,**5**]; [12,6,**6**]; [8,6,**5**]; [10,7,**6**] [7,2,**2**]; [11,5,**5**] [Total rod synaptic terminals: 266; Total rod synaptic ribbons: 155; Tangential ribbons: 135]	0,2902 ± 0,0067 (n=135)	ND

GCAP2+ 60d cyclic light	**#22:** [16,8,**6**]; [12,6,**5**]; [9,7,**6**]; [12,7,**4**]; [16,10,**8**]; [7,4,**3**] **#23:** [14,8,**3**]; [13,7,**6**]; [9,7,**4**]; [11,10,**7**]; [13,10,**5**]; [16,12,**3**] **#24:** [16,10,**7**]; [13,5,**3**]; [15,7,**6**]; [12,7,**5**] **#25:** [17,11,**10**]; [13,6,**5**]; [14,6,**5**]; [14,10,**4**]; [18,10,**6**]; [16,9,**8**]; [9,4,**4**]; [9,9,**8**] [Total rod synaptic terminals: 314; Total rod synaptic ribbons: 190; Tangential ribbons: 131]	0,2621 ± 0,0059 (n=131)	ND
GCAPs-/- 40d dark	**#26**: [21,18,**9**]; [20,10,**7**] **#27**: [20,13,**11**]; [21,12,**10**]; [15,10,**7**]; [19,13,**7**]; [18,13,**11**] **#28**: [30,18,**13**]; [29,12,**10**]; [11,9,**7**], [22,19,**17**]; [15,15,**13**]; [15,14,**14**] **#29**: [18,13,**12**]; [15,8,**4**]; [17,8,**5**], [18,10,**2**]; [11,10,**3**]; [12,9,**4**]; [17,12,**8**]¸ [16,13,**9**]; [15,12,**12**]; [17,9,**7**]; [13,12,**12**] **#30**: [16,7,**4**]; [16,10,**8**]; [10,5,**3**], [10,6,**6**] **#31**: [9,7,**6**]; [9,5,**2**]; [13,9,**7**], [12,7,**6**] [Total rod synaptic terminals: 520; Total rod synaptic ribbons: 332; Tangential ribbons: 256]	0,2791 + 0.0175 (n=256)	ND
GCAPs-/- GCAP2+ 40d dark	**#32**: [19,5,**3**]; [15,8,**5**]; [18,6,**2**]; [19,14,**8**] **#33**: [17,11,**9**]; [13,11,**5**]; [23,11,**8**]; [16,10,**6**]; [23,8,**5**] **#34**:[13,7,**5**]; [10,7,**3**]; [12,8,**4**]; [14,7,**3**] **#35**:[15,6,**3**]; [10,9,**7**]; [14,7,**5**]; [18,8,**8**] **#36**: [20,13,**9**]; [16,7,**9**]; [22,15,**11**]; [20,10,**8**]; [13,7,**6**]; [8,5,**5**] **#37**: [10,3,**3**]; [18,5,**4**]; [16,6,**6**]; [16,7,**5**]; [14,10,**5**]; [23,10,**5**]; [17,11,**6**]; [18,11,**7**] [Total rod synaptic terminals: 500; Total rod synaptic ribbons: 263; Tangential ribbons:178]	0,1798 ± 0,004 (n=178)	ND
GCAPs-/- GCAP2+ 40d cyclic light	#38: [16,7,**5**]; [17,10,**8**]; [14,8,**8**]; [14,8,**6**]; [10,5,**2**]; [15,7,**5**]; [13,8,**5**] [Total rod synaptic terminals: 99; Total rod synaptic ribbons: 53; Tangential ribbons:39]	0,1788 ± 0,007 (n=39)	#16: 0; 0; 1; 1; 1; 1; 1

Table R.4. ***Ribbon length and percentage of club-shaped/spherical ribbons at ribbon synapses of the different mouse lines.*** *Two to ten 16×16 µm frames at 8,000× magnification were delimited in the opl region of each specimen. Each frame typically contained 10 to 22 rod synaptic terminals. Every synaptic terminal in the frame was individually scanned at 100,000× magnification, and length measurements were determined in ribbons resulting from tangential cuts (ImageJ software). Values are expressed as the Mean ± Standard error. The percentage of club-shaped/spherical ribbons is expressed as the ratio of club-shaped ribbons and spherical ribbons to total rod synaptic ribbons (tangential, longitudinal and sagital). Cone synaptic terminals were excluded from the analysis.*

- *Color code in Mouse ID indicates that mice are littermates.*
- *% of csr/sr is expressed as the ratio of club-shaped ribbons and spherical ribbons to total rod synaptic ribbons (tangential, longitudinal and sagital).*
- *1-5h light indicates that mice were exposed to either a 1h or a 5h light step (no differences found between these light conditions).*

were light-adapted for 1–5 h the percentage of club-shaped/spherical ribbons increased to 8%, while in GCAP2+ or GCAP2+/+ mice exposed to these same light conditions the increase was even higher (14% and 18% of assembly intermediates respectively, Table R.4).

Figure R.21B shows two representative visual fields from light-adapted GCAP2+ and GCAP2+/+ samples, in which two and three club-shaped/spherical ribbons are present per visual field, respectively [shown by arrows and magnified in subsequent panels]. This density of club-shaped/spherical ribbons is not observed in the C57Bl samples.

Taken together, the reduction of ribbon length and the increase in the frequency of ribbon morphology intermediates indicate that GCAP2 overexpression causes ribbon disassembly *in vivo*.

Occasionally, accumulations of electrodense particles that seem like clusters of small vesicles (smaller in diameter than synaptic vesicles) were observed in the vicinity of the ribbon and horizontal cell processes (Figure R.21A, GCAP2+/+ panel, dark condition). These clouds of particles of unknown nature, that appear in synaptic terminals irrespective of whether a synaptic ribbon is observed or not, were more voluminous and appeared more frequently in GCAP2+/+ mice than in wildtype mice. We speculate that they might represent debris resulting from bulk membrane retrieval in the process of synaptic vesicle recycling. This observation suggests that GCAP2 might somehow interfere with their clearance.

5.3.3. GCAP2 and RIBEYE Partially Colocalize at Synaptic Ribbons

In order to study whether GCAP2 colocalizes with RIBEYE at synaptic ribbons at the ultrastructural level and whether it localizes to ribbon assembly intermediates, we performed immunohistochemistry at the electron microscopy level. For these studies we used an affinity purified polyclonal antibody anti-GCAP2 generated in rabbit against recombinant GCAP2 protein. This antibody is highly specific, recognizing a single protein band at 24 kDa in Western blots.

Immunolocalization of GCAP2 was assayed in sections from GCAPs−/−GCAP2+ mice. Figure R.22A shows that the anti-GCAP2 antibody decorates the disc membranes at the rod outer segment compartment, as expected. At the synaptic terminal, GCAP2 was observed sparsed in the cytosolic space and occasionally associated to synaptic ribbons, to the plasma membrane and to the presynaptic membrane apposing horizontal cell processes (5nm-gold particles, arrows in Figure R.22B and R.22C). This

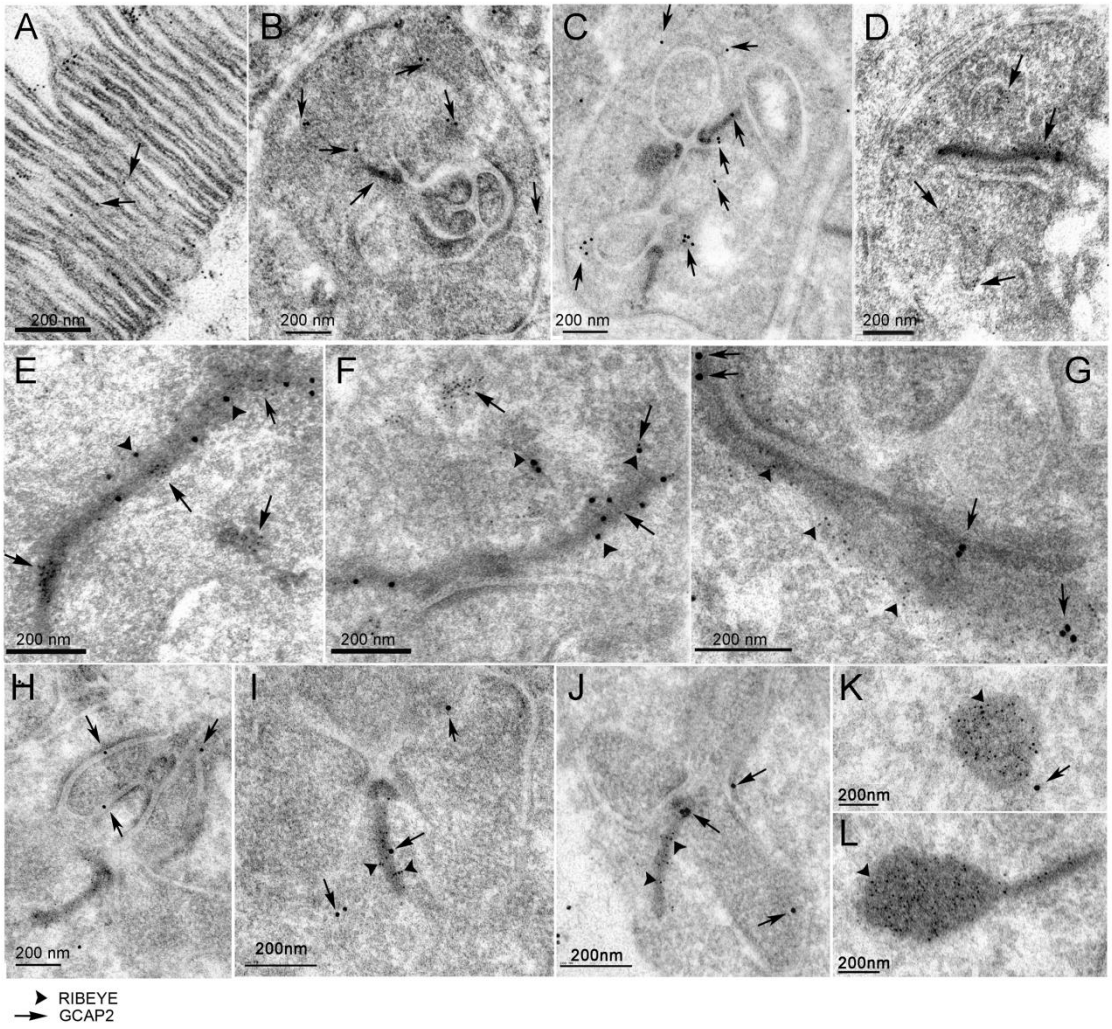

Figure R.22. ***Immunoelectron microscopic localization of GCAP2 and RIBEYE at rod synaptic terminals of GCAPs−/−GCAP2+ mice. A.*** *Localization of GCAP2 in ultrathin sections of the retina at the outer segment layer region, as an intrinsic control of the immunoelectron microscopic localization protocol. GCAP2 [5nm-gold particles, arrows] associates to the disc membranes, as expected.* ***B-C.*** *View of entire synaptic terminals, to show GCAP2 immunoreactivity sparsed in the cytosolic space and also associated to the plasma membrane, the membrane apposing invaginating horizontal processes and the ribbon.* ***D.*** *Gold-particles decorating the border of an invaginating horizontal process.* ***E-G.*** *Selected examples of longitudinal ribbons showing GCAP2 [5nm-gold particles in E, F, 15-nm gold particles in G, pointed by arrows in all panels] colocalizing with RIBEYE [arrowheads in all panels].* ***H-J.*** *Selected ribbon transversal sections showing GCAP2 localization at the ribbon or its proximity [arrows point to GCAP2 associated particles, arrowheads to RIBEYE associated particles].* ***K, L.*** *Representative examples of club-shaped ribbon transversal sections, densely immunolabeled for RIBEYE but not GCAP2. Scale bar corresponds to 200 nm in all panels.*

staining pattern reproduces the GCAP2 immunostaining reported by confocal microscopy, although the density of GCAP2 signal is much lower at the ultrastructural level.

In order to assess the specificity of the occasional immunostaining of synaptic ribbons and the presynaptic membrane apposing horizontal cell processes, the gold particles were counted in more than 70 randomly selected synaptic terminals in the GCAPs−/−GCAP2+ sample (e.g. synaptic terminals presented in Figure R.22B and C)

and GCAPs−/− control sections. In the GCAPs−/−GCAP2+ sample 16% of the analyzed synaptic terminals presented at least one gold particle associated to the ribbon, whereas only 6% of the synaptic terminals analyzed in the GCAPs−/− control presented gold particle association to the ribbon. About 27% of synaptic terminals in GCAPs−/−GCAP2+ sections presented association of the gold particles to the plasma membrane surrounding horizontal cell processes, whereas only 16% presented this association in the GCAPs−/−. Panels R.22E-G show longitudinal sections of synaptic ribbons in which GCAP2 immunostaining is observed in clusters (Figure R.22E-F, 5nm-gold particles, arrows; Figure R.22G, 15nm-gold particles, arrows] colocalizing with RIBEYE, that selectively marks the ribbon (arrowheads in all panels). In tangential sections, GCAP2 is occasionally observed in the ribbon (Figure R.22 I, arrow) and/or in the proximity of the arciform density (Figure R.22J, arrow). Pictures showing GCAP2 association to the membrane apposing invaginating dendritic processes of horizontal cells are shown in Figure R.22H-J. Club-shaped ribbons that were extensively labeled with anti-RIBEYE antibody did not show labeling with the anti-GCAP2 antibody (Figure R.22K,L).

The fact that GCAP2 appears to be occasionally associated with the ribbon in clusters rather than showing a more extensive and homogeneous ribbon distribution might reflect a transient nature of the interaction of GCAP2 with the ribbon structural components.

5.3.4. GCAP1/GCAP2 Double Knockout Mice have Unaltered Ribbons, but the Effect of GCAP2 Overexpression at Shortening Synaptic Ribbons is Magnified in the Absence of GCAP1

In order to study how the loss-of-function of both GCAP1 and GCAP2 affected synaptic ribbon length, ribbon length measurements were taken in rod terminals from GCAPs−/− and compared to those of wildtype mice. For the comparison in Figure R.23 mice were reared in constant darkness. GCAP1 and GCAP2 ablation leads to an increase in light sensitivity, due to suppression of the Ca^{2+}-feedback loop to cGMP synthesis (Mendez *et al.* 2001). This would have the effect of magnifying the change in cell membrane potential and Ca^{2+} dynamics upon light exposure. However, dark-adapted GCAPs−/− mice show a similar dark current value to that of wildtype mice. Therefore, we reasoned that by rearing the mice in darkness any difference detected in ribbon length between wildtype and GCAPs−/− mice could be assigned to their direct effect on ribbon dynamics at the synaptic terminal. However, no significative differences in length were

observed between GCAPs−/− ribbons (0,2791±0,0175 µm, n = 256) and WT ribbons (0,2915±0,00665 µm, n = 103), Figure R.23A-B, Histogram in Figure R.23F and Table R.4, which indicates that GCAP1 and GCAP2 are both dispensable for the normal development and basic structural maintenance of synaptic ribbons, at least when raised in darkness.

Surprisingly, GCAPs−/−GCAP2+ mice raised in darkness showed a remarkable reduction in ribbon length at p40 (0,1798±0,004 µm, n = 178), Figure R.23F and Table R.4. This represents a 36% reduction of ribbon length in GCAPs−/−GCAP2+ compared to GCAPs−/− littermate controls. This 36% reduction of ribbon length in GCAPs−/−GCAP2+ mice that express GCAP2 to 1,5-fold the endogenous level is much higher than the 14% reduction of ribbon length observed in GCAP2+/+ mice, that overexpress GCAP2 to 4-fold the endogenous levels in the wildtype genetic background. These results suggest that endogenous GCAP1 somehow counteracts GCAP2 effect at shortening synaptic ribbons.

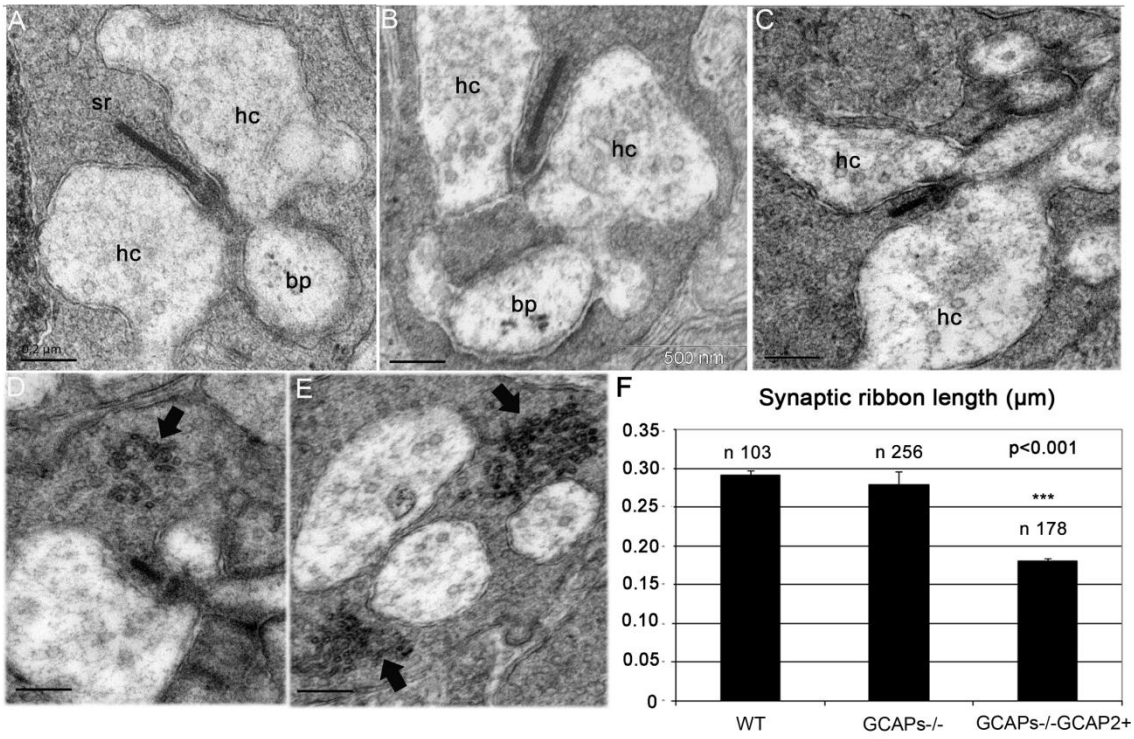

Figure R.23. ***Expression of GCAP2 in the absence of GCAP1 exacerbates the effect of GCAP2 at promoting ribbon disassembly. A-C.*** *Electron micrographs from WT (A), GCAPs−/− (B) and GCAPs−/−GCAP2+ (C) ultrathin retinal sections obtained from dark-reared mice at postnatal day 40, showing a representative rod synaptic ribbon from each phenotype. While GCAPs−/− mice show ribbons that are undistinguishable in length from wildtype ribbons, GCAPs−/−GCAP2+ mice show ribbons that are on average about 40% shorter than wildtype ribbons. hc: horizontal cell process; bc: bipolar cell process; sr: synaptic ribbon.* ***D, E.*** *Examples of GCAPs−/−GCAP2+ synaptic terminals containing accumulations of vesicle-like particles in the vicinity of the active zone (arrows). These aggregates, that might appear in terminals with or without ribbons, might generate as by-products in the bulk endocytosis for synaptic vesicle recycling process.* ***F.*** *Histogram of synaptic ribbon length in WT, GCAPs−/− and GCAPs−/−GCAP2+ mice. Plotted are mean values ± standard errors. * denotes P<0.001 in ANOVA analysis [F(2, 196532) = 97,37, P = 0.000] using the PASW program package (IBM)*

We have observed that GCAP1 also localizes at the synaptic terminal, by immunolocalizing GCAP1 with an affinity-purified anti-GCAP1 polyclonal antibody raised against the whole recombinant protein (Figure R.24). GCAP1 immunolocalization signal partially overlaps with RIBEYE at the synaptic ribbon, indicating that GCAP1 could have a role at the synaptic terminal.

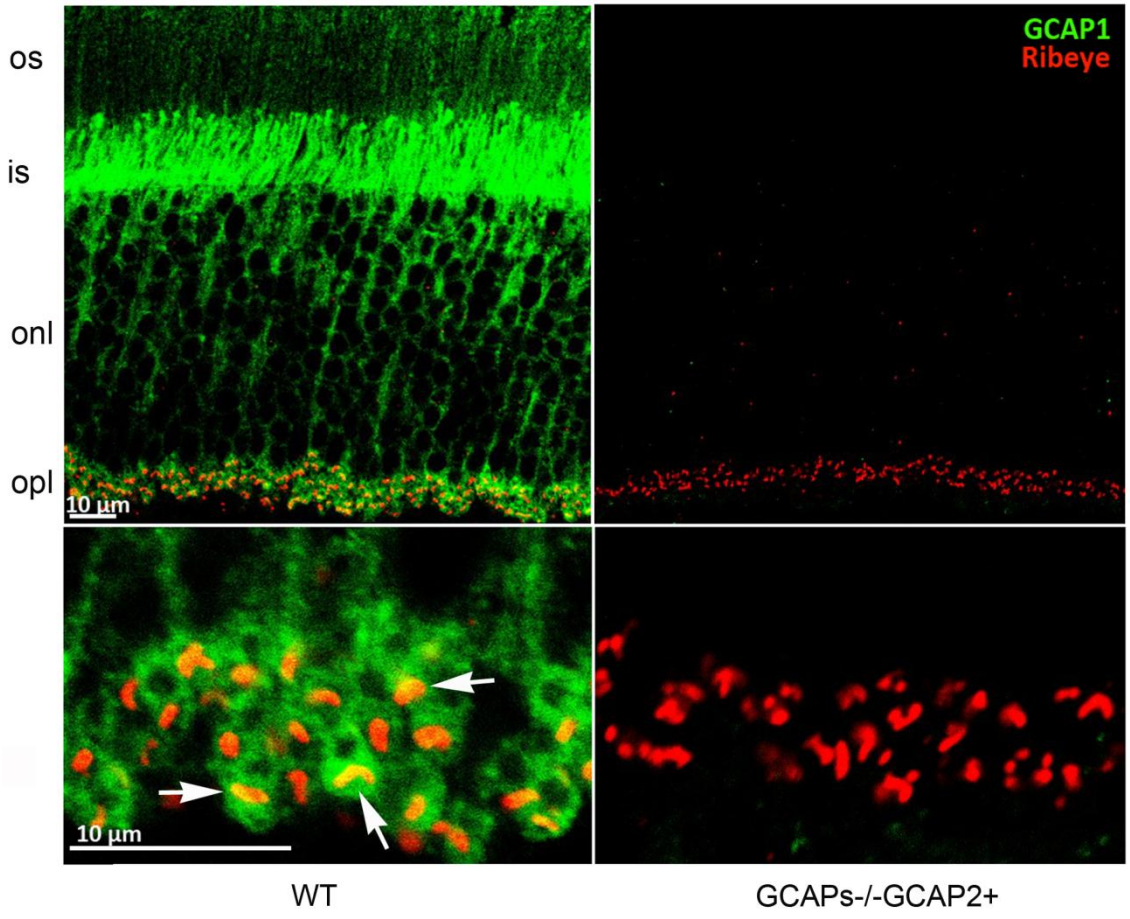

Figure R.24. ***GCAP1 localizes to the synaptic terminal and partially overlaps with RIBEYE.*** *Immunolabeling of vertical retinal sections from WT and GCAPs−/−GCAP2+ mice with rabbit polyclonal antibody anti-GCAP1 and a monoclonal antibody against RIBEYE/CtBP2. GCAP1 is found at the outer segment (os) inner segment (is) and outer plexiform layer (opl) of the retina, where it colocalizes with RIBEYE at synaptic ribbons (white arrows). GCAP1 antibody immunolabeling signal was absent in GCAPs−/−GCAP2+ sections when identical laser power and acquisition gain parameters were used at the confocal microscope, excluding that the signal originates from cross-reactivity of anti-GCAP1 antibody with GCAP2 at this working dilution.*

To study whether there are other ultrastructural changes at the synaptic terminal between GCAPs−/−GCAP2+ mice and their GCAPs−/− littermate controls, the dimensions of individual synaptic terminals were determined in five 16×16 μm^2 visual fields in the OPL region. The size of the synaptic terminals was determined to be smaller in GCAPs−/−GCAP2+ mice than in GCAPs−/− littermate controls, that were in turn smaller than the wildtype. A Duncan's test established the size of the synaptic terminals as follows: GCAPs−/−GCAP2+ (2.47±0.09 μm^2, X+SE, n = 69) < GCAPs−/−

(3.18±0.12 μm^2, n = 88) < WT (3,58±0,13 μm^{2}n = 69), with P<0,05 (Figure R.25). The percentage of synaptic terminals that contained a synaptic ribbon was also reduced in GCAPs−/−GCAP2+ versus the two other groups. Mean values were [WT 70,1±1,8 n = 69; GCAPs−/−67,3±2,3 n = 88; GCAPs−/−GCAP2+57,6±2,3 n = 69]. An ANOVA analysis showed a statistically significant difference between the GCAPs−/−GCAP2+ values and the two other groups, F [2], [12] = 9,36, P = 0,004 (Figure R.25C).

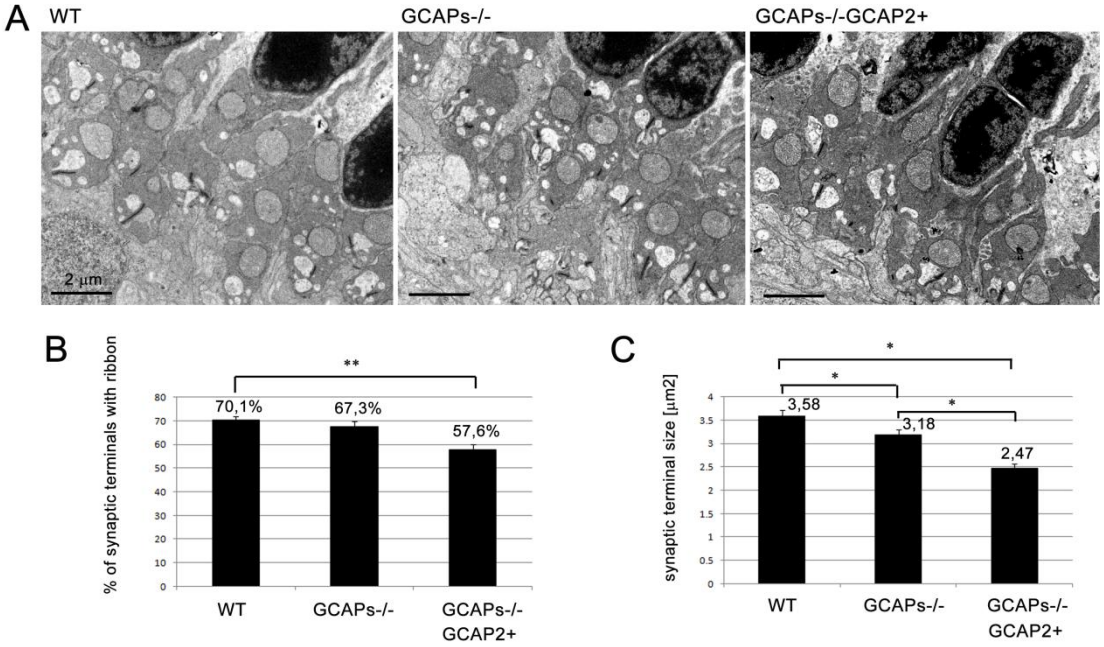

Figure R.25. ***GCAPs-/-GCAP2+ mice present smaller synaptic terminals than GCAPs-/- and WT mice, and fewer synaptic terminals with ribbon. A****. Low magnification micrographs of the opl region of WT, GCAPs-/- and GCAPs-/-GCAP2+ mice. Scale bar, 2μm.* ***B.*** *Histogram comparing the percentage of synaptic terminals with ribbon in the three phenotypes. The number of synaptic terminals that contain a synaptic ribbon was determined in five representative visual fields per phenotype and expressed as the percentage of the total [Mean ± Standard Error]. Mean values were [WT 70,1±1,8 μm^2 n=69; GCAPs-/- 67,3±2,3 μm^2 n=88; GCAPs-/-GCAP2+ 57,6±2,3 μm^2 n=69]. The ANOVA analysis showed a statistically significant difference between the GCAPs-/-GCAP2+ values and the two other groups of values, F[2,12] = 9,36, P=0,004. Asterisc in histogram denotes P< 0,01. No statistically significant difference was observed between WT and GCAPs-/- values [Duncan's test].* ***C.*** *Histogram comparing synaptic terminal size in WT, GCAPs-/- and GCAPs-/-GCAP2+ mice. Statistically significant differences were observed among groups by ANOVA analysis F[2,223] =20,37, P=0,000. A Duncan's test established GCAPs-/-GCAP2+ mice synaptic terminals (2.47±0.09 μm^2 , X+SE, n=69,) < GCAPs-/- (3.18±0.12 μm^2 n=88) < WT (3,58±0,13 μm^2 n=69), with P< 0,05.*

That is, synaptic terminals are smaller in GCAPs−/−GCAP2+ mice, and there is a lower percentage of synaptic terminals that contain a ribbon. This figure explains our observation in Figure R.18 that OPL thickness is substantially reduced in GCAPs−/−GCAP2+ mice, and reflects that the integrity of the ribbon synapse is compromised to some extent in these mice. However, neurodegeneration in these mice appears to be milder than the neurodegeneration described for other mouse models with mutations in presynaptic proteins (Dick *et al.* 2003) (tom Dieck *et al.* 2005) (Reim

et al. 2005) (Schmitz *et al.* 2006) (Biehlmaier *et al.* 2007) (Grossman *et al.* 2009) (Sharma *et al.* 2011), and signs of autophagia like vacuolization or mitochondria swelling were not appreciated in GCAPs−/−GCAP2+ mice compared to GCAPs−/− or WT controls (Figure R.25).

When GCAPs−/−GCAP2+ mice were raised in 12 h:12 h dark:light standard cyclic light they showed a similar reduction in ribbon length at p40 (0,1788±0,007 µm, n = 43) than when raised in darkness, whereas GCAPs−/− littermate control mice raised under the same cyclic light conditions showed a more subtle reduction in ribbon length (0,2412±0,01 µm, n = 29).

Taken together, these results indicate that abolishing the expression of both GCAP1 and GCAP2 does not alter the length or morphology of synaptic ribbons in dark-reared mice, or substantially affect the thickness and connectivity of the OPL. However, expressing GCAP2 in the absence of GCAP1 (GCAPs−/−GCAP2+ mice) had a severe effect at shortening the ribbons, lowering the number of synaptic ribbons, reducing the dimensions of synaptic terminals and ultimately causing a thinning of the OPL. We conclude that altering the ratio of GCAP1 to GCAP2 in rod photoreceptor cells *in vivo* leads to morphological alterations at the synaptic terminal including a substantial shortening of the synaptic ribbon. Because alteration of GCAP1 to GCAP2 relative levels has a bigger effect than the overexpression of GCAP2, we infer that it is the balanced action of these proteins in rods that is required to maintain the integrity of synaptic terminals.

5.3.5. Mice that Express GCAP2 in the Absence of GCAP1 and are Raised in Darkness have Severely Impaired Light Responses in the Scotopic Range

To study whether the phenotype observed at the ultrastructural level in these mouse lines correlates with a functional phenotype, electroretinogram responses to a family of flashes of increasing intensities were recorded in the scotopic and the photopic range.

Rod b-wave amplitudes in the scotopic range (I = −4 to I = −2 Log cd.s/m^2), as well as a-wave and b-wave amplitudes from rod and cone mixed responses (I = 1,5 Log cd.s/m^2) and pure cone responses (I = 2,0 Log cd.s/m^2) were averaged for the different mouse lines, and are presented in Table R.5. Representative recordings are shown in Figure R.26. While dark-reared GCAPs−/− mice presented minor reductions in the amplitude of the rod b-wave and the a-wave from mixed responses (compare blue traces to red traces), dark-reared GCAPs−/−GCAP2+ mice showed very diminished

responses in the scotopic range as well as diminished a-wave amplitudes in the rod-cone mixed responses (compare black traces to red traces). In contrast, pure-cone responses in the photopic range were unaffected (Table R.5, Figure R.26 bottom traces). Photopic responses in GCAPs−/−GCAP2+ mice are not expected to differ from GCAPs−/− responses because the transgene is not expressed in cones.

ERG wave amplitude **Intensity (cd·s·m-2)**		**b – rod** **-2,0**	**a – mixed** **1,5**	**b - mixed** **1,5**	**b - cone** **2,0**
WT [D-D]	n = 4	304,08 ± 15,39	277,90 ± 34,30	529,48 ± 34,29	188,75 ± 8,84
GCAPs -/- [D-D]	n = 4	230,98 ± 22,62	177,01 ± 18,07	380,65 ± 32,78	140,81 ± 19,78
GCAPs -/- GCAP 2+ [D-D]	n = 10	69,91 ± 16,57***	54,44 ± 19,18***	228,38 ± 24,65***	180,69 ± 13,77
WT [L-D]	n = 4	255,84 ± 11,53	203,62 ± 7,83	474,29 ± 14,46	188,75 ± 8,84
GCAPs -/- [L-D]	n = 4	158,81 ± 7,04	183,59 ± 9,28	446,52 ± 53,77	237,84 ± 28,33
GCAPs -/- GCAP 2+ [L-D]	n = 6	178,76 ± 37,57	185,89 ± 31,38	455,33 ± 68,24	256,87 ± 31,43
GCAP 2+ [L-D]	n = 3	224,31 ± 25,01	175,22 ± 12,54#	420,08 ± 33,97	234,25 ± 8,04

Table R.5 ***ERG response parameters in the different mouse lines.*** *Statistical analysis of ERG data was performed using GraphPad InStat software; each experimental group was considered independent. A general linear model procedure with analysis of the variance (ANOVA) was carried out. Post hoc multiple comparisons Tukey test was used. Data are expressed as mean ± SEM. The results were considered significant at p<0.05.*

WT [D-D] vs.

- GCAPs -/- [D-D]: n.s.
- GCAPs -/- GCAP 2+ [D-D]: *** p<0.001

WT [L-D] vs.

- GCAPs-/- [L-D] : n.s.
- GCAP 2+ [L-D] : n.s.
- GCAPs -/- GCAP 2+ [L-D]: n.s

The reduction in the magnitude of the rod component of the ERG response was more severe in GCAPs−/−GCAP2+ rods when mice were raised in constant darkness than when mice were raised in standard 12 h:12 h dark:light cycles (Figure R.26, compare superimposed traces in left and middle panels).

Because both the a-wave and b-wave are reduced in dark-reared GCAPs−/−GCAP2+ ERG responses, this visual impairment cannot be solely attributed to ribbon shortening.

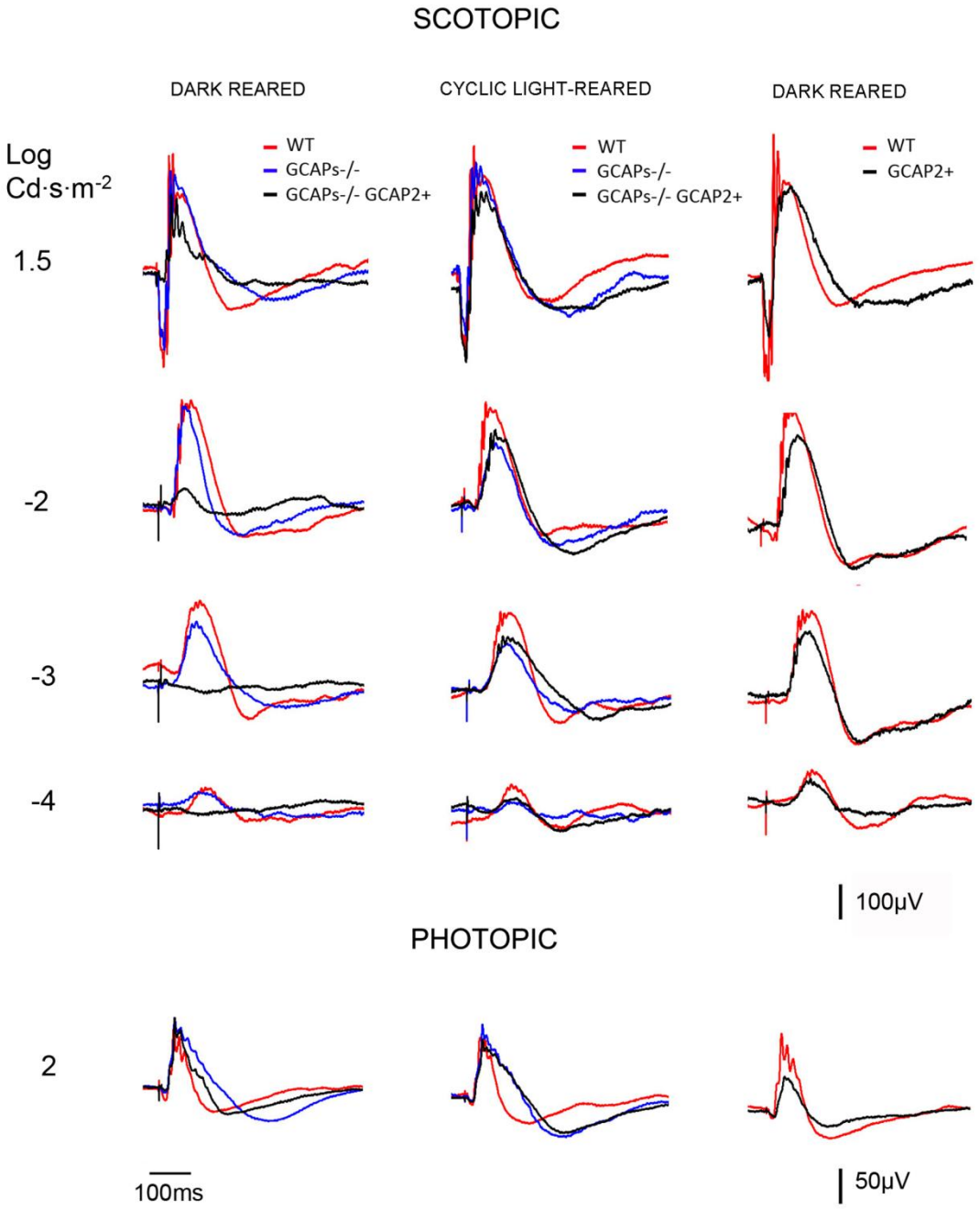

Figure R.26. ***Comparison of electroretinogram responses from WT, GCAP2+, GCAPs−/− and GCAPs−/−GCAP2+ mice that were either raised in constant darkness or in 12h:12h dark:light standard cyclic light.*** *Left panel, superimposed representative responses of WT (red), GCAPs−/− (blue) and GCAPs−/−GCAP2+ (black) mice at p40 that were reared in constant darkness, in the scotopic and photopic range. The a-wave amplitude is severely reduced in GCAPs−/−GCAP2+ mice (black trace) compared to wildtype and GCAPs−/− traces in the scotopic range. This difference is absent in the photopic range, since the transgene is only expressed in rods. Central panel, superimposed representative responses of the same phenotypes, but raised in 12h:12h dark:light standard cyclic light and dark-adapted previous to the experiment. ERG responses from GCAPs−/−GCAP2+ mice were similar to GCAPs−/− and wildtype responses. Right panel, superimposed traces of cyclic light reared wildtype and GCAP2+ mice at p40. There were no statistically significant differences in the a-wave and b-wave amplitudes of these responses, whether the mice were raised in constant darkness or in 12h:12h dark:light standard cyclic light (cyclic reared mice results shown).*

Furthermore, the same shortening of the ribbons takes place when GCAPs−/−GCAP2+ mice are raised in cyclic light, but ERG responses are indistinguishable from GCAPs−/− responses. These results indicate that the rod component of the ERG response is very diminished in dark-reared GCAPs−/−GCAP2+ mice; and, on the other side, that a shortening of 40% of ribbon length in cyclic-light reared GCAPs−/−GCAP2+ mice has little effect on the amplitude of the B-wave of ERG responses in the scotopic range. That is, ribbon shortening has a limited effect on synaptic strength.

The decreased contribution of the rod component of the ERG response to dark-reared GCAPs−/−GCAP2+ responses is not due to the loss of rod photoreceptor cells. GCAPs−/−GCAP2+ mice that have been raised in constant darkness show at p40 the same number of photoreceptor nuclei rows that wildtype mice, as shown by morphometric analysis of outer nuclear layer thickness at different regions covering the whole length of the retina in these mice (Figure R.18C). Therefore, we infer that the rods in GCAPs−/−GCAP2+ mice raised in darkness have a diminished contribution to ERG responses because they are unable to respond to light, likely due to electrical saturation (see Discussion).

5.4. DISCUSSION

Guanylate Cyclase Activating Proteins (GCAPs) are neuronal Ca^{2+} sensors from the calmodulin superfamily. They play a fundamental role in the recovery of the light response by conferring Ca^{2+} modulation to retinal guanylate cyclase at the membrane discs of rod and cone outer segments where phototransduction takes place (Arshavsky *et al.* 2012). The main isoforms GCAP1 and GCAP2 also localize to the inner segment and synaptic terminal of photoreceptor cells, where their function is unknown (Cuenca *et al.* 1998). A recent study has demonstrated that GCAP2 interacts with RIBEYE, a unique and major protein component of synaptic ribbons, and partially colocalizes with RIBEYE at these structures, and pointed to GCAP2 as a candidate that might mediate the Ca^{2+}-dependent disassembly of synaptic ribbons (Venkatesan *et al.* 2010).

In this study we set to test this hypothesis *in vivo*, by analyzing alterations in the density and morphology of synaptic ribbons in GCAP2 models of gain-of-function (GCAP2 overexpression) and loss-of-function (GCAP1/GCAP2 double knockout, GCAPs−/−) and their correlation with a functional phenotype. We here report that mice that lack GCAP1 and GCAP2 develop synaptic ribbons that are similar in length and morphology to wildtype ribbons, indicating that the GCAP2-RIBEYE interaction is not required for the initial assembly or anchoring of the ribbon to the active zone. By

characterizing transgenic mice that overexpress GCAP2 in rods (GCAP2+ and GCAP2+/+ mice) or mice in which GCAP2 expression was restored in the GCAPs−/− genetic background (GCAPs−/−GCAP2+ mice) we have confirmed that GCAP2 overexpression leads to the shortening of synaptic ribbons. This phenotype is manifested when mice are reared either in standard cyclic light or in constant darkness, and it worsens when GCAP2 is expressed in the absence of GCAP1, in which case it severely impairs visual function when mice are dark-reared. We also demonstrate GCAP2 colocalization with RIBEYE at the ultrastructural level. Based on our results we suggest that both GCAP1 and GCAP2 isoforms, and particularly the relative levels of GCAP1 to GCAP2, might contribute to mediate the ribbon morphological changes triggered by light through a combination of effects: a secondary effect on the ribbon due to their role at regulating cGMP synthesis at rod outer segments; and a more direct effect on the ribbons exerted at the synaptic terminal. We here analyze our findings and their physiological significance in the context of the current knowledge of GCAP1 and GCAP2 function and biochemical properties.

5.4.1. GCAP1 and GCAP2 are not Required for the Early Assembly of Photoreceptor Ribbon Synapses

The group of Frank Schmitz has identified GCAP2 as an interacting partner of RIBEYE. In their localization assays, Venkatesan and collaborators showed that the GCAP2 immunofluorescence signal filled the cytosolic space of the synaptic terminal, partially overlapping with RIBEYE at the ribbons (Venkatesan *et al.* 2010).

Synaptogenesis in rod photoreceptors of the mouse retina is initiated at P6–P8, and is completed by the time mice open their eyes at P13–P14. The assembly of photoreceptor ribbons during synaptogenesis involves the formation of sphere-like structures from protein aggregates of ribbon cytomatrix proteins: Bassoon, RIBEYE, Piccolo and RIM1. These non-membranous electrodense “precursor spheres” were proposed to be the transport units of the ribbon cytomatrix active zone (CAZ) proteins that assemble into immature floating ribbons and subsequently give rise to mature anchored ribbons (Regus-Leidig *et al.* 2009). Mice that lack Bassoon show impaired aggregation of ribbon cytomatrix proteins at early stages, delayed formation of precursor spheres (Regus-Leidig *et al.* 2010b) and a failure to form anchored ribbons (Dick *et al.* 2003). The fact that GCAP2 interacts with RIBEYE raises the question of whether GCAP2 might be required for the developmental assembly of synaptic ribbons. In this study we have observed that the GCAP1/GCAP2 double knockout mice

(GCAPs−/−) present a largely normal OPL at p40 with the typical pattern of RIBEYE staining (Figures R.18, R.19, and R.20); and the usual number of synaptic ribbons, with standard size and morphology by transmission electron microscopy (Figure R.23 and Figure R.25).

Measurements of synaptic ribbon length in GCAPs−/− mice were initially taken from mice that were reared in constant darkness (Figure R.23). The reason for this is that GCAPs−/− rod photoreceptors show a higher sensitivity to light than wildtype rods, and the same prolonged light stimuli could have different effects on WT and GCAPs−/− mice (Mendez *et al.* 2001). Nevertheless, we have subsequently observed that either dark-reared or cyclic-light reared GCAPs−/− mice yielded similar to wildtype ERG responses in a range of light intensities that covered the scotopic and photopic ranges (Figure R.26). These results indicate that GCAP1 and GCAP2 are not required for the developmental assembly of synaptic ribbons in rod photoreceptors. However, they do not exclude that these proteins play more subtle roles: e.g. at regulating ribbon dynamic turn-over (see below).

5.4.2. Ultrastructural Localization of GCAP2 at the Synaptic Terminal

Original immunolocalization studies of GCAP1 and GCAP2 reported that GCAP1 localized more abundantly to cone outer segments whereas GCAP2 appeared to be present in the outer segment, the inner segment and the synaptic terminals of both rods and cones in different species (Cuenca *et al.* 1998) (Kachi *et al.* 1999). Venkatesan's study has shown that the GCAP2 immunofluorescence signal filled the synaptic terminal and to some extent overlapped with synaptic ribbons (Venkatesan *et al.* 2010). Our localization data at the confocal microscopy level confirms this observation (Figure R.18), which is relevant because our assays overcome two previously identified limitations in GCAP localization studies. First, the fact that antibodies raised against one specific isoform might cross-react with the other (e.g. Antibodies raised against GCAP2 typically crossreact with GCAP1, and vice versa). Second, the fact that antibodies raised against a particular species isoform yield different results in retinal tissue from different species (Howes *et al.* 1998) (Otto-Bruc *et al.* 1997). Our antibodies were raised against the bovine isoform of GCAP2, and they were used to immunolocalize the bovine isoform of GCAP2 expressed in transgenic mice. The bovine GCAP2 isoform has been shown to restore endogenous GCAP2 localization and function in GCAPs−/− mice (Mendez *et al.* 2001).

Our immunoelectron localization study revealed for the first time at the ultrastructural level that GCAP2 co-localizes with RIBEYE in about 16% of the synaptic ribbons analyzed in the GCAPs−/−GCAP2+ mice (Figure R.22). Instead of a homogeneous distribution along the ribbon, we found that GCAP2 was present in clusters, easier to detect in longitudinal sections [with up to two or three clusters per ribbon, Figure R.22E-G) than in tangential sections. That GCAP2 appears associated to the ribbon in only 16% of the ribbons analyzed might be indicative of a transient interaction. It has been described that, following the *in vitro* EGTA treatment of retinas, ribbon disassembly begins with the formation of protrusions and the pinching off of spherical ribbon material (Spiwoks-Becker *et al.* 2004), (Regus-Leidig *et al.* 2009), that are seen as club-shaped ribbons and as floating spheres in tangential sections. Therefore, in our immunolabeled ultrathin sections we thoroughly looked for clusters of RIBEYE and GCAP2 outside the ribbon that might reflect modules of disassembly containing both proteins, but could not detect them. Taken together, our results confirm GCAP2 localization at the ribbons at the ultrastructural level, and would sustain GCAP2 involvement in the regulation of ribbon morphological changes triggered by changes in Ca^{2+}.

In addition to the synaptic ribbon, GCAP2 was also associated to the plasma membrane and particularly to the presynaptic membrane apposing the invaginating processes of horizontal cells (Figure R.22D,H-J). The whole delimiting membrane was decorated, and not just the active zone. This result points to GCAP2 having additional functions at the synaptic terminal, where it could be imparting Ca^{2+} sensitivity to new molecular targets. Future experiments will attempt to identify GCAP2 molecular targets in this compartment.

5.4.3. GCAPs Effect on Ribbon Length

Synaptic ribbons in photoreceptor cells of the mouse retina in the albino strain Balb/c tend to disassemble in response to illumination by releasing ribbon material in spherical modules; and elongate by regaining ribbon material during dark-adaptation (Vollrath *et al.* 1996) (Adly *et al.* 1999) (Vollrath *et al.* 2001) (Spiwoks-Becker *et al.* 2004) (Regus-Leidig *et al.* 2009) (Regus-Leidig *et al.* 2010a). Although the physiological significance of this ribbon remodeling with light is not yet clear and strong variations in the extent of these changes have been reported between different mouse strains (Fuchs, Sendelbeck *et al.* 2013), we have observed in this study that 1 h of light exposure can cause a 13% reduction of ribbon length in pigmented C57Bl/6 mice (Figure R.21 and

Table R.4). While we doubt that this might be a relevant mechanism to regulate synaptic strength or serve to extend the operational range of rods, it might represent a turn-over mechanism of the ribbon set in place by light, e.g. following photic damage.

It has been shown in albino mice that ribbon disassembly depends on the drop in intracellular Ca^{2+} at the synapse caused by the light-triggered hyperpolarization of the cell (Spiwoks-Becker *et al.* 2004) (Regus-Leidig *et al.* 2010a). Because GCAP2 has been shown to interact with RIBEYE and localize to the ribbon (Venkatesan *et al.* 2010), we here wanted to test whether GCAP2 might mediate the Ca^{2+} -dependent structural changes of ribbons as proposed (Venkatesan *et al.* 2010).

Our findings indicate that, although both GCAP1 and GCAP2 isoforms are dispensable for developmental ribbon formation and basic structural maintenance, altering the GCAP1 to GCAP2 ratio does have an effect on the morphology of synaptic terminals and does alter ribbon length.

Mice that express GCAP2 to 2,5-fold the endogenous levels (GCAP2+ line, Table R.3) presented a 10%reduction in ribbon length compared to wildtype mice when both transgenic and wildtype mice were raised in constant darkness, or in standard cyclic light (Figure R.21, Table R.4). Mice that express GCAP2 to 4,5-fold the endogenous level [GCAP2+/+] showed a 14% reduction in ribbon length when mice were raised in constant darkness and a 24% reduction when they were raised in constant darkness and subsequently exposed to light for 1–5 h. In addition, the percentage of ribbon shapes that identify a disassembling ribbon (club-shaped and spherical ribbons versus bar-shaped ribbons in transversal sections) was higher in transgenic mice than in wildtype mice. These ultrastructural effects on the synaptic ribbons show that GCAP2 overexpression causes ribbon disassembly. This noticeable change in ribbon dimensions, however, had only minor effects on the functional response to light, as measured by electroretinogram (ERG). GCAP2+ mice elicited light responses by ERG that were similar to wildtype responses in a-wave and b-wave amplitude and kinetics, when they were raised either in constant darkness or in standard cyclic light (traces from cyclic light-reared mice shown in Figure R.26; traces from dark-reared mice not shown). This indicates that a 10% reduction in ribbon length is not enough to produce a significative change in the b-wave of the ERG response, and that more extensive remodeling of the ribbon might be necessary to affect synaptic strength.

As discussed above, GCAPs−/− synaptic ribbon length did not differ from wildtype synaptic ribbons at p40, and ERG responses of GCAPs−/− mice at p40 were similar to wildtype.

Intriguingly, mice in which GCAP2 expression was selectively restored in the GCAPs−/− background (GCAPs−/−GCAP2+) showed synaptic ribbons that were 40% shorter than wildtype ribbons at p40 when raised in constant darkness (Figure R.23). GCAPs−/−GCAP2+ mice, when raised in constant darkness, had severely impaired rod visual function at p40. Both the a-wave and b-wave amplitudes of ERG responses were severely reduced in the scotopic range. Because the a-wave amplitude of the ERG reflects the change in membrane potential elicited by the phototransduction cascade and the inverted-sign b-wave reflects postreceptoral activation of rod on-bipolar cells, genetic defects affecting synaptic transmission typically affect predominantly the b-wave (Ball *et al.* 2002) (Haeseleer *et al.* 2004) (Van Epps *et al.* 2004) (Mansergh *et al.* 2005). Therefore the GCAPs−/−GCAP2+ visual impairment could not be solely attributed to the shortening of rod ribbons. Instead, the ERG phenotype of dark-reared GCAPs−/−GCAP2+ mice revealed a diminished capacity to respond to light at the rod outer segment (ROS) level.

The ratio of the Ca^{2+}-bound inhibitory state to the Mg^{2+}-bound stimulatory state of each GCAP isoform is what determines the rate of cGMP synthesis by retinal guanylate cyclase in rod outer segments at any given $[Ca^{2+}]_i$. Given the well characterized difference in the Ca^{2+}sensitivities of GCAP1 and GCAP2, there is a narrow range of $[Ca^{2+}]_i$ -around the $[Ca^{2+}]_i$typical of the dark-adapted steady state- for which GCAP1 molecules would be in the stimulatory state while most GCAP2 molecules would be inhibitory state of the cyclase, and these antagonistic effects would cancel each other (Mendez *et al.* 2001). It is therefore not surprising that chronic darkness might result in an alteration in the free cGMP levels at ROS in GCAPs−/−GCAP2+ mice in which GCAP2 is expressed in the absence of GCAP1, reducing cGMP levels gradually over time. Abnormally low levels of free cGMP would cause the closure of cGMP-gated channels and the electrical saturation of rods, and could explain the diminished rod component of the ERG despite retention of a normal number of rods in these retinas (Figure R.26 and Figure R.18C). Therefore it cannot be excluded that shortening of the ribbons might result from a chronic alteration of $[Ca^{2+}]_l$ at the synapse due to abnormally low levels of cGMP. That is, when GCAPs−/−GCAP2+ mice are raised in constant darkness, alterations in ribbon morphology could be a secondary consequence of GCAP2 effect on cGMP metabolism. The involvement of the phototransduction cascade and cGMP metabolism on the light-triggered morphological changes of ribbons has been established (Spiwoks-Becker *et al.* 2004) .

In contrast to mice raised in constant darkness, GCAPs−/−GCAP2+ mice reared in 12 h:12 h dark:light cycles preserved scotopic ERG traces at p40 similar to wildtype in

magnitude and kinetics (Figure R.26, Table R.5). Noteworthy, synaptic ribbons in GCAPs−/−GCAP2+ mice raised in cyclic light at p40 are shortened to the same extent as GCAPs−/−GCAP2+ mice raised in darkness (Table R.4). These mice have been reported to have dark current values similar to wildtype, in association with normal free cGMP levels (Mendez *et al.* 2001). This makes it unlikely that changes in ribbon length observed in these animals are secondary to altered cGMP metabolism at ROS. Strikingly, the absence of GCAP1 exacerbates the effect of GCAP2 at shortening ribbon length, even when mice are raised in cyclic light. We infer that altering the balance between GCAP1 and GCAP2 leads to the shortening of the ribbons.

Altering the balanced action of GCAP1 and GCAP2 also compromises the ribbon synapse integrity, as shown by the reduction in the size of the synaptic terminals in GCAPs−/−GCAP2+ mice (Figure R.25). Therefore, we cannot completely rule out that ribbon disassembly might be a secondary consequence of a presynaptic defect caused at some other level. There are numerous examples in the literature of mutations in presynaptic proteins that cause presynaptic defects that are accompanied by changes in ribbon structure. Mutations in Cav1.4, bassoon, complexin, synaptojanin and laminin produce floating ribbons (Dick *et al.* 2003) (Reim *et al.* 2005) (tom Dieck *et al.* 2005) (Chang *et al.* 2006) (Biehlmaier *et al.* 2007). Mutations in tubby-like protein 1 (TULP1), which impairs rhodopsin trafficking to the outer segment, also affect synaptic ribbon morphology (Grossman *et al.* 2009). Mutations in cysteine string protein alpha, a chaperone required for SNAP25 and SNARE complex assembly cause photoreceptor degeneration and the appearance of floating ribbons (Schmitz *et al.* 2006), (Sharma *et al.* 2011). Myosin Va mutant mice have both anatomical and physiological abnormalities at rod synapses (Libby *et al.* 2004). However some of these mouse models [e.g. Tulp1 KO, CSPα KO] manifest a rapid retinal degeneration with a substantial loss of photoreceptor cells that is accompanied by severe functional defects before one month of age (Hagstrom *et al.* 1999) (Schmitz *et al.* 2006). GCAPs−/−GCAP2+ transgenic mice, in contrast, preserve the normal number of photoreceptor cells for months (Figure R.18) and do not present obvious signs of neurodegeneration like vacuolization or mitochondria swelling at the synapse (Figure R.25). The fact that the absence of GCAP1 exacerbates the effect of GCAP2 at shortening ribbons argues against a non-specific toxic effect of overexpressed GCAP2 at the synaptic terminal. Rather, it seems that the balanced action of GCAP1 and GCAP2 might be needed to preserve the integrity of the synapse and the ribbon.

Together with Venkatesan's report that GCAP2 interacts with RIBEYE, our observation that GCAP2 can appear associated to the ribbon at the ultrastructural level and the

marked reduction in ribbon length that is observed in GCAPs−/−GCAP2+ mice leads us to suggest that GCAPs might be involved in mediating the morphological changes at the ribbons triggered by changes in Ca^{2+}.

Further genetic and biochemical experiments will be needed to confirm the direct implication of GCAP2 and GCAP1 in this process, and to study whether GCAP1 and GCAP2 might have new molecular targets and new functions at the synapse.

5.5. CONCLUSION

The central observation of this study is that the overexpression of GCAP2 in rods *in vivo* has an impact at shortening synaptic ribbons that is exacerbated in the absence of GCAP1. These results, together with the lack of phenotype when both GCAP1 and GCAP2 isoforms are absent in the double knockout, point to the balanced action of GCAP1 and GCAP2 having an effect on the ultrastructure of the synaptic terminals and on synaptic ribbon length, likely through a combination of mechanisms: i) an indirect or secondary effect on the ribbon would be caused by their primary effect on cGMP metabolism at rod outer segments, manifested in this study when GCAP2 is expressed in the absence of GCAP1 and mice are reared in constant darkness; and ii) an effect on the ribbon through a mechanism independent of cGMP metabolism, manifested when GCAP2 is overexpressed or expressed in the absence of GCAP1 and mice are reared in cyclic light. We have observed that a 40% reduction of ribbon length *in vivo* in GCAPs−/−GCAP2+ mice raised in cyclic light had only subtle effects on ERG responses in the scotopic range, indicating that ribbons can withstand dimensional restrictions without a severe functional effect.

VI. FINAL DISCUSSION AND FUTURE PERSPECTIVES

RESUMEN EN ESPAÑOL

Las guanilato ciclasas de retina (RetGCs) y las proteínas activadoras de las guanilato ciclasas (GCAPs) están ensambladas en un complejo (RetGC/GCAPs) que tiene un papel fundamental en el compartimento sensorial de células fotorreceptor para la terminación de la señal a la luz y para la adaptación a la luz, y un nodo clave en la señal de retrorregulación recíproca entre el cGMP y el Ca^{2+}.

A pesar de la extensa caracterización bioquímica de estas proteínas, otros aspectos relacionados con su función en la célula se desconocen todavía, como: a) – Qué determina su distribución subcelular?; b) - Qué otras funciones desempeñan en los otros compartimentos celulares, fuera del segmento externo?; c) – Cómo desencadenan la muerte celular las formas mutadas de las proteínas GCAP1 y GCAP2 asociadas a ceguera hereditaria?

En este estudio hemos abordado estas cuestiones mediante la caracterización de un modelo de ratón que expresa una forma mutada de GCAP2 en que todos los dominios de unión a Ca^{2+} han sido inactivados. La expresión de esta forma mutada de la proteína en fotorreceptores bastón conduce a una degeneración retinal rápida.

Primero demostramos que este mutante causaba toxicidad por un mecanismo independiente del metabolismo de cGMP, un resultado inesperado dado que las mutaciones en GCAP1 que reducen su afinidad de unión a Ca^{2+} conducen a la activación constitutiva de cGMP, tanto *in vitro* como *in vivo*. Sin embargo, la forma mutada EF^{-}GCAP2 es retenida en los compartimentos proximales de la célula y no se transporta al segmento externo. Además, en el segmento interno y compartimentos proximales de la célula, se acumula en una forma incompetente para la activación de la actividad guanilato ciclasa en ensayos de reconstitución.

Para estudiar cómo la acumulación de la forma mutada EF^{-}GCAP2 en el segmento interno conduce al daño celular, investigamos qué interacciones establece la forma mutada EF^{-}GCAP2 de forma selectiva respecto a la forma wildtype de GCAP2. El análisis proteómico identificó a las proteínas 14-3-3 como interactores de mayor afinidad a la forma mutada que a la wildtype. La identificación de las distintas isoformas de 14-3-3 como interactores de GCAP2 nos llevó a desvelar un mecanismo molecular clave en el control de la distribución intracelular de GCAP2, con implicaciones importantes en enfermedad. GCAP2 se fosforila *in vivo* principalmente cuando se encuentra en su forma libre de Ca^{2+}. La fosforilación es lo que incita la unión de 14-3-3, y su retención en el segmento interno. En ratones wildtype, un 50% del total de la forma endógena de GCAP2 se fosforila; y esto se correlaciona con el

porcentaje de GCAP2 que se localiza en los compartimentos proximales de la célula (50%). En ratones que expresan EF$^-$GCAP2, casi la totalidad de la proteína se encuentra fosforilada, y casi la totalidad de la proteína es retenida en los compartimentos proximales. La asociación de GCAP2 y 14-3-3 *in vivo* se manifiesta claramente también en separaciones de extractos de retina por cromatografía de exclusión en tamaño.

De nuestros resultados emerge el siguiente modelo: GCAP2 se sintetiza en el segmento interno. Si une Ca^{2+} tras su síntesis (cuando la $[Ca^{2+}]_i$ es alta, en períodos de oscuridad), entonces se une a RetGC y es transportada al segmento externo. Si no une Ca^{2+} tras su síntesis (a baja $[Ca^{2+}]_i$, en períodos de exposición a luz), entonces une Mg2+ y adquiere una conformación tridimensional que es menos estable. La forma libre de Ca^{2+} de GCAP2 forma dímeros, es fosforilada y une dímeros de 14-3-3. Esta unión podría explicar la retención de GCAP2-P en el segmento interno y compartimentos proximales, ya que las isoformas de 14-3-3 están excluídas del segmento externo. De hecho, en este estudio presentamos la comprobación genética de que la fosforilación de GCAP2 es la responsable de su retención. Al mutar la Ser201 en EF$^-$GCAP2 revertimos su retención, y la proteína se transporta al segmento externo. De acuerdo con nuestro modelo, la distribución subcelular de GCAP2 (una proteína citosólica) es un proceso altamente regulado, dictado por interacciones proteína-proteína que ocurren de forma diferente en los períodos de luz que en los períodos de oscuridad, y no como resultado de la equilibración de su concentración en el espacio citosólico. Las mutaciones en GCAP2 que disminuyen o impiden su unión a Ca^{2+} alteran este mecanismo de distribución de la proteína, creando un desequilibrio –por acumulación de GCAP2 en el segmento interno en una forma conformacional inestable- que en último término conduce a la muerte celular.

Esto es, aquí describimos un nuevo mecanismo de toxicidad de mutaciones en las proteínas GCAP que es independiente del metabolismo de cGMP. La expresión transgénica de bEF$^-$GCAP2 condujo a una degeneración retinal rápida. Por tanto, la acumulación en exceso en el segmento interno de GCAP2 en su conformación "libre de Ca^{2+}" resulta en toxicidad para la célula. Nuestros resultados sugieren que la toxicidad deriva de la inestabilidad térmica de la proteína. Está bien establecido que GCAP2 en su conformación libre de Ca^{2+} es térmicamente inestable y muestra tendencia a la agregación. La propensión de GCAP2 en su forma "libre de Ca^{2+}" a precipitar es lo que ha impedido hasta ahora la determinación de su estructura tridimensional por NMR, mientras que la estructura de GCAP2 en su forma "unida a Ca^{2+}" sí ha podido ser determinada. Hay muchos estudios que han descrito una

asociación entre 14-3-3 y enfermedades neurodegenerativas progresivas. Las proteínas 14-3-3 se han detectado en depósitos amiloides de la proteína Tau hiperfosforilada de las placas seniles (ovillos neurofibrilares) en la enfermedad de Alzheimer. En la enfermedad de Parkinson, 14-3-3 es detectada en cuerpos de Lewy formados por depósitos de sinucleina, y también se ha descrito la colocalizacion de 14-3-3 con formas mutadas de ataxin en la ataxia cerebelar espinosa.

Como resultado de este estudio proponemos que la forma mutada de GCAP2 bloqueada en su forma libre de Ca^{2+} causa toxicidad *in vivo* por la formación progresiva de oligomeros solubles de alto peso molecular GCAP2-14-3-3 que son toxicos para la celula. De acuerdo con esta hipótesis, observamos una fracción mucho mayor de EF$^-$GCAP2 que de GCAP2 control asociada a 14-3-3 en experimentos de fraccionamiento por tamaño de extractos de retina de ratones transgénicos. Las fracciones que muestran asociación entre GCAP2 y 14-3-3 muestran también especies de GCAP2 de alto peso molecular (dimeros y multimeros). La acumulación de complejos EF$^-$GCAP2-14-3-3 muestra cierta tendencia a formar agregados insolubles, como se muestra en la fracción de EF$^-$GCAP2-14-3-3 que aparece en la fracción resistente a Triton X-100, soluble en SDS.

Proponemos que el efecto deletéreo de la forma de GCAP2 libre de Ca^{2+} conformacionalmente inestable es un factor que contribuye a la patología de un numero considerable de distrofias hereditarias de la retina: a) las causadas por mutaciones en GUCA1B(GCAP2) que afecten a su afinidad de unión a Ca^{2+}, b) distrofias causadas por mutaciones en diferentes genes que en ultimo termino causen una reducción en la concentración intracelular de Ca^{2+} de forma sostenida, que son aquellas distrofias conocidas como "escenarios equivalentes a luz".

Ejemplos de defectos genéticos que resultan en un fenotipo "escenario equivalente a luz" son a) mutaciones nulas en GUCY2E (RetGC) asociadas a Amaurosis Congénita de Leber, en que falla el transporte de las proteínas GCAP debido a la ausencia de RetGC, a la vez que hay una reducción sostenida de los niveles de Ca^{2+} debido al cierre de los canales en ausencia de síntesis de cGMP; b) mutaciones en RD3, al afectar el transporte de los complejos RetGC/GCAPs al segmento externo crean las condiciones anteriormente citadas; c) mutaciones nulas en RPE65, que al afectar al ciclo visual –impidiendo el reciclaje del cromóforo- crean un escenario en que el pigmento visual se encuentra como opsina (apoproteína en ausencia de cromóforo), generando una actividad constitutiva basal y creando, por tanto, una reducción en los niveles de Ca^{2+} intracelular de forma sostenida.

En el futuro próximo diseñaremos experimentos para determinar en cuales de estos desórdenes hereditarios la acumulación de GCAP2 térmicamente inestable esta contribuyendo a la patología. Ademas, trataremos de identificar la quinasa responsable de la fosforilación de GCAP2, y las vías implicadas en la degradación de los agregados de GCAP2-14-3-3, asi como su reciclaje ("turnover").

Además de localizarse en el segmento externo de los fotorreceptores, las proteínas GCAP también se localizan en el segmento interno y en la terminal sináptica de fotorreceptores, donde hasta ahora se desconoce su función. Este trabajo demuestra que tanto GCAP1 como GCAP2 se localizan en la terminal sináptica colocalizando con RIBEYE, el componente estructural mayoritario de las cintillas sinápticas, y que tanto la sobreexpresión de GCAP2 como la reducción de GCAP1 *in vivo* (la alteración de la relación molar GCAP1:GCAP2) provoca el desensamblaje de las cintillas sinápticas y reduce la sensibilidad a la luz de los fotorreceptores. Este dato es importante porque aporta nueva información acerca de la organización/regulación de las cintillas sinápticas, un orgánulo presumiblemente fundamental en fotorreceptores para coordinar los cambios de calcio en la terminal presináptica con la maquinaria de exocitosis/ endocitosis de vesículas sinápticas, y sin embargo aún poco caracterizado.

Futuros experimentos trataran de continuar la caracterización de las funciones de GCAP1 y GCAP2 en terminal sináptica, mediante la caracterización funcional de nuevas interacciones de las GCAP en este compartimento.

DISCUSSION

The guanylate cyclase/guanylate cyclase activating proteins (RetGC/GCAP proteins) are assembled in a complex that has a key role at the light-sensitive compartment of photoreceptor cells. This complex is responsible for the synthesis of cGMP, the second messenger in phototransduction. It synthesizes cGMP at basal levels in darkness that counter-balances the basal activity of cGMP-phosphodiesterase, keeping a constant level of free cGMP that sets the fraction of open cGMP-channels at the plasma membrane and the inward current of Ca^{2+} that keeps photoreceptors partially depolarized (Figure I.4, upper diagram). Light activates an enzymatic cascade that ultimately causes the hydrolysis of cGMP. As cGMP drops, some cGMP-gated channels are closed and the inward current –including Ca^{2+} influx– is reduced, so that photoreceptors hyperpolarize and emit a signal (Figure I.4, middle diagram). As the light is dimmed or extinguished, the darkness equilibrium must be restored by reinstating the dark levels of cGMP. This is achieved as the GCAP proteins sense the drop in Ca^{2+} during the light response and exert a robust stimulation of RetGC activity (Figure I.4, lower diagram). Therefore, the RetGC/GCAPs complexes are essential for termination of the light response and light adaptation, and a key node in the cGMP and Ca^{2+} reciprocal feedback loop in photoreceptors (Burns and Arshavsky 2005).

Extensive biochemical analysis of the two major isoforms of guanylate cyclase activating proteins in mammals, GCAP1 and GCAP2 , has led to the proposal of the Ca^{2+}-relay model of action of GCAP proteins in the light response of rods and cones. Intracellular free [Ca^{2+}] declines from ~ 250nM in darkness to 23nM in saturating light in mouse rod outer segments. The models proposes that this Ca^{2+} decrease is first sensed at GC/GCAP complexes comprising GCAP1 and successively at those comprising GCAP2 [Ca^{2+} EC_{50} for GCAP1 ~130nM; for GCAP2 ~50nM], in a sequential mode of action -referred to as a Ca^{2+}-relay model-. Altogether, the rate of cGMP synthesis upon light exposure is stimulated up to ~12-fold over its basal levels, serving to restore the cGMP levels and to reopen the channels during the recovery of the light response and light adaptation (Kock and Dell'Orco 2013).

However, despite their extensive biochemical characterization, there are still important questions regarding GCAP1 and GCAP2 : a) – What determines their subcellular distribution?, b) – What other functions do GCAP1 and GCAP2 exert at other cellular compartments, other than the light-sensitive compartment? , c) – How do they result in photoreceptor cell death when mutated?

In this study we have addressed these questions by combining mouse genetic techniques with biochemical, physiological and histological analysis. We undertook an extensive characterization of a transgenic line expressing a mutant form of GCAP2 impaired to bind Ca^{2+}, in which all functional EF-hands were mutated, the EF$^-$GCAP2 (Figure R.2.). This mutant resulted in severe retinal degeneration, reproducing the phenotype caused by human mutations that impair Ca^{2+}-binding. We first demonstrated that this mutant was causing toxicity by a mechanism independent of cGMP metabolism, which was unexpected (Figure R.5.). Its toxicity was not caused by unabated cGMP synthesis, the mechanism underlying the pathology of mutations in GCAP1 that have been associated to autosomal dominant cone/rod dystrophies (adCORD). In the case of GCAP1 mutations, most of the mutations that have been identified cause protein conformational distorsions that affect the Ca^{2+}-coordination capacity of EF-hand 3 or EF-hand 4. It has been demonstrated both *in vitro* and *in vivo* that the effect of impairing Ca^{2+}-binding to GCAP1 is the constitutive activation of the cyclase, leading to elevated levels of cGMP, a higher-than-normal fraction of open cGMP-gated channels and therefore an abnormally elevated entry of Ca^{2+}, with ensuing apoptosis (Dizhoor *et al.* 1998) (Dizhoor 2000) (Jiang and Baehr 2010). In contrast, in our transgenic line, the mutant form of GCAP2 impaired at binding Ca^{2+}, EF$^-$GCAP2, failed to be transported to rod outer segments and accumulated at the photoreceptor inner segment and proximal compartments (Figure R.6.). In order to study how the mutant protein was causing damage to the cell by accumulating at the inner segment, we undertook the characterization of protein interactions established by the mutant protein, by designing a differential proteomic analysis using the mutant transgenic line, a transgenic control line and the GCAPs knockout strain. As a result of the proteomic analysis, we identified the 14-3-3 phosphobinding proteins as the major EF$^-$GCAP2 interactors (Table R.1. and Table R.2.).

The identification of 14-3-3 protein isoforms as binding proteins of GCAP2 led us to unveil an important mechanism governing GCAP2 subcellular distribution *in vivo*, with important implications for disease. We here demonstrate that GCAP2 is phosphorylated *in vivo*, to a much higher extent in its Ca^{2+}-free form than in its Ca^{2+}-loaded form (Figure R.9). Phosphorylation of GCAP2 is what triggers 14-3-3 binding (Figure R.8), and the retention of the protein at the inner segment and proximal compartments (Figure R.12).. In wildtype mice, we have seen that about 50% of the total protein is phosphorylated at steady state (Figure R.10), and that about 50% of the protein localizes to proximal compartments, whereas about 50% of the protein is distributed to the rod outer segment (Figure R.13. and R.14.). We have also shown

that GCAP2 and 14-3-3 co-fractionate during separation of murine retinal homogenates by size exclusion chromatography, which indicates that these proteins might be associated *in vivo* (Figure R.11).

Our results, taken together, suggest the following model (Figure R.16): GCAP2 is synthesized at the inner segment. If it binds Ca^{2+} immediately upon synthesis (at the high $[Ca^{2+}]_i$ typical of dark periods), then it would bind to Ret-GCs and be transported to rod outer segments. If it does not bind Ca^{2+} upon synthesis (at the low $[Ca^{2+}]_i$ typical of prolonged light exposures), then it would bind Mg^{2+} and the protein would acquire a tridimensional conformation that would be less stable. It would form dimers. It would be phosphorylated, and it would bind a dimer of 14-3-3. Because 14-3-3 isoforms distribute to proximal compartments of photoreceptors and are excluded from the outer segments (Figure R.12) (Nakano *et al.* 2001), the binding of 14-3-3 to phosphorylated GCAP2 could account for GCAP2 retention at proximal compartments. In fact, we revert GCAP2 retention at the inner segment in the bEF-GCAP2 transgenic line when we mutate Ser201, precluding the phosphorylation of the protein. When phosphorylated and bound to 14-3-3, GCAP2 would be retained and precluded from binding RetGC for its transport to rod outer segments.

Therefore, our model envisages the subcellular localization of GCAP2 (a cytosolic protein) as a highly regulated process, dictated by protein-protein interactions that occur differently in dark or light conditions, rather than the result of equalizing its concentrations in the cytosolic space. Mutations in GCAP2 that disrupt or preclude Ca^{2+}-binding would alter this mechanism of protein distribution, creating an imbalance that would ultimately lead to cell death (see below).

We here uncover a mechanism by which mutations in GCAP2 may lead to cell death which is independent of cGMP metabolism. Transgenic expression of bEF$^-$GCAP2 led to a rapid retinal degeneration. Therefore, GCAP2, when building up in excess at the inner segment in its conformationally unstable Ca^{2+}-free conformation results in severe toxicity. Data suggests that toxicity comes from Ca^{2+}-free GCAP2 thermal instability.

It is well established that the Ca^{2+}-free conformation of GCAP2 is conformationally unstable and has a natural tendency to aggregate (Olshevskaya *et al.* 1999b) (Pettelkau *et al.* 2013). The propensity of Ca^{2+}-free GCAP2 to precipitate *in vitro* has precluded so far the determination of its NMR structure, whereas the structure of the Ca^{2+}-bound form of GCAP2 has been resolved (Ames *et al.* 1999). By homology to the reported Ca^{2+}-dependent structural changes in GCAP1, the release of Ca^{2+} from the EF-hand domains in the GCAP2 molecule would likely result in the swiveling of the

interdomain region, separating the N-terminus and C-terminus domains of the protein (Stephen *et al.* 2007). This would result in the release of the C-terminus from a three-element network of intramolecular interactions involving the N-terminus, the buried myristoyl group and the C-terminus, so that the C-terminus becomes more exposed, and more susceptible to phosphorylation at Ser201. Phosphorylation at this residue triggers 14-3-3 binding (Peshenko *et al.* 2004b).

Several investigations in the last decade have linked 14-3-3 proteins with progressive neurodegenerative diseases: 14-3-3s colocalize with hyperphosphorylated tau in Alzheimer disease neurofibrillary tangles (Layfield *et al.* 1996) (Lee *et al.* 2001), with α-synuclein in Lewy bodies typical of PD (Kawamoto *et al.* 2002), with ataxin in spinocerebellar ataxia (SCA, Chen *et al.* 2003). Moreover, phosphorylation of ataxin-1 at S776 stabilizes the protein by inducing 14-3-3 binding (zeta and epsilon isoforms), delaying its degradation and reinforcing its aggregation in Drosophila (Chen et al 2003).

We propose that it is the gradual formation of GCAP2-14-3-3 soluble oligomers that results in toxicity for the photoreceptor cell. We have observed in size exclusion chromatography experiments that those fractions that present the highest colocalization of GCAP2 and 14-3-3 are enriched in high molecular weight species of GCAP2 (Figure R.11). These GCAP2-14-3-3 complexes are shifted towards “higher molecular weight” fractions in these assays when retinal extracts are solubilized in 1% SDS rather than in TritonX100, which is to say that higher molecular weight complexes have a tendency to precipitate (Figure R.11).

We propose that the deletereous effects of the conformationally unstable Ca^{2+}-free GCAP2 will be contributing to the pathology of a number of inherited retinal dystrophies: a) those caused by mutations in the GUCA1B gene (GCAP2 protein) that preclude Ca^{2+}-binding; and b) dystrophies caused by mutations in different genes that ultimately result in a sustained reduction in the intracellular concentration of Ca^{2+} [e.g, mutations impairing termination of the light response or mutations in the visual pigment resulting in opsin basal constitutive activity (Singhal *et al.* 2013), (Woodruff *et al.* 2003)], the so-called “equivalent-light” genetic scenario (Fain and Lisman 1999) (Figure D.1.).

An example of mutations leading to “equivalent-light” conditions, for which this mechanism could be of relevance, follows:

- **Null mutations in RetGC1 (GUCY2E), associated to Lebers Congenital Amaurosis, LCA1**. GUCY2E was the first gene identified that was involved in

LCA and accounts for ~20% LCA cases (Perrault *et al.*2000). In the absence of functional RetGC in photoreceptors: a) there is no transport of GCAP1 or GCAP2 to rod outer segments, and GCAP1 and GCAP2 accumulate at proximal compartments; and b) synthesis of cGMP is reduced, cGMP levels are lower than normal, consequently the fraction of open cGMP channels is lower than normal, mimicking the effect of light, and Ca^{2+} entry is therefore lower than normal (Baehr *et al.* 2007). In the "equivalent-light" situation, the conditions converge that: a) GCAPs accumulate at the inner segment; and b) intracellular Ca^{2+} is abnormally low.

- **Null mutations in RD3, associated to Lebers Congenital Amaurosis, LCA12.** RD3 is an accesory protein required for the transport of RetGC/GCAP complexes to the outer segments. Therefore the consequences of lacking a functional RD3 are the same of lacking functional RetGC1 (Azadi *et al.* 2010).
- **Null mutations in RPE65, associated to Lebers Congenital Amaurosis , LCA12.** Mutations in RPE65 disrupt synthesis of the opsin chromophore ligand 11-cis-retinal, leading to light-independent constitutive signaling by unliganded opsin, therefore resulting in a sustained decrease in intracellular Ca^{2+} (Marlhens *et al.* 1997) (Gu *et al.* 1997).

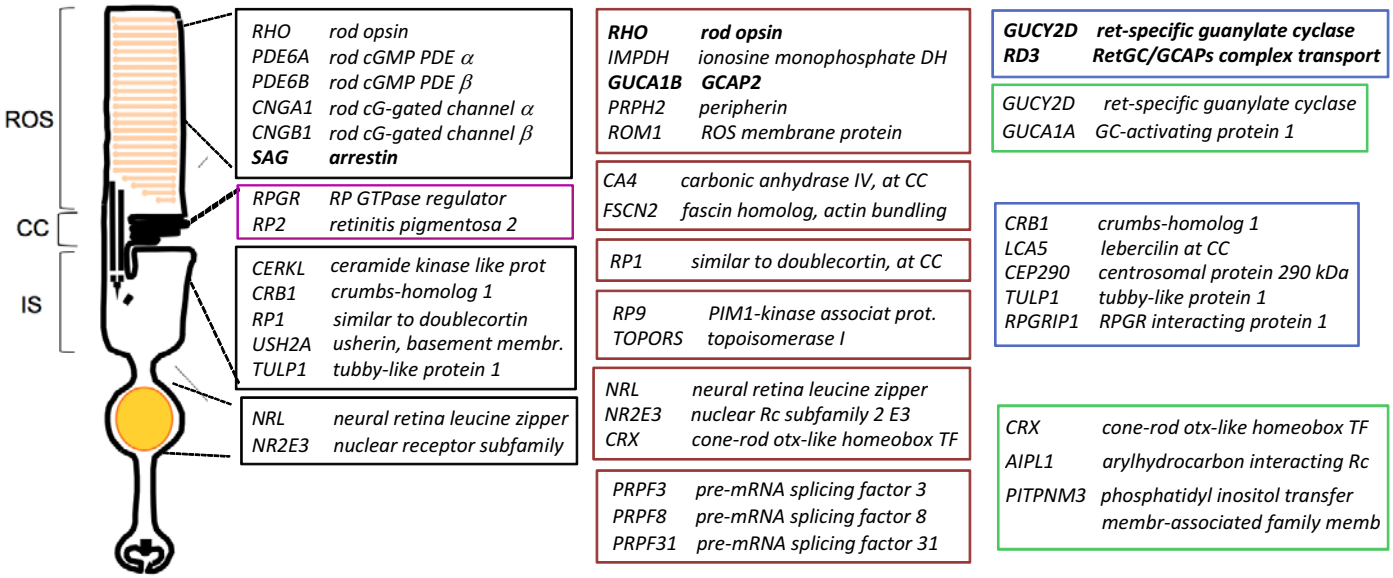

Figure D1. ***Retinal dystrophies in which mutations result in a sustained reduction in intracellular Ca^{2+}, shown in bold in the broader context of mutations leadingto different forms of inherited blindness. arRP; adRP, XlRP**: **autosomal recessive/dominant/ X-linked retinitis pigmentosa.*** *Mutations impair rod function, leading initially to "night blindness" and loss of peripheral vision. As the disease progresses, at a certain threshold of rod cell death cones are also compromised, and there is loss of central visual acuity (tunnel vision) and eventually total blindness.* ***LCA**: **Leber congenital amaurosis**. Severe retinal dystrophy, evident in the first year of life. Near complete impairment of visual function (both rods and cones typically affected).**adCORD**: **autosomal dominant cone-rod dystrophy.** Gene defects affect initially cone and subsequently rod function; leading to loss of visual acuity and central vision.*

- **G90D-rhodopsin.** Mutations in rhodopsin that abolish chromophore binding would have the same functional consequences that null mutations in RPE65 (that not having chromophore) (Woodruff *et al.* 2007) (Dizhoor *et al.* 2008).
- **Null mutations in proteins involved in termination of the light response: such as rhodopsin kinase (Yamamoto *et al.* 1997) or arrestin (Fuchs *et al.* 1995), associated to Congenital Stationary Night Blindness or Oguchi disease.** Abnormally prolonged signaling initiated by rhodopsin in response to light, by not being terminated when the light is extinguished , would lead to sustained reduced intracellular Ca^{2+} (Chen *et al.* 1999) (Lamb and Pugh 2004) (Metayé *et al.* 2006)

Future experiments will test whether the mechanism here outlined contributes to the pathology of these inherited retinal dystrophies by using mouse models of these diseases. Also, experiments will be addressed at characterizing the kinase involved and its regulation, the stoichiometry and turn-over of GCAP2-14-3-3 complexes, as well as at characterizing the deletereous effects that GCAP2 and GCAP2-14-3-3 aggregates have in the cell (the link with cell death).

Besides its localization at the photoreceptor sensory compartment and at the metabolic compartment, GCAP proteins also localize to the synaptic terminal, where its function is unknown (Howes *et al.* 1998). This study confirms that both GCAP1 and GCAP2 are localized at the synaptic terminal, and further demonstrates GCAP2 colocalization with RIBEYE, the major structural component of synaptic ribbons (Venkatesan *et al.* 2010) both at the confocal level (Figures R.18, R.19 and R.20) and at the ultrastructural level (Figure R.22). We here demonstrate the colocalization of GCAP1 with RIBEYE at synaptic ribbons as well (Figure R.24).

GCAP2 overexpression *in vivo* (altering the GCAP1:GCAP2 molar ratio) causes synaptic ribbon disassembly (Figure R.21 and R.23) and reduces photoreceptors light sensitivity (Figures R.26). This study is relevant because it points to a role of GCAP2 (and GCAP1) at the synaptic terminal, at regulating the dynamic reorganization of ribbons during light exposure.

Because RetGC and RD3 are also present at the synaptic terminal, it cannot be discarded that GCAPs could be regulating cGMP synthesis at this compartment as well (Liu *et al.* 1994) (Cooper *et al.* 1995) (Duda *et al.* 2002) (Venkataram *et al.* 2003)

(Azadi *et al.* 2010) (Peshenko *et al.* 2011b), although this seems unlikely given that the $[Ca^{2+}]_i$ is much higher at the synaptic terminal than at rod outer segments.

Future experiments will also aim at further investigating the role of GCAP2 and GCAP1 at the synaptic terminal, by continuing the characterization of protein-protein interactions that GCAP2 and GCAP1 establish in this compartment, besides RIBEYE

VII. CONCLUSIONS

RESUMEN EN ESPAÑOL

1. Demostramos la presencia de GCAP1 y GCAP2 en las cintillas sinápticas de la terminal sináptica de los bastones mediante microscopia electrónica y confocal.
2. GCAP1 y GCAP2 son prescindibles en el ensamblaje y mantenimiento básico de las cintillas sinápticas.
3. La sobreexpresión de GCAP2 en el fenotipo salvaje, que incrementa el ratio GCAP2:GCAP1, promueve el desensamblaje de las cintillas.
4. Proponemos que GCAP2 podría jugar un papel mediando cambios morfológicos en las cintillas sinápticas promovidas por cambios en los niveles de Ca^{2+}.
5. La expresión *in vivo* de la proteína bEF$^-$GCAP2, que no une Ca^{2+}, provoca degeneración retinal a un ritmo que se correlaciona con la pérdida de función visual, y esto es debido a la mutación en sí y no a la sobreexpresión del transgén.
6. bEF$^-$GCAP2 se localiza en los compartimentos proximales de los fotoreceptores y no transloca al segmento externo, por lo que no activa GC.
7. bEF$^-$GCAP2 está anormalmente fosforilada *in vivo*.
8. La fosforilación de GCAP2 promueve la unión de 14-3-3.
9. La fosforilación de GCAP2 en la serina 201 retiene a GCAP2 en el segmento interno y evita su translocación al segmento externo. *In vivo*, esta retención es revertida cuando la serina 201 se muta a una glicina.
10. Proponemos que la fosforilación de GCAP2 y su unión a 14-3-3 determina la localización de GCAP2 en la celula.
11. Proponemos que mutaciones en GCAP2 o condiciones de luz que promuevan la acumulación de GCAP2 en su forma libre de Ca^{2+}en el segmento interno de la célula, conducen a la muerte celular por la inestabilidad conformacional de GCAP2. Y más importante, proponemos que esto aplicaría también a condiciones genéticas que mimetizan los efectos de exposición a luz prolongada, los escenarios recogidos bajo la hipótesis de “equivalente a luz”.

CONCLUSIONS

1. GCAP1 and GCAP2, in addition to their role at confering Ca^{2+} sensitivity to cGMP synthesis at rod outer segments, are also present at the synaptic terminal. At confocal and electron microscopy level, we have shown that GCAP1 and GCAP2 localize to ribbon synapses in rod synaptic terminals.
2. The absence of GCAP1 and GCAP2 does not alter synaptic ribbon length. If both GCAP1 and GCAP2 isoforms are ablated, there is no overall effect on synaptic ribbon length at the ultrastructural level. GCAP1 and GCAP2 proteins are not required for the early assembly or basic maintenance of synaptic ribbons.
3. The overexpression of GCAP2 in the wildtype background (increasing GCAP2 to GCAP1 ratio) promotes ribbon disassembly, as observed by the shortened ribbons in GCAP2+/+ mice compared to WT and by the higher abundance of club-shaped and spherical ribbons, representative of assembly intermediates. This effect is exacerbated in the absence of GCAP1.
4. We propose that GCAP2 is involved in mediating the morphological changes at the synaptic ribbons triggered by changes in Ca^{2+} levels.
5. Expression of a mutant form of GCAP2 impaired to bind Ca2+, bEF$^-$GCAP2, in the rods of transgenic mice leads to a retinal degeneration that correlates with the loss of visual function that can be specifically assigned to the mutation and not to overexpression of the transgene.
6. Transgenic bEF$^-$GCAP2 in photoreceptors is excluded from rod outer segments where Ca2+-dependent GC modulation takes place, and accumulates at the inner segment and proximal compartments of the cell in a form incompetent to activate the cyclase.
7. bEF$^-$GCAP2 shows an abnormally enhanced phosphorylation *in vivo* as seen by in situ phosphorylation assays as well as by isoelectrofocusing gels.
8. GCAP2 phosphorylation triggers 14-3-3 binding, as assessed by immunoprecipitation assays, and as indicated by retinal homogenate separation by size-exclusion chromatography.
9. GCAP2 phosphorylation at Ser201 retains GCAP2 at the inner segment and proximal compartments, precluding its distribution to rod outer segments. Ser201 mutation to Gly reverts this retention in vivo.
10. We propose that GCAP2 phosphorylation and 14-3-3 binding determine GCAP2 subcellular localization.

11. We propose that mutations in GCAP2 or light conditions that result in accumulation of GCAP2 in its Ca2+-free form at the inner segment of the cell lead to cell death due to GCAP2 conformational instability. Importantly, we propose that this would also apply to genetic conditions mimicking the effects of prolonged light exposure, the so-called "equivalent-light" scenarios.

VIII. BIBLIOGRAPHY

BIBLIOGRAPHY

Adly MA, Spiwoks-Becker I, Vollrath L. 1999. Ultrastructural changes of photoreceptor synaptic ribbons in relation to time of day and illumination. Invest Ophthalmol Vis Sci 40(10):2165-2172.

Aitken A. 1996. 14-3-3 and its possible role in co-ordinating multiple signalling pathways. Trends Cell Biol 6(9):341-347.

Ames JB, Dizhoor AM, Ikura M, Palczewski K, Stryer L. 1999. Three-dimensional structure of guanylyl cyclase activating protein-2, a calcium-sensitive modulator of photoreceptor guanylyl cyclases. J Biol Chem 274(27):19329-19337.

Ames JB, Lim S. 2012. Molecular structure and target recognition of neuronal calcium sensor proteins. Biochim Biophys Acta 1820(8):1205-1213.

Arshavsky VY, Burns ME. 2012. Photoreceptor signaling: supporting vision across a wide range of light intensities. J Biol Chem 287(3):1620-1626.

Azadi S, Molday LL, Molday RS. 2010. RD3, the protein associated with Leber congenital amaurosis type 12, is required for guanylate cyclase trafficking in photoreceptor cells. Proc Natl Acad Sci U S A 107(49):21158-21163.

Baehr W, Karan S, Maeda T, Luo DG, Li S, Bronson JD, Watt CB, Yau KW, Frederick JM, Palczewski K. 2007. The function of guanylate cyclase 1 and guanylate cyclase 2 in rod and cone photoreceptors. J Biol Chem 282(12):8837-8847.

Baehr W, Palczewski K. 2007. Guanylate cyclase-activating proteins and retina disease. Subcell Biochem 45:71-91.

Balkema GW, Cusick K, Nguyen TH. 2001. Diurnal variation in synaptic ribbon length and visual threshold. Vis Neurosci 18(5):789-797.

Ball SL, Powers PA, Shin HS, Morgans CW, Peachey NS, Gregg RG. 2002. Role of the beta(2) subunit of voltage-dependent calcium channels in the retinal outer plexiform layer. Invest Ophthalmol Vis Sci 43(5):1595-1603.

Biehlmaier O, Alam M, Schmidt WJ. 2007. A rat model of Parkinsonism shows depletion of dopamine in the retina. Neurochem Int 50(1):189-195.

Boston P, Jackson P. 1980. Purification and properties of a brain-specific protein, human 14-3-3 protein. Biochem Soc Trans 8(5):617-618.

Brennan GP, Jimenez-Mateos EM, McKiernan RC, Engel T, Tzivion G, Henshall DC. 2013. Transgenic overexpression of 14-3-3 zeta protects hippocampus against endoplasmic reticulum stress and status epilepticus in vivo. PLoS One 8(1):e54491.

Buch PK, Mihelec M, Cottrill P, Wilkie SE, Pearson RA, Duran Y, West EL, Michaelides M, Ali RR, Hunt DM. 2011. Dominant cone-rod dystrophy: a mouse model generated by gene targeting of the GCAP1/Guca1a gene. PLoS One 6(3):e18089.

Burgoyne RD. 2007. Neuronal calcium sensor proteins: generating diversity in neuronal Ca2+ signalling. Nat Rev Neurosci 8(3):182-193.

Burgoyne RD, Haynes LP. 2012. Understanding the physiological roles of the neuronal calcium sensor proteins. Mol Brain 5(1):2.

Burgoyne RD, O'Callaghan DW, Hasdemir B, Haynes LP, Tepikin AV. 2004. Neuronal Ca2+-sensor proteins: multitalented regulators of neuronal function. Trends Neurosci 27(4):203-209.

Burns ME, Arshavsky VY. 2005. Beyond counting photons: trials and trends in vertebrate visual transduction. Neuron 48(3):387-401.

Burns ME, Mendez A, Chen J, Baylor DA. 2002. Dynamics of cyclic GMP synthesis in retinal rods. Neuron 36(1):81-91.

Chang B, Heckenlively JR, Bayley PR, Brecha NC, Davisson MT, Hawes NL, Hirano AA, Hurd RE, Ikeda A, Johnson BA, McCall MA, Morgans CW, Nusinowitz S, Peachey NS, Rice DS, Vessey KA, Gregg RG. 2006. The nob2 mouse, a null mutation in Cacna1f: anatomical and functional abnormalities in the outer retina and their consequences on ganglion cell visual responses. Vis Neurosci 23(1):11-24.

Chang S, Vaccarella L, Olatunji S, Cebulla C, Christoforidis J. 2011. Diagnostic challenges in retinitis pigmentosa: genotypic multiplicity and phenotypic variability. Curr Genomics 12(4):267-275.

Chapple JP, Grayson C, Hardcastle AJ, Saliba RS, van der Spuy J, Cheetham ME. 2001. Unfolding retinal dystrophies: a role for molecular chaperones? Trends Mol Med 7(9):414-421.

Chen CK, Burns ME, Spencer M, Niemi GA, Chen J, Hurley JB, Baylor DA, Simon MI. 1999. Abnormal photoresponses and light-induced apoptosis in rods lacking rhodopsin kinase. Proc Natl Acad Sci U S A 96(7):3718-3722.

Chen HK, Fernandez-Funez P, Acevedo SF, Lam YC, Kaytor MD, Fernandez MH, Aitken A, Skoulakis EM, Orr HT, Botas J, Zoghbi HY. 2003. Interaction of Akt-phosphorylated ataxin-1 with 14-3-3 mediates neurodegeneration in spinocerebellar ataxia type 1. Cell 113(4):457-468.

Coleman JE, Zhang Y, Brown GA, Semple-Rowland SL. 2004. Cone cell survival and downregulation of GCAP1 protein in the retinas of GC1 knockout mice. Invest Ophthalmol Vis Sci 45(10):3397-3403.

Concepcion F, Mendez A, Chen J. 2002. The carboxyl-terminal domain is essential for rhodopsin transport in rod photoreceptors. Vision Res 42(4):417-426.

Cuenca N, Lopez S, Howes K, Kolb H. 1998. The localization of guanylyl cyclase-activating proteins in the mammalian retina. Invest Ophthalmol Vis Sci 39(7):1243-1250.

Daiger SP, Sullivan LS, Bowne SJ. 2013. Genes and mutations causing retinitis pigmentosa. Clin Genet 84(2):132-141.

den Hollander AI, Roepman R, Koenekoop RK, Cremers FP. 2008. Leber congenital amaurosis: genes, proteins and disease mechanisms. Prog Retin Eye Res 27(4):391-419.

Diamond JS. 2011. Grilled RIBEYE stakes a claim for synaptic ribbons. Nat Neurosci 14(9):1097-1098.

Dick O, tom Dieck S, Altrock WD, Ammermüller J, Weiler R, Garner CC, Gundelfinger ED, Brandstätter JH. 2003. The presynaptic active zone protein bassoon is essential for photoreceptor ribbon synapse formation in the retina. Neuron 37(5):775-786.

Dizhoor AM. 2000. Regulation of cGMP synthesis in photoreceptors: role in signal transduction and congenital diseases of the retina. Cell Signal 12(11-12):711-719.

Dizhoor AM, Boikov SG, Olshevskaya EV. 1998. Constitutive activation of photoreceptor guanylate cyclase by Y99C mutant of GCAP-1. Possible role in causing human autosomal dominant cone degeneration. J Biol Chem 273(28):17311-17314.

Dizhoor AM, Hurley JB. 1996. Inactivation of EF-hands makes GCAP-2 (p24) a constitutive activator of photoreceptor guanylyl cyclase by preventing a Ca2+-induced "activator-to-inhibitor" transition. J Biol Chem 271(32):19346-19350.

Dizhoor AM, Lowe DG, Olshevskaya EV, Laura RP, Hurley JB. 1994. The human photoreceptor membrane guanylyl cyclase, RetGC, is present in outer segments and is regulated by calcium and a soluble activator. Neuron 12(6):1345-1352.

Dizhoor AM, Olshevskaya EV, Henzel WJ, Wong SC, Stults JT, Ankoudinova I, Hurley JB. 1995. Cloning, sequencing, and expression of a 24-kDa Ca(2+)-binding protein activating photoreceptor guanylyl cyclase. J Biol Chem 270(42):25200-25206.

Dizhoor AM, Olshevskaya EV, Peshenko IV. 2010. Mg2+/Ca2+ cation binding cycle of guanylyl cyclase activating proteins (GCAPs): role in regulation of photoreceptor guanylyl cyclase. Mol Cell Biochem 334(1-2):117-124.

Dizhoor AM, Woodruff ML, Olshevskaya EV, Cilluffo MC, Cornwall MC, Sieving PA, Fain GL. 2008. Night blindness and the mechanism of constitutive signaling of mutant G90D rhodopsin. J Neurosci 28(45):11662-11672.

Domino SE, Tubb DJ, Garbers DL. 1991. Assay of guanylyl cyclase catalytic activity. Methods Enzymol 195:345-355.

Downes SM, Holder GE, Fitzke FW, Payne AM, Warren MJ, Bhattacharya SS, Bird AC. 2001. Autosomal dominant cone and cone-rod dystrophy with mutations in the guanylate cyclase activator 1A gene-encoding guanylate cyclase activating protein-1. Arch Ophthalmol 119(1):96-105.

Ermilov AN, Olshevskaya EV, Dizhoor AM. 2001. Instead of binding calcium, one of the EF-hand structures in guanylyl cyclase activating protein-2 is required for targeting photoreceptor guanylyl cyclase. J Biol Chem 276(51):48143-48148.

Fain GL, Lisman JE. 1999. Light, Ca2+, and photoreceptor death: new evidence for the equivalent-light hypothesis from arrestin knockout mice. Invest Ophthalmol Vis Sci 40(12):2770-2772.

Fain GL, Matthews HR, Cornwall MC, Koutalos Y. 2001. Adaptation in vertebrate photoreceptors. Physiol Rev 81(1):117-151.

Fesenko EE, Kolesnikov SS, Lyubarsky AL. 1985. Induction by cyclic GMP of cationic conductance in plasma membrane of retinal rod outer segment. Nature 313(6000):310-313.

Friedman JS, Chang B, Kannabiran C, Chakarova C, Singh HP, Jalali S, Hawes NL, Branham K, Othman M, Filippova E, Thompson DA, Webster AR, Andréasson S, Jacobson SG, Bhattacharya SS, Heckenlively JR, Swaroop A. 2006. Premature truncation of a novel protein, RD3, exhibiting subnuclear localization is associated with retinal degeneration. Am J Hum Genet 79(6):1059-1070.

Frins S, Bönigk W, Müller F, Kellner R, Koch KW. 1996. Functional characterization of a guanylyl cyclase-activating protein from vertebrate rods. Cloning, heterologous expression, and localization. J Biol Chem 271(14):8022-8027.

Fu Y, Yau KW. 2007. Phototransduction in mouse rods and cones. Pflugers Arch 454(5):805-819.

Fuchs M, Scholz M, Sendelbeck A, Atorf J, Schlegel C, Enz R, Brandstätter JH. 2012. Rod photoreceptor ribbon synapses in DBA/2J mice show progressive age-related structural changes. PLoS One 7(9):e44645.

Fuchs M, Sendelbeck A, Atorf J, Kremers J, Brandstätter JH. 2013. Strain differences in illumination-dependent structural changes at mouse photoreceptor ribbon synapses. J Comp Neurol 521(1):69-78.

Fuchs S, Nakazawa M, Maw M, Tamai M, Oguchi Y, Gal A. 1995. A homozygous 1-base pair deletion in the arrestin gene is a frequent cause of Oguchi disease in Japanese. Nat Genet 10(3):360-362.

Gorczyca WA, Gray-Keller MP, Detwiler PB, Palczewski K. 1994. Purification and physiological evaluation of a guanylate cyclase activating protein from retinal rods. Proc Natl Acad Sci U S A 91(9):4014-4018.

Gorczyca WA, Polans AS, Surgucheva IG, Subbaraya I, Baehr W, Palczewski K. 1995. Guanylyl cyclase activating protein. A calcium-sensitive regulator of phototransduction. J Biol Chem 270(37):22029-22036.

Grossman GH, Pauer GJ, Narendra U, Peachey NS, Hagstrom SA. 2009. Early synaptic defects in tulp1-/- mice. Invest Ophthalmol Vis Sci 50(7):3074-3083.

Gu SM, Thompson DA, Srikumari CR, Lorenz B, Finckh U, Nicoletti A, Murthy KR, Rathmann M, Kumaramanickavel G, Denton MJ, Gal A. 1997. Mutations in RPE65 cause autosomal recessive childhood-onset severe retinal dystrophy. Nat Genet 17(2):194-197.

Haeri M, Knox BE. 2012. Rhodopsin mutant P23H destabilizes rod photoreceptor disk membranes. PLoS One 7(1):e30101.

Haeseleer F, Imanishi Y, Maeda T, Possin DE, Maeda A, Lee A, Rieke F, Palczewski K. 2004. Essential role of Ca2+-binding protein 4, a Cav1.4 channel regulator, in photoreceptor synaptic function. Nat Neurosci 7(10):1079-1087.

Hagstrom SA, Duyao M, North MA, Li T. 1999. Retinal degeneration in tulp1-/- mice: vesicular accumulation in the interphotoreceptor matrix. Invest Ophthalmol Vis Sci 40(12):2795-2802.

Hamel C. 2006. Retinitis pigmentosa. Orphanet J Rare Dis 1:40.

Hamel CP. 2007. Cone rod dystrophies. Orphanet J Rare Dis 2:7.

Hartong DT, Berson EL, Dryja TP. 2006. Retinitis pigmentosa. Lancet 368(9549):1795-1809.

Heidelberger R, Thoreson WB, Witkovsky P. 2005. Synaptic transmission at retinal ribbon synapses. Prog Retin Eye Res 24(6):682-720.

Helten A, Säftel W, Koch KW. 2007. Expression level and activity profile of membrane bound guanylate cyclase type 2 in rod outer segments. J Neurochem 103(4):1439-1446.

Howes K, Bronson JD, Dang YL, Li N, Zhang K, Ruiz C, Helekar B, Lee M, Subbaraya I, Kolb H, Chen J, Baehr W. 1998. Gene array and expression of mouse retina guanylate cyclase activating proteins 1 and 2. Invest Ophthalmol Vis Sci 39(6):867-875.

Howes KA, Pennesi ME, Sokal I, Church-Kopish J, Schmidt B, Margolis D, Frederick JM, Rieke F, Palczewski K, Wu SM, Detwiler PB, Baehr W. 2002. GCAP1 rescues rod photoreceptor response in GCAP1/GCAP2 knockout mice. EMBO J 21(7):1545-1554.

Hughes RE, Brzovic PS, Dizhoor AM, Klevit RE, Hurley JB. 1998. Ca2+-dependent conformational changes in bovine GCAP-2. Protein Sci 7(12):2675-2680.

Hwang JY, Koch KW. 2002. Calcium- and myristoyl-dependent properties of guanylate cyclase-activating protein-1 and protein-2. Biochemistry 41(43):13021-13028.

Hwang JY, Lange C, Helten A, Höppner-Heitmann D, Duda T, Sharma RK, Koch KW. 2003. Regulatory modes of rod outer segment membrane guanylate cyclase differ in catalytic efficiency and Ca(2+)-sensitivity. Eur J Biochem 270(18):3814-3821.

Imanishi Y, Li N, Sokal I, Sowa ME, Lichtarge O, Wensel TG, Saperstein DA, Baehr W, Palczewski K. 2002. Characterization of retinal guanylate cyclase-activating protein 3 (GCAP3) from zebrafish to man. Eur J Neurosci 15(1):63-78.

Imanishi Y, Yang L, Sokal I, Filipek S, Palczewski K, Baehr W. 2004. Diversity of guanylate cyclase-activating proteins (GCAPs) in teleost fish: characterization of three novel GCAPs (GCAP4, GCAP5, GCAP7) from zebrafish (Danio rerio) and prediction of eight GCAPs (GCAP1-8) in pufferfish (Fugu rubripes). J Mol Evol 59(2):204-217.

Jacobson SG, Cideciyan AV, Peshenko IV, Sumaroka A, Olshevskaya EV, Cao L, Schwartz SB, Roman AJ, Olivares MB, Sadigh S, Yau KW, Heon E, Stone EM, Dizhoor AM. 2013. Determining consequences of retinal membrane guanylyl cyclase (RetGC1) deficiency in human Leber congenital amaurosis en route to therapy: residual cone-photoreceptor vision correlates with biochemical properties of the mutants. Hum Mol Genet 22(1):168-183.

Jiang L, Baehr W. 2010. GCAP1 mutations associated with autosomal dominant cone dystrophy. Adv Exp Med Biol 664:273-282.

Jiang L, Katz BJ, Yang Z, Zhao Y, Faulkner N, Hu J, Baird J, Baehr W, Creel DJ, Zhang K. 2005. Autosomal dominant cone dystrophy caused by a novel mutation in the GCAP1 gene (GUCA1A). Mol Vis 11:143-151.

Jiang L, Wheaton D, Bereta G, Zhang K, Palczewski K, Birch DG, Baehr W. 2008. A novel GCAP1(N104K) mutation in EF-hand 3 (EF3) linked to autosomal dominant cone dystrophy. Vision Res 48(23-24):2425-2432.

Kachi S, Nishizawa Y, Olshevskaya E, Yamazaki A, Miyake Y, Wakabayashi T, Dizhoor A, Usukura J. 1999. Detailed localization of photoreceptor guanylate cyclase activating protein-1 and -2 in mammalian retinas using light and electron microscopy. Exp Eye Res 68(4):465-473.

Kajiwara K, Hahn LB, Mukai S, Travis GH, Berson EL, Dryja TP. 1991. Mutations in the human retinal degeneration slow gene in autosomal dominant retinitis pigmentosa. Nature 354(6353):480-483.

Karan S, Frederick JM, Baehr W. 2010. Novel functions of photoreceptor guanylate cyclases revealed by targeted deletion. Mol Cell Biochem 334(1-2):141-155.

Karan S, Tam BM, Moritz OL, Baehr W. 2011. Targeting of mouse guanylate cyclase 1 (Gucy2e) to Xenopus laevis rod outer segments. Vision Res 51(21-22):2304-2311.

Kawamoto Y, Akiguchi I, Nakamura S, Honjyo Y, Shibasaki H, Budka H. 2002. 14-3-3 proteins in Lewy bodies in Parkinson disease and diffuse Lewy body disease brains. J Neuropathol Exp Neurol 61(3):245-253.

Kitiratschky VB, Behnen P, Kellner U, Heckenlively JR, Zrenner E, Jägle H, Kohl S, Wissinger B, Koch KW. 2009. Mutations in the GUCA1A gene involved in hereditary cone dystrophies impair calcium-mediated regulation of guanylate cyclase. Hum Mutat 30(8):E782-796.

Koch KW. 2012. Biophysical investigation of retinal calcium sensor function. Biochim Biophys Acta 1820(8):1228-1233.

Koch KW. 2013. The guanylate cyclase signaling system in zebrafish photoreceptors. FEBS Lett 587(13):2055-2059.

Koch KW, Dell'orco D. 2013. A Calcium-Relay Mechanism in Vertebrate Phototransduction. ACS Chem Neurosci.

Koch KW, Stryer L. 1988. Highly cooperative feedback control of retinal rod guanylate cyclase by calcium ions. Nature 334(6177):64-66.

Kosmaoglou M, Schwarz N, Bett JS, Cheetham ME. 2008. Molecular chaperones and photoreceptor function. Prog Retin Eye Res 27(4):434-449.

Kraskiewicz H, FitzGerald U. 2012. InterfERing with endoplasmic reticulum stress. Trends Pharmacol Sci 33(2):53-63.

Krylov DM, Niemi GA, Dizhoor AM, Hurley JB. 1999. Mapping sites in guanylyl cyclase activating protein-1 required for regulation of photoreceptor membrane guanylyl cyclases. J Biol Chem 274(16):10833-10839.

Lamb TD, Pugh EN. 2004. Dark adaptation and the retinoid cycle of vision. Prog Retin Eye Res 23(3):307-380.

Laura RP, Dizhoor AM, Hurley JB. 1996. The membrane guanylyl cyclase, retinal guanylyl cyclase-1, is activated through its intracellular domain. J Biol Chem 271(20):11646-11651.

Layfield R, Fergusson J, Aitken A, Lowe J, Landon M, Mayer RJ. 1996. Neurofibrillary tangles of Alzheimer's disease brains contain 14-3-3 proteins. Neurosci Lett 209(1):57-60.

Leber T. 1869. Ueber retinitis pigmentosa und angeborene Amaurose. Graefes Arch Clin Exp Ophthalmol. 1869;15:1–25.

Lee BY, Thulin CD, Willardson BM. 2004. Site-specific phosphorylation of phosducin in intact retina. Dynamics of phosphorylation and effects on G protein beta gamma dimer binding. J Biol Chem 279(52):54008-54017.

Lee VM, Goedert M, Trojanowski JQ. 2001. Neurodegenerative tauopathies. Annu Rev Neurosci 24:1121-1159.

Libby RT, Lillo C, Kitamoto J, Williams DS, Steel KP. 2004. Myosin Va is required for normal photoreceptor synaptic activity. J Cell Sci 117(Pt 19):4509-4515.

Lim S, Peshenko I, Dizhoor A, Ames JB. 2009. Effects of Ca2+, Mg2+, and myristoylation on guanylyl cyclase activating protein 1 structure and stability. Biochemistry 48(5):850-862.

Lim S, Peshenko IV, Dizhoor AM, Ames JB. 2013a. Backbone (1)H, (13)C, and (15)N resonance assignments of guanylyl cyclase activating protein-1, GCAP1. Biomol NMR Assign 7(1):39-42.

Lim S, Peshenko IV, Dizhoor AM, Ames JB. 2013b. Structural insights for activation of retinal guanylate cyclase by GCAP1. PLoS One 8(11):e81822.

LoGiudice L, Matthews G. 2009. The role of ribbons at sensory synapses. Neuroscientist 15(4):380-391.

Lopez-del Hoyo N, Fazioli L, Lopez-Begines S, Fernandez-Sanchez L, Cuenca N, Llorens J, de la Villa P, Mendez A. 2012. Overexpression of Guanylate Cyclase Activating Protein 2 in Rod Photoreceptors In Vivo Leads to Morphological Changes at the Synaptic Ribbon. Plos One 7(8):20.

Lucas KA, Pitari GM, Kazerounian S, Ruiz-Stewart I, Park J, Schulz S, Chepenik KP, Waldman SA. 2000. Guanylyl cyclases and signaling by cyclic GMP. Pharmacol Rev 52(3):375-414.

Magupalli VG, Schwarz K, Alpadi K, Natarajan S, Seigel GM, Schmitz F. 2008. Multiple RIBEYE-RIBEYE interactions create a dynamic scaffold for the formation of synaptic ribbons. J Neurosci 28(32):7954-7967.

Makino CL, Peshenko IV, Wen XH, Olshevskaya EV, Barrett R, Dizhoor AM. 2008. A role for GCAP2 in regulating the photoresponse. Guanylyl cyclase activation and rod electrophysiology in GUCA1B knock-out mice. J Biol Chem 283(43):29135-29143.

Makino CL, Wen XH, Olshevskaya EV, Peshenko IV, Savchenko AB, Dizhoor AM. 2012. Enzymatic relay mechanism stimulates cyclic GMP synthesis in rod photoresponse: biochemical and physiological study in guanylyl cyclase activating protein 1 knockout mice. PLoS One 7(10):e47637.

Mansergh F, Orton NC, Vessey JP, Lalonde MR, Stell WK, Tremblay F, Barnes S, Rancourt DE, Bech-Hansen NT. 2005. Mutation of the calcium channel gene Cacna1f disrupts calcium signaling, synaptic transmission and cellular organization in mouse retina. Hum Mol Genet 14(20):3035-3046.

Marlhens F, Bareil C, Griffoin JM, Zrenner E, Amalric P, Eliaou C, Liu SY, Harris E, Redmond TM, Arnaud B, Claustres M, Hamel CP. 1997. Mutations in RPE65 cause Leber's congenital amaurosis. Nat Genet 17(2):139-141.

Matsuda T, Cepko CL. 2004. Electroporation and RNA interference in the rodent retina in vivo and in vitro. Proc Natl Acad Sci U S A 101(1):16-22.

McCue HV, Haynes LP, Burgoyne RD. 2010. The diversity of calcium sensor proteins in the regulation of neuronal function. Cold Spring Harb Perspect Biol 2(8):a004085.

Mendes HF, van der Spuy J, Chapple JP, Cheetham ME. 2005. Mechanisms of cell death in rhodopsin retinitis pigmentosa: implications for therapy. Trends Mol Med 11(4):177-185.

Mendez A, Burns ME, Sokal I, Dizhoor AM, Baehr W, Palczewski K, Baylor DA, Chen J. 2001. Role of guanylate cyclase-activating proteins (GCAPs) in setting the flash sensitivity of rod photoreceptors. Proc Natl Acad Sci U S A 98(17):9948-9953.

Mendez A, Chen J. 2002. Mouse models to study GCAP functions in intact photoreceptors. Adv Exp Med Biol 514:361-388.

Michaelides M, Wilkie SE, Jenkins S, Holder GE, Hunt DM, Moore AT, Webster AR. 2005. Mutation in the gene GUCA1A, encoding guanylate cyclase-activating protein 1, causes cone, cone-rod, and macular dystrophy. Ophthalmology 112(8):1442-1447.

Molday LL, Djajadi H, Yan P, Szczygiel L, Boye SL, Chiodo VA, Gregory-Evans K, Sarunic MV, Hauswirth WW, Molday RS. 2013. RD3 gene delivery restores guanylate cyclase localization and rescues photoreceptors in the Rd3 mouse model of Leber congenital amaurosis 12. Hum Mol Genet 22(19):3894-3905.

Moreno JA, Halliday M, Molloy C, Radford H, Verity N, Axten JM, Ortori CA, Willis AE, Fischer PM, Barrett DA, Mallucci GR. 2013. Oral treatment targeting the unfolded protein response prevents neurodegeneration and clinical disease in prion-infected mice. Sci Transl Med 5(206):206ra138.

Muslin AJ, Tanner JW, Allen PM, Shaw AS. 1996. Interaction of 14-3-3 with signaling proteins is mediated by the recognition of phosphoserine. Cell 84(6):889-897.

Métayé T, Perdrisot R, Kraimps JL. 2006. [GRKs and arrestins: the therapeutic pathway?]. Med Sci (Paris) 22(5):537-543.

Nakano K, Chen J, Tarr GE, Yoshida T, Flynn JM, Bitensky MW. 2001. Rethinking the role of phosducin: light-regulated binding of phosducin to 14-3-3 in rod inner segments. Proc Natl Acad Sci U S A 98(8):4693-4698.

Nishiguchi KM, Sokal I, Yang L, Roychowdhury N, Palczewski K, Berson EL, Dryja TP, Baehr W. 2004. A novel mutation (I143NT) in guanylate cyclase-activating protein 1 (GCAP1) associated with autosomal dominant cone degeneration. Invest Ophthalmol Vis Sci 45(11):3863-3870.

Olshevskaya EV, Boikov S, Ermilov A, Krylov D, Hurley JB, Dizhoor AM. 1999a. Mapping functional domains of the guanylate cyclase regulator protein, GCAP-2. J Biol Chem 274(16):10823-10832.

Olshevskaya EV, Calvert PD, Woodruff ML, Peshenko IV, Savchenko AB, Makino CL, Ho YS, Fain GL, Dizhoor AM. 2004. The Y99C mutation in guanylyl cyclase-activating protein 1 increases intracellular Ca2+ and causes photoreceptor degeneration in transgenic mice. J Neurosci 24(27):6078-6085.

Olshevskaya EV, Ermilov AN, Dizhoor AM. 1999b. Dimerization of guanylyl cyclase-activating protein and a mechanism of photoreceptor guanylyl cyclase activation. J Biol Chem 274(36):25583-25587.

Olshevskaya EV, Hughes RE, Hurley JB, Dizhoor AM. 1997. Calcium binding, but not a calcium-myristoyl switch, controls the ability of guanylyl cyclase-activating protein GCAP-2 to regulate photoreceptor guanylyl cyclase. J Biol Chem 272(22):14327-14333.

Omi K, Hachiya NS, Tanaka M, Tokunaga K, Kaneko K. 2008. 14-3-3zeta is indispensable for aggregate formation of polyglutamine-expanded huntingtin protein. Neurosci Lett 431(1):45-50.

Orban T, Bereta G, Miyagi M, Wang B, Chance MR, Sousa MC, Palczewski K. 2010. Conformational changes in guanylate cyclase-activating protein 1 induced by Ca2+ and N-terminal fatty acid acylation. Structure 18(1):116-126.

Otto-Bruc A, Fariss RN, Haeseleer F, Huang J, Buczyłko J, Surgucheva I, Baehr W, Milam AH, Palczewski K. 1997. Localization of guanylate cyclase-activating protein 2 in mammalian retinas. Proc Natl Acad Sci U S A 94(9):4727-4732.

Otto-Bruc AE, Fariss RN, Van Hooser JP, Palczewski K. 1998. Phosphorylation of photolyzed rhodopsin is calcium-insensitive in retina permeabilized by alpha-toxin. Proc Natl Acad Sci U S A 95(25):15014-15019.

Palczewski K, Polans AS, Baehr W, Ames JB. 2000. Ca(2+)-binding proteins in the retina: structure, function, and the etiology of human visual diseases. Bioessays 22(4):337-350.

Palczewski K, Subbaraya I, Gorczyca WA, Helekar BS, Ruiz CC, Ohguro H, Huang J, Zhao X, Crabb JW, Johnson RS. 1994. Molecular cloning and characterization of retinal photoreceptor guanylyl cyclase-activating protein. Neuron 13(2):395-404.

Papermaster DS, Schneider BG, Zorn MA, Kraehenbuhl JP. 1978. Immunocytochemical localization of a large intrinsic membrane protein to the incisures and margins of frog rod outer segment disks. J Cell Biol 78(2):415-425.

Parsons TD, Sterling P. 2003. Synaptic ribbon. Conveyor belt or safety belt? Neuron 37(3):379-382.

Payne AM, Downes SM, Bessant DA, Taylor R, Holder GE, Warren MJ, Bird AC, Bhattacharya SS. 1998. A mutation in guanylate cyclase activator 1A (GUCA1A) in an autosomal dominant cone dystrophy pedigree mapping to a new locus on chromosome 6p21.1. Hum Mol Genet 7(2):273-277.

Pennesi ME, Howes KA, Baehr W, Wu SM. 2003. Guanylate cyclase-activating protein (GCAP) 1 rescues cone recovery kinetics in GCAP1/GCAP2 knockout mice. Proc Natl Acad Sci U S A 100(11):6783-6788.

Perrault I, Rozet JM, Calvas P, Gerber S, Camuzat A, Dollfus H, Châtelin S, Souied E, Ghazi I, Leowski C, Bonnemaison M, Le Paslier D, Frézal J, Dufier JL, Pittler S, Munnich A, Kaplan J. 1996. Retinal-specific guanylate cyclase gene mutations in Leber's congenital amaurosis. Nat Genet 14(4):461-464.

Perrault I, Rozet JM, Gerber S, Ghazi I, Ducroq D, Souied E, Leowski C, Bonnemaison M, Dufier JL, Munnich A, Kaplan J. 2000. Spectrum of retGC1 mutations in Leber's congenital amaurosis. Eur J Hum Genet 8(8):578-582.

Peshenko IV, Dizhoor AM. 2004. Guanylyl cyclase-activating proteins (GCAPs) are Ca2+/Mg2+ sensors: implications for photoreceptor guanylyl cyclase (RetGC) regulation in mammalian photoreceptors. J Biol Chem 279(17):16903-16906.

Peshenko IV, Dizhoor AM. 2006. Ca2+ and Mg2+ binding properties of GCAP-1. Evidence that Mg2+-bound form is the physiological activator of photoreceptor guanylyl cyclase. J Biol Chem 281(33):23830-23841.

Peshenko IV, Dizhoor AM. 2007. Activation and inhibition of photoreceptor guanylyl cyclase by guanylyl cyclase activating protein 1 (GCAP-1): the functional role of Mg2+/Ca2+ exchange in EF-hand domains. J Biol Chem 282(30):21645-21652.

Peshenko IV, Moiseyev GP, Olshevskaya EV, Dizhoor AM. 2004a. Factors that determine Ca2+ sensitivity of photoreceptor guanylyl cyclase. Kinetic analysis of the interaction between the Ca2+-bound and the Ca2+-free guanylyl cyclase activating proteins (GCAPs) and recombinant photoreceptor guanylyl cyclase 1 (RetGC-1). Biochemistry 43(43):13796-13804.

Peshenko IV, Olshevskaya EV, Azadi S, Molday LL, Molday RS, Dizhoor AM. 2011a. Retinal degeneration 3 (RD3) protein inhibits catalytic activity of retinal membrane guanylyl cyclase (RetGC) and its stimulation by activating proteins. Biochemistry 50(44):9511-9519.

Peshenko IV, Olshevskaya EV, Dizhoor AM. 2004b. Ca(2+)-dependent conformational changes in guanylyl cyclase-activating protein 2 (GCAP-2) revealed by site-specific phosphorylation and partial proteolysis. J Biol Chem 279(48):50342-50349.

Peshenko IV, Olshevskaya EV, Dizhoor AM. 2008. Binding of guanylyl cyclase activating protein 1 (GCAP1) to retinal guanylyl cyclase (RetGC1). The role of individual EF-hands. J Biol Chem 283(31):21747-21757.

Peshenko IV, Olshevskaya EV, Dizhoor AM. 2012a. Interaction of GCAP1 with retinal guanylyl cyclase and calcium: sensitivity to fatty acylation. Front Mol Neurosci 5:19.

Peshenko IV, Olshevskaya EV, Lim S, Ames JB, Dizhoor AM. 2012b. Calcium-myristoyl Tug is a new mechanism for intramolecular tuning of calcium sensitivity and target enzyme interaction for guanylyl cyclase-activating protein 1: dynamic connection between N-fatty acyl group and EF-hand controls calcium sensitivity. J Biol Chem 287(17):13972-13984.

Peshenko IV, Olshevskaya EV, Savchenko AB, Karan S, Palczewski K, Baehr W, Dizhoor AM. 2011b. Enzymatic properties and regulation of the native isozymes of retinal membrane guanylyl cyclase (RetGC) from mouse photoreceptors. Biochemistry 50(25):5590-5600.

Pettelkau J, Thondorf I, Theisgen S, Lilie H, Schröder T, Arlt C, Ihling CH, Sinz A. 2013. Structural analysis of guanylyl cyclase-activating protein-2 (GCAP-2) homodimer by stable isotope-labeling, chemical cross-linking, and mass spectrometry. J Am Soc Mass Spectrom 24(12):1969-1979.

Prescott ED, Zenisek D. 2005. Recent progress towards understanding the synaptic ribbon. Curr Opin Neurobiol 15(4):431-436.

Pugh EN, Nikonov S, Lamb TD. 1999. Molecular mechanisms of vertebrate photoreceptor light adaptation. Curr Opin Neurobiol 9(4):410-418.

Regus-Leidig H, Specht D, Tom Dieck S, Brandstätter JH. 2010a. Stability of active zone components at the photoreceptor ribbon complex. Mol Vis 16:2690-2700.

Regus-Leidig H, tom Dieck S, Brandstätter JH. 2010b. Absence of functional active zone protein Bassoon affects assembly and transport of ribbon precursors during early steps of photoreceptor synaptogenesis. Eur J Cell Biol 89(6):468-475.

Regus-Leidig H, Tom Dieck S, Specht D, Meyer L, Brandstätter JH. 2009. Early steps in the assembly of photoreceptor ribbon synapses in the mouse retina: the involvement of precursor spheres. J Comp Neurol 512(6):814-824.

Reim K, Wegmeyer H, Brandstätter JH, Xue M, Rosenmund C, Dresbach T, Hofmann K, Brose N. 2005. Structurally and functionally unique complexins at retinal ribbon synapses. J Cell Biol 169(4):669-680.

Rodieck, R. 1998.The First Steps in Seeing. Sinauer Associates, Massachusetts.

Rudnicka-Nawrot M, Surgucheva I, Hulmes JD, Haeseleer F, Sokal I, Crabb JW, Baehr W, Palczewski K. 1998. Changes in biological activity and folding of guanylate cyclase-activating protein 1 as a function of calcium. Biochemistry 37(1):248-257.

Sato M, Nakazawa M, Usui T, Tanimoto N, Abe H, Ohguro H. 2005a. Mutations in the gene coding for guanylate cyclase-activating protein 2 (GUCA1B gene) in patients with autosomal dominant retinal dystrophies. Graefes Arch Clin Exp Ophthalmol 243(3):235-242.

Schmitz F. 2009. The making of synaptic ribbons: how they are built and what they do. Neuroscientist 15(6):611-624.

Schmitz F, Königstorfer A, Südhof TC. 2000. RIBEYE, a component of synaptic ribbons: a protein's journey through evolution provides insight into synaptic ribbon function. Neuron 28(3):857-872.

Schmitz F, Tabares L, Khimich D, Strenzke N, de la Villa-Polo P, Castellano-Muñoz M, Bulankina A, Moser T, Fernández-Chacón R, Südhof TC. 2006. CSPalpha-deficiency causes massive and rapid photoreceptor degeneration. Proc Natl Acad Sci U S A 103(8):2926-2931.

Schröder T, Lilie H, Lange C. 2011. The myristoylation of guanylate cyclase-activating protein-2 causes an increase in thermodynamic stability in the presence but not in the absence of Ca^{2+}. Protein Sci 20(7):1155-1165.

Sharma M, Burré J, Südhof TC. 2011. CSPα promotes SNARE-complex assembly by chaperoning SNAP-25 during synaptic activity. Nat Cell Biol 13(1):30-39.

Singhal A, Ostermaier MK, Vishnivetskiy SA, Panneels V, Homan KT, Tesmer JJ, Veprintsev D, Deupi X, Gurevich VV, Schertler GF, Standfuss J. 2013. Insights into congenital stationary night blindness based on the structure of G90D rhodopsin. EMBO Rep 14(6):520-526.

Sizova OS, Shinde VM, Lenox AR, Gorbatyuk MS. 2013. Modulation of cellular signaling pathways in P23H rhodopsin photoreceptors. Cell Signal 26(4):665-672.

Smith AJ, Daut J, Schwappach B. 2011. Membrane proteins as 14-3-3 clients in functional regulation and intracellular transport. Physiology (Bethesda) 26(3):181-191.

Snellman J, Mehta B, Babai N, Bartoletti TM, Akmentin W, Francis A, Matthews G, Thoreson W, Zenisek D. 2011. Acute destruction of the synaptic ribbon reveals a role for the ribbon in vesicle priming. Nat Neurosci 14(9):1135-1141.

Sokal I, Dupps WJ, Grassi MA, Brown J, Affatigato LM, Roychowdhury N, Yang L, Filipek S, Palczewski K, Stone EM, Baehr W. 2005. A novel GCAP1 missense mutation (L151F) in a large family with autosomal dominant cone-rod dystrophy (adCORD). Invest Ophthalmol Vis Sci 46(4):1124-1132.

Sokal I, Li N, Klug CS, Filipek S, Hubbell WL, Baehr W, Palczewski K. 2001. Calcium-sensitive regions of GCAP1 as observed by chemical modifications, fluorescence, and EPR spectroscopies. J Biol Chem 276(46):43361-43373.

Sokal I, Li N, Surgucheva I, Warren MJ, Payne AM, Bhattacharya SS, Baehr W, Palczewski K. 1998. GCAP1 (Y99C) mutant is constitutively active in autosomal dominant cone dystrophy. Mol Cell 2(1):129-133.

Sokal I, Otto-Bruc AE, Surgucheva I, Verlinde CL, Wang CK, Baehr W, Palczewski K. 1999. Conformational changes in guanylyl cyclase-activating protein 1 (GCAP1) and its tryptophan mutants as a function of calcium concentration. J Biol Chem 274(28):19829-19837.

Sokolov M, Strissel KJ, Leskov IB, Michaud NA, Govardovskii VI, Arshavsky VY. 2004. Phosducin facilitates light-driven transducin translocation in rod photoreceptors. Evidence from the phosducin knockout mouse. J Biol Chem 279(18):19149-19156.

Spiwoks-Becker I, Glas M, Lasarzik I, Vollrath L. 2004. Mouse photoreceptor synaptic ribbons lose and regain material in response to illumination changes. Eur J Neurosci 19(6):1559-1571.

Steinacker P, Aitken A, Otto M. 2011. 14-3-3 proteins in neurodegeneration. Semin Cell Dev Biol 22(7):696-704.

Stephen R, Bereta G, Golczak M, Palczewski K, Sousa MC. 2007. Stabilizing function for myristoyl group revealed by the crystal structure of a neuronal calcium sensor, guanylate cyclase-activating protein 1. Structure 15(11):1392-1402.

Sterling P, Matthews G. 2005. Structure and function of ribbon synapses. Trends Neurosci 28(1):20-29.

Strissel KJ, Lishko PV, Trieu LH, Kennedy MJ, Hurley JB, Arshavsky VY. 2005. Recoverin undergoes light-dependent intracellular translocation in rod photoreceptors. J Biol Chem 280(32):29250-29255.

Subbaraya I, Ruiz CC, Helekar BS, Zhao X, Gorczyca WA, Pettenati MJ, Rao PN, Palczewski K, Baehr W. 1994. Molecular characterization of human and mouse photoreceptor guanylate cyclase-activating protein (GCAP) and chromosomal localization of the human gene. J Biol Chem 269(49):31080-31089.

Surguchov A, Bronson JD, Banerjee P, Knowles JA, Ruiz C, Subbaraya I, Palczewski K, Baehr W. 1997. The human GCAP1 and GCAP2 genes are arranged in a tail-to-tail array on the short arm of chromosome 6 (p21.1). Genomics 39(3):312-322.

Thoreson WB. 2007. Kinetics of synaptic transmission at ribbon synapses of rods and cones. Mol Neurobiol 36(3):205-223.

Thulin CD, Savage JR, McLaughlin JN, Truscott SM, Old WM, Ahn NG, Resing KA, Hamm HE, Bitensky MW, Willardson BM. 2001. Modulation of the G protein regulator phosducin by Ca2+/calmodulin-dependent protein kinase II phosphorylation and 14-3-3 protein binding. J Biol Chem 276(26):23805-23815.

tom Dieck S, Altrock WD, Kessels MM, Qualmann B, Regus H, Brauner D, Fejtová A, Bracko O, Gundelfinger ED, Brandstätter JH. 2005. Molecular dissection of the photoreceptor ribbon synapse: physical interaction of Bassoon and RIBEYE is essential for the assembly of the ribbon complex. J Cell Biol 168(5):825-836.

tom Dieck S, Brandstätter JH. 2006. Ribbon synapses of the retina. Cell Tissue Res 326(2):339-346.

van der Spuy J, Chapple JP, Clark BJ, Luthert PJ, Sethi CS, Cheetham ME. 2002. The Leber congenital amaurosis gene product AIPL1 is localized exclusively in rod photoreceptors of the adult human retina. Hum Mol Genet 11(7):823-831.

Van Epps HA, Hayashi M, Lucast L, Stearns GW, Hurley JB, De Camilli P, Brockerhoff SE. 2004. The zebrafish nrc mutant reveals a role for the polyphosphoinositide phosphatase synaptojanin 1 in cone photoreceptor ribbon anchoring. J Neurosci 24(40):8641-8650.

Venkatesan JK, Natarajan S, Schwarz K, Mayer SI, Alpadi K, Magupalli VG, Sung CH, Schmitz F. 2010. Nicotinamide adenine dinucleotide-dependent binding of the neuronal Ca2+ sensor protein GCAP2 to photoreceptor synaptic ribbons. J Neurosci 30(19):6559-6576.

Vollrath L, Spiwoks-Becker I. 1996. Plasticity of retinal ribbon synapses. Microsc Res Tech 35(6):472-487.

Vollrath L, Spiwoks-Becker I, Adly MA, Schaaff U, Lasarzik I, Neumann S. 2001. Synaptic ribbon dynamics in photoreceptors of mice. Ital J Anat Embryol 106(2 Suppl 1):499-507.

von Gersdorff H. 2001. Synaptic ribbons: versatile signal transducers. Neuron 29(1):7-10.

Werblin FS. 2011. The retinal hypercircuit: a repeating synaptic interactive motif underlying visual function. J Physiol 589(Pt 15):3691-3702.

Wilkie SE, Li Y, Deery EC, Newbold RJ, Garibaldi D, Bateman JB, Zhang H, Lin W, Zack DJ, Bhattacharya SS, Warren MJ, Hunt DM, Zhang K. 2001. Identification and functional consequences of a new mutation (E155G) in the gene for GCAP1 that causes autosomal dominant cone dystrophy. Am J Hum Genet 69(3):471-480.

Woodruff ML, Olshevskaya EV, Savchenko AB, Peshenko IV, Barrett R, Bush RA, Sieving PA, Fain GL, Dizhoor AM. 2007. Constitutive excitation by Gly90Asp rhodopsin rescues rods from degeneration caused by elevated production of cGMP in the dark. J Neurosci 27(33):8805-8815.

Woodruff ML, Sampath AP, Matthews HR, Krasnoperova NV, Lem J, Fain GL. 2002. Measurement of cytoplasmic calcium concentration in the rods of wild-type and transducin knock-out mice. J Physiol 542(Pt 3):843-854.

Woodruff ML, Wang Z, Chung HY, Redmond TM, Fain GL, Lem J. 2003. Spontaneous activity of opsin apoprotein is a cause of Leber congenital amaurosis. Nat Genet 35(2):158-164.

Yamamoto S, Sippel KC, Berson EL, Dryja TP. 1997. Defects in the rhodopsin kinase gene in the Oguchi form of stationary night blindness. Nat Genet 15(2):175-178.

Yang RB, Robinson SW, Xiong WH, Yau KW, Birch DG, Garbers DL. 1999. Disruption of a retinal guanylyl cyclase gene leads to cone-specific dystrophy and paradoxical rod behavior. J Neurosci 19(14):5889-5897.

Yang X, Lee WH, Sobott F, Papagrigoriou E, Robinson CV, Grossmann JG, Sundström M, Doyle DA, Elkins JM. 2006. Structural basis for protein-protein interactions in the 14-3-3 protein family. Proc Natl Acad Sci U S A 103(46):17237-17242.

Yau KW, Hardie RC. 2009. Phototransduction motifs and variations. Cell 139(2):246-264.

Yildiz O, Khanna H. 2012. Ciliary signaling cascades in photoreceptors. Vision Res 75:112-116.

Yu H, Olshevskaya E, Duda T, Seno K, Hayashi F, Sharma RK, Dizhoor AM, Yamazaki A. 1999. Activation of retinal guanylyl cyclase-1 by Ca2+-binding proteins involves its dimerization. J Biol Chem 274(22):15547-15555.

Zampighi GA, Schietroma C, Zampighi LM, Woodruff M, Wright EM, Brecha NC. 2011. Conical tomography of a ribbon synapse: structural evidence for vesicle fusion. PLoS One 6(3):e16944.

Zanazzi G, Matthews G. 2009. The molecular architecture of ribbon presynaptic terminals. Mol Neurobiol 39(2):130-148.

Zavzavadjian JR, Couture S, Park WS, Whalen J, Lyon S, Lee G, Fung E, Mi Q, Liu J, Wall E, Santat L, Dhandapani K, Kivork C, Driver A, Zhu X, Chang MS, Randhawa B, Gehrig E, Bryan H, Verghese M, Maer A, Saunders B, Ning Y, Subramaniam S, Meyer T, Simon MI, O'Rourke N, Chandy G, Fraser ID. 2007. The alliance for cellular signaling plasmid collection: a flexible resource for protein localization studies and signaling pathway analysis. Mol Cell Proteomics 6(3):413-424.

Zenisek D, Horst NK, Merrifield C, Sterling P, Matthews G. 2004. Visualizing synaptic ribbons in the living cell. J Neurosci 24(44):9752-9759.

Zhang H, Constantine R, Frederick JM, Baehr W. 2012. The prenyl-binding protein PrBP/δ: a chaperone participating in intracellular trafficking. Vision Res 75:19-25.

Zhang H, Constantine R, Vorobiev S, Chen Y, Seetharaman J, Huang YJ, Xiao R, Montelione GT, Gerstner CD, Davis MW, Inana G, Whitby FG, Jorgensen EM, Hill CP, Tong L, Baehr W. 2011. UNC119 is required for G protein trafficking in sensory neurons. Nat Neurosci 14(7):874-880.

.

IX. ACKNOWLEDGEMENTS

ACKNOWLEDGEMENTS- AGRADECIMIENTOS

We acknowledge the expert assistance of Dr. P. de la Villa in the acquisition and interpretation of ERG recordings, Dr. J.L. Rosa for his expert advise on proteomic analysis, Dr J.Llorens for his expert advice on acquisition and interpretation of transmission electron micrographs, as well as his assistance on statistical analysis; Drs. J.M. Estanyol and M.J. Fidalgo at the Proteomics Facility of the Clinic Hospital of Barcelona, Scientific and Technological Services of the University of Barcelona (CCiT-UB). We kindly acknowledge the excellent technical assistance of Dr. Nuria Cortadellas, Almudena García and Dr. Eva Fernández at the electron microscopy facility of the CCiT-UB. Also we thank Isidre Casals and Dr. Eva María del Álamo from the Separative Techniques Facility of Cluster Building in PCB (Parc Científic de Barcelona), CCiT-UB for their help and advice in the use of HPLC. We are in debt with Dr. Benjamín Torrejón for his kind assistance with image acquisition at the Leica TCS-SL, at the CCiT-UB; with Dr. Alvaro Gimeno at the Vivarium facility and with Dr. Aurea Navarro at the IRA2105 Radioactive facility at the CCiT-UB-Bellvitge. We also acknowledge funding from the Spanish Ministry of Economy and Competitiveness (MINECO): *BFU2008-04199/BFI, BFU2011-26519/BFI, PRI-PIBIN-2011-1151;* from the European Community*: MIRG-CT-2007-210042;* and from the ONCE Foundation, from the European Community to A.M. (Marie-Curie Reintegration grant 210042/RODCELL) and from IDIBELL to A.M. (10IDB012).

Also, I gratefully acknowledge being the recipient of a PhD fellowship from Research Foundation for the predoctoral fellowship from the IDIBELL PhD Program that allowed me to do this work here presented.

Permitidme los agradecimientos más personales en mi lengua materna.

Esta tesis es el resultado de cinco años de intenso trabajo en equipo, humano y profesional. Tras el paso de éstos, finalmente caí en la cuenta que no había hecho más que empezar a crecer en una pequeña nueva familia. Una familia científica.

Mis primeras horas de vuelo terminan aquí. Hemos pasado la travesía del desierto, quemado las últimas naves y nos vemos sumidos en economía de guerra, batallando incesantes día tras día. Gracias por vuestro apoyo, Ana, Santi y Lucrezia.

Ana, eres una muy buena narradora de historias, científicas y no tan científicas. Además, me has sabido transmitir ánimos cuando has visto tentaciones de abandonar

las armas, abanderando tenazmente la ciencia a pesar de las siempre acechantes adversidades. Por esto y más, me has enseñado que los triunfos más contundentes se consiguen con esfuerzo, perseverancia, dedicación de infinitas horas y disciplina.

Qué decir Santi, podría llenar hojas y hojas. Contigo me ha tocado la lotería. Lo he dicho siempre, y lo mantengo. Eres una de las personas más noble, trabajadora y sana de espíritu con las que me he topado. Y también eres un rato paciente. El que siempre ha estado ahí, codo con codo, dispuesto a ayudar y a hacer alguna que otra payasada. El compi genial y el más normal de la jaula de grillos que es el laboratorio. Tu mayor pega, que no te guste compartir la comida ☺ Te voy a echar mucho de menos, y te agradezco todo el soporte que siempre me has dado.

Lucrezia, te fui queriendo cada vez más. Buena, bella, alegre, luchadora y con gran sentido de la justicia son las palabras que me vienen a la cabeza cuando pienso en ti.

Sinceramente, junto con Santi, los dos habéis sido buenos ejemplos de los que he aprendido mucho, y obviamente, esta tesis es también vuestra.

También gracias a los dos estudiantes que nos ayudaron unos meses. Laura, me encantas. Se te iba la pinza más que a mí y me arrancabas la sonrisa y la carcajada todas las mañanas con tu inagotable verborrea. David eres el mejor piropeador de todos los tiempos. Y muy freak y detallista, ¡menudo crack!

Bueno, rubia, es tu turno. Mercè, eres la responsable de que acabase aquí haciendo un doctorado. Así que ¿gracias? ☺ Con la broma, hace 9 años que nos conocemos, y en ellos te he visto más que a mi familia, y es literal, y me parece a mí que recíproco. ¡¡¡Eres mi relación diaria más larga!!! ¿Qué voy a hacer ahora sin ti? Jeje Tengo una lista infinita de momento especiales contigo, y la mayoría de ellos, los mejores, surgían de la nada, de una iluminación “gloriosa” por parte de una de las dos, y no nos iba tan mal. Sigamos haciéndolo pues, improvisemos a ver qué tal se nos sigue dando.

Núria, de mayor quiero ser como tú. Tal cual. Eres muy apañada con la cocina, las compritas, estás a la última en la actualidad social y tecnológica (esto último por todas tus aventuras con el móvil, “of course”), sabes escuchar y dar unos consejos cojonudos y muy prácticos. Ariadna, aunque mi pueblo sea más pequeño, eres más chunga que yo. Pero la chunga de corazón más gordo con la que me he topado. Y adoro lo ordenado que tienes todo. Sois amor, me habéis hecho el año más desesperante mucho más liviano y en definitiva, sois mis “cooks” preferidas ♥ Silvia hemos compartido botes de nutella, tiramisús, consejos de tricot, tardes dispersas de charlas pseudofilosóficas y más. Marisabel, aparte de tus múltiples sabios consejos, para algo eras algo así como la mami, me río acordándome de ti cuando me viene a la

cabeza: “Sabe más el diablo por viejo, que por diablo.” ¡Qué cierto! También quiero dar las gracias a todo el resto de los miembros del grupo de Pau Gorostiza, con quiénes desde los inicios hemos compartido laboratorio y de todo, cual familia adoptiva.

Motivos de fuerza mayor me llevan a dar las gracias también a los coleguillas del labo de Concepció Soler, Diana y Joan (venga va, y ahora Mercè, “la otra Mercè”), que han sido los vecinos con los que compartes azúcar, aceite o lo que haga falta. Diana, lo dicho, eres la extranjera más linda del mundo que he conocido en mi vida (tienes más cuento que yo, pero cuento bonito) y Joan, eres un “person”, nunca dejarás de sorprenderme. Y aunque seguro que me dejo a mucha gente, que nadie se lo tome a mal, sino los agradecimientos se extenderían más que la propia tesis.

Los inicios en Bellvitge, poniendo a punto el laboratorio, fueron más fáciles gracias a buenos favores. Doy las gracias por los seminarios semanales de los primeros años y a todos los que a ellos asistían, entre ellos, David Albrecht, me dedicaste unas generosas horas para que usase solita el HPLC y así purificar proteína, amenizándolo siempre con tu encanto chileno y tus chistes tan potentes. Para ir acortando un poco, gracias a todas esas personas que en algún momento me echaron un capote con alguna técnica y recomendaciones entre la cuarta y quinta planta de Bellvitge, o en congresos, o en los serveis del Parc y el Clínic, etc.

Ya pasando a un plano más personal, en esta andadura científica también tuvo su peso el máster el primer año. Allí nos conocimos, Lara Sedó, Anna Nualart y la ya Dra. Ana García. Nada que ver las primeras impresiones del doctorado con lo que luego nos hemos encontrado, pero siempre sacando un rato para compartirlo y cambiar la desesperación por esperanza. Gracias por todos esos momentos en los que empatizamos contándonos nuestras vidas, como salidas de “Sexo en Nueva York”, mientras tomamos unas buenas tapitas o nos corremos alguna juerga. En esa misma línea, no me olvido de aquellos con los que comenzó esta aventura científica en la Universidad y que durante estos años han seguido allí pico y pala: “evidentemente Marta”, Sergio (siempre me has transmitido serenidad, ¡maldito!), la también Dra. Carmen Aguilar, Laura Tatjer, María, Alberto, Nikita, Jurdan, Gemma…

Y para ir acabando, no quiero olvidarme de dar las mil gracias a los que siempre están ahí, escuchándote y mimándote, aunque algunos no siempre entiendan esto de la tesis ni los disgustos y quebraderos de cabeza que te produce, porque al igual que todos los anteriores, han sabido reconfortarme y alentarme a seguir adelante investigando.

Gracias a los amigos de toda la vida: Maite, Paulita, Naiara, Celia, Mireia, Lara, Nerea, Ainara, Arnau, Marta Canadell, Cristina Arauz, Paula Gutiérrez, Sanjur, Ariadna, Laura, Cristina Masnou, Nuria Crous, Lara Laso, Varona…

Y finalmente, gracias a mi magnífica y extensa familia, por parte de padre y por parte de madre. Y en esta última, quiero elogiar las multitudinarias comidas familiares, que resultan ser la inspiración definitiva para acabar una tesis, arreglar y conquistar el mundo.

X. APPENDIX

A.1. LIST OF ABBREVIATIONS

A	Å	Armstrong
	aa	amino acid
	Ab	antibody
	ad	arciform density
	AD	Alzheimer disease
	adCD	autosomal dominant cone dystrophy
	adCORD	autosomal dominant cone-rod dystrophy
	adRP	autosomal dominant retinitis pigmentosa
	AMPA	α-amino-3-hydroxy-5-methyl-4-isoxazole propionic acid
	APP	amyloid precursor protein
B	bc	bipolar cell
	b or bov GCAP	bovine GCAP
	bp	base pairs
	BSA	bovine serum albumin
C	Ca^{2+}	calcium
	$[Ca^{2+}]_{free}$	calcium free concentration
	$[Ca^{2+}]_{I}$	calcium initial concentration
	$CaCl_2$	calcium chloride
	CaM	calmodulin
	cAMP	cyclic adenosine monophosphate
	cGMP	cyclic guanosine monophosphate
	CO_2	carbon dioxide
	csr	club-shaped ribbons
	CV	column volume
D	DNA	deoxyribonucleic acid
	dNTPs	nucleotides
	DTT	dithiothreitol
E	EC_{50}	half maximal effective concentration
	ECL	enhanced chemiluminescence
	EDTA	ethylene diamine tetraacetic acid
	e.g.	for example
	EGTA	ethylene glycol tetraacetic acid
	ER	endoplasmic reticulum

	ERG	electroretinogram
	etc.	et cetera
G	G_α, G_β, G_γ	Subunits of transducin protein
	GAP	GTPase- activating protein
	GC	guanylate cyclase
	GCAP	guanylate cyclase activating protein
	GCIP	guanylate cyclase inhibiting protein
	GDNF	glial cell-derived neurotrophic factor
	GDP	guanosine diphosphate
	GFP	green fluorescent protein
	GMP	guanosine monophosphate
	GRK1	G protein-coupled receptor kinase 1
	GTP	guanosine triphosphate
H	hc	horizontal cell
	HCl	hydrochloric acid
	HD	Huntington disease
	HEPES	2-[4-(2-hydroxyethyl)piperazin-1-yl] ethanesulfonic acid
	HPLC	high-performance liquid chromatography
I	IBMX	1-methyl-3-(2-methylpropyl)-7H-purine-2,6-dione
	IEF	isoelectric focusing
	IgG	immunoglobulin G
K	K^+	potassium
	KChIP	K^+ channel-interacting protein
	KCl	potassium chloride
	kDa	kilodalton
	KO	knockout
	KOH	potassium hydroxide
	Kv channel	voltage-gated K^+ channel
L	LTD	long-term depression
	LCA	Leber's Congenital Amaurosis
M	MAPK	mitogen-activated protein kinases
	Mg^{2+}	magnesium
	$MgCl_2$	magnesium chloride
	mM	millimolar
	MOPS	3-(N-morpholino)propanesulfonic acid

	ms	millisecond
	myr	myristoylated
N	Na^+	sodium
	NaCl	sodium chloride
	NAD(H)	nicotinamide adenine dinucleotide
	NaFl	sodium fluoride
	NaH_2PO_4	sodium phosphate
	Na_2CO_3	sodium carbonate
	NCS	neuronal calcium sensor
	nM	nanomolar
	NMR	nuclear magnetic resonance
O	OCT	optimal cutting temperature compound
	ONL	outer nuclear layer
	OPL	outer plexiform layer
P	$^{32}P_i$	radioactively labeled inorganic phosphate
	PBS	phosphate buffered saline
	PCR	polymerase chain reaction
	PD	Parkinson disease
	PDE	phosphodiesterase
	PKC	protein kinase C
	PKG	protein kinase G
	PMA	plant plasma membrane H^+-ATPase
	PMSF	phenylmethanesulfonylfluoride
R	R9AP	RGS9 anchoring protein
	RD3	retinal degeneration 3 protein
	RetGC	retinal guanylate cyclase
	RGS9	regulator of G-protein signalling 9
	RIS	rod inner segment
	ROS	rod outer segment
	RP	retinitis pigmentosa
	RRP	readily releasable pool
S	s	second
	SCA	spinocerebellar ataxin
	SDS	sodium dodecyl sulfate
	SDS-PAGE	sodium dodecyl sulfate polyacrylamide gel
	SNARE complex	SNAP (Soluble NSF Attachment Protein) REceptor complex

	sr	synaptic ribbon
	ss	synaptic sphere
U	µM	micromolar
	µCi	microcurie
V	VSNL	visinin-like protein
W	wt	wildtype
Z	zGCAP	GCAP from zebrafish
	$Zn(OAc)_2$	zinc acetate

A.2. STANDARD AMINOACIDS

Amino Acid	3-Letter	1-Letter	Side-chain polarity	Side-chain charge (pH 7.4)	Hydropathy
Alanine	Ala	A	Nonpolar	neutral	1.8
Arginine	Arg	R	Basic polar	positive	−4.5
Asparagine	Asn	N	Polar	neutral	−3.5
Aspartic acid	Asp	D	acidic polar	negative	−3.5
Cysteine	Cys	C	Nonpolar	neutral	2.5
Glutamic acid	Glu	E	acidic polar	negative	−3.5
Glutamine	Gln	Q	Polar	neutral	−3.5
Glycine	Gly	G	Nonpolar	neutral	−0.4
Histidine	His	H	Basic polar	positive(10%)/ neutral(90%)	−3.2
Isoleucine	Ile	I	Nonpolar	neutral	4.5
Leucine	Leu	L	Nonpolar	neutral	3.8
Lysine	Lys	K	Basic polar	positive	−3.9
Methionine	Met	M	Nonpolar	neutral	1.9
Phenylalanine	Phe	F	Nonpolar	neutral	2.8
Proline	Pro	P	Nonpolar	neutral	−1.6
Serine	Ser	S	Polar	neutral	−0.8
Threonine	Thr	T	Polar	neutral	−0.7
Tryptophan	Trp	W	Nonpolar	neutral	−0.9
Tyrosine	Tyr	Y	Polar	neutral	−1.3
Valine	Val	V	Nonpolar	neutral	4.2

Table A.1. Standard amino acid abbreviations and properties

A.3. GCAPs AND DISEASE

Until now, GCAPs mutant proteins have been described to be involved in the following retinal diseases (all of them with a dominant phenotype) (Table A.2): on one hand, GCAP1 mutants lead to autosomal dominant cone dystrophy (adCD) and autosomal dominant cone-rod dystrophy (adCORD) (see *INTRODUCTION: Molecular basis of inherited retinal dystrophies: GCAPs mutations and disease*). On the other hand, in three independent Asian families was found G157R mutation in GCAP2 that leads to retinitis pigmentosa (RP) and in some cases to dominant macular dystrophy (Sato *et al.* 2005).

Symbols; OMIM Numbers	Location	Diseases; Protein	How Identified; Comments	References
GUCA1A, COD3, CORD14, GCAP1; 120970, 602093, 600364	6p21.1	Dominant cone dystrophy; dominant cone-rod dystrophy; protein: guanylate cyclase activating protein 1A [Gene]	linkage mapping, candidate gene; British family with constitutively active mutant; variable phenotype within families	Downes 01; Payne 97; Payne 98, Sokal 98
GUCA1B, GCAP2, RP48; 268000, 602275, 613827	6p21.1	Dominant retinitis pigmentosa; dominant macular dystrophy; protein: guaylate cyclase activating protein 1B [Gene]	Candidate gene ; Gly157Arg mutation in Japanese families with variable phenotype ; no pathologic changes found in 400 Bristish patients with dominant retinopathies	Payne 99a; Sato 04

Table A.2. *GUCA1A and GUCA1B data extracted from "Genes and map loci causing general disease" in webpage: https://sph.uth.edu/Retnet/home.htm.*

XI. PUBLICATION

OPEN ACCESS Freely available online

PLOS ONE

Overexpression of Guanylate Cyclase Activating Protein 2 in Rod Photoreceptors *In Vivo* Leads to Morphological Changes at the Synaptic Ribbon

Natalia López-del Hoyo[1☯], Lucrezia Fazioli[1☯], Santiago López-Begines[1], Laura Fernández-Sánchez[2], Nicolás Cuenca[2], Jordi Llorens[1,3], Pedro de la Villa[4], Ana Méndez[1,5]*

1 Bellvitge Biomedical Research Institute (IDIBELL), Barcelona, Spain, **2** Department of Physiology, Genetics and Microbiology, Universidad de Alicante, Alicante, Spain, **3** Department of Physiological Sciences II, University of Barcelona-Bellvitge Health Science Campus, Barcelona, Spain, **4** Department of Physiology, University of Alcalá de Henares, Madrid, Spain, **5** Department of Pathology and Experimental Therapeutics, University of Barcelona-Bellvitge Health Science Campus, Barcelona, Spain

Abstract

Guanylate cyclase activating proteins are EF-hand containing proteins that confer calcium sensitivity to retinal guanylate cyclase at the outer segment discs of photoreceptor cells. By making the rate of cGMP synthesis dependent on the free intracellular calcium levels set by illumination, GCAPs play a fundamental role in the recovery of the light response and light adaptation. The main isoforms GCAP1 and GCAP2 also localize to the synaptic terminal, where their function is not known. Based on the reported interaction of GCAP2 with Ribeye, the major component of synaptic ribbons, it was proposed that GCAP2 could mediate the synaptic ribbon dynamic changes that happen in response to light. We here present a thorough ultrastructural analysis of rod synaptic terminals in loss-of-function (GCAP1/GCAP2 double knockout) and gain-of-function (transgenic overexpression) mouse models of GCAP2. Rod synaptic ribbons in GCAPs−/− mice did not differ from wildtype ribbons when mice were raised in constant darkness, indicating that GCAPs are not required for ribbon early assembly or maturation. Transgenic overexpression of GCAP2 in rods led to a shortening of synaptic ribbons, and to a higher than normal percentage of club-shaped and spherical ribbon morphologies. Restoration of GCAP2 expression in the GCAPs−/− background (GCAP2 expression in the absence of endogenous GCAP1) had the striking result of shortening ribbon length to a much higher degree than overexpression of GCAP2 in the wildtype background, as well as reducing the thickness of the outer plexiform layer without affecting the number of rod photoreceptor cells. These results indicate that preservation of the GCAP1 to GCAP2 relative levels is relevant for maintaining the integrity of the synaptic terminal. Our demonstration of GCAP2 immunolocalization at synaptic ribbons at the ultrastructural level would support a role of GCAPs at mediating the effect of light on morphological remodeling changes of synaptic ribbons.

Citation: López-del Hoyo N, Fazioli L, López-Begines S, Fernández-Sánchez L, Cuenca N, et al. (2012) Overexpression of Guanylate Cyclase Activating Protein 2 in Rod Photoreceptors *In Vivo* Leads to Morphological Changes at the Synaptic Ribbon. PLoS ONE 7(8): e42994. doi:10.1371/journal.pone.0042994

Editor: Karl-Wilhelm Koch, University of Oldenburg, Germany

Received March 14, 2012; **Accepted** July 16, 2012; **Published** August 13, 2012

Funding: This work was supported by grants from the Spanish Ministry of Science and Innovation to A.M. (BFU2008-04199/BFI and BFU2011-26519/BFI), to J.Ll. (BFU2009-06945), to P.dlV. (SAF2010-21879 and RETICS RD07/0062/0008), to N.C. (BFU2009-07793/BFI and RETICS RD07/0062/0012); from the European Community to A.M. (Marie-Curie Reintegration grant 210042/RODCELL) and from The Bellvitge Biomedical Research Institute (IDIBELL) to A.M. (10IDB012). N.L.-H. was the recipient of an Bellvitge Biomedical Research Institute (IDIBELL) PhD fellowship. The funders had no role in study design, data collection and analysis, decision to publish, or preparation of the manuscript.

Competing Interests: The authors have declared that no competing interests exist.

* E-mail: mendezzu@idibell.cat

☯ These authors contributed equally to this work.

Introduction

Photoreceptor cells in the retina sense the light intensity at different points in the visual field. They transduce absorbed photons into graded changes in membrane potential that set the rate of neurotransmitter release to bipolar and horizontal cells. A neural signal is thereby relayed from photoreceptor to bipolar cells that is in turn conveyed to ganglion cells. The neural circuitry involved in the convergence of this signal is what emphasizes the spatial differences in light intensity that are processed by ganglion cells to evoke the distinct visual functions [1].

Because light intensities in the natural world can vary over ten orders of magnitude, one fundamental ability of rod and cone photoreceptor cells is to sense and reliably transmit fine gradations in light intensity covering a broad dynamic range. To accomplish this, photoreceptor cells avoid spikes and finely grade the quantized synaptic output with graded changes in membrane potential [2,3]. Like sensory receptors in the auditory and vestibular systems, they rely on specialized synapses that support the continuous neurotransmitter release at high rates [4,5]. A hallmark of these synapses is a specialized structure, the "ribbon" or "dense body", a plate-like proteinaceous scaffold that anchors to the active zone just adjacent to the clustered voltage-gated calcium channels[6–9]. Ribbons presumably facilitate focal exocytosis at high throughput by targeting vesicular fusion and the molecular components that trigger this fusion to the proximity of sites of Ca^{2+} influx[10–12].

Synaptic ribbons are heterogeneous organelles present in various forms in different cell types, such as spherical, ellipsoid, or bar-shaped structures, with different shapes in hair cells being

associated with different functional properties [5,6]. In rod synapses of the mouse retina of the albino Balb/c strain synaptic ribbons undergo dynamic turn-over changes depending on illumination. Ribbons tend to disassemble in response to illumination by releasing ribbon material in spherical modules; and elongate by regaining ribbon material during dark-adaptation[13–16]. This illumination-dependent ribbon remodeling was reported to affect visual function in Balb/c mice [13]. Whether these light-dependent ribbon turn-over changes can be regarded as a general mechanism for light adaptation is questionable based on the variability observed between mouse strains. Illumination-dependent ribbon remodeling changes are minor in pigmented C57Bl/6 mice compared to Balb/c [17]. Therefore the physiological significance of the light-dependent ribbon turn-over changes is not yet clear.

Mechanistically, the illumination-dependent disassembly of ribbons is known to depend on the drop in intracellular Ca^{2+} at the synapse caused by the light-triggered hyperpolarization of the cell. Disassembly has been experimentally induced in *in situ* retinas by chelating extracellular Ca^{2+} with EGTA/BAPTA[14–16,18]. A member of the neuronal calcium sensor (NCS) family of EF-hand containing proteins, Guanylate Cyclase Activating Protein 2 (GCAP2), has been recently proposed as a prime candidate for mediating the Ca^{2+}-dependent structural changes of ribbons [19].

Guanylate Cyclase Activating Proteins (GCAPs) are EF-hand containing Ca^{2+} binding proteins that were characterized as the proteins that confer Ca^{2+} sensitivity to retinal guanylate cyclase at the outer segment discs of rods and cones[20–23]. The two main isoforms, GCAP1 and GCAP2, are thought to be associated to the cyclase and regulate its catalytic activity in response to small fluctuations in Ca^{2+}. GCAPs shift between a "Ca^{2+}-bound state" that inhibits the cyclase catalytic activity, and a "Mg^{2+}-bound state" that stimulates cyclase activity. Both GCAPs display high Ca^{2+} sensitivity, with GCAP2 Ca^{2+} sensitivity being slightly higher than GCAP1 (EC_{50Ca} for GCAP1 $\sim$ 132–139 nM and EC_{50Ca} for GCAP2 $\sim$ 50–59 nM, [24]). At the high intracellular Ca^{2+} concentration typical of rod outer segments in the dark steady-state GCAPs inhibit guanylate cyclase activity. When the intracellular free Ca^{2+} is reduced in response to light, GCAP1 and GCAP2 sequentially respond to this Ca^{2+} decline by shifting from their "inhibitory" to their "stimulatory" state of the cyclase, to promote the restoration of cGMP to the levels of the darkness equilibrium [25]. By counteracting the effect of light this way, GCAPs play a fundamental role in termination of the light response and in the process of light adaptation [26,27].

In addition to the outer segment, GCAP1 and GCAP2 also localize to the inner segment compartment and to the synaptic terminal of photoreceptor cells, where their function is unclear [28,29]. GCAP2 has been proposed to mediate the Ca^{2+} -dependent structural changes of ribbons based on the following observations: i) GCAP2 interacts with Ribeye, the main protein component of synaptic ribbons; ii) GCAP2 colocalizes with Ribeye at ribbon synapses; and iii) GCAP2 overexpression in photoreceptor cells achieved by viral infection of retinal explants led to the disassembly of the synaptic ribbon in a high percentage of synaptic terminals [19].

To study the function of GCAPs at rod synaptic terminals, and to test whether GCAP2 (and/or GCAP1) might mediate the Ca^{2+}-dependent ribbon morphological changes that take place during dark/light adaptation, we analyzed structural alterations in ribbons from GCAP1/GCAP2 double knockout or GCAP2-overexpressing mice. We here demonstrate that GCAP2 overexpression in rods leads to the shortening of synaptic ribbons *in vivo*. Interestingly, we have seen that mice that lack GCAP1 and GCAP2 (GCAPs−/− mice) develop and maintain normal ribbons whereas mice that lack GCAP1 but express GCAP2 (GCAPs−/−GCAP2+ mice) display severely shortened ribbons at 40 days of age. That is, the lack of GCAP1 exacerbates GCAP2 effect at shortening synaptic ribbons. These histological observations, together with the functional phenotype of these mice, indicate that GCAP1 and GCAP2 can have opposing effects on ribbon length, likely through a combination of indirect (through their effect on cGMP metabolism and membrane potential) and more direct (at the synapse) effects. A direct function of GCAP2 at promoting the disassembly of ribbon material from the ribbon would be supported by GCAP2 ultrastructural localization in clusters at the ribbon.

Materials and Methods

Ethics Statement

The care and use of animals was done in compliance with Acts 5/1995 and 214/1997 for the welfare of experimental animals of the Autonomous Community (Generalitat) of Catalonia, and approved by the Ethics Committee on Animal Experiments of the University of Barcelona.

Mouse Genetic Models

The GCAP1/GCAP2 double knockout line (GCAPs−/− mice) was produced by simultaneous disruption of the GUCA1A and GUCA1B genes that are organized in a head-to-head gene array in the genome [27]. The generation of transgenic mice that express bovGCAP2 in rods under the control of the mouse opsin promoter and the determination of GCAP2 transgene expression levels have been described [27].

Antibodies and Fluorescent Dyes

The GCAP2 antibody used in Western blots, indirect immunofluorescence assays and electron microscopic immunolocalization is a polyclonal antibody raised in rabbit against a His-tagged recombinant form of bovGCAP2 expressed in bacteria. Antibodies were affinity-purified with a recombinant GCAP2 affinity column. For indirect immunofluorescence assays GCAP2 Ab was used at a 1:400 working dilution from a 1 mg/ml stock. Ribeye immunolabeling of synaptic ribbons was performed with a monoclonal antibody anti-CtBP2 (BD biosciences 612044, 1:250). The GCAP1 antibody is a polyclonal antibody raised in rabbit against a His-tagged recombinant form of human GCAP1, and was affinity-purified.

To label retinal cell types we used primary antibodies directed against the following molecules: Transducin Gγ c subunit (Cytosignal PAB-00801-G Ab, 1:200, for cone pedicules); Calbindin D (Swant CB-38a Ab, 1:500, for horizontal cells); Protein Kinase C α isoform, PKCα (Santa Cruz Biotechnology sc-10800 Ab, 1:100, for rod-on bipolar cells); Bassoon (Stressgen VAM-PS003 mAb, 1:1000, for arciform densities in rods and cones); and Synaptophysin, SYP (Chemicon MAB5258 mAb, 1:1000, for rod spherules and cone pedicules). Secondary antibodies for immunofluorescence were Alexa 488 goat anti-rabbit IgG [Molecular Probes A-21206]; Alexa 555 goat anti-mouse IgG [Molecular Probes A-31570] and Alexa 633 goat anti-guinea pig IgG [Molecular Probes A-21105], used at a 1:100 dilution.

Immunofluorescence Microscopy

For immunofluorescence microscopy, mice were sacrificed and eyes were marked at the superior center for orientation purposes. Immediately after enucleation the eyes were punctured with a

needle and submerged in fixative: 4% paraformaldehyde; 0,02% glutaraldehyde in phosphate buffer saline at pH7.4. At 5 min into the fixation step the cornea was excised, at 20 min the lens was removed and eye cups were further fixed for a total of 2 h at room temperature. Eye cups were infiltrated in acrylamide (8,4% acrylamide, 0,014% bisacrylamide in PBS pH7.4 for 14 h before acrylamide polymerization was induced) or in sucrose (30% w/v in PBS pH7.4 for 14 h), and included in OCT compound. Cryosections along the vertical axis of the eyecup were obtained at 20 µm-thickness using a CM1510S Leica cryostat (Leica Microsystems). Sections were incubated with blocking solution (3% normal goat serum, 1% BSA, 0,3% Triton X100 in PBS pH7.4, 1 h at room temperature); first antibody (14 h at 4°C), secondary antibody (1 h at room temperature), and fixed for 15 min in 4% paraformaldehyde prior to being mounted with Mowiol [Calbiochem 475904]. An antigen retrieval treatment of retinal sections (incubation in 0,05 mg/ml proteinase K in PBS pH7.4 for 2 min at room temperature followed by a heat shock at 70°C for 10 sec) was needed for GCAP2 immunostaining. Images were acquired at a laser scanning confocal microscope (Leica TCS-SL and TCS-SP2). For measurements of outer plexiform layer (OPL) thickness, pictures were taken at four different positions in the retinal vertical meridian (A, B, C and D). These regions, at 800 µm from the superior edge (A), equidistant from point A and the optic nerve (B), at 750 µm from the optic nerve in the inferior retina (C) and equidistant from C and the inferior edge (D) were marked at 10× magnification by photobleaching the fluorescent signal next to the point of interest. By using the photobleached areas as a reference, pictures at A, B, C and D positions were taken at 63× magnification. Measurements of OPL thickness were taken at each point in the different phenotypes by determining the width of the GCAP2 (or Ribeye) immunolabeled bands with the Leica LAS AF Lite image acquisition software. Three different measurements were taken per point to calculate the average for each retina specimen, and at least four mice per phenotype were analyzed to calculate the mean.

Retinal Preparation for Light Microscopy and Electron Microscopy

For the ultrastructural analysis of rod synaptic terminals the different mouse lines were raised in constant darkness by maintaining cages in aerated dark cabinets. They were sacrificed under dim red light at postnatal day 40 (dark conditions); or exposed to 1500 lux white fluorescent light for 1 or 5 h after pupil dilation with a mixture of 0.75% tropicamide and 2.5% phenylephrine hydrochloride (light conditions) and immediately sacrificed. For orientation purposes, a mark was imprinted at the superior center of the eye before enucleation. Immediately after enucleation the eye was punctured with a 30-G needle and fixed in 2% paraformaldehyde, 2.5% glutaraldehyde in 0.1 M cacodylate buffer for 5 min. An incision was made around the ora serrata and fixation was allowed to proceed for 1 h. The cornea and lens were removed and the eye cup was further fixed for 12 h at 4°C. After this fixation step, eye cups were washed with 0.1 M cacodylate buffer and fixed with 1% osmium tetroxide (OsO4) in 0.1 M cacodylate buffer for 2 h at room temperature. Specimens were dehydrated in ethanol (30–100%) or acetone, infiltrated with propylene oxide and embedded in Epoxi embedding medium (Fluka Analytical).

To measure synaptic ribbons in GCAP2+ and WT littermate control mice, 4 GCAP2+ and 3 WT littermate controls were raised in 12 h:12 h dark-light standard cyclic light and were processed at p60 at the end of the dark period. Processing of the eyes for conventional electron microscopy was done as described.

Ultrathin Sectioning, Image Acquisition and Analysis at the Transmission Electron Microscope

Ultrathin sections (70–90 nm) in the vertical meridian of the eye cup were made using a Reichert Ultracut S ultramicrotome (Leica), collected on 200 mesh copper grids, counterstained with heavy metal staining (2% uranyl acetate in 50% ethanol for 30 min) and contrasted with 2% lead citrate for 10 min. Ultrathin sections were analyzed in a JEOL 1010 or a Tecnai Spirit Twin [FEI] 120 Kv LaB6 transmission electron microscope. Images were obtained with a Bioscan Gatan wide angle slow scan CCD camera. In order to determine the ribbon length in the different mouse lines, at least two different specimens were analyzed per phenotype. Two to ten 16×16 µm frames at 8,000× magnification were delimited per Epon block, that typically contained 10 to 22 rod synaptic terminals. At a given plane of sectioning along the vertical axis in the center of the eye cup, the synaptic ribbon was visible in about 60–70% of the synaptic terminals, and about 40% of all terminals presented ribbons discernible as resulting from transversal cuts (Table S1). Contrary to ribbons from longitudinal or oblique cuts that result in variable shapes and sizes, transversal cuts are easily recognized as defined lines anchored at the arciform density between the two invaginating processes of horizontal cells, and their length should represent the length of the ribbon plate at any point. Therefore, once the 8,000× magnification frames were delimited, all synaptic terminals contained in the frame were individually scanned at 100,000× magnification, and length measurements were taken from ribbons resulting from tangential cuts by using the ImageJ software. Cone synaptic terminals were excluded from the analysis.

For determination of synaptic terminal size [μm^2], micrographs of the OPL area were obtained at the electron microscope at low magnification [x8000], and ImageJ was used to obtain the dimensions of delimited regions of interest with the form of the synaptic terminals.

To determine the percentage of synaptic terminals containing a synaptic ribbon, the number of total synaptic terminals was determined in five 16×16 -μm^2 frames per fenotype, and the number of terminals containing a longitudinal, transversal or sagittal ribbon were counted. A percentage was calculated per frame, and the five results obtained per phenotype were averaged.

Immunoelectron Microscopy

For immunoelectron labeling of GCAP2 and Ribeye in GCAPs−/−GCAP2+ mice and GCAPs−/− negative control mice, dark-reared mice at p40 were sacrificed in dim light. The eyes were marked, enucleated and immediately fixed in 2% paraformaldehyde in phosphate buffer saline at pH7.4 for 2 h at room temperature, following the puncture and dissection steps described above. In order to preserve antigenicity while maintaining ultrastructure, immediately after fixation eye cups were processed by a progressive lowering temperature (PLT) protocol of dehydration and embedding in Lowicryl resin. Dehydration protocol was: [0°C, 30 min 30% ethanol; −20°C, 60 min 50% ethanol; −35°C, 60 min 70% ethanol; −35°C, 60 min 95% ethanol; −35°C, 60 min 100% ethanol; −35°C, 60 min 100% ethanol]. Infiltration was performed with Lowicryl embedding media K4M: [−35°C, 60 min resin:ethanol 1:3; −35°C, 60 min pure resin; −35°C, 16 h pure resin]. The resin was polymerized by long wavelength UV irradiation for at least 24 h. Ultrathin sections were incubated at room temperature in blocking solution (1% BSA, 20 mM glycine in PBS pH7.4, for 30 min), first antibody (anti-Ribeye Ab, for 2 h) and secondary antibody (5 nm or 15 nm gold-conjugated goat anti-mouse IgG, BBInternational, for 1 h); and the process was subsequently repeated for GCAP2

immunolabeling, by repeating the blocking step and incubating with antibody (anti-GCAP2 Ab, for 2 h) and secondary antibody (5 nm or 15 nm gold-conjugated goat anti-rabbit IgG, BBInternational, for 1 h). After washes, sections in the gold grids were counterstained with heavy metal staining (2% uranyl acetate in 50% ethanol for 10 min) and contrasted with 2% lead citrate for 5 min.

Sections were observed at a JEOL JEM1010 transmission electron microscope at 80 Kv and images were obtained with a Bioscan Gatan wide angle slow scan CCD camera.

To assess specificity of the association of gold-particles to GCAP2 antigenicity in the GCAPs−/−GCAP2+ specimens, the number of gold particles associated to synaptic ribbons were counted in 74 synaptic terminals randomly selected from two specimens, and compared to that of GCAPs−/− negative control samples. Out of 74 randomly selected synaptic terminals in the GCAPs−/−GCAP2+ sample, 12 out of 74 (about 16%) had at least one gold particle associated to the synaptic ribbon, and 20 out of 74 (about 27%) showed association of gold particles to the presynaptic plasma membrane in apposition to the invaginated processes of horizontal cells; whereas in the GCAPs−/− only 6% of the ribbons analyzed showed associated gold particles and only 16% showed association of gold particles to the membrane delineating the invaginating horizontal dendritic processes. Therefore, we consider the micrographs presented in this study to be an accurate illustration of GCAP2 intracellular localization at the synaptic terminal.

Electroretinogram Analysis

Electroretinogram (ERG) recordings were performed in 12 h dark-adapted deeply anesthetized mice. Recordings were acquired with a Burian-Allen mouse electrode set on a corneal lens specifically designed to fit the mouse eye (Hansen Ophthalmic Development Lab), with the reference electrode positioned at the mouth and the ground grasped on the tail. Pupil from the right eye was dilated, and flash-induced ERG responses were recorded in response to light stimuli produced with a Gansfeld stimulator. The intensity of light stimuli ranged from −4 to 2 log cd.s.m^{-2}. For each light intensity, responses from four consecutive light presentations were averaged. The range of light intensities from −4 to −1,52 log cd.s.m^{-2} elicited rod-mediated responses. In the range from −1,52 to 0,48 log cd.s.m^{-2} ERG recordings reflected mixed responses from rods and cones. Pure cone responses were recorded after inducing rod saturation by exposing the mouse to a 30 cd/m^2 background light for 10 min, and then applying light stimuli in the range of −0,52 to 2 log cd.s.m^{-2} superimposed to the background. ERG signals were amplified and band filtered between 0.3 and 1000 Hz (Grass CP511 AC amplifier), digitized at 10 kHz with a Power Lab data acquisition board (ADI instruments) and analyzed off-line by measuring the amplitudes of the a-wave (from the baseline to the peak of the a-wave) and of the b-wave (from the peak of the a-wave to the peak of the b-wave). ERG measurements were done on a blind basis with respect to the mouse phenotype.

Retinal Morphometry

For retinal morphometry analysis of GCAPs−/− and GCAPs−/−GCAP2+ retinas, a high magnification picture of the whole retina under study was obtained by fusion (HUGIN software) of three 20× overlapping frames covering the length of a vertical section from central retina. Pictures were taken with the ProgResCapturePro 2.6 software in a Stereo Lumar V12 stereoscopic microscope (Zeiss) coupled to a Jenoptik camera. On whole retina-pictures, lines were traced from an imaginary point at the center of the retina semicircumference to the optic nerve and to the superior and inferior borders, dividing the retina in its superior and inferior quadrants; and then to marks traced at 200 μm intervals starting from the optic nerve that divided the superior retina into 12 equal divisions and the inferior retina into 11 divisions. Marks were numbered 1 to 10 starting at the second mark from the optic nerve towards the superior edge, and from −1 to −10 at equivalent positions in the inferior retina. At each marked position the onl thickness was determined by taking three measurements with the ProgResCapturePro 2.6 software and averaging them. To obtain the graph comparing the morphometric analysis in GCAPs−/−GCAP2+ versus GCAPs−/−, at least three animals per phenotype were used.

Results

Mouse Models of Gain-of-function and Loss-of-function of GCAP2 Show Morphological Alterations at the Outer Plexiform Layer, Pointing to a Role of GCAP2 at the Synaptic Terminal of Photoreceptors

In order to gain insight into the roles that GCAP1 and GCAP2 may play at the synaptic terminal, and whether they might mediate the light-triggered morphological changes of photoreceptor ribbons, we performed a detailed morphological analysis of the outer plexiform layer (OPL) in retinas from mouse models of gain-of-function of GCAP2 and loss-of-function of GCAP1 and GCAP2.

The mouse lines used in this study are summarized in Fig. 1 and Table 1. To study the effect of GCAP2 overexpression on the morphology and function of rod synaptic terminals *in vivo*, we used a previously characterized transgenic line that expresses GCAP2 in rods under the mouse opsin promoter [Fig. 1A]. This line expresses heterologous GCAP2 (bovine GCAP2, bigger than the murine isoform in three amino acids) at 1,5-fold the endogenous GCAP2 levels [Fig. 1B], and is referred to as GCAP2+ in Table 1. By breeding this original transgenic line to transgene homozygosis we obtained a line in which transgenic GCAP2 was expressed to 3-fold the endogenous level of GCAP2 (GCAP2+/+, Fig. 1D, Table 1). These mice showed virtually normal retinas for up to six months of age when raised in standard cyclic light conditions. No noticeable signs of retinal degeneration were observed by light microscopy in mice raised in constant darkness at postnatal day 40 [Fig. 1C].

As a mouse model of loss-of-function we used the double knock-out in GCAP1 and GCAP2 (referred to as GCAPs−/− [27]). These mice were originally obtained by homologous recombination in embryonic stem cells with a single replacement vector, because the GUCA1A and GUCA1B genes encoding GCAP1 and GCAP2 are contiguous in the genome. Mice deficient in GCAP1 and GCAP2 lack the rapid and robust Ca^{2+} feedback signal to cGMP synthesis set in place by light, and show slower light response kinetics, enhanced sensitivity to light and impaired light adaptation. Despite this marked functional phenotype, retinas from GCAPs−/− mice show normal appearance for up to 5 months of age when mice are raised in standard cyclic light [27] [Fig. 1E]. A transgenic line that expresses GCAP2 in the absence of GCAP1 was obtained by breeding the GCAP2+ line to the GCAPs−/− line. GCAP2 expression in this line restores the endogenous GCAP2 localization and function [27]. Retinas from these mice show a normal outer nuclear layer thickness for at least 5 months of age [Fig. 1E].

To study whether the loss of expression of both GCAP1 and GCAP2 in the GCAPs−/− mice or the selective restoration of GCAP2 expression in this line has an effect on the synaptic

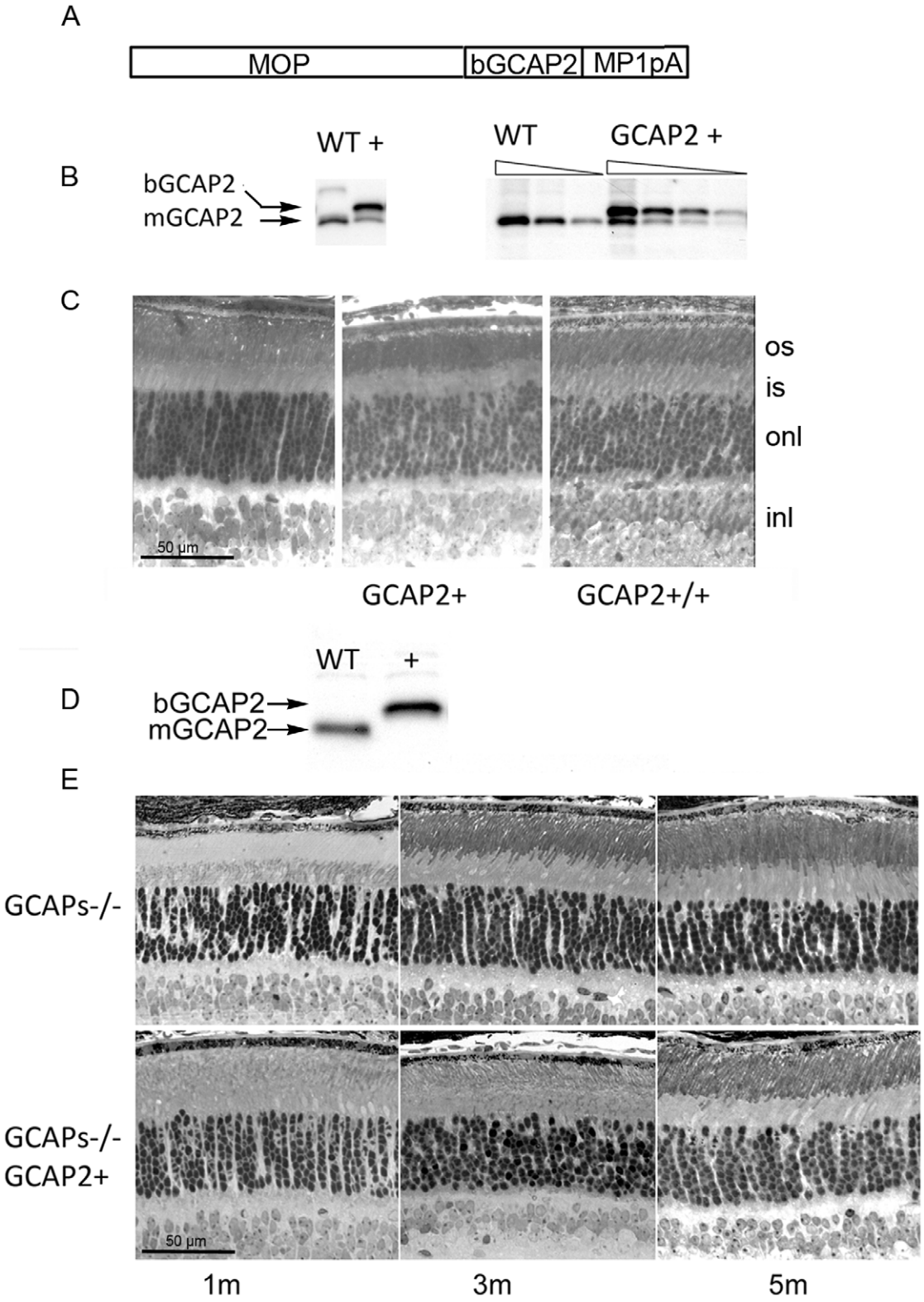

Figure 1. Mouse models of overexpression of GCAP2 and loss-of-function of GCAP1 and GCAP2 used in the study. A. GCAP2 transgene construct. MOP, 4.4 kb-version of the mouse opsin promoter; bGCAP2, cDNA of bovine GUCA1B gene encoding guanylate cyclase activator protein 2 (GCAP2); MP1pA, polyadenylation signal of mouse protamine gene 1. B. Western blot of total retinal homogenates illustrating GCAP2 level of expression in the GCAP2+ line. Equivalent fractions of a retina (1/10) of WT and GCAP2+ mice were resolved in a 12% SDS-PAGE, transferred to a nitrocellulose membrane and incubated with a polyclonal Ab anti-GCAP2. The bovine (transgenic) and murine (endogenous) isoforms of GCAP2 can be resolved on the basis of their 3-aa difference in size. In the GCAP2+ transgenic line bGCAP2 is expressed to 1.5-fold the endogenous GCAP2 expression [27]. C. Light micrographs of vertical sections of the retina of dark-reared WT, GCAP2+ and GCAP2+/+ (transgenic line bred to homozygosity, that expresses transgenic GCAP2 to 3-fold the endogenous GCAP2 level) at postnatal day 40. Mice overexpressing GCAP2 show at this

age a normal retinal morphology. D. Expression of bGCAP2 transgene in the GCAP1/GCAP2 double knockout background (GCAPs−/− background). Western blot shows expression of transgenic bGCAP2 in the absence of endogenous GCAP2 in the GCAPs−/−GCAP2+ mice. E. Light micrographs of vertical sections of the retina from GCAPs−/− and GCAPs−/−GCAP2+ at 1, 3 or 5 months of age, when reared in standard cyclic light. Mice lacking GCAP1 and GCAP2 retain the normal thickness of outer nuclear layer, that is, the normal number of photoreceptor cells for up to 8 months of age. Mice in which GCAP2 expression is restored in the GCAPs−/− background do not show obvious signs of retinal degeneration at the light microscopy level.
doi:10.1371/journal.pone.0042994.g001

terminals of rods and cones, the OPL in retinal sections from p40 mice was immunolabeled with an antibody anti-Ribeye, the major protein component of synaptic ribbons. Sections were co-stained with an antibody anti-GCAP2. Measurements of OPL thickness were taken at the confocal microscope at four points along the retinal vertical meridian (A, B, C and D shown in Fig. 2B inset, see Methods). The retinas analyzed in this study were obtained from mice raised in complete darkness to avoid secondary changes at the synaptic terminal that could derive from differences in the gain of the light response at the rod outer segment among different mouse models. The absence of both GCAP1 and GCAP2 in the GCAPs−/− mice had a minor effect on OPL thickness, which was significant only in the upper retina. However, expression of GCAP2 in the absence of GCAP1 caused a 40% reduction in OPL thickness along the entire length of the retina, indicating that the size or the number of synaptic terminals was reduced [Fig. 2A].

This reduction of OPL thickness was not preceded by photoreceptor cell death. GCAP2 expression in the absence of GCAP1 did not cause noticeable morphological changes at the outer segment, inner segment or outer nuclear layers of the retina [Fig. 2A]. GCAPs−/−GCAP2+ mice showed an outer nuclear layer undistinguishable in thickness from that of GCAPs−/− littermate control mice along the entire length of the retina [Fig. 2C], indicating that the thinning of the OPL was not a secondary consequence of ongoing photoreceptor cell death.

To study whether the magnitude of the reduction of the OPL thickness in the GCAPs−/−GCAP2+ mice depends on whether the mice are raised in constant darkness (with constant intracellular Ca^{2+} levels at rod outer segments and tonic neurotransmitter release at the synapse) or exposed to regular 12 h:12 h dark:light cycles (with photoreceptor intracellular Ca^{2+} levels varying daily between its dark and daylight values), the OPL from 40 day-old mice raised either in constant darkness or in standard 12 h:12 h dark:light cycles was stained with an anti-Bassoon antibody [Fig. 3] and measurements of OPL thickness were taken at four points in the retina vertical meridian. GCAPs−/−GCAP2+ mice raised in cyclic light also presented an statistically significant reduction in OPL thickness when compared to wildtype controls, although slightly lower in magnitude than when mice were raised in constant darkness (20–30% reduction of OPL thickness depending on the retinal region, versus the 40% uniform reduction in dark reared-mice, data not shown). Immunolabeling of cone pedicules with an antibody for the Transducin Gγ c subunit did not reveal noticeable alterations in the synaptic terminals of cones or the density of their synaptic ribbons among the different mouse phenotypes [Fig. 3].

Table 1. transgene expression levels in the different mouse lines.

Mouse strain	GCAP1 expression *	GCAP2 expression *
WT (C57Bl)	1 -fold	1 -fold
GCAPs−/−	0	0
GCAPs−/−GCAP2+	0	1.5 -fold
GCAP2+	1 -fold	1.5+1 = 2.5 -fold
GCAP2+/+	1 -fold	3+1 = 4 -fold

*expressed respect to the endogenous protein level (1 -fold).
doi:10.1371/journal.pone.0042994.t001

To determine whether the connections between photoreceptor cells and horizontal and bipolar cells were affected, horizontal and bipolar cells were immunolabeled with antibodies for Calbindin and PKCα, respectively [Fig. 4]. Photoreceptor synaptic terminals were highlighted with an antibody for Synaptophysin, SYP. There was a reduction in the density and size of horizontal cell processes, both in GCAPs−/− and in GCAPs−/−GCAP2+ mice. Remodeling changes were also apparent in the dendrites of bipolar cells, which were more dramatic in GCAPs−/−GCAP2+ mice that were raised in constant darkness than in mice raised in cyclic light, with shorter bipolar dendrites and loss of dendritic tip terminals. Immunostaining of retinal sections with Bassoon also showed a reduction in the density and size of synaptic ribbons in the OPL of GCAPs−/−GCAP2+ mice respect to wildtype mice, while no variation in OPL thickness is observed in GCAPs−/− mice versus wildtype mice.

Together these results show that mice that express GCAP2 in the absence of GCAP1 have a severe reduction in the thickness of the OPL, with a decrease in the density of synaptic ribbons. GCAP2 expression effect on retinal morphology is specific to the outer plexiform layer, and is not accompanied by photoreceptor cell loss by postnatal day 40. These OPL alterations are more dramatic when mice are raised in constant darkness than when they are raised under cyclic light conditions, and are accompanied by remodeling changes that reduce the density of connecting horizontal and bipolar cell processes.

Overexpression of GCAP2 in Rod Photoreceptors Leads to Shorter Synaptic Ribbons and Increases the Abundance of Ribbon Assembly Intermediates

To study whether GCAP2 overexpression in rods leads to the shortening of synaptic ribbons at the ultrastructural level, the OPL region of retinal ultrathin sections from transgenic mice expressing GCAP2 to 2.5 or 4-fold the endogenous GCAP2 levels [GCAP2+ or GCAP2+/+ transgenic mice respectively, see Table 1] was examined by transmission electron microscopy. The lengths of transversal rod synaptic ribbons contained in two to eight 16×16-μm frames of OPL per specimen from at least two specimens per phenotype were determined and averaged, and compared to those of C57Bl control mice [Fig. 5 and Table S1, see Methods]. Mice were reared in complete darkness and sacrificed at p40 under dark-adapted conditions or following a 1–5 h period of light exposure.

C57Bl mice that were raised in constant darkness to postnatal day 40 and were processed in darkness presented ribbons that measured on average 0,2915±0,0066 μm (n = 103 synaptic ribbons from 5 mice), whereas littermate mice that were processed after 1–5 h of light exposure showed ribbons that measured on average 0,2534±0,0082 (n = 98 synaptic ribbons from 5 mice), Table S1. This represents a 13% reduction of ribbon length in

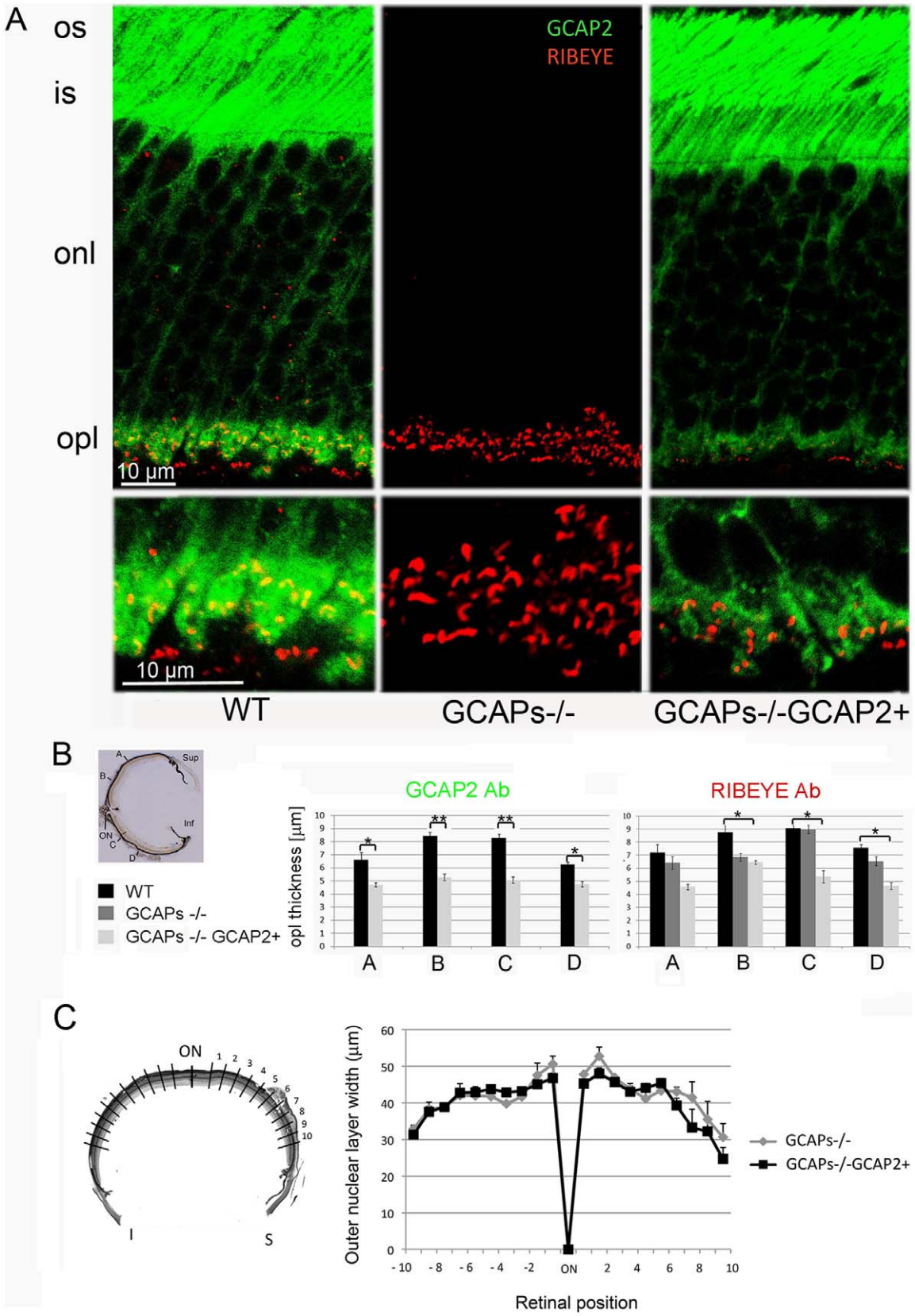

Figure 2. Mice that express GCAP2 in the GCAPs−/− background show a reduction of outer plexiform layer (OPL) thickness compared to wildtype mice. A. Immunolabeling of vertical retinal sections from WT, GCAPs−/− and GCAPs−/−GCAP2+ mice with rabbit polyclonal antibodies anti-GCAP2 and a monoclonal antibody against Ribeye(B)/CtBP2. GCAP2 antibodies give a strong immunolabeling signal at the outer segment (os), inner segment (is) and outer plexiform layer (opl) of the retina. This signal is absent in GCAPs−/− mice, and is restored in

GCAPs−/−GCAP2+ mice, in which the GCAP2 transgenic protein reproduces the endogenous GCAP2 intracellular localization. GCAP2 partially colocalizes with Ribeye at ribbon synapses, as pointed by white arrows in WT magnified OPL panel, as previously reported [19]. This figure shows that the expression of GCAP2 in the GCAPs−/− background, that is, GCAP2 expression in the absence of GCAP1, leads to a substantial shortening of the OPL: compare immunolabeling intensity and thickness of the OPL in WT and GCAPs−/−GCAP2+ panels. B. Statistical analysis of the outer plexiform layer thickness in the WT, GCAPs−/− and GCAPs−/−GCAP2+ phenotypes. Measurements of OPL thickness were taken at four different regions along vertical sections of the central retina (A, B, C and D in inset) for each phenotype. WT, GCAPs−/− and GCAPs−/−GCAP2+ mice were raised in constant darkness and processed at p40. OPL thickness was determined at each position based on measurements of the anti-GCAP2 Ab immunolabeled region (left histogram) or anti-Ribeye mAb immunolabeled region (right histogram) at the laser scanning confocal microscope. In GCAPs−/−GCAP2+ mice the OPL thickness is reduced to 60–65% of the wildtype OPL. Values in histograms are the mean ± standard deviation from measurements taken from four mice per phenotype. * denotes $P<0.01$; ** denotes $P<0.001$ in the Student's t-test. C. Mice that express GCAP2 in the absence of GCAP1 (GCAPs−/−GCAP2+) retain the normal quantity of photoreceptor cells at p40 when raised in constant darkness. The retinal morphometry analysis shows that outer nuclear layer thickness (in μm) at 200 μm intervals covering the whole length of the vertical central retina (left diagram) is undistinguishable in GCAPs−/− and GCAPs−/−GCAP2+ mice at p40 (overlapping graphs). Mean values ± standard error were obtained from at least three littermate mice per phenotype.
doi:10.1371/journal.pone.0042994.g002

C57Bl mice following a 1–5 h period of light exposure, that was statistically significant [Fig. 5A and 5C].

Transgenic expression of GCAP2 led to a shortening of synaptic ribbons that correlated with transgene dosage, independently of whether the mice were sacrificed in the dark or following light exposure. GCAP2+ mice presented a 9,6% reduction whereas GCAP2+/+ mice presented a 13,7% reduction in ribbon length versus the C57Bl control when processed under dark-adapted conditions [representative ribbons shown in Fig. 5A, statistical analysis shown by black bars in Fig. 5C, see Table S1]. Under light-adapted conditions the reduction was of 4% for GCAP2+ and of 17% for GCAP2+/+ when compared to the C57Bl light value [Fig. 5A, grey bars in Fig. 5C].

Because illumination-dependent changes of photoreceptor ribbon structure were shown to differ between mouse strains [17] it was important to discard that minor variations in the genetic background between GCAP2-transgenic and C57Bl mice may account for the phenotype observed, given that the analysis of GCAP2 gene dosage effect on ribbon length could not be performed on littermate mice. Although the GCAP2-expressing transgenic mice used in this study were back-crossed to C57Bl/6

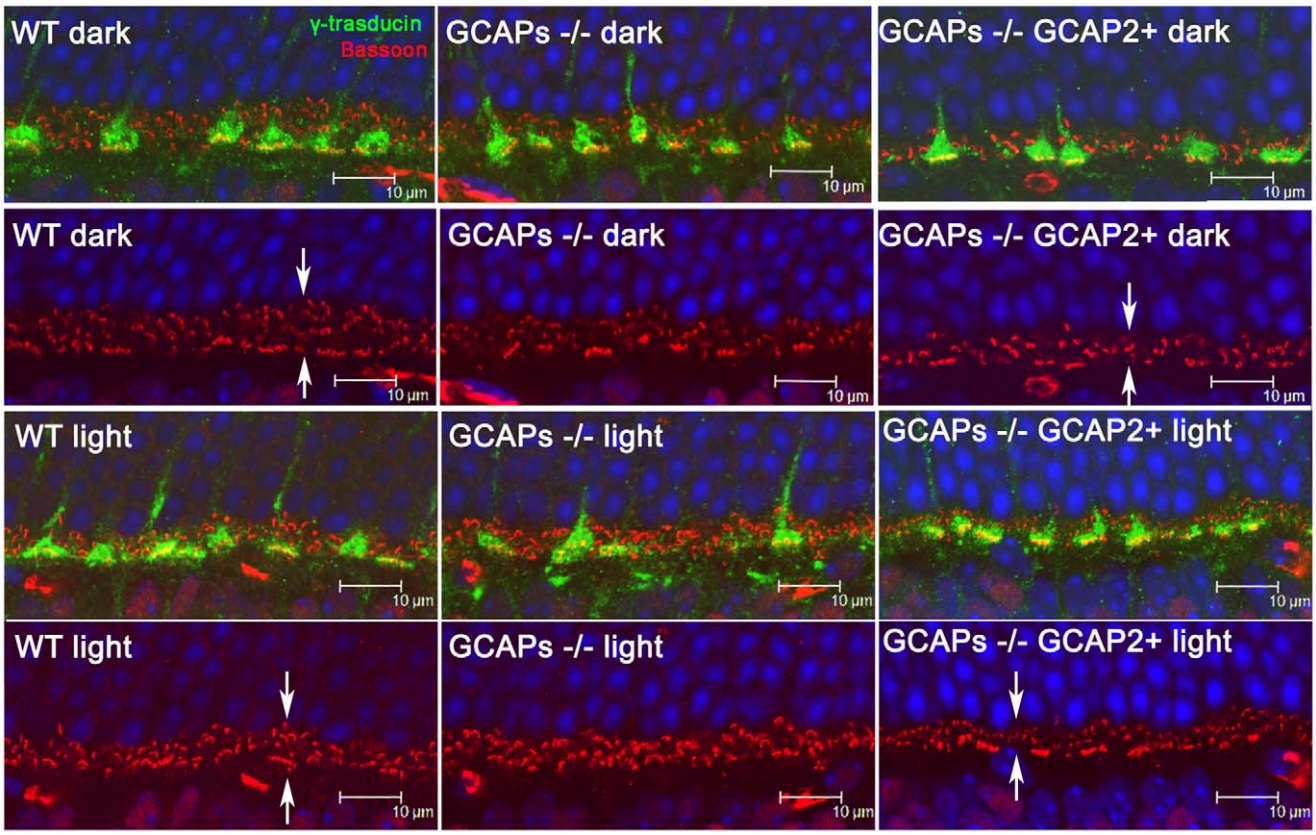

Figure 3. Outer plexiform layer reduction in GCAPs−/−GCAP2+ mice takes place regardless of whether the mice are raised in constant darkness or in 12 h dark : 12 h light cyclic light. Immunolabeling of synaptic active zones (arciform densities) with a monoclonal antibody anti-Bassoon (in red), and cone pedicules with a polyclonal antibody anti-transducin γ (in green) in WT, GCAPs−/− and GCAPs−/−GCAP2+ retinas. Mice were either raised in darkness (two upper rows) or were raised in standard 12 h dark : 12 h cyclic light (two lower rows) and processed at p40. OPL thickness in GCAPs−/−GCAP2+ mice was reduced to about 65% of wildtype thickness independently of the light-rearing conditions [compare OPL thickness in WT and GCAPs−/− GCAP2+ panels, arrows].
doi:10.1371/journal.pone.0042994.g003

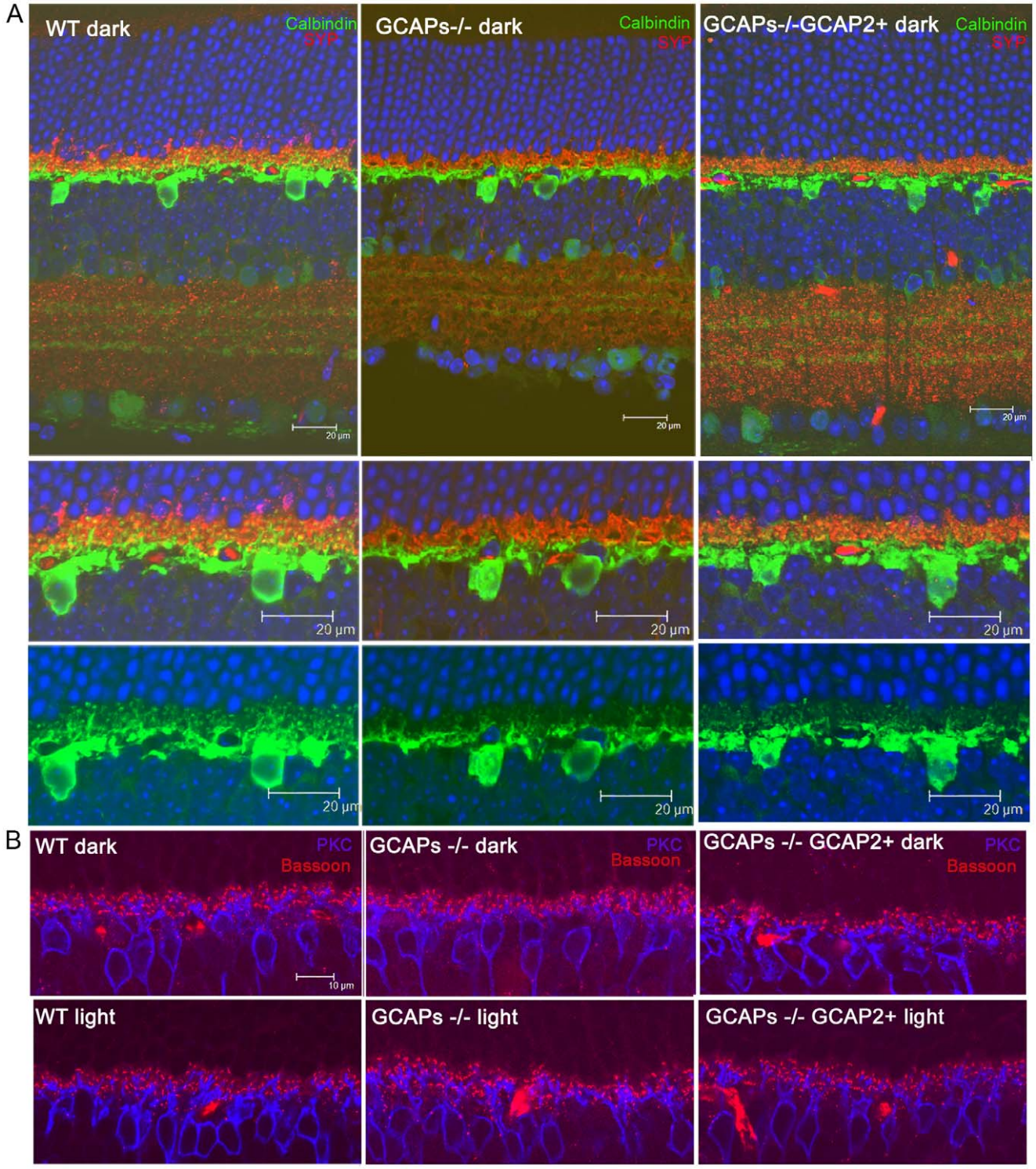

Figure 4. Reduction in the density of horizontal and bipolar cell dendritic processes in mice that express GCAP2 in the GCAPs−/− background. A. Immunolabeling of horizontal cells by indirect immunofluorescence with anti-Calbindin polyclonal antibodies [green signal] and rod and cone synaptic terminals with a monoclonal antibody anti-Synaptophysin [SYP, red signal] in WT, GCAPs−/− and GCAPs−/−GCAP2+ mice raised in constant darkness. Note the reduction in density and complexity of horizontal cell processes in GCAPs−/− and GCAPs−/−GCAP2+ retinas compared to WT samples. B. Immunolabeling of bipolar cells with a polyclonal antibody against PKCα [blue signal] and detection of arciform densities in rod and cone synaptic terminals with a monoclonal antibody anti-Bassoon [red signal]. Note the remodeling of bipolar cell dendrites that is taking place at p40 in GCAPs−/−GCAP2+ samples associated to a reduction in the number and dimensions of synaptic ribbons and arciform density structures at rod and cone synaptic terminals.
doi:10.1371/journal.pone.0042994.g004

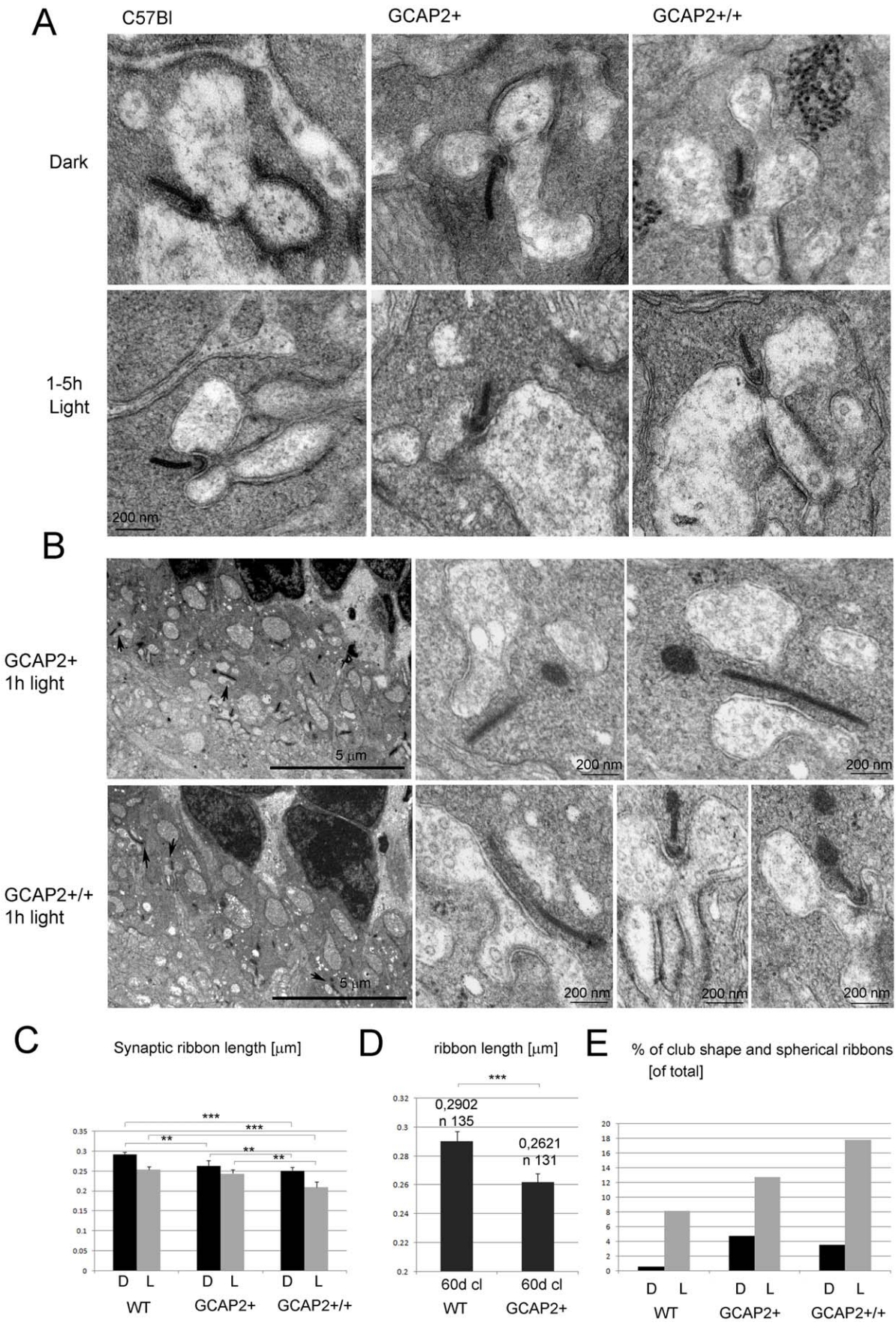
A
C57Bl
GCAP2+
GCAP2+/+
Dark
1-5h Light
200 nm
B
GCAP2+ 1h light
GCAP2+/+ 1h light
5 μm
200 nm
C
Synaptic ribbon length [μm]
D L
WT
GCAP2+
GCAP2+/+
D
ribbon length [μm]
0,2902 n 135
0,2621 n 131
60d cl
WT
GCAP2+
E
% of club shape and spherical ribbons [of total]

Figure 5. Overexpression of GCAP2 in transgenic mice leads to shortening of ribbon length and to an increase in the fraction of club-shape and spherical morphologies representing disassembling ribbons. A. Electron micrographs of rod synaptic terminals of dark-reared C57Bl, GCAP2+ or GCAP2+/+ mice at p40 that were processed in darkness or immediately after 1–5 h of light exposure, showing transversal sections of synaptic ribbons. Notice the difference in length in C57Bl [left], GCAP2+ [middle] and GCAP2+/+ [right panel] ribbons. In addition to synaptic vesicles, vesicle-like particles that are smaller in diameter than synaptic vesicles were seen forming clusters in the cytosol [GCAP2+/+ panel]. These clusters found in the vicinity of the ribbons were more extensive in GCAP2+/+ samples than in C57Bl samples. B. Club-shape ribbons were more abundant in GCAP2+ and GCAP2+/+ than in C57Bl samples. Two examples of the density of club-shape and spherical-ribbons are shown in 8,000× visual fields of GCAP2+ and GCAP2+/+ retinal sections. Club-shape and spherical ribbons pointed by arrows are shown at higher magnification in the right panels. C. Statistical analysis of ribbon length in C57Bl, GCAP2+ and GCAP2+/+ mice that were either raised in constant darkness (D); or raised in constant darkness and subsequently exposed to 1–5 h light (L). A minimum of forty synaptic ribbons were measured from at least two mice per phenotype. Plotted in the histogram are mean values ± standard error. *** denotes $P<0.0001$ in Student's t-test. ** denotes P≤0,001 in Student's t-test. *denotes PP≤0,01 in Student's t-test. D. Statistical analysis of ribbon length in GCAP2+ and WT littermate control mice raised in standard cyclic light and processed at p60. GCAP2-expressing mice showed a 10% reduction in ribbon length compared to WT littermate controls. Notice the difference in the Y-axis scale. *** denotes P≤0,0001 in Student's t-test. E. Histogram comparing the percentage of club-shape and spherical ribbons [of total synaptic ribbons] in C57Bl, GCAP2+ and GCAP2+/+ at p40 processed in darkness [D] or immediately after 1 h or 5 h of light exposure.
doi:10.1371/journal.pone.0042994.g005

for at least four generations, they were originally obtained in a C57Bl × DBA mixed genetic background [27].

To discard the contribution of genetic background effects, synaptic ribbon length was compared in GCAP2+ versus transgene-negative control mice [herein called WT] in the same litter, raised in the same cage under standard cyclic light and analyzed at p60. GCAP2 transgene expression led to a 10% reduction in ribbon length compared to WT mice [0,2621±0,0059 μm in transgene-positive mice, n = 131 from four mice; versus 0,2902±0,0067 μm in WT mice, n = 135 from three mice; Student's t = 3,114, 264d.f., P = 0,002] [Fig. 5D].

Taken together these results indicate that the overexpression of GCAP2 promotes the loss of ribbon material, both in dark-adapted and light-adapted retinas.

It has been reported that as synaptic ribbons loose material in the light adaptation process, different morphologies are observed at the ultrastructural level, such as club-shape ribbons (csr) or ribbons with a spherical form (sr) in tangential sections. This is probably due to the fact that the ribbons, laminar in nature, assemble and disassemble material in preformed spherical blocks at focal points[14–16].

To study whether the overexpression of GCAP2 led to a higher abundance of these "assembly intermediate" morphologies, the percentage of club-shape and spherical ribbons was determined in GCAP2+ and GCAP2+/+ versus C57Bl mice [Histogram in Fig. 5E, Table S1]. While C57Bl mice that were raised in darkness showed less than 1% of club-shaped/spherical ribbons, GCAP2+ and GCAP2+/+ mice raised in darkness showed a 4.8% and 3.6% of these structures respectively, which represents at least a four-fold increase in their relative abundance [Table S1]. In C57Bl mice that were light-adapted for 1–5 h the percentage of club-shaped/spherical ribbons increased to 8%, while in GCAP2+ or GCAP2+/+ mice exposed to these same light conditions the increase was even higher [14% and 18% of assembly intermediates respectively, Table S1].

Fig. 5B shows two representative visual fields from light-adapted GCAP2+ and GCAP2+/+ samples, in which two and three club-shape/spherical ribbons are present per visual field, respectively [shown by arrows and magnified in subsequent panels]. This density of club-shaped/spherical ribbons is not observed in the C57Bl samples.

Taken together, the reduction of ribbon length and the increase in the frequency of ribbon morphology intermediates indicate that GCAP2 overexpression causes ribbon disassembly *in vivo*.

Occasionally, accumulations of electrodense particles that seem like clusters of small vesicles (smaller in diameter than synaptic vesicles) were observed in the vicinity of the ribbon and horizontal cell processes [Fig. 5A, GCAP2+/+ panel, dark condition]. These clouds of particles of unknown nature, that appear in synaptic terminals irrespective of whether a synaptic ribbon is observed or not, were more voluminous and appeared more frequently in GCAP2+/+ mice than in wildtype mice. We speculate that they might represent debris resulting from bulk membrane retrieval in the process of synaptic vesicle recycling. This observation suggests that GCAP2 might somehow interfere with their clearance.

GCAP2 and Ribeye Partially Colocalize at Synaptic Ribbons

In order to study whether GCAP2 colocalizes with Ribeye at synaptic ribbons at the ultrastructural level and whether it localizes to ribbon assembly intermediates, we performed immunohistochemistry at the electron microscopy level. For these studies we used an affinity purified polyclonal antibody anti-GCAP2 generated in rabbit against recombinant GCAP2 protein. This antibody is highly specific, recognizing a single protein band at 24 kDa in Western blots (data not shown).

Immunolocalization of GCAP2 was assayed in sections from GCAPs−/−GCAP2+ mice. Fig. 6A shows that the anti-GCAP2 antibody decorates the disc membranes at the rod outer segment compartment, as expected. At the synaptic terminal, GCAP2 was observed sparsed in the cytosolic space and occasionally associated to synaptic ribbons, to the plasma membrane and to the presynaptic membrane apposing horizontal cell processes [5nm-gold particles, arrows in Fig. 6B and 6C]. This staining pattern reproduces the GCAP2 immunostaining reported by confocal microscopy, although the density of GCAP2 signal is much lower at the ultrastructural level.

In order to assess the specificity of the occasional immunostaining of synaptic ribbons and the presynaptic membrane apposing horizontal cell processes, the gold particles were counted in more than 70 randomly selected synaptic terminals in the GCAPs−/−GCAP2+ sample [e.g. synaptic terminals presented in Fig. 6B and C] and GCAPs−/− control sections. In the GCAPs−/−GCAP2+ sample 16% of the analyzed synaptic terminals presented at least one gold particle associated to the ribbon, whereas only 6% of the synaptic terminals analyzed in the GCAPs−/− control presented gold particle association to the ribbon. About 27% of synaptic terminals in GCAPs−/−GCAP2+ sections presented association of the gold particles to the plasma membrane surrounding horizontal cell processes, whereas only 16% presented this association in the GCAPs−/−. Panels 6E-G show longitudinal sections of synaptic ribbons in which GCAP2 immunostaining is observed in clusters [Fig. 6E-F, 5nm-gold particles, arrows; Fig. 6G, 15nm-gold particles, arrows] colocalizing with Ribeye, that selectively marks the ribbon (arrowheads in all panels). In tangential sections, GCAP2 is occasionally observed

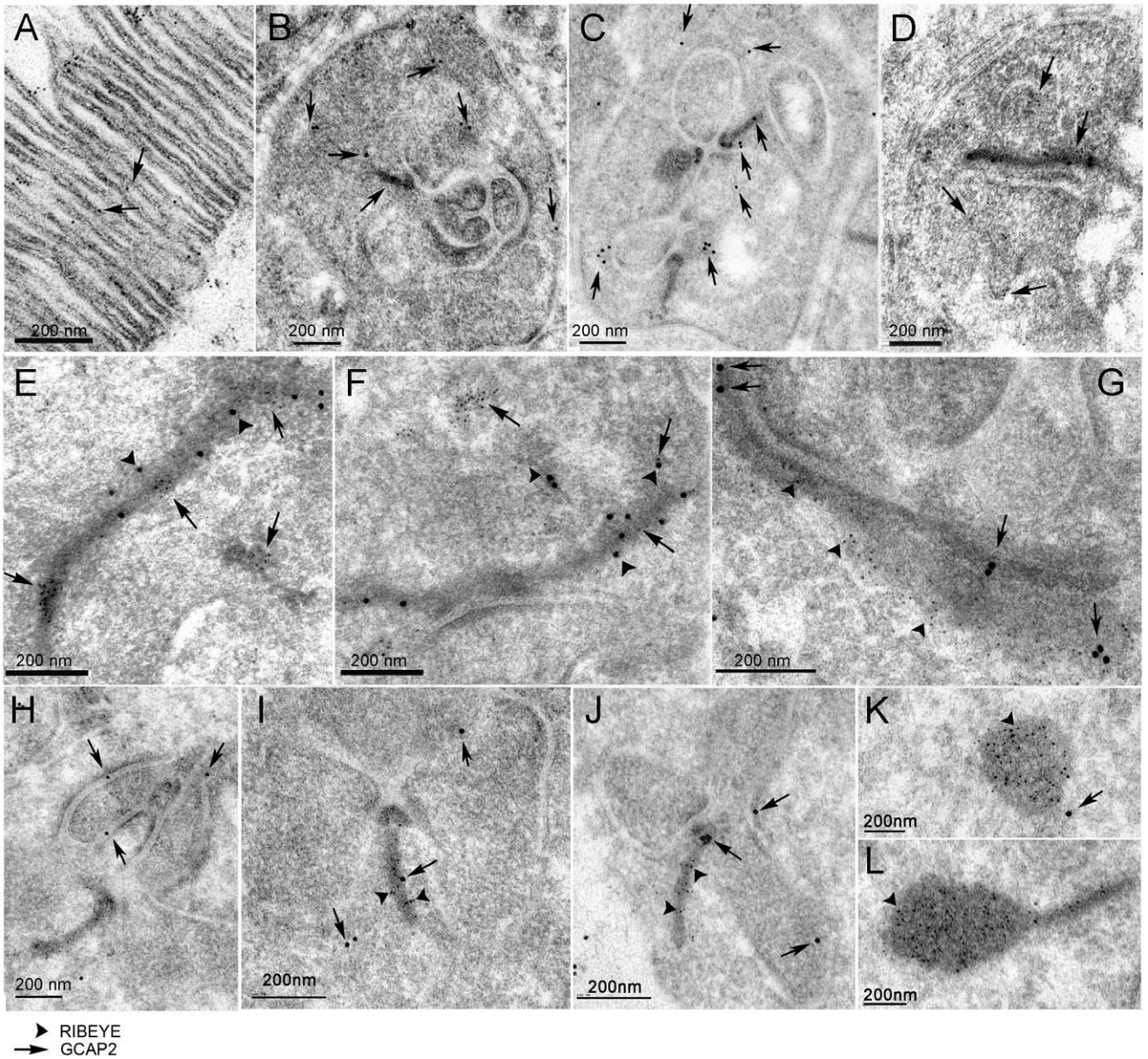

Figure 6. Immunoelectron microscopic localization of GCAP2 and Ribeye at rod synaptic terminals of GCAPs−/−GCAP2+ mice. A. Localization of GCAP2 in ultrathin sections of the retina at the outer segment layer region, as an intrinsic control of the immunoelectron microscopic localization protocol. GCAP2 [5nm-gold particles, arrows] associates to the disc membranes, as expected. B-C. View of entire synaptic terminals, to show GCAP2 immunoreactivity sparsed in the cytosolic space and also associated to the plasma membrane, the membrane apposing invaginating horizontal processes and the ribbon. D. Gold-particles decorating the border of an invaginating horizontal process. E-G. Selected examples of longitudinal ribbons showing GCAP2 [5nm-gold particles in E, F, 15-nm gold particles in G, pointed by arrows in all panels] colocalizing with RIBEYE [arrowheads in all panels]. H-J. Selected ribbon transversal sections showing GCAP2 localization at the ribbon or its proximity [arrows point to GCAP2 associated particles, arrowheads to RIBEYE associated particles]. K, L. Representative examples of club-shape ribbon transversal sections, densely immunolabeled for Ribeye but not GCAP2. Scale bar corresponds to 200 nm in all panels.
doi:10.1371/journal.pone.0042994.g006

in the ribbon [Fig. 6I, arrow] and/or in the proximity of the arciform density [Fig. 6J, arrow]. Pictures showing GCAP2 association to the membrane apposing invaginating dendritic processes of horizontal cells are shown in Fig. 6H-J. Club-shaped ribbons that were extensively labeled with anti-Ribeye antibody did not show labeling with the anti-GCAP2 antibody [Fig. 6K,L].

The fact that GCAP2 appears to be occasionally associated with the ribbon in clusters rather than showing a more extensive and homogeneous ribbon distribution might reflect a transient nature of the interaction of GCAP2 with the ribbon structural components.

GCAP1/GCAP2 Double Knockout Mice have Unaltered Ribbons, but the Effect of GCAP2 Overexpression at Shortening Synaptic Ribbons is Magnified in the Absence of GCAP1

In order to study how the loss-of-function of both GCAP1 and GCAP2 affected synaptic ribbon length, ribbon length measure-

ments were taken in rod terminals from GCAPs−/− and compared to those of wildtype mice. For the comparison in Fig. 7 mice were reared in constant darkness. GCAP1 and GCAP2 ablation leads to an increase in light sensitivity, due to suppression of the Ca^{2+}-feedback loop to cGMP synthesis [27]. This would have the effect of magnifying the change in cell membrane potential and Ca^{2+} dynamics upon light exposure. However, dark-adapted GCAPs−/− mice show a similar dark current value to that of wildtype mice. Therefore, we reasoned that by rearing the mice in darkness any difference detected in ribbon length between wildtype and GCAPs−/− mice could be assigned to their direct effect on ribbon dynamics at the synaptic terminal. However, no significative differences in length were observed between GCAPs−/− ribbons (0,2791±0,0175 μm, n = 256) and WT ribbons (0,2915±0,00665 μm, n = 103), Fig. 7A-B, Histogram in Fig. 7F and Table S1, which indicates that GCAP1 and GCAP2 are both dispensable for the normal development and basic structural maintenance of synaptic ribbons, at least when raised in darkness.

Surprisingly, GCAPs−/−GCAP2+ mice raised in darkness showed a remarkable reduction in ribbon length at p40 (0,1798±0,004 μm, n = 178), Fig. 7F and Table S1. This represents a 36% reduction of ribbon length in GCAPs−/−GCAP2+ compared to GCAPs−/− littermate controls. This 36% reduction of ribbon length in GCAPs−/−GCAP2+ mice that express GCAP2 to 1,5-fold the endogenous level is much higher than the 14% reduction of ribbon length observed in GCAP2+/+ mice, that overexpress GCAP2 to 4-fold the endogenous levels in the wildtype genetic background. These results suggest that endogenous GCAP1 somehow counteracts GCAP2 effect at shortening synaptic ribbons.

We have observed that GCAP1 also localizes at the synaptic terminal, by immunolocalizing GCAP1 with an affinity-purified anti-GCAP1 polyclonal antibody raised against the whole recombinant protein [Fig. 8]. GCAP1 immunolocalization signal partially overlaps with Ribeye at the synaptic ribbon, indicating that GCAP1 could have a role at the synaptic terminal.

To study whether there are other ultrastructural changes at the synaptic terminal between GCAPs−/−GCAP2+ mice and their GCAPs−/− littermate controls, the dimensions of individual synaptic terminals were determined in five 16×16 μm^2 visual fields in the OPL region. The size of the synaptic terminals was determined to be smaller in GCAPs−/−GCAP2+ mice than in GCAPs−/− littermate controls, that were in turn smaller than the

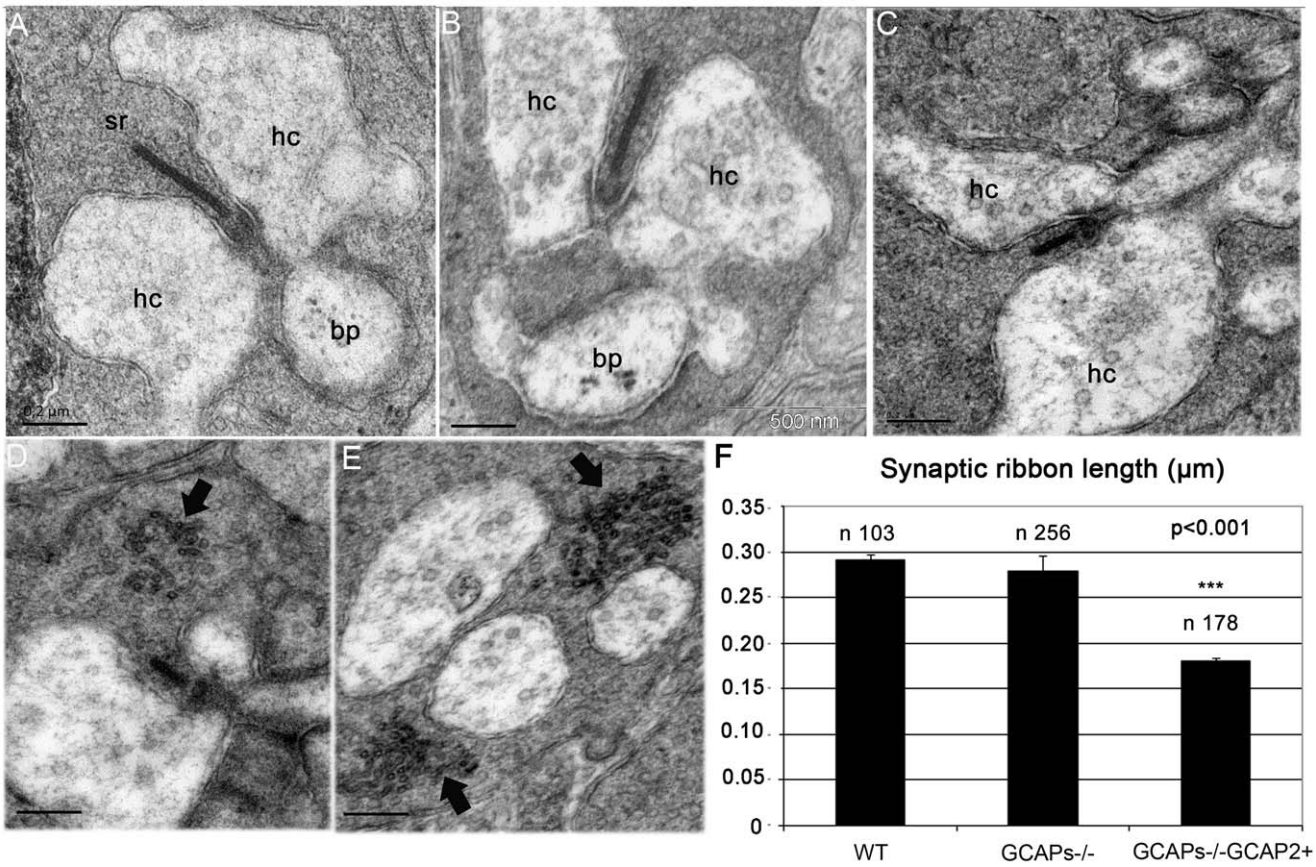

Figure 7. Expression of GCAP2 in the absence of GCAP1 exacerbates the effect of GCAP2 at promoting ribbon disassembly. A-C. Electron micrographs from WT (A), GCAPs−/− (B) and GCAPs−/−GCAP2+ (C) ultrathin retinal sections obtained from dark-reared mice at postnatal day 40, showing a representative rod synaptic ribbon from each phenotype. While GCAPs−/− mice show ribbons that are undistinguishable in length from wildtype ribbons, GCAPs−/−GCAP2+ mice show ribbons that are on average about 40% shorter than wildtype ribbons. hc: horizontal cell process; bc: bipolar cell process; sr: synaptic ribbon. D, E. Examples of GCAPs−/−GCAP2+ synaptic terminals containing accumulations of vesicle-like particles in the vicinity of the active zone (arrows). These aggregates, that might appear in terminals with or without ribbons, might generate as by-products in the bulk endocytosis for synaptic vesicle recycling process. F. Histogram of synaptic ribbon length in WT, GCAPs−/− and GCAPs−/−GCAP2+ mice. Plotted are mean values ± standard errors. * denotes $P<0.001$ in ANOVA analysis [$F(2, 196532) = 97,37$, $P = 0.000$] using the PASW program package (IBM).
doi:10.1371/journal.pone.0042994.g007

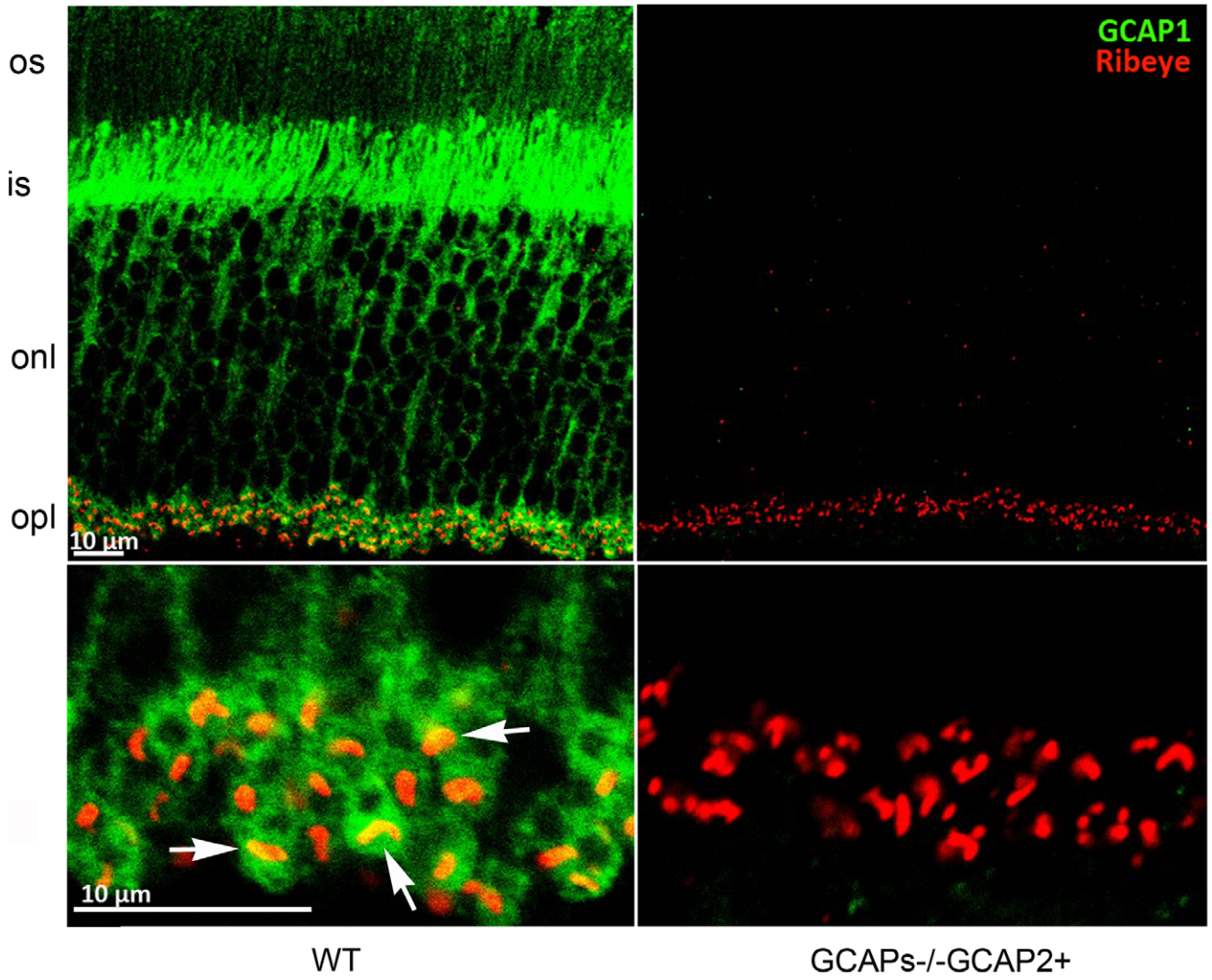

Figure 8. GCAP1 localizes to the synaptic terminal and partially overlaps with Ribeye. Immunolabeling of vertical retinal sections from WT and GCAPs−/−GCAP2+ mice with rabbit polyclonal antibody anti-GCAP1 and a monoclonal antibody against Ribeye/CtBP2. GCAP1 is found at the outer segment (os) inner segment (is) and outer plexiform layer (opl) of the retina, where it colocalizes with Ribeye at synaptic ribbons (white arrows). GCAP1 antibody immunolabeling signal was absent in GCAPs−/−GCAP2+ sections when identical laser power and acquisition gain parameters were used at the confocal microscope, excluding that the signal originates from cross-reactivity of anti-GCAP1 antibody with GCAP2 at this working dilution.
doi:10.1371/journal.pone.0042994.g008

wildtype. A Duncan's test established the size of the synaptic terminals as follows: GCAPs−/−GCAP2+ (2.47±0.09 µm^2, X+SE, n = 69) < GCAPs−/− (3.18±0.12 µm^2, n = 88) < WT (3,58±0,13 µm^2 n = 69), with P<0,05 [Fig. S1]. The percentage of synaptic terminals that contained a synaptic ribbon was also reduced in GCAPs−/−GCAP2+ versus the two other groups. Mean values were [WT 70,1±1,8 n = 69; GCAPs−/−67,3±2,3 n = 88; GCAPs−/−GCAP2+57,6±2,3 n = 69]. An ANOVA analysis showed a statistically significant difference between the GCAPs−/−GCAP2+ values and the two other groups, F [2,12] = 9,36, P = 0,004 [Fig. S1C].

That is, synaptic terminals are smaller in GCAPs−/−GCAP2+ mice, and there is a lower percentage of synaptic terminals that contain a ribbon. This figure explains our observation in Fig. 2 that OPL thickness is substantially reduced in GCAPs−/−GCAP2+ mice, and reflects that the integrity of the ribbon synapse is compromised to some extent in these mice. However, neurodegeneration in these mice appears to be milder than the neurodegeneration described for other mouse models with mutations in presynaptic proteins[30–36], and signs of autophagia like vacuolization or mitochondria swelling were not appreciated in GCAPs−/−GCAP2+ mice compared to GCAPs−/− or WT controls [Fig. S1].

When GCAPs−/−GCAP2+ mice were raised in 12 h:12 h dark:light standard cyclic light they showed a similar reduction in ribbon length at p40 (0,1788±0,007 µm, n = 43) than when raised in darkness, whereas GCAPs−/− littermate control mice raised under the same cyclic light conditions showed a more subtle reduction in ribbon length (0,2412±0,01 µm, n = 29).

Taken together, these results indicate that abolishing the expression of both GCAP1 and GCAP2 does not alter the length or morphology of synaptic ribbons in dark-reared mice, or substantially affect the thickness and connectivity of the OPL. However, expressing GCAP2 in the absence of GCAP1

(GCAPs−/−GCAP2+ mice) had a severe effect at shortening the ribbons, lowering the number of synaptic ribbons, reducing the dimensions of synaptic terminals and ultimately causing a thinning of the OPL. We conclude that altering the ratio of GCAP1 to GCAP2 in rod photoreceptor cells *in vivo* leads to morphological alterations at the synaptic terminal including a substantial shortening of the synaptic ribbon. Because alteration of GCAP1 to GCAP2 relative levels has a bigger effect than the overexpression of GCAP2, we infer that it is the balanced action of these proteins in rods that is required to maintain the integrity of synaptic terminals.

Mice that Express GCAP2 in the Absence of GCAP1 and are Raised in Darkness have Severely Impaired Light Responses in the Scotopic Range

To study whether the phenotype observed at the ultrastructural level in these mouse lines correlates with a functional phenotype, electroretinogram responses to a family of flashes of increasing intensities were recorded in the scotopic and the photopic range.

Rod b-wave amplitudes in the scotopic range (I = −4 to I = −2 Log cd.s/m^2), as well as a-wave and b-wave amplitudes from rod and cone mixed responses (I = 1,5 Log cd.s/m^2) and pure cone responses (I = 2,0 Log cd.s/m^2) were averaged for the different mouse lines, and are presented in Table 2. Representative recordings are shown in Fig. 9. While dark-reared GCAPs−/− mice presented minor reductions in the amplitude of the rod b-wave and the a-wave from mixed responses (compare blue traces to red traces), dark-reared GCAPs−/−GCAP2+ mice showed very diminished responses in the scotopic range as well as diminished a-wave amplitudes in the rod-cone mixed responses (compare black traces to red traces). In contrast, pure-cone responses in the photopic range were unaffected [Table 1, Fig. 9 bottom traces]. Photopic responses in GCAPs−/−GCAP2+ mice are not expected to differ from GCAPs−/− responses because the transgene is not expressed in cones.

The reduction in the magnitude of the rod component of the ERG response was more severe in GCAPs−/−GCAP2+ rods when mice were raised in constant darkness than when mice were raised in standard 12 h:12 h dark:light cycles [Fig. 9, compare superimposed traces in left and middle panels].

Because both the a-wave and b-wave are reduced in dark-reared GCAPs−/−GCAP2+ ERG responses, this visual impairment cannot be solely attributed to ribbon shortening. Furthermore, the same shortening of the ribbons takes place when GCAPs−/−GCAP2+ mice are raised in cyclic light, but ERG responses are indistinguishable from GCAPs−/− responses. These results indicate that the rod component of the ERG response is very diminished in dark-reared GCAPs−/−GCAP2+ mice; and, on the other side, that a shortening of 40% of ribbon length in cyclic-light reared GCAPs−/−GCAP2+ mice has little effect on the amplitude of the B-wave of ERG responses in the scotopic range. That is, ribbon shortening has a limited effect on synaptic strength.

The decreased contribution of the rod component of the ERG response to dark-reared GCAPs−/−GCAP2+ responses is not due to the loss of rod photoreceptor cells. GCAPs−/−GCAP2+ mice that have been raised in constant darkness show at p40 the same number of photoreceptor nuclei rows that wildtype mice, as shown by morphometric analysis of outer nuclear layer thickness at different regions covering the whole length of the retina in these mice [Fig. 2C]. Therefore, we infer that the rods in GCAPs−/−GCAP2+ mice raised in darkness have a diminished contribution to ERG responses because they are unable to respond to light, likely due to electrical saturation (see Discussion).

Discussion

Guanylate Cyclase Activating Proteins (GCAPs) are neuronal Ca^{2+} sensors from the calmodulin superfamily. They play a fundamental role in the recovery of the light response by conferring Ca^{2+} modulation to retinal guanylate cyclase at the membrane discs of rod and cone outer segments where phototransduction takes place [37]. The main isoforms GCAP1 and GCAP2 also localize to the inner segment and synaptic terminal of photoreceptor cells, where their function is unknown [28]. A recent study has demonstrated that GCAP2 interacts with Ribeye, a unique and major protein component of synaptic

Table 2. ERG response parameters in the different mouse lines.

ERG wave amplitude		b - rod	a - mixed	b - mixed	b - cone
Intensity (cd·s·m-2)		**−2,0**	**1,5**	**1,5**	**2,0**
WT [D-D]	n = 4	304,08±15,39	277,90±34,30	529,48±34,29	188,75±8,84
GCAPs −/− [D-D]	n = 4	230,98±22,62	177,01±18,07	380,65±32,78	140,81±19,78
GCAPs −/− GCAP 2+ [D-D]	n = 10	69,91±16,57***	54,44±19,18***	228,38±24,65***	180,69±13,77
WT [L-D]	n = 4	255,84±11,53	203,62±7,83	474,29±14,46	188,75±8,84
GCAPs −/− [L-D]	n = 4	158,81±7,04	183,59±9,28	446,52±53,77	237,84±28,33
GCAPs −/− GCAP 2+ [L-D]	n = 6	178,76±37,57	185,89±31,38	455,33±68,24	256,87±31,43
GCAP 2+ [L-D]	n = 3	224,31±25,01	175,22±12,54#	420,08±33,97	234,25±8,04

Statistical analysis: Statistical analysis of ERG data was performed using GraphPad InStat software; each experimental group was considered independent. A general linear model procedure with analysis of the variance (ANOVA) was carried out. Post hoc multiple comparisons Tukey test was used. Data are expressed as mean ± SEM. The results were considered significant at $p<0.05$.

WT [D-D] vs.

- GCAPs −/− [D-D]: n.s.
- GCAPs −/− GCAP 2+ [D-D]:

***$p<0.001$.

WT [L-D] vs.

- GCAPs−/− [L-D] : n.s.
- GCAP 2+ [L-D] : n.s.
- GCAPs −/− GCAP 2+ [L-D]: n.s.

doi:10.1371/journal.pone.0042994.t002

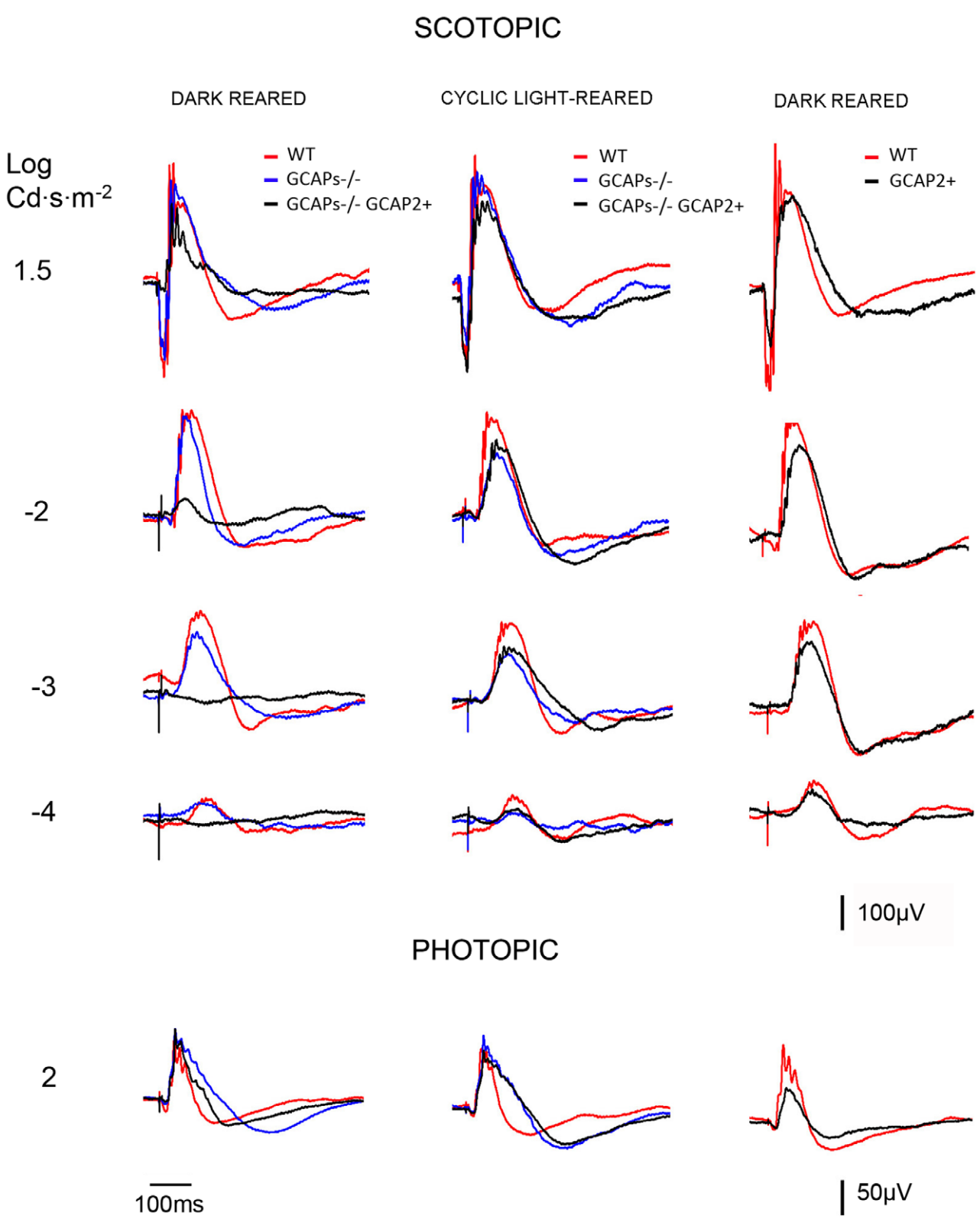

Figure 9. Comparison of electroretinogram responses from WT, GCAP2+, GCAPs−/− and GCAPs−/−GCAP2+ mice that were either raised in constant darkness or in 12 h:12 h dark:light standard cyclic light. Left panel, superimposed representative responses of WT (red), GCAPs−/− (blue) and GCAPs−/−GCAP2+ (black) mice at p40 that were reared in constant darkness, in the scotopic and photopic range. The a-wave amplitude is severely reduced in GCAPs−/−GCAP2+ mice (black trace) compared to wildtype and GCAPs−/− traces in the scotopic range. This difference is absent in the photopic range, since the transgene is only expressed in rods. Central panel, superimposed representative responses of the same phenotypes, but raised in 12h:12h dark:light standard cyclic light and dark-adapted previous to the experiment. ERG responses from GCAPs−/−GCAP2+ mice were similar to GCAPs−/− and wildtype responses. Right panel, superimposed traces of cyclic light reared wildtype and GCAP2+

mice at p40. There were no statistically significant differences in the a-wave and b-wave amplitudes of these responses, whether the mice were raised in constant darkness or in 12h:12h dark:light standard cyclic light (cyclic reared mice results shown).
doi:10.1371/journal.pone.0042994.g009

ribbons, and partially colocalizes with Ribeye at these structures, and pointed to GCAP2 as a candidate that might mediate the Ca^{2+}-dependent disassembly of synaptic ribbons [19].

In this study we set to test this hypothesis *in vivo*, by analyzing alterations in the density and morphology of synaptic ribbons in GCAP2 models of gain-of-function (GCAP2 overexpression) and loss-of-function (GCAP1/GCAP2 double knockout, GCAPs−/−) and their correlation with a functional phenotype. We here report that mice that lack GCAP1 and GCAP2 develop synaptic ribbons that are similar in length and morphology to wildtype ribbons, indicating that the GCAP2-Ribeye interaction is not required for the initial assembly or anchoring of the ribbon to the active zone. By characterizing transgenic mice that overexpress GCAP2 in rods (GCAP2+ and GCAP2+/+ mice) or mice in which GCAP2 expression was restored in the GCAPs−/− genetic background (GCAPs−/−GCAP2+ mice) we have confirmed that GCAP2 overexpression leads to the shortening of synaptic ribbons. This phenotype is manifested when mice are reared either in standard cyclic light or in constant darkness, and it worsens when GCAP2 is expressed in the absence of GCAP1, in which case it severely impairs visual function when mice are dark-reared. We also demonstrate GCAP2 colocalization with Ribeye at the ultrastructural level. Based on our results we suggest that both GCAP1 and GCAP2 isoforms, and particularly the relative levels of GCAP1 to GCAP2, might contribute to mediate the ribbon morphological changes triggered by light through a combination of effects: a secondary effect on the ribbon due to their role at regulating cGMP synthesis at rod outer segments; and a more direct effect on the ribbons exerted at the synaptic terminal. We here analyze our findings and their physiological significance in the context of the current knowledge of GCAP1 and GCAP2 function and biochemical properties.

GCAP1 and GCAP2 are not Required for the Early Assembly of Photoreceptor Ribbon Synapses

The group of Frank Schmitz has identified GCAP2 as an interacting partner of Ribeye. In their localization assays, Venkatesan and collaborators showed that the GCAP2 immunofluorescence signal filled the cytosolic space of the synaptic terminal, partially overlapping with Ribeye at the ribbons [19].

Synaptogenesis in rod photoreceptors of the mouse retina is initiated at P6–P8, and is completed by the time mice open their eyes at P13–P14. The assembly of photoreceptor ribbons during synaptogenesis involves the formation of sphere-like structures from protein aggregates of ribbon cytomatrix proteins: Bassoon, Ribeye, Piccolo and RIM1. These non-membranous electrodense "precursor spheres" were proposed to be the transport units of the ribbon cytomatrix active zone (CAZ) proteins that assemble into immature floating ribbons and subsequently give rise to mature anchored ribbons [38]. Mice that lack Bassoon show impaired aggregation of ribbon cytomatrix proteins at early stages, delayed formation of precursor spheres [39] and a failure to form anchored ribbons [31]. The fact that GCAP2 interacts with Ribeye raises the question of whether GCAP2 might be required for the developmental assembly of synaptic ribbons. In this study we have observed that the GCAP1/GCAP2 double knockout mice (GCAPs−/−) present a largely normal OPL at p40 with the typical pattern of Ribeye staining [Figs 2, 3, and 4]; and the usual number of synaptic ribbons, with standard size and morphology by transmission electron microscopy [Fig. 7 and Fig. S1].

Measurements of synaptic ribbon length in GCAPs−/− mice were initially taken from mice that were reared in constant darkness [Fig. 7]. The reason for this is that GCAPs−/− rod photoreceptors show a higher sensitivity to light than wildtype rods and, and the same prolonged light stimuli could have different effects on WT and GCAPs−/− mice [27]. Nevertheless, we have subsequently observed that either dark-reared or cyclic-light reared GCAPs−/− mice yielded similar to wildtype ERG responses in a range of light intensities that covered the scotopic and photopic ranges [Fig. 9]. These results indicate that GCAP1 and GCAP2 are not required for the developmental assembly of synaptic ribbons in rod photoreceptors. However, they do not exclude that these proteins play more subtle roles: e.g. at regulating ribbon dynamic turn-over (see below).

Ultrastructural Localization of GCAP2 at the Synaptic Terminal

Original immunolocalization studies of GCAP1 and GCAP2 reported that GCAP1 localized more abundantly to cone outer segments whereas GCAP2 appeared to be present in the outer segment, the inner segment and the synaptic terminals of both rods and cones in different species [28,29]. Venkatesan's study has shown that the GCAP2 immunofluorescence signal filled the synaptic terminal and to some extent overlapped with synaptic ribbons [19]. Our localization data at the confocal microscopy level confirms this observation [Fig. 2], which is relevant because our assays overcome two previously identified limitations in GCAP localization studies. First, the fact that antibodies raised against one specific isoform might cross-react with the other (e.g. Antibodies raised against GCAP2 typically crossreact with GCAP1, and vice versa). Second, the fact that antibodies raised against a particular species isoform yield different results in retinal tissue from different species [40,41]. Our antibodies were raised against the bovine isoform of GCAP2, and they were used to immunolocalize the bovine isoform of GCAP2 expressed in transgenic mice. The bovine GCAP2 isoform has been shown to restore endogenous GCAP2 localization and function in GCAPs−/− mice [27].

Our immunoelectron localization study revealed for the first time at the ultrastructural level that GCAP2 co-localizes with Ribeye in about 16% of the synaptic ribbons analyzed in the GCAPs−/−GCAP2+ mice [Fig. 6]. Instead of a homogeneous distribution along the ribbon, we found that GCAP2 was present in clusters, easier to detect in longitudinal sections [with up to two or three clusters per ribbon, Fig. 6E-G] than in tangential sections. That GCAP2 appears associated to the ribbon in only 16% of the ribbons analyzed might be indicative of a transient interaction. It has been described that, following the *in vitro* EGTA treatment of retinas, ribbon disassembly begins with the formation of protrusions and the pinching off of spherical ribbon material [14,38], that are seen as club-shaped ribbons and as floating spheres in tangential sections. Therefore, in our immunolabeled ultrathin sections we thoroughly looked for clusters of Ribeye and GCAP2 outside the ribbon that might reflect modules of disassembly containing both proteins, but could not detect them. Taken together, our results confirm GCAP2 localization at the ribbons at the ultrastructural level, and would sustain GCAP2 involvement in the regulation of ribbon morphological changes triggered by changes in Ca^{2+}.

In addition to the synaptic ribbon, GCAP2 was also associated to the plasma membrane and particularly to the presynaptic membrane apposing the invaginating processes of horizontal cells [Fig. 6D,H-J]. The whole delimiting membrane was decorated, and not just the active zone. This result points to GCAP2 having additional functions at the synaptic terminal, where it could be imparting Ca^{2+} sensitivity to new molecular targets. Future experiments will attempt to identify GCAP2 molecular targets in this compartment.

GCAPs Effect on Ribbon Length

Synaptic ribbons in photoreceptor cells of the mouse retina in the albino strain Balb/c tend to disassemble in response to illumination by releasing ribbon material in spherical modules; and elongate by regaining ribbon material during dark-adaptation[14–16,18,38,42]. Although the physiological significance of this ribbon remodeling with light is not yet clear and strong variations in the extent of these changes have been reported between different mouse strains [17], we have observed in this study that 1 h of light exposure can cause a 13% reduction of ribbon length in pigmented C57Bl/6 mice [Fig. 5 and Table S1]. While we doubt that this might be a relevant mechanism to regulate synaptic strength or serve to extend the operational range of rods, it might represent a turn-over mechanism of the ribbon set in place by light, e.g. following photic damage.

It has been shown in albino mice that ribbon disassembly depends on the drop in intracellular Ca^{2+} at the synapse caused by the light-triggered hyperpolarization of the cell [14,18]. Because GCAP2 has been shown to interact with Ribeye and localize to the ribbon [19], we here wanted to test whether GCAP2 might mediate the Ca^{2+} -dependent structural changes of ribbons as proposed [19].

Our findings indicate that, although both GCAP1 and GCAP2 isoforms are dispensable for developmental ribbon formation and basic structural maintenance, altering the GCAP1 to GCAP2 ratio does have an effect on the morphology of synaptic terminals and does alter ribbon length.

Mice that express GCAP2 to 2,5-fold the endogenous levels [GCAP2+ line, Table 1] presented a 10% reduction in ribbon length compared to wildtype mice when both transgenic and wildtype mice were raised in constant darkness, or in standard cyclic light [Fig. 5, Table S1]. Mice that express GCAP2 to 4,5-fold the endogenous level [GCAP2+/+] showed a 14% reduction in ribbon length when mice were raised in constant darkness and a 24% reduction when they were raised in constant darkness and subsequently exposed to light for 1–5 h. In addition, the percentage of ribbon shapes that identify a disassembling ribbon (club-shaped and spherical ribbons versus bar-shaped ribbons in transversal sections) was higher in transgenic mice than in wildtype mice. These ultrastructural effects on the synaptic ribbons show that GCAP2 overexpression causes ribbon disassembly. This noticeable change in ribbon dimensions, however, had only minor effects on the functional response to light, as measured by electroretinogram (ERG). GCAP2+ mice elicited light responses by ERG that were similar to wildtype responses in a-wave and b-wave amplitude and kinetics, when they were raised either in constant darkness or in standard cyclic light (traces from cyclic light-reared mice shown in Fig. 9; traces from dark-reared mice not shown). This indicates that a 10% reduction in ribbon length is not enough to produce a significative change in the b-wave of the ERG response, and that more extensive remodeling of the ribbon might be necessary to affect synaptic strength.

As discussed above, GCAPs−/− synaptic ribbon length did not differ from wildtype synaptic ribbons at p40, and ERG responses of GCAPs−/− mice at p40 were similar to wildtype.

Intriguingly, mice in which GCAP2 expression was selectively restored in the GCAPs−/− background (GCAPs−/−GCAP2+) showed synaptic ribbons that were 40% shorter than wildtype ribbons at p40 when raised in constant darkness [Fig. 7]. GCAPs−/−GCAP2+ mice, when raised in constant darkness, had severely impaired rod visual function at p40. Both the a-wave and b-wave amplitudes of ERG responses were severely reduced in the scotopic range. Because the a-wave amplitude of the ERG reflects the change in membrane potential elicited by the phototransduction cascade and the inverted-sign b-wave reflects postreceptoral activation of rod on-bipolar cells, genetic defects affecting synaptic transmission typically affect predominantly the b-wave[43–46]. Therefore the GCAPs−/−GCAP2+ visual impairment could not be solely attributed to the shortening of rod ribbons. Instead, the ERG phenotype of dark-reared GCAPs−/−GCAP2+ mice revealed a diminished capacity to respond to light at the rod outer segment (ROS) level.

The ratio of the Ca^{2+}-bound inhibitory state to the Mg^{2+}-bound stimulatory state of each GCAP isoform is what determines the rate of cGMP synthesis by retinal guanylate cyclase in rod outer segments at any given $[Ca^{2+}]_i$. Given the well characterized difference in the Ca^{2+} sensitivities of GCAP1 and GCAP2, there is a narrow range of $[Ca^{2+}]_i$ -around the $[Ca^{2+}]_i$ typical of the dark-adapted steady state- for which GCAP1 molecules would be in the stimulatory state while most GCAP2 molecules would be inhibitory state of the cyclase, and these antagonistic effects would cancel each other [27]. It is therefore not surprising that chronic darkness might result in an alteration in the free cGMP levels at ROS in GCAPs−/−GCAP2+ mice in which GCAP2 is expressed in the absence of GCAP1, reducing cGMP levels gradually over time. Abnormally low levels of free cGMP would cause the closure of cGMP-gated channels and the electrical saturation of rods, and could explain the diminished rod component of the ERG despite retention of a normal number of rods in these retinas [Fig. 9 and Fig. 2C]. Therefore it cannot be excluded that shortening of the ribbons might result from a chronic alteration of $[Ca^{2+}]_i$ at the synapse due to abnormally low levels of cGMP. That is, when GCAPs−/−GCAP2+ mice are raised in constant darkness, alterations in ribbon morphology could be a secondary consequence of GCAP2 effect on cGMP metabolism. The involvement of the phototransduction cascade and cGMP metabolism on the light-triggered morphological changes of ribbons has been established [14].

In contrast to mice raised in constant darkness, GCAPs−/−GCAP2+ mice reared in 12 h:12 h dark:light cycles preserved scotopic ERG traces at p40 similar to wildtype in magnitude and kinetics [Fig. 9, Table 2]. Noteworthy, synaptic ribbons in GCAPs−/−GCAP2+ mice raised in cyclic light at p40 are shortened to the same extent as GCAPs−/−GCAP2+ mice raised in darkness [Table S1]. These mice have been reported to have dark current values similar to wildtype, in association with normal free cGMP levels [27]. This makes it unlikely that changes in ribbon length observed in these animals are secondary to altered cGMP metabolism at ROS. Strikingly, the absence of GCAP1 exacerbates the effect of GCAP2 at shortening ribbon length, even when mice are raised in cyclic light. We infer that altering the balance between GCAP1 and GCAP2 leads to the shortening of the ribbons.

Altering the balanced action of GCAP1 and GCAP2 also compromises the ribbon synapse integrity, as shown by the reduction in the size of the synaptic terminals in GCAPs−/

−GCAP2+ mice [Fig. S1]. Therefore, we cannot completely rule out that ribbon disassembly might be a secondary consequence of a presynaptic defect caused at some other level. There are numerous examples in the literature of mutations in presynaptic proteins that cause presynaptic defects that are accompanied by changes in ribbon structure. Mutations in Cav1.4, bassoon, complexin, synaptojanin and laminin produce floating ribbons [30,31,33,36,47]. Mutations in tubby-like protein 1 (TULP1), which impairs rhodopsin trafficking to the outer segment, also affect synaptic ribbon morphology [32]. Mutations in cysteine string protein alpha, a chaperone required for SNAP25 and SNARE complex assembly cause photoreceptor degeneration and the appearance of floating ribbons [34,35]. Myosin Va mutant mice have both anatomical and physiological abnormalities at rod synapses [48]. However some of these mouse models [e.g. Tulp1 ko, CSPα ko] manifest a rapid retinal degeneration with a substantial loss of photoreceptor cells that is accompanied by severe functional defects before one month of age [34,49]. GCAPs−/−GCAP2+ transgenic mice, in contrast, preserve the normal number of photoreceptor cells for months [Fig. 2] and do not present obvious signs of neurodegeneration like vacuolization or mitochondria swelling at the synapse [Fig. S1]. The fact that the absence of GCAP1 exacerbates the effect of GCAP2 at shortening ribbons argues against a non-specific toxic effect of overexpressed GCAP2 at the synaptic terminal. Rather, it seems that the balanced action of GCAP1 and GCAP2 might be needed to preserve the integrity of the synapse and the ribbon.

Together with Venkatesan's report that GCAP2 interacts with Ribeye, our observation that GCAP2 can appear associated to the ribbon at the ultrastructural level and the marked reduction in ribbon length that is observed in GCAPs−/−GCAP2+ mice leads us to suggest that GCAPs might be involved in mediating the morphological changes at the ribbons triggered by changes in Ca^{2+}.

Further genetic and biochemical experiments will be needed to confirm the direct implication of GCAP2 and GCAP1 in this process, and to study whether GCAP1 and GCAP2 might have new molecular targets and new functions at the synapse.

Conclusion

The central observation of this study is that the overexpression of GCAP2 in rods *in vivo* has an impact at shortening synaptic ribbons that is exacerbated in the absence of GCAP1. These results, together with the lack of phenotype when both GCAP1 and GCAP2 isoforms are absent in the double knockout, point to the balanced action of GCAP1 and GCAP2 having an effect on the ultrastructure of the synaptic terminals and on synaptic ribbon length, likely through a combination of mechanisms: i) an indirect or secondary effect on the ribbon would be caused by their primary effect on cGMP metabolism at rod outer segments, manifested in this study when GCAP2 is expressed in the absence of GCAP1 and mice are reared in constant darkness; and ii) an effect on the ribbon through a mechanism independent of cGMP metabolism, manifested when GCAP2 is overexpressed or expressed in the absence of GCAP1 and mice are reared in cyclic light. We have observed that a 40% reduction of ribbon length *in vivo* in GCAPs−/−GCAP2+ mice raised in cyclic light had only subtle effects on ERG responses in the scotopic range, indicating that ribbons can withstand dimensional restrictions without a severe functional effect.

Supporting Information

Figure S1 GCAPs−/−GCAP2+ mice present smaller synaptic terminals than GCAPs−/− and WT mice, and fewer synaptic terminals that contain a ribbon. A. Low magnification micrographs of the opl region of WT, GCAPs−/− and GCAPs−/−GCAP2+ mice. Scale bar, 2 μm. B. Histogram comparing the percentage of synaptic terminals with ribbon in the three phenotypes. The number of synaptic terminals that contain a synaptic ribbon was determined in five representative visual fields per phenotype and expressed as the percentage of the total [Mean ± Standard Error]. Mean values were [WT 70,1±1,8 n = 69; GCAPs−/−67,3±2,3 n = 88; GCAPs−/−GCAP2+57,6±2,3 n = 69]. The ANOVA analysis showed a statistically significant difference between the GCAPs−/−GCAP2+ values and the two other groups of values, F [2,12] = 9,36, P = 0,004. Asterisc in histogram denotes P<0,01. No statistically significant difference was observed between WT and GCAPs−/− values [Duncan's test]. C. Histogram comparing synaptic terminal size in WT, GCAPs−/− and GCAPs−/−GCAP2+ mice. Statistically significant differences were observed among groups by ANOVA analysis F [2,223] = 20,37, P = 0,000. A Duncan's test established GCAPs−/−GCAP2+ mice synaptic terminals (2.47±0.09 μm^2, X+SE, n = 69,) < GCAPs−/− (3.18±0.12 μm^2 n = 88) < WT (3,58±0,13 μm^2 n = 69), with P<0,05.
(TIF)

Table S1 Ribbon length and percentage of club-shaped/spherical ribbons at ribbon synapses of the different mouse lines. Two to ten 16×16 μm frames at 8,000× magnification were delimited in the opl region of each specimen. Each frame typically contained 10 to 22 rod synaptic terminals. Every synaptic terminal in the frame was individually scanned at 100,000× magnification, and length measurements were determined in ribbons resulting from tangential cuts (ImageJ software). Values are expressed as the Mean ± Standard error. The percentage of club-shaped/spherical ribbons is expressed as the ratio of club-shaped ribbons and spherical ribbons to total rod synaptic ribbons (tangential, longitudinal and sagital). Cone synaptic terminals were excluded from the analysis.
(DOC)

Acknowledgments

We kindly acknowledge the excellent technical assistance of Eva Fernández, Almudena García, Nieves Hernández, Carmen López and Nuria Cortadellas at the electron microscopy technical facility at the Scientific and Technological Services of the University of Barcelona (CCiT-UB). We are in debt with Benjamín Torrejón for his kind assistance with image acquisition at the Leica TCS-SL, at the CCiT-UB Bellvitge. We kindly acknowledge the technical help received from Laura Ramírez.

Author Contributions

Conceived and designed the experiments: NLH LF SLB LFS NC JL PV AM. Performed the experiments: NLH LF SLB LFS NC JL PV AM. Analyzed the data: NLH LF SLB LFS NC JL PV AM. Wrote the paper: AM.

References

1. Werblin FS (2011) The retinal hypercircuit: a repeating synaptic interactive motif underlying visual function. J Physiol 589: 3691–3702.
2. Parsons TD, Sterling P (2003) Synaptic ribbon. Conveyor belt or safety belt? Neuron 37: 379–382.
3. Thoreson WB (2007) Kinetics of synaptic transmission at ribbon synapses of rods and cones. Mol Neurobiol 36: 205–223.
4. Prescott ED, Zenisek D (2005) Recent progress towards understanding the synaptic ribbon. Curr Opin Neurobiol 15: 431–436.

5. von Gersdorff H (2001) Synaptic ribbons: versatile signal transducers. Neuron 29: 7–10.
6. LoGiudice L, Matthews G (2009) The role of ribbons at sensory synapses Neuroscientist 15: 380–391.
7. Schmitz F (2009) The making of synaptic ribbons: how they are built and what they do. Neuroscientist 15: 611–624.
8. Tom Dieck S, Brandstatter JH (2006) Ribbon synapses of the retina. Cell Tissue Res 326: 339–346.
9. Zanazzi G, Matthews G (2009) The molecular architecture of ribbon presynaptic terminals. Mol Neurobiol 39: 130–148.
10. Snellman J, Mehta B, Babai N, Bartoletti TM, Akmentin W, et al. (2011) Acute destruction of the synaptic ribbon reveals a role for the ribbon in vesicle priming. Nat Neurosci 14: 1135–1141.
11. Zampighi GA, Schietroma C, Zampighi LM, Woodruff M, Wright, et al. (2011) PLoS One 6, e16944.
12. Zenisek D, Horst NK, Merrifield C, Sterling P, Matthews G (2004) Visualizing synaptic ribbons in the living cell. J Neurosci 24: 9752–9759.
13. Balkema GW, Cusick K, Nguyen TH (2001) Diurnal variation in synaptic ribbon length and visual threshold. Vis Neurosci 18: 789–797.
14. Spiwoks-Becker I, Glas M, Lasarzik I, Vollrath L (2004) Mouse photoreceptor synaptic ribbons lose and regain material in response to illumination changes. Eur J Neurosci 19: 1559–1571.
15. Vollrath L, Spiwoks-Becker I (1996) Plasticity of retinal ribbon synapses. Microsc Res Tech 35: 472–487.
16. Vollrath L, Spiwoks-Becker I, Adly MA, Schaaff U, Lasarzik I, et al. (2001) Synaptic ribbon dynamics in photoreceptors of mice. Ital J Anat Embryol 106: 499–507.
17. Fuchs M, Sendelbeck A, Atorf J, Kremers J. Brandstatter JH (2012) Strain differences in illumination-dependent structural changes at mouse photoreceptor ribbon synapses. J Comp Neurol. In Press.
18. Regus-Leidig H, Specht D, Tom Dieck S, Brandstatter JH (2010) Stability of active zone components at the photoreceptor ribbon complex. Mol Vis 16: 2690–2700.
19. Venkatesan JK, Natarajan S, Schwarz K, Mayer SI, Alpadi K, et al. (2010) Nicotinamide adenine dinucleotide-dependent binding of the neuronal Ca2+ sensor protein GCAP2 to photoreceptor synaptic ribbons. J Neurosci 30: 6559–6576.
20. Dizhoor AM, Olshevskaya EV, Henzel WJ, Wong SC, Stults JT, et al. (1995) Cloning, sequencing, and expression of a 24-kDa Ca(2+)-binding protein activating photoreceptor guanylyl cyclase. J Biol Chem 270: 25200–25206.
21. Frins S, Bonigk W, Muller F, Kellner R, Koch KW (1996) Functional characterization of a guanylyl cyclase-activating protein from vertebrate rods. Cloning, heterologous expression, and localization. J Biol Chem 271: 8022–8027.
22. Gorczyca WA, Gray-Keller MP, Detwiler PB, Palczewski K (1994) Purification and physiological evaluation of a guanylate cyclase activating protein from retinal rods. Proc Natl Acad Sci U S A 91: 4014–4018.
23. Palczewski K, Subbaraya I, Gorczyca WA, Helekar BS, Ruiz, et al. (1994) Molecular cloning and characterization of retinal photoreceptor guanylyl cyclase-activating protein. Neuron 13: 395–404.
24. Peshenko IV, Olshevskaya EV, Savchenko AB, Karan S, Palczewski K, et al. (2011) Enzymatic properties and regulation of the native isozymes of retinal membrane guanylyl cyclase (RetGC) from mouse photoreceptors. Biochemistry 50: 5590–5600.
25. Peshenko IV, Dizhoor AM (2004) Guanylyl cyclase-activating proteins (GCAPs) are Ca2+/Mg2+ sensors: implications for photoreceptor guanylyl cyclase (RetGC) regulation in mammalian photoreceptors. J Biol Chem 279: 16903–16906.
26. Burns ME, Mendez A, Chen J, Baylor DA (2002) Dynamics of cyclic GMP synthesis in retinal rods. Neuron 36: 81–91.
27. Mendez A, Burns ME, Sokal I, Dizhoor AM, Baehr W, et al. (2001) Role of guanylate cyclase-activating proteins (GCAPs) in setting the flash sensitivity of rod photoreceptors. Proc Natl Acad Sci U S A 98: 9948–9953.
28. Cuenca N, Lopez S, Howes K, Kolb H (1998) The localization of guanylyl cyclase-activating proteins in the mammalian retina. Invest Ophthalmol Vis Sci 39: 1243–1250.
29. Kachi S, Nishizawa Y, Olshevskaya E, Yamazaki A, Miyake, et al.(1999) Detailed localization of photoreceptor guanylate cyclase activating protein-1 and -2 in mammalian retinas using light and electron microscopy. Exp Eye Res 68: 465–473.
30. Biehlmaier O, Alam M, Schmidt WJ (2007) A rat model of Parkinsonism shows depletion of dopamine in the retina. Neurochem Int 50: 189–195.
31. Dick O, tom Dieck S, Altrock WD, Ammermuller J, Weiler R, et al. (2003) The presynaptic active zone protein bassoon is essential for photoreceptor ribbon synapse formation in the retina. Neuron 37: 775–786.
32. Grossman GH, Pauer GJ, Narendra U, Peachey NS, Hagstrom SA (2009) Early synaptic defects in tulp1−/− mice. Invest Ophthalmol Vis Sci 50: 3074–3083.
33. Reim K, Wegmeyer H, Brandstatter JH, Xue M, Rosenmund, et al. (2005) Structurally and functionally unique complexins at retinal ribbon synapses. J Cell Biol 169: 669–680.
34. Schmitz F, Tabares L, Khimich D, Strenzke N, de la Villa-Polo, et al. (2006) CSPalpha-deficiency causes massive and rapid photoreceptor degeneration. Proc Natl Acad Sci U S A 103: 2926–2931.
35. Sharma M, Burre J, Sudhof TC (2011) CSPα promotes SNARE-complex assembly by chaperoning SNAP-25 during synaptic activity. Nat Cell Biol 13: 30–39.
36. tom Dieck S, Altrock WD, Kessels MM, Qualmann B, Regus, et al. (2005) Molecular dissection of the photoreceptor ribbon synapse: physical interaction of Bassoon and RIBEYE is essential for the assembly of the ribbon complex. J Cell Biol 168: 825–836.
37. Arshavsky VY, Burns ME (2012) Photoreceptor signaling: supporting vision across a wide range of light intensities. J Biol Chem 287: 1620–1626.
38. Regus-Leidig H, Tom Dieck S, Specht D, Meyer L, Brandstatter JH (2009) Early steps in the assembly of photoreceptor ribbon synapses in the mouse retina: the involvement of precursor spheres. J Comp Neurol 512: 814–824.
39. Regus-Leidig H, tom Dieck S, Brandstatter JH (2010) Absence of functional active zone protein Bassoon affects assembly and transport of ribbon precursors during early steps of photoreceptor synaptogenesis. Eur J Cell Biol 89: 468–475.
40. Howes K, Bronson JD, Dang YL, Li N, Zhang K, et al. (1998) Gene array and expression of mouse retina guanylate cyclase activating proteins 1 and 2. Invest Ophthalmol Vis Sci 39: 867–875.
41. Otto-Bruc A, Fariss RN, Haeseleer F, Huang J, Buczylko J, et al. (1997) Localization of guanylate cyclase-activating protein 2 in mammalian retinas. Proc Natl Acad Sci U S A 94: 4727–4732.
42. Adly MA, Spiwoks-Becker I, Vollrath L (1999) Ultrastructural changes of photoreceptor synaptic ribbons in relation to time of day and illumination. Invest Ophthalmol Vis Sci 40: 2165–2172.
43. Ball SL, Powers PA, Shin HS, Morgans CW, Peachey NS, et al. (2002) Role of the beta(2) subunit of voltage-dependent calcium channels in the retinal outer plexiform layer. Invest Ophthalmol Vis Sci 43: 1595–1603.
44. Haeseleer F, Imanishi Y, Maeda T, Possin DE, Maeda A, et al. (2004) Essential role of Ca2+-binding protein 4, a Cav1.4 channel regulator, in photoreceptor synaptic function. Nat Neurosci 7: 1079–1087.
45. Mansergh F, Orton NC, Vessey JP, Lalonde MR, Stell WK, et al. (2005) Mutation of the calcium channel gene Cacna1f disrupts calcium signaling, synaptic transmission and cellular organization in mouse retina. Hum Mol Genet 14, 3035–3046.
46. Van Epps HA, Hayashi M, Lucast L, Stearns GW, Hurley JB, et al. (2004) The zebrafish nrc mutant reveals a role for the polyphosphoinositide phosphatase synaptojanin 1 in cone photoreceptor ribbon anchoring. J Neurosci 24: 8641–8650.
47. Chang B, Heckenlively JR, Bayley PR, Brecha NC, et al. (2006) The nob2 mouse, a null mutation in Cacna1f: anatomical and functional abnormalities in the outer retina and their consequences on ganglion cell visual responses. Vis Neurosci 23: 11–24.
48. Libby RT, Lillo C, Kitamoto J, Williams DS, Steel KP (2004) Myosin Va is required for normal photoreceptor synaptic activity. J Cell Sci 117: 4509–4515.
49. Hagstrom SA, Duyao M, North MA, Li T (1999) Retinal degeneration in tulp1−/− mice: vesicular accumulation in the interphotoreceptor matrix. Invest Ophthalmol Vis Sci 40: 2795–2802.